

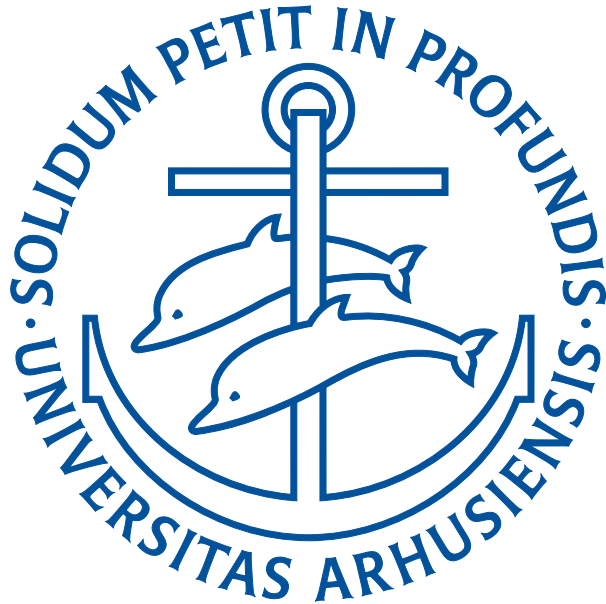
---

# Two- and three-dimensional few-body systems in the universal regime

---

**Filipe Furlan Bellotti**

Department of Physics and Astronomy  
Aarhus University, Denmark



Dissertation for the degree of  
Doctor of Philosophy

October 2014

Filipe Furlan Bellotti  
Department of Physics and Astronomy  
Aarhus University  
Ny Munkegade, Bldg. 1520  
8000 Århus C  
Denmark  
E-mail: [filipe@phys.au.dk](mailto:filipe@phys.au.dk)

This dissertation has been submitted to the Faculty of Science and Technology at Aarhus University, Denmark, in partial fulfillment of the requirements for the PhD degree in physics. The work presented has been performed in the period from August 2012 to July 2014 under the supervision of Aksel S. Jensen from Aarhus University/Denmark and Tobias Frederico from Instituto Tecnológico de Aeronáutica/Brazil. The work is the result of an agreement on joint supervision of doctoral studies and was carried out at the Department of Physics and Astronomy in Aarhus and at the Department for Natural Sciences in São José dos Campos.

*"... A boy walks and walking he reaches the wall.  
And there, right ahead, the future is waiting for us.  
And the future is a spacecraft which we try to fly  
It has neither moment, nor compassion, nor time to arrive.  
Without asking permission it changes our lives and next it invites us to either  
laugh or cry.  
In this road, we are not supposed to either know or see what is coming.  
Nobody does quite know for sure where it ends. ..."*

— TOQUINHO / VINICIUS DE MORAIS / MAURIZIO FABRIZIO / GUIDO  
MORRA  
FREE TRANSLATION OF PART OF *Aquarela*



# Acknowledgment

---

The project, which is ended by this thesis, has started approximately three years ago. During the Master studies, my advisor Prof. Tobias Frederico (ITA/Brazil) trusted and gave me the opportunity to visit Aarhus University for three months. I have been very well received and the visit was very fruitful. After getting my M.Sc. degree, Prof. Aksel S. Jensen (AU/Denmark) proposed the joint supervision of the PhD studies. Since then, I have two official advisors and I would like to thank them: Profs. Tobias and Aksel. They have taught me about Physics, Mathematics, numerical calculation, writing papers and reports, oral presentation, politics in the academic area and other uncountable subjects. In practice, they have given me guidelines to become a good, independent and honest Scientist. Thank you so much for all the time spent and patience with me. I am very proud in saying that you were my supervisors.

In practice, I had also three more advisors, who I should properly acknowledge: Dmitri Fedorov and Nikolaj Zinner from Aarhus University (AU/Denmark) and Marcelo Yamashita from Instituto de Física Teórica (IFT-UNESP/Brazil). They were always available to discuss about any topic and their suggestions and comments have improved a lot my formation. In particular, Dmitri has always been exceptionally supportive during my visits to Aarhus, as well as the secretaries Brigitte Henderson, Trine Binderup and Karin Vittrup. They have always helped me with the administrative and logistic issues. A special thank goes for Tobias and Nikolaj for having proofread the thesis.

The enjoyable time I had in Aarhus was in great extension due to the company of Jeremy Armstrong, Artem Volosniev, Oleksandr Marchukov and Jakob Knorborg, who were constantly present apart of the working time.

At my work place in Brazil, Instituto de Fomento e Coordenação Industrial, I would like to firstly thank Cel. Eng. Augusto Luiz de Castro Otero, who gave me conditions to study without quitting my job. I also appreciate the support from my boss, Dr. Cesar Augusto Botura, and the advices from Dr. Pedro José Pompéia.

My parents are the basis of my journey and they know how grateful I am. The time spent in Aarhus has contributed a lot for my personal and professional development, but it was one of the toughest periods I have ever experienced, since I had to spent almost half of the first year of my daughter away from my family. Therefore, the most special acknowledgement goes to my beloved wife Mônica, who has also passed through very hard times in order to support me in this project. Without her support, this project would not have been started, constructed and concluded. I am very thankful to my young Cecilia, who has showed me that the mathematical and abstract concept of infinity has a meaning: is the love I feel by her.

# Abstract

---

Macro properties of cold atomic gases are driven by few-body correlations, even if the gas has thousands of particles. Quantum systems composed of two and three particles with attractive zero-range pairwise interactions are considered for general masses and interaction strengths in two and three dimensions (2D and 3D). The Faddeev decomposition is used to derive the equations for the bound state, which is the starting point for the investigation of universal properties of few-body systems, i.e. those that all potentials with the same physics at low energy are able to describe in a model-independent form. In 2D, the number of bound states in a three-body system increases without bound as the mass of one particle becomes much lighter than the other two. The analytic form of an effective potential between the heavy particles explains the mass-dependence on the number of bound energy levels. An exact analytic expression for the large-momentum asymptotic behavior of the spectator function in the Faddeev equation is presented. The spectator function and its asymptotic form define the two- and three-body contact parameters. The two-body parameter is found to be independent of the quantum state in some specific 2D systems. The 2D and 3D momentum distributions have a distinct sub-leading form whereas the 3D term depends on the mass of the particles. A model that interpolates between 2D and 3D is proposed and a sharp transition in the energy spectrum of three-body systems is found.





# Resumé

---

Makroskopiske egenskaber af ultrakolde atomare gasser styres af få-legeme korrelationer, det på trods af at gassen har tusindvis af partikler. Vi studerer kvantesystemer bestående af to og tre partikler med attraktive to-partikel vekselvirkninger med nul rækkevidde for generelle partikelmasser og vekselvirkningsstyrker i to og tre dimensioner (2D og 3D). Vi benytter Faddeev dekomposition til at udlede ligningerne for bundne tilstande, hvilket er udgangspunktet for studier af universielle egenskaber ved få-legeme systemer. Dvs. de egenskaber som er uafhængig af den specifikke model for potentialer der giver samme fysik ved lav energi. I 2D vokser antallet af bundne tilstande i et tre-partikel system uden grænse når en af de tre masser er meget lettere end de andre to. Et analytisk udtryk for et effektivt potential mellem de to tunge partikler kan forklare hvorledes antal bundne energiniveauer afhænger af massen. Vi udleder et analytisk udtryk for den såkaldte tilskuer-funktion fra Faddeev dekompositionen i den grænse hvor impulsen bliver stor. Denne tilskuer-funktionen og den asymptotiske opførsel benyttes til at bestemme to- og tre-partikel kontakt-parameteren. To-partikel kontakt parameteren viser sig at være uafhængig af kvantetilstand i nogle bestemte 2D systemer. Impulsfordelingen i 2D og 3D har en karakteristisk opførsel når man betragter den første korrektion til den ledende orden og i 3D får man her en korrektion der afhænger af massen af partiklerne. Vi foreslår en model der interpolerer mellem 2D og 3D grænserne og finder en veldefineret og skarp overgang i energispektret for bundne tilstande af tre partikler.



# Contents

Acknowledgment	v
Abstract	vii
Resumé	ix
Table of Contents	xiii
List of Publications	xv
List of Figures	xix
List of Tables	xxi
<b>1 Introduction</b>	<b>1</b>
<b>2 Two- and Three-body dynamics</b>	<b>7</b>
2.1 Zero-range model and Renormalization . . . . .	8
2.1.1 Two-body T-matrix in 2D . . . . .	10
2.1.2 Two-body T-matrix in 3D . . . . .	13
2.2 Notation and three-body dynamics . . . . .	13
2.2.1 Three-body T-matrix . . . . .	15
2.3 Three-body bound state equation in 2D . . . . .	18
2.4 Three-body bound state equation in 3D . . . . .	23
2.4.1 Renormalization of the 3B transition operator . . . . .	24
2.4.2 Three-body bound state integral equation in 3D . . . . .	25
<b>3 Universal 2D three-body bound states</b>	<b>27</b>
3.1 Symmetry relations . . . . .	28
3.2 Survey of mass dependence . . . . .	29
3.3 Three-body energies for given masses . . . . .	33
3.4 Parametrization of three-body energies . . . . .	36
<b>4 Adiabatic approximation</b>	<b>41</b>
4.1 Adiabatic potential . . . . .	42
4.2 Asymptotic expressions . . . . .	46
4.3 Numerical results . . . . .	49
4.4 Estimate of the number of bound states . . . . .	51

<b>5</b>	<b>Momentum distribution in 2D</b>	<b>55</b>
5.1	Asymptotic spectator function . . . . .	57
5.1.1	Parameterizing from small to large momenta . . . . .	63
5.2	Asymptotic one-body densities . . . . .	64
5.2.1	Asymptotic contribution from $n_1(q_\alpha)$ . . . . .	66
5.2.2	Asymptotic contribution from $n_2(q_\alpha)$ . . . . .	66
5.2.3	Asymptotic contribution from $n_3(q_\alpha)$ . . . . .	67
5.2.4	Asymptotic contribution from $n_4(q_\alpha)$ . . . . .	70
5.2.5	Asymptotic contribution from $n_5(q_\alpha)$ . . . . .	70
5.3	Contact parameters . . . . .	72
5.3.1	Analytic expressions . . . . .	72
5.3.2	Identical Bosons . . . . .	74
5.3.3	Mass-imbalanced systems . . . . .	78
5.4	Discussion about possible experiments . . . . .	85
<b>6</b>	<b>Momentum distribution in 3D</b>	<b>87</b>
6.1	Formalism and definitions . . . . .	88
6.2	Asymptotic spectator function . . . . .	90
6.2.1	Scaling parameter . . . . .	93
6.3	Asymptotic one-body densities . . . . .	95
6.4	Leading and sub-leading terms . . . . .	97
6.5	Numerical examples . . . . .	101
<b>7</b>	<b>Dimensional crossover</b>	<b>105</b>
7.1	Renormalization with a compact dimension . . . . .	107
7.2	3D - 2D transition with PBC . . . . .	109
7.2.1	Two-body scattering amplitude . . . . .	109
7.2.2	Dimer binding energy . . . . .	112
7.2.3	Trimer bound state equation . . . . .	114
7.3	2D - 1D with PBC . . . . .	115
7.3.1	Two-body scattering amplitude . . . . .	116
7.3.2	Trimer bound state equation . . . . .	117
7.4	Trimer at 3D - 2D crossover with PBC . . . . .	118
<b>8</b>	<b>Summary and outlook</b>	<b>121</b>
<b>A</b>	<b>Revision of the scattering theory</b>	<b>131</b>
A.1	Brief presentation of the quantum scattering . . . . .	131
A.2	Scattering equation for the two-body T-matrix . . . . .	134

<b>B</b>	<b>Jacobi relative momenta</b>	<b>137</b>
B.1	Classical three-body problem . . . . .	137
B.2	Jacobi relative momenta . . . . .	139
<b>C</b>	<b>Matrix elements of the three-body resolvent</b>	<b>143</b>
<b>D</b>	<b>Numerical methods</b>	<b>147</b>
D.1	Three-body energy (eigenvalue) . . . . .	147
D.2	Spectator functions (eigenvector) . . . . .	154
<b>E</b>	<b>Asymptotic one-body density in 3D</b>	<b>157</b>
E.0.1	Asymptotic contribution from $n_1(q_B)$ . . . . .	157
E.0.2	Asymptotic contribution from $n_2(q_B)$ . . . . .	157
E.0.3	Asymptotic contribution from $n_3(q_B)$ . . . . .	159
E.0.4	Asymptotic contribution from $n_4(q_B)$ . . . . .	167
<b>F</b>	<b>Detailed calculation of the residue</b>	<b>177</b>
	<b>Bibliography</b>	<b>194</b>



# List of Publications

---

Bellotti, F. F.; Frederico, T.; Yamashita, M. T.; Fedorov, D. V.; Jensen, A. S.; Zinner, N. T. Scaling and universality in two dimensions: three-body bound states with short-ranged interactions. **Journal of Physics B**, v. 44, n. 20, p. 205302, 2011. Labtalk:

<http://iopscience.iop.org/0953-4075/labtalk-article/47307>.

Bellotti, F. F.; Frederico, T.; Yamashita, M. T.; Fedorov, D. V.; Jensen, A. S.; Zinner, N. T. Supercircle description of universal three-body states in two dimensions. **Physical Review A**, v. 85, p. 025601, 2012.

Bellotti, F. F.; Frederico, T.; Yamashita, M. T.; Fedorov, D. V.; Jensen, A. S.; Zinner, N. T. Dimensional effects on the momentum distribution of bosonic trimer states. **Physical Review A**, v. 87, n. 1, p. 013610, Jan. 2013.

Bellotti, F. F.; Frederico, T.; Yamashita, M. T.; Fedorov, D. V.; Jensen, A. S.; Zinner, N. T. Mass-imbalanced three-body systems in two dimensions. **Journal of Physics B**, v. 46, n. 5, p. 055301, May 2013. Labtalk:

<http://iopscience.iop.org/0953-4075/labtalk-article/52615>.

Yamashita, M. T.; Bellotti, F. F.; Frederico, T.; Fedorov, D. V.; Jensen, A. S.; Zinner, N. T. Single-particle momentum distributions of efimov states in mixed-species systems. **Physical Review A**, v. 87, p. 062702, Jun 2013.

Bellotti, F. F.; Frederico, T.; Yamashita, M. T.; Fedorov, D. V.; Jensen, A. S.; Zinner, N. T. Contact parameters in two dimensions for general three-body systems. **New Journal of Physics**, v. 16, n. 1, p. 013048, 2014.

Bellotti, F. F.; Frederico, T.; Yamashita, M. T.; Fedorov, D. V.; Jensen, A. S.; Zinner, N. T. Mass-imbalanced three-body systems in 2d: Bound states and the analytical approach to the adiabatic potential. **Few-Body Systems**, v. 55, p. 847, 2014.

Bellotti, F. F.; Frederico, T.; Yamashita, M. T.; Fedorov, D. V.; Jensen, A. S.; Zinner, N. T. Universality of three-body systems in 2d: Parametrization of the bound states energies. **Few-Body Systems**, v. 55, p. 1025, 2014.

Yamashita, M. T.; Bellotti, F. F.; Frederico, T.; Fedorov, D. V.; Jensen, A. S.; Zinner, N. T. Dimensional crossover transitions of strongly interacting two- and three-boson systems. **ArXiv e-prints**, Apr. 2014.



# List of Figures

2.1	Jacobi relative momenta . . . . .	15
3.1	Mass diagram of the number of three-body bound states as functions of two mass ratios, $\frac{m_b}{m_a}$ and $\frac{m_c}{m_a}$ . The three two-body energies are equal, i.e., $E_{ab} = E_{bc} = E_{ac}$ . . . . .	30
3.2	Mass diagram of the number of three-body bound states as functions of two mass ratios, $\frac{m_b}{m_a}$ and $\frac{m_c}{m_a}$ . The two-body energies are $E_{ab} = 0$ and $E_{ac} = E_{bc}$ . . . . .	31
3.3	Mass diagram of the number of three-body bound states as functions of two mass ratios, $\frac{m_b}{m_a}$ and $\frac{m_c}{m_a}$ . The two-body energies are $E_{ab} = 10E_{ac}$ and $E_{bc} = 0.1E_{ac}$ . . . . .	33
3.4	Contour diagrams with lines of fixed $\epsilon_3$ values as function of the two-body energies $\epsilon_{ac}$ and $\epsilon_{bc}$ . . . . .	35
3.5	The functions, $R_0$ and $R_1$ , of the three-body energy $\epsilon_3$ in the super-ellipse fit for three sets of mass ratios. . . . .	37
3.6	The exponents, $t_0$ and $t_1$ , in the super-ellipse fit as functions of the three-body energy $\epsilon_3$ for three sets of mass ratios. . . .	38
4.1	Three-body relative coordinates used in the adiabatic approximation. . . . .	43
4.2	Ratio $\epsilon_{asymptotic}(s)/\epsilon_{exact}(s)$ as function of the dimensionless coordinate $s(R)$ , showing the validity of asymptotic expressions. . . . .	47
4.3	Adiabatic potential $ \epsilon_{asymptotic}(R)/E_2 $ as function of the dimensionless coordinate $s(R)$ . . . . .	48
4.4	Number of possible bound states ( $N_B$ ) for a system with mass ratio $m$ and $E_{ab} = 0$ . Comparison between the adiabatic approximation and the full solution of the set of coupled homogeneous integral equations. . . . .	51

4.5	Number of possible bound states ( $N_B$ ) for a system with mass ratio $m$ for $E_{ab} = 0$ and $E_{ab} = 1$ . . . . .	53
5.1	Spectator function, $f(q)$ , for the ground state calculated numerically and using the ansatz $f(q) = A_0 \frac{\ln q}{q^2}$ . . . . .	57
5.2	The difference $f_\alpha(q) - \frac{\Gamma}{m_{\beta\gamma}} \frac{\ln q}{q^2}$ as a function of the momentum $q$ for three different systems. . . . .	61
5.3	Ratios between the three distinct spectator function for a generic case of three distinct particles. . . . .	62
5.4	Comparison between the analytic spectator function estimated for the ground state given and the numeric solution of the set of coupled homogeneous integral equations. . . . .	64
5.5	LO momentum distribution tail, $q^4 n(q)$ , for ground and excited three-body states. . . . .	75
5.6	NLO momentum distribution comparison of 3D and 2D. . . . .	78
5.7	The leading order term of the one-body momentum density divided by $E_3^n$ for each bound state labeled as $n$ . . . . .	81
5.8	The two-body parameters $C_{aa}$ and $C_{ac}$ as function of the mass ratio $m$ . . . . .	82
5.9	Comparison between the analytic estimative and numerical calculation of $C_{aa}$ . . . . .	83
5.10	The sub-leading order of the one-body momentum density divided by $E_3^n$ for each bound state labeled as $n$ . . . . .	85
6.1	Comparison between the numerical solution of the set of coupled homogeneous integral equations and the asymptotic formula of the spectator function $\chi_{AA}(q)$ . . . . .	92
6.2	Scaling parameter $s$ as a function of the mass ratio $\mathcal{A}$ for $E_{AA} = 0$ (resonant interactions) and with no interaction between AA. . . . .	95
6.3	$C/\kappa_0$ for mass ratios in the range $6/133 \leq \mathcal{A} \leq 25$ . . . . .	98
6.4	Non-oscillatory contributions for $n_1, n_2, n_3$ and $n_4$ as a function of the mass ratio $\mathcal{A}$ . . . . .	99

6.5	Individual non-oscillatory contributions for $n_1, n_2, n_3$ and $n_4$ as a function of the mass ratio $\mathcal{A}$ . . . . .	100
6.6	Scaling plot of the Efimov states indicating the points where the momentum distributions have been calculated. . . . .	102
6.7	Momentum distribution for the second excited state as a function of the relative momentum of one particle to the CM of the remaining pair. . . . .	103
6.8	Rescaled momentum distribution for the ground, first and second excited states as a function of the relative momenta of one particle to the CM of the remaining pair. . . . .	104
7.1	Dimensional crossover of the three-body binding energy spectrum. . . . .	119
A.1	Schematic figure showing the quantum scattering process. . .	131
B.1	Three-body coordinates in laboratory frame. . . . .	138
B.2	Relation of the new coordinates with the coordinates in frame of the laboratory. . . . .	140
E.1	Closed path used in the calculation of complex integrals. . . .	163



# List of Tables

5.1	The coefficients $\frac{C_{ac}}{E_3}$ , $\frac{C_{aa}}{E_3}$ and $\frac{2\pi}{E_3} \int_0^\infty dk k  f_c(k) ^2 \dots \dots \dots$	81
-----	---	----



# Introduction

---

In the last decade scientists around the world found experimental evidences [Kraemer 2006, Ferlaino 2010] of a remarkable phenomenon in few-body systems that was predicted long time ago [Efimov 1970] and today is known as the Efimov effect. It corresponds to an accumulation of three-boson energy levels when the two-body scattering length tends to infinity. In the exact limit - when the dimer energy is zero - the energies of successive states are geometrically spaced obeying a universal ratio. Experiments [Kraemer 2006] were able to identify few of these Efimov states, bringing the attention of the physics community to few-body problems of short-ranged interactions with large scattering lengths.

The experiments were realized using Feshbach resonances in cold atomic gases (see, e.g., Ref. [Chin 2010]). Using this technique it is possible to tune the scattering length to large values bringing the system into a universal regime, where their properties are essentially model-independent. In this regime the properties of the system are defined by the knowledge of only few physical low-energy observables that the short-ranged potentials should produce. The possibility of manipulating the interaction between trapped cold atoms also opened new avenues to probe few-body physics as, for example, by studying systems restricted to two dimensions [Martianov 2010, Fröhlich 2011, Dyke 2011]. Mostly, the theoretical background in few-body physics was built for systems in three dimensions. However, the experimental possibility to squeeze one of the dimensions, forming trapped atomic systems in layers, asks for deeper and larger theoretical investigations of lower dimensional few-particle systems.

The number of spatial dimensions plays an important role in quantum

systems. For instance, let us consider the kinetic energy operator written in angular coordinates. The dependence on the angle variables comes through the centrifugal barrier operator, that in three dimensions has eigenvalues always zero or positive, while in two dimensions, for zero angular momentum, it is negative. This means that a minimum amount of attraction is necessary to bind a three dimensional system, while any infinitesimal attractive potential produce a  $s$ -wave bound state in a two dimensional system [Nielsen 1997, Nielsen 1999, Nielsen 2001]. In fact this was already pointed out a long time ago. The Landau criterion says that potentials with negative volume integral will produce a bound state for any value of the strength in two-dimensions (see, e.g., Ref. [Landau 1977]). This topic continues to be of interest and it was found that when the volume integral is exactly zero a bound state is still present [Simon 1976, Armstrong 2010, Volosniev 2011].

All this recent effort towards the two dimensional (2D) physics is supported by the relevance of the field for several different applications like, e.g., high-temperature superconductors, localization of atoms on surfaces, in semi-conducting micro-cavities, for carbon nanotubes and organic interface. There is an interest among the ultracold atomic gas laboratories to produce quantum degenerate gases in low dimensions, with the aim to probe the two-dimensional physics of quantum systems. Early experiments already produced quasi-2D samples of  $^{133}\text{Cs}$  [Vuletić 1998, Morinaga 1999, Hammes 2003],  $^{23}\text{Na}$  [Görlitz 2001], and  $^{87}\text{Rb}$  [Burger 2002]. Two-dimensional gases with mixtures of  $^{40}\text{K}$  and  $^{87}\text{Rb}$  have been produced [Modugno 2003, Günter 2005] and two-component gases of  $^6\text{Li}$  [Dyke 2011, Martiyanov 2010] and  $^{40}\text{K}$  [Fröhlich 2011] have also been studied. Quasi-2D pancakes of trapped heteronuclear diatomic molecules of  $^{40}\text{K}^{87}\text{Rb}$  were produced in stacked layers [de Miranda 2011].

Theoretically one can define precisely the dynamics of quantum systems in two-dimensions, while in a real experiment the confinement to 2D is typically done using an optical lattice. This introduces a transverse energy scale,  $\hbar\omega_0$ , and below it the physics is effectively 2D, while it becomes 3D at



or above  $\hbar\omega_0$ . To produce a 2D sample of trapped atoms in an experimental setup, one starts with a three dimensional system. Therefore, it is important to find observables that make possible to distinguish experimentally when the system can be considered really in two dimensions.

The work consists in the study of two- and three- dimensional (2D and 3D) few-body systems close to the universal regime, where the word “universal”, which is extensively used along the work, means that the discussed properties of the quantum systems are independent of the model utilized to describe the interaction between two particles, namely, the weakly bound system is much larger than the size of the interaction. A natural way to study such properties is to describe the pairwise interaction with Dirac- $\delta$  potentials, since the condition for universality  $|a|/r_0 \gg 1$ , where  $a$  is the scattering length and  $r_0$  the range of the potential, is always fulfilled.

The introduction/motivation to the work given in Chapter 1 are followed by the derivation of the equations that describe the 2D and 3D dynamics of two- and three-body systems interacting through zero-ranged potentials in Chapter 2. Notice that the problem consists basically in the solution of an eigenvalue-eigenvector problem, where the energy and the wave function of the three-body system must be determined. However, the complexity of the three-body problem, which does not have a closed solution even at the classical level, leads the problem to be described for an elaborated set of homogeneous coupled integral equations.

The behavior of three-boson systems changes remarkably from two to three dimensions, since the dynamics and properties of quantum systems drastically change when the system is restricted to different dimensions. Two important examples illustrating the influence of the spatial dimension in the three-body sector are the Efimov effect [Efimov 1970] and the Thomas collapse [Thomas 1935]. The Efimov states (see the beginning of Chapter 1), which were predicted and observed for three identical bosons in 3D systems [Kraemer 2006, Ferlaino 2010], are absent in 2D even in the most favorable scenario of mass-imbalanced systems [Lim 1980, Adhikari 1988]. Similarly, Thomas found in 1935 that the energy of a three identical bosons

system subjected to short-range pairwise interactions in 3D grows without boundaries (collapses) when the range of the interaction approaches zero ( $r_0 \rightarrow 0$ ). Nevertheless, this effect was not observed in 2D systems yet. It is shown in Ref. [Adhikari 1988] that both the Thomas collapse and the Efimov effect are mathematically related to the same anomaly in the kernel of the three-body equations and they take place whenever  $|a|/r_0 \rightarrow \infty$ . For instance, starting with finite and non-null values of  $|a|$  and  $r_0$ , the finite and well-behaved three-body spectrum will collapse when  $r_0 \rightarrow 0$ . On the other hand, infinitely many weakly bound states will appear for  $|a| \rightarrow \infty$ . Notice that the condition  $|a|/r_0 \rightarrow \infty$  is fulfilled in both cases.

The sparseness of information about 2D three-bosons system has motivated the systematic investigation of the universal properties of mass-imbalanced systems using zero-range interactions in momentum space [Bellotti 2011, Bellotti 2012] and the results are shown in Chapter 3. The focus is particularly on the dependence of the three-body binding energy with masses and two-body binding energies. The critical values of these parameters (masses and two-body binding energies) allowing a given number of three-particle bound states with zero total angular momentum are determined in a form of boundaries in the multidimensional parametric space. Besides the dependence of the three-particle binding energy on the parameters be highly non-trivial, even in the simpler case of two identical particles and a distinct one, this dependence is parametrized for the ground and first excited state in terms of *supercircles* functions in the most general case of three distinguishable particles, as also presented in Chapter 3.

The study of the universal properties of 2D three-body systems has shown an increasing number of bound states for the decreasing mass of one of the particles [Bellotti 2011, Bellotti 2012]. The situation where one particle is much lighter than the other two is suitably handled in the adiabatic approximation, namely the Born-Oppenheimer (BO) approximation, which is presented in Chapter 4. The adiabatic potential between the heavy particles due to the light one found as the solution of a transcendental equation is mass-dependent and reveals an increasing number of bound states by

decreasing the mass of one of the particles [Bellotti 2013b]. Besides, an asymptotic expression for the adiabatic potential is derived and is shown that this analytic expression faithfully corresponds to the numerically calculated adiabatic potential, even in the non-asymptotic region. The number of bound states for a heavy-heavy-light system is estimated as a function of the light-heavy mass ratio and infinitely many bound states are expected as this ratio approaches zero. However, for finite masses only finite number of bound states is always present.

While Chapters 2 and 3 are focused in the eigenvalue of the three-body Hamiltonian problem, Chapters 5 and 6 are related to the eigenstate in momentum space, constructed from the spectator function and giving the momentum density. A key result presented in Chapter 5 is the derivation of an analytical expression for the asymptotic behavior of the spectator function large momentum of three-body systems in two dimensions [Bellotti 2013a, Bellotti 2014]. This asymptotic behavior defines the one-body large momentum density, which is a strong candidate as observable quantity able to unequivocally determine whether the quantum system is restricted to two or three dimensions [Bellotti 2013a]. The two- and three-dimensional one-body momentum densities are discussed respectively in Chapters 5 and 6. Besides, the one-body density defines the two- and three-body contact parameters, which relate few- and many-body properties of quantum atomic gases [Tan 2008]. It is shown in Chapter 5 that the two-body contact parameter, which is the coefficient in the leading order in the large momentum expansion of the one-body density, of specific 2D systems is a universal constant, in the sense that it does not depend on the quantum level considered [Bellotti 2013a, Bellotti 2014]. The three-body contact parameter, which is the coefficient in the sub-leading order in the large momentum expansion of the one-body density is not found to be universal, but the sub-leading functional form is independent of the mass of the constituents in 2D. The same does not happen in 3D systems, where the functional form of the sub-leading term in the one-body momentum density depends on the mass [Yamashita 2013], as shown in Chapter 6. Furthermore, the discus-

sion of how the one-body momentum density can be used to determine the dimensionality of the system is also made in Chapter 5.

As current experimental set ups are able to continuously squeeze one dimension in order to build 2D experiments (see for instance Ref. [Dyke 2011]), it is interesting to find theoretical methods which are able to produce a continuous squeezing of one of the dimensions. In Chapter 7 it is presented a method that allows to study the dimensional crossover transitions of strongly interacting two- and three-bosons systems by continuously “squeezing” one of the dimensions [Yamashita 2014]. The particles are placed in a flat surface plus a transverse direction (compact dimension), which imposes the discretization of the momentum accordingly to the chosen type of boundary conditions. Employing periodic boundary conditions in the compact dimension, it is shown that a sharp transition occurs in the energy spectrum of three-body system as the system is squeezed from 3D to 2D. However, more studies are still necessary in order to relate the parameter which dials between the different situations to real experiments.

Summary and outlook are presented in Chapter 8. In order to motivate the reading, the beginning of Chapters 2 to 7 brings a brief motivation/introduction to the topic that will be discussed. Further details are given in Appendices A to F.

# Two- and Three-body dynamics

---

The surprisingly fast and ongoing technological advances, which permeate our daily life, has also given tools for an extraordinary growth on the experimental studies of cold atomic quantum gases. However, the cornerstone in the study of quantum systems in laboratories is still the same: these systems are probed through collision experiments.

In this way, the background tools for the theoretical understanding of such experiments are given by the scattering theory and some concepts of this theory are presented in the following. While, even for low density gases, the experiments are taken with several thousands of particles, it turns out that some macro properties of the systems are driven by two- and three-body correlations. This work is focused on the *universal* properties of three-body quantum systems, i.e., when the size of the system is much larger than the range of the interaction between the particles. Such problem is already challenging and interesting in itself, since there is no classical equivalent.

A brief presentation of the quantum theory of scattering for two-body zero-range potentials is given in Appendix A and the focus here is only on the concepts and equations that are needed in order to make the reading of this thesis easier. More details are given in Appendices A, B and C. Complete and formal descriptions of the scattering theory in the three-body quantum problem are given, for instance, in Refs. [Schmid 1974, Mitra 1969]. The main point here is the derivation of the integral equations for the two- and three-body transition matrix ( $T$ -matrix) when the particles are assumed to interact through zero-range potentials. Although these potentials

are not realistic, their importance in the study of two- and three-body quantum systems is explained in the next section.

## 2.1 Zero-range model and Renormalization

The  $s$ -wave zero-range potentials have a separable operator form (see Eq. (A.15))

$$V = \lambda |\chi\rangle \langle \chi| \quad (2.1)$$

and will be used to solve the two-body  $T$ -matrix (see Eq. (A.13))

$$t = V + V g_0 t, \quad (2.2)$$

as shown in Appendix A.2. For a  $s$ -wave separable potential, the transition matrix is (see Eqs. (A.19) and (A.21))

$$t(E) = |\chi\rangle \tau(E) \langle \chi| \quad (2.3)$$

with

$$\tau(E) = \left( \lambda^{-1} - \int d^D p \frac{g(p)^2}{E - \frac{p^2}{2m_{red}} + i\epsilon} \right)^{-1}. \quad (2.4)$$

Despite of the fact that Eq. (A.21) holds for any generic separable potential that has the operator form given in Eq. (A.15), no local potential has this form besides the zero-range one.

Zero-range potentials are very interesting. Although they do not correspond any realistic interaction, they allow to study the phenomenology and to understand the driven physics, which dominates the properties of large quantum systems, namely systems with size much larger than the range of the potential. They guide our intuition on the expected behavior of the quantum few-body systems, since any realistic short-range potential must reproduce the results obtained with zero-range potential when the system is very large.

The  $s$ -wave zero-range model is introduced through a Dirac- $\delta$  interac-

tion which is also called contact interaction. This means that the particles only interact when they touch each other. Besides, the Dirac- $\delta$  potential has the operator form given by Eq. (A.15). In configuration space, the matrix element of a local potential  $V$  is written as

$$\langle \mathbf{R}' | V | \mathbf{R} \rangle = V(\mathbf{R})\delta(\mathbf{R}' - \mathbf{R}) . \quad (2.5)$$

The Dirac- $\delta$  potential is local and  $V(\mathbf{R}) = \lambda\delta(\mathbf{R})$ . So, Eq. (2.5) becomes

$$\langle \mathbf{R}' | V | \mathbf{R} \rangle = \lambda\delta(\mathbf{R})\delta(\mathbf{R}' - \mathbf{R}) = \lambda\delta(\mathbf{R})\delta(\mathbf{R}') , \quad (2.6)$$

meaning that this potential is also separable.

In momentum space, the matrix element of the Dirac- $\delta$  potential for a  $n$ -dimensional system is

$$\langle \mathbf{p}' | V | \mathbf{p} \rangle = \frac{\lambda}{(2\pi)^D} \int d^D R \int d^D R' e^{i\mathbf{p}'\cdot\mathbf{R}'} e^{-i\mathbf{p}\cdot\mathbf{R}} \delta(\mathbf{R}')\delta(\mathbf{R}) = \frac{\lambda}{(2\pi)^D} . \quad (2.7)$$

It is possible to redefine  $|\chi\rangle \equiv (2\pi)^{n/2} |\tilde{\chi}\rangle$  so that Eq. (2.7) is equal to  $\lambda$ . In this way, the form factor  $\langle \chi | \mathbf{p} \rangle = \langle \mathbf{p} | \chi \rangle = g(p)$  is equal to one for the Dirac- $\delta$  potential, as can be seen below

$$g(p) = \langle \mathbf{p} | \chi \rangle = (2\pi)^{D/2} \int d^D R \frac{e^{-i\mathbf{p}\cdot\mathbf{R}}}{(2\pi)^{D/2}} \delta(\mathbf{R}) = 1 . \quad (2.8)$$

The form factor of the Dirac- $\delta$  potential in Eq. (2.8) introduces a divergence in the momentum integration of Eq. (A.21). In 2D and 3D the divergence can be treated by introducing a physical scale in the problem [Fred-erico 2012], but another way to render finite the integral could be done by introducing a cut-off. It was shown in Ref. [Yamashita 2004b] that both methods are equivalent when the momentum cut-off is let to be infinite.

The scale is introduced by defining a physical value for the two-body  $T$ -matrix ,  $\lambda_R$ , in a subtracted energy point defined by  $E = -\mu^2$ . The

$T$ -matrix becomes

$$\tau_R(-\mu^2) = \lambda_R(-\mu^2) , \quad (2.9)$$

where the subscript  $R$  means renormalized, and  $\lambda_R(-\mu^2)$  is given by a physical condition.

Inserting the condition from Eq. (2.9) in the matrix element given by Eq. (A.21) gives

$$\tau_R(-\mu^2) = \left( \lambda^{-1} - \int d^D p \frac{1}{-\mu^2 - \frac{p^2}{2m_{red}}} \right)^{-1} = \lambda_R(-\mu^2) , \quad (2.10)$$

which allows to express the bare strength  $\lambda$  as

$$\lambda^{-1} = \lambda_R^{-1}(-\mu^2) + \int d^D p \frac{1}{-\mu^2 - \frac{p^2}{2m_{red}}} . \quad (2.11)$$

A finite expression for the scattering amplitude is found by replacing  $\lambda$ , as given in Eq. (2.11), into the matrix element in Eq. (A.21). The result is

$$\tau_R(E)^{-1} = \lambda_R^{-1}(-\mu^2) + \int d^D p \left( \frac{1}{-\mu^2 - \frac{p^2}{2m_{red}}} - \frac{1}{E - \frac{p^2}{2m_{red}} + i\epsilon} \right) . \quad (2.12)$$

### 2.1.1 Two-body T-matrix in 2D

Considering only bound states, i.e.,  $E < 0$ , the integral on the right-hand-side of Eq. (2.12) for two-dimensional systems ( $D = 2$ ) is

$$I(E) = \int d^2 p \left( \frac{1}{-\mu^2 - \frac{p^2}{2m_{red}}} - \frac{1}{E - \frac{p^2}{2m_{red}}} \right) = -4\pi m_{red} \ln \left( \sqrt{\frac{-E}{\mu^2}} \right) , \quad (2.13)$$

and from Eqs. (2.12) and (2.13), the renormalized two-body  $T$ -matrix is given by

$$\tau_R(E)^{-1} = \lambda_R^{-1}(-\mu^2) - 4\pi m_{red} \ln \left( \sqrt{\frac{-E}{\mu^2}} \right) . \quad (2.14)$$

For positive energies, i.e.,  $E > 0$  (scattering states), the scattering amplitude is obtained from the analytic continuation of Eq. (2.14) in the upper



complex semi-plane of  $E$ , as shown below:

$$\begin{aligned}\tau_R(E)^{-1} &= \lambda_R^{-1}(-\mu^2) - 4\pi m_{red} \ln \left( \sqrt{\frac{-E}{\mu^2}} \right), \\ &= \lambda_R^{-1}(-\mu^2) - 4\pi m_{red} \ln \left( \sqrt{\frac{E}{\mu^2}} \right) + 2\pi^2 i m_{red},\end{aligned}\quad (2.15)$$

where the choice  $-1 = e^{-i\pi}$  is used due to the analytic continuation in the upper half semi-plane of the energy.

The matrix elements of the transition operator in Eq. (A.20) are expressed as

$$\langle \mathbf{p}' | t_R(E) | \mathbf{p} \rangle = \tau_R(E), \quad (2.16)$$

and for the sake of notation simplicity, the subscript  $R$  will be suppressed in the equations from now on, i.e.,  $\tau_R(E) \equiv \tau(E)$ ,  $\lambda_R(-\mu^2) \equiv \lambda(-\mu^2)$  and  $t_R(E) \equiv t(E)$ .

Looking at the matrix element in Eq. (2.14), it is not straightforward to identify the  $s$ -wave scattering phase-shift and cross-section for the zero-range model, as they were presented in Ref. [Adhikari 1993]. In units of  $\hbar = 2m_{red} = 1$ , Eq. (2.14) becomes

$$\tau(E)^{-1} = \lambda^{-1}(-\mu^2) - \pi \ln \left( \frac{-E}{\mu^2} \right), \quad (2.17)$$

where the respective analytic continuation for  $E > 0$  is given in Eq. (2.15). Using that  $\langle p' | t(E) | p \rangle = 2\pi \langle \mathbf{p}' | t(E) | \mathbf{p} \rangle$ , the matrix elements in Eq. (2.16) are written as

$$\langle p' | t(E) | p \rangle = \frac{2\pi}{\lambda^{-1} - \pi \ln \left( \frac{E}{\mu^2} \right) + i\pi^2} = \frac{2}{\pi (-\cot \delta_2 + i)}, \quad (2.18)$$

where the  $s$ -wave phase-shift for the zero-range model is defined as

$$\cot \delta_2 = -\frac{1}{\pi^2 \lambda(-\mu^2)} + \frac{1}{\pi} \ln \left( \frac{E}{\mu^2} \right). \quad (2.19)$$

Then, the two-dimensional scattering length,  $a_2$ , is found to be

$$\bar{a}_2 = -\frac{1}{\pi^2 \lambda(-\mu^2)} + \frac{1}{\pi} \ln(\mu^2) = a_2 + \frac{1}{\pi} \ln(\mu^2). \quad (2.20)$$

Notice that the logarithmic term, which appears in the low energy expansion, leads to an ambiguity in the definition of the scattering length in 2D, which depends on the scale used to measure the energy. So, the binding energy of the pair,  $E_B$ , is chosen as the physical scale in the problem. The bound state energy ( $E < 0$ ) is the pole of Eq. (2.18), i.e.,

$$\ln\left(\frac{-E}{\mu^2}\right) = \frac{1}{\pi^2 \lambda(-\mu^2)}, \quad (2.21)$$

which gives

$$E = -\mu^2 e^{-a_2} = e^{-\bar{a}_2} = E_B. \quad (2.22)$$

Remember that  $\lambda(-\mu^2)$  is the physical information which was introduced in the two-body  $T$ -matrix integral equation to handle the ultraviolet divergence. Then, the subtraction point  $\mu^2$  can be choose as the physical scale of the problem, i.e.,  $\mu^2 = -E_B$ , where the binding energy of the pair is the zero of Eq. (2.14). This choice also fixes the value of  $\lambda(-\mu^2)$ , namely

$$\tau(E)^{-1} = \lambda^{-1}(E_B) - 4\pi m_{red} \ln\left(\sqrt{\frac{E}{E_B}}\right) = 0, \quad (2.23)$$

at the bound-state pole and therefore

$$\lambda^{-1}(E_B) = 0. \quad (2.24)$$

Finally, the renormalized 2D two-body  $T$ -matrix for the zero-range model is

$$\tau(E)^{-1} = -4\pi m_{red} \ln\left(\sqrt{\frac{-E}{E_B}}\right), \quad (2.25)$$

which will be used in the calculation of the properties of three-body systems in 2D.

### 2.1.2 Two-body T-matrix in 3D

The 3D equivalent of Eq. (2.12) is given by

$$\tau_R(E)^{-1} = \lambda_R^{-1}(-\mu^2) + \int d^3p \left( \frac{1}{-\mu^2 - \frac{p^2}{2m_{red}}} - \frac{1}{E - \frac{p^2}{2m_{red}} + i\epsilon} \right), \quad (2.26)$$

where, as before,  $E$  is the energy,  $\mu^2$  the subtraction point,  $m_{red}$  the reduced mass and the subscript  $R$  means renormalized. For  $E < 0$  (bound states), the integral on the right-hand-side of Eq. (2.26) is

$$I(E) = \int d^3p \left( \frac{1}{-\mu^2 - \frac{p^2}{2m_{red}}} - \frac{1}{E - \frac{p^2}{2m_{red}}} \right) = -4\pi^2 m_{red} \left( \sqrt{2m_{red}|E|} - \sqrt{2m_{red}\mu^2} \right). \quad (2.27)$$

As in the 2D case, the subtraction point is chosen as the two-body binding energy, i.e.,  $-\mu^2 = E_B$  and Eq. (2.24) also holds in the 3D case, namely  $\lambda_R^{-1}(E_B) = 0$ . Then, dropping the subscript  $R$ , the two-body  $T$ -matrix for 3D systems is given by

$$\tau(E)^{-1} = -2\pi^2 (2m_{red})^{3/2} \left( \sqrt{|E|} - \sqrt{|E_B|} \right), \quad (2.28)$$

which will be used in the calculation of the properties of three-body systems in 3D.

## 2.2 Notation and three-body dynamics

The system consists of three distinguishable particles of masses  $m_\alpha$ , momenta  $\mathbf{k}_\alpha$  and pairwise interactions  $v_\alpha$ , where  $\alpha = a, b, c$  labels the particles ( $a, b, c$ ) and the notation of the potential is such that  $v_a$  is the interaction between particles  $b$  and  $c$ . The eigenvalue equation for the Hamiltonian

$$(H_0 + V) \Psi = E \Psi, \quad (2.29)$$

is fulfilled by states in the discrete ( $E < 0$ ) and continuum ( $E > 0$ ) regions. The potential given by two-body terms is  $V = v_a + v_b + v_c$  and the free and full propagators are respectively given by

$$G_0(Z) \equiv \frac{1}{Z - H_0} \quad \text{and} \quad G(Z) \equiv \frac{1}{Z - H}, \quad (2.30)$$

with  $H = H_0 + V$ . The free Hamiltonian, in frame of the laboratory, is given by the sum over the individual kinetic energies of the particles and is written as

$$H_0 = \sum_{\alpha=a,b,c} \frac{k_\alpha^2}{2m_\alpha}. \quad (2.31)$$

A set of Jacobi coordinates and the canonical conjugate momenta, which are shown in Fig. 2.1, are useful when dealing with three-body problems, since the CM motion is separated out. In this case the free Hamiltonian becomes

$$H_0 = \frac{p_\alpha^2}{2m_{\beta\gamma}} + \frac{q_\alpha^2}{2m_{\beta\gamma,\alpha}} + \frac{Q^2}{m_\alpha + m_\beta + m_\gamma}, \quad (2.32)$$

where  $\mathbf{Q} = \sum_\alpha \mathbf{k}_\alpha$  is the CM momentum. Taking into account the frame of particle  $\alpha$  with respect to the CM of the pair  $(\beta, \gamma)$ ,  $\mathbf{q}_\alpha$  is the momentum of particle  $\alpha$  with respect to the CM of the pair,  $\mathbf{p}_\alpha$  is the relative momentum of the pair,  $m_{\beta\gamma}$  is the reduced mass of the pair and  $m_{\beta\gamma,\alpha}$  is the three-body reduced mass. The relative momenta and reduced masses are given by

$$\mathbf{q}_\alpha = \frac{m_\beta + m_\gamma}{m_\alpha + m_\beta + m_\gamma} \left[ \mathbf{k}_\alpha - \frac{m_\alpha}{m_\beta + m_\gamma} (\mathbf{k}_\beta + \mathbf{k}_\gamma) \right], \quad (2.33)$$

$$\mathbf{p}_\alpha = \frac{m_\gamma \mathbf{k}_\beta - m_\beta \mathbf{k}_\gamma}{m_\beta + m_\gamma}, \quad (2.34)$$

$$m_{\beta\gamma} = \frac{m_\beta m_\gamma}{m_\beta + m_\gamma}, \quad (2.35)$$

$$m_{\beta\gamma,\alpha} = \frac{m_\alpha (m_\beta + m_\gamma)}{m_\alpha + m_\beta + m_\gamma}, \quad (2.36)$$

with  $(\alpha, \beta, \gamma)$  as cyclic permutations of  $(a, b, c)$  (see Appendix B for more details about Jacobi relative momenta). It is also useful to specify an operator notation, where all two-body operators are represented with small

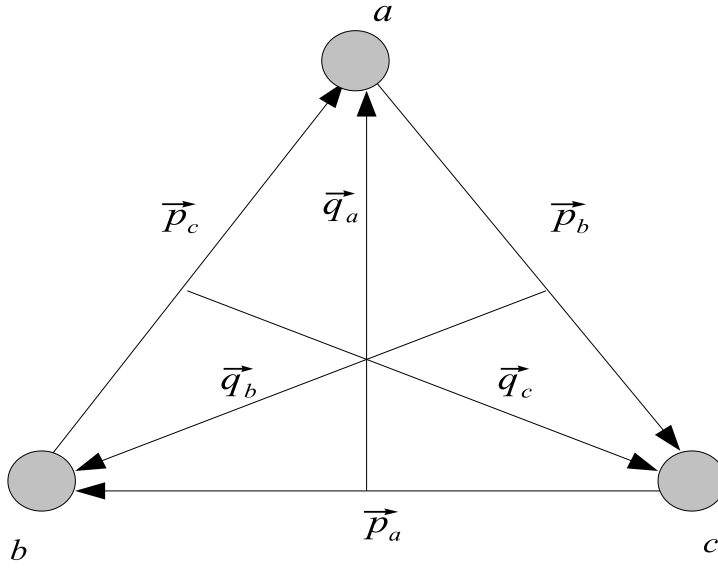


Figure 2.1: Jacobi relative momenta

letters, i.e.,  $v_\alpha, g_0$  and three-particle operators are represented by capital letters, i.e.,  $H, V$ .

### 2.2.1 Three-body T-matrix

The three-body transition operator is written as

$$T(E) = V + VG(E + i\epsilon)V, \quad (2.37)$$

that is the formal analogue of the two-body  $T$ -matrix in Eq. (A.11). Besides that the operator in Eq. (2.37) is not directly related to the scattering cross section as in the two-body case, the relations in Eqs. (A.13) and (A.14) also hold and read

$$T(E) = V + VG_0(E + i\epsilon)T(E) = V + T(E)G_0(E + i\epsilon)V. \quad (2.38)$$

The Faddeev components of the three-body  $T$ -matrix (see Ref. [Fad-

deev 1965, Schmid 1974]) are given by

$$T_a(E) = v_a + v_a G_0(E + i\epsilon) T(E) \quad (2.39)$$

and since that  $V = v_a + v_b + v_c$ , the transition operator from Eq. (2.38) can be written in term of the components given by Eq. (2.39) as

$$T(E) = T_a(E) + T_b(E) + T_c(E) . \quad (2.40)$$

Inserting Eq. (2.40) back into Eq. (2.39) results in a system of coupled equations, which are written in matrix form as

$$\begin{pmatrix} T_a \\ T_b \\ T_c \end{pmatrix} = \begin{pmatrix} v_a \\ v_b \\ v_c \end{pmatrix} + \begin{pmatrix} v_a & v_a & v_a \\ v_b & v_b & v_b \\ v_c & v_c & v_c \end{pmatrix} G_0 \begin{pmatrix} T_a \\ T_b \\ T_c \end{pmatrix} . \quad (2.41)$$

Isolating the component  $T_a$  in Eq. (2.41) results in

$$(1 - v_a G_0) T_a = v_a + v_a G_0 (T_b + T_c) , \quad (2.42)$$

which multiplied by  $(1 - v_a G_0)^{-1}$  from the left gives

$$T_a = t_a + t_a G_0 (T_b + T_c) , \quad (2.43)$$

where the relation  $t_a = [1 - v_a G_0]^{-1} v_a$  was used in third line. The renormalized two-body  $T$ -matrix  $t_a$  in the  $abc$  system is given by

$$t_a \equiv t_a(E) = |\chi_a\rangle \tau_a(E) \langle \chi_a| \quad \text{with} \quad \tau_a(E)^{-1} = -4\pi m_{bc} \ln \left( \sqrt{\frac{-E}{E_{bc}}} \right) . \quad (2.44)$$

Finally, the set of coupled equations for the Faddeev components of the

three-body transition operator are written in matrix form as

$$\begin{pmatrix} T_a \\ T_b \\ T_c \end{pmatrix} = \begin{pmatrix} t_a \\ t_b \\ t_c \end{pmatrix} + \begin{pmatrix} 0 & t_a & t_a \\ t_b & 0 & t_b \\ t_c & t_c & 0 \end{pmatrix} G_0 \begin{pmatrix} T_a \\ T_b \\ T_c \end{pmatrix}. \quad (2.45)$$

These equations have the advantage to contain the only the two-body  $T$ -matrix, and consequently two-body energies, instead of the potential. The power of such formulation is better explained and explored in Chapter 3. Besides, Eq. (2.45) shows how the two-body scattering amplitude connects with the three-body scattering. In detail, the equation for one Faddeev component of the transition operator is given by

$$T_a(E_3) = t_a \left( E_3 - \frac{q_a^2}{2m_{bc,a}} \right) \left\{ 1 + G_0(E_3 + i\epsilon) \left[ T_b(E_3) + T_c(E_3) \right] \right\}, \quad (2.46)$$

where  $E_3$  is the three-body energy and the other components are found by cyclic permutation of the particle labels.

Notice that the argument of the two-body  $T$ -matrix in Eq. (2.15) is the relative two-body energy,  $E_2^R$ , which was replaced by  $E_3 - \frac{q^2}{2m_{bc,a}}$  in Eq. (2.46). The relative two-body energy connects with the total energy,  $E_2^T$ , through  $E_2^T = E_2^R + \frac{q_2^2}{2(m_b+m_c)}$ , where  $q_2$  is the total momentum of the pair. At the frame of the CM in a three-body system, i.e.,  $Q = 0$ , the total energy of the pair is the difference between the three-body energy  $E_3$  and the kinetic energy of the third particle, namely  $E_2^T = E_3 - \frac{q_1^2}{2m_a}$ . Moreover, if  $Q = 0$  the momentum of the pair is exactly the momentum of the third particle. In other words,  $|\mathbf{q}_1| = |-\mathbf{q}_2| = q$  and the relative two-body energy as function of the three-body energy is written as

$$E_2^R = E_3 - \frac{q^2}{2m_a} - \frac{q^2}{2(m_b + m_c)} = E_3 - \frac{q^2}{2m_{bc,a}}, \quad (2.47)$$

which is exactly the argument of the two-body  $T$ -matrix in Eq. (2.46).

## 2.3 Three-body bound state equation in 2D

The three-body  $T$ -matrix in Eq. (2.45) describes the three-body scattering process with pairwise short-range potentials. The transition operator generally contains all the strong interaction properties of the three-body system or, in other words, it allows to construct the resolvent of the interacting model. Therefore, the  $T$ -matrix gives information about both bound ( $E_3 < 0$ ) and scattering ( $E_3 > 0$ ) states. The focus in the following Chapters is on three-body bound states, then the coupled homogeneous integral equations for the bound state are derived here, starting from the transition operator. It is possible to instead use directly the Faddeev decomposition for the bound-state wave function [Mitra 1969].

The completeness relation is defined as

$$\hat{1} = \sum_B |\Phi_B\rangle \langle \Phi_B| + \int d^2k |\Psi_c^{(+)}\rangle \langle \Psi_c^{(+)}|, \quad (2.48)$$

where  $|\Phi_B\rangle$  and  $|\Psi_c^{(+)}\rangle$  represent the wave functions of bound and scattering states, respectively. The  $T$ -matrix (2.37), written in terms of the interacting resolvent decomposed in eigenstates of  $H$ , is written as

$$T(E_3) = V + \sum_B \frac{V |\Phi_B\rangle \langle \Phi_B| V}{E_3 - E_B + i\epsilon} + \int d^2k \frac{V |\Psi_c^{(+)}\rangle \langle \Psi_c^{(+)}| V}{E - E_c + i\epsilon}, \quad (2.49)$$

where the bound-state poles of the transition operator appear explicitly. When the three-body system is close to a bound state ( $E_3 \approx E_B$ ), the second term on the right-hand-side of Eq.(2.49) is dominant, due to the pole, and the part concerning to the scattering states can be neglected. Defining the bound state vertex function by  $|\Gamma_B\rangle = V |\Phi_B\rangle$ , the three-body  $T$ -matrix (2.49) near the pole becomes

$$T(E_3) \approx \frac{|\Gamma_B\rangle \langle \Gamma_B|}{E_3 - E_B} = \frac{|\Gamma_B\rangle \langle \Gamma_B|}{E_3 + |E_B|}. \quad (2.50)$$

Then, Eq. (2.50) is decomposed in three Faddeev components, as in Eq. (2.39),



which reads

$$T_a(E_3) \approx \frac{|\Gamma_a\rangle\langle\Gamma_B|}{E_3 + |E_B|}, \quad (2.51)$$

where  $|\Gamma_a\rangle = v_a|\Phi_B\rangle$  and  $\langle\Gamma_B| = \langle\Phi_B|V$ . Inserting the  $T$ -matrix (2.51) in Eq. (2.46) gives

$$\frac{|\Gamma_a\rangle\langle\Gamma_B|}{E_3 + |E_B|} \approx t_a \left( E_3 - \frac{q_a^2}{m_{bc,a}} \right) \left[ 1 + G_0(E_3) \left( \frac{|\Gamma_b\rangle\langle\Gamma_B|}{E_3 + |E_B|} + \frac{|\Gamma_c\rangle\langle\Gamma_B|}{E_3 + |E_B|} \right) \right]. \quad (2.52)$$

When the three-body system is bound,  $E_3 \rightarrow -|E_B|$  and in this limit Eq. (2.52) becomes a homogeneous equation, which reads

$$|\Gamma_a\rangle = t_a \left( E_3 - \frac{q_a^2}{m_{bc,a}} \right) G_0(E_3) (|\Gamma_b\rangle + |\Gamma_c\rangle). \quad (2.53)$$

Writing the two-body  $T$ -matrix for the one term separable potential, as in Eq. (A.19), gives

$$|\Gamma_a\rangle = |\chi_a\rangle\tau_a \left( E_3 - \frac{q_a^2}{m_{bc,a}} \right) \langle\chi_a|G_0(E_3)(|\Gamma_b\rangle + |\Gamma_c\rangle), \quad (2.54)$$

and the projection of Eq. (2.54) in states  $|\mathbf{p}_a, \mathbf{q}_a\rangle$  results in

$$\langle\mathbf{p}_a, \mathbf{q}_a|\Gamma_a\rangle = \langle\mathbf{p}_a|\chi_a\rangle\tau_a \left( E_3 - \frac{q_a^2}{m_{bc,a}} \right) \langle\chi_a, \mathbf{q}_a|G_0(E_3)(|\Gamma_b\rangle + |\Gamma_c\rangle). \quad (2.55)$$

For Dirac- $\delta$  potentials,  $\langle\mathbf{p}_a, \mathbf{q}_a|\Gamma_a\rangle = \langle\mathbf{p}_a|\chi_a\rangle\langle\mathbf{q}_a|f_a\rangle = g_a(\mathbf{p}_a)f_a(\mathbf{q}_a) = f_a(\mathbf{q}_a)$  and the  $i^{\text{th}}$  Faddeev component of the three-body bound state vertex, which satisfies an homogeneous integral equation, is given by

$$f_a(\mathbf{q}_a) = \tau_a \left( E_3 - \frac{q_a^2}{2m_{bc,a}} \right) \langle\chi_a, \mathbf{q}_a|G_0(E_3)(|\chi_b\rangle|f_b\rangle + |\chi_c\rangle|f_c\rangle), \quad (2.56)$$

where  $f_a$  is the spectator function, which describes the interaction of each spectator particle with the corresponding two-body subsystem. The spectator functions  $f_b$  and  $f_c$  are easily found by cyclic permutation of the labels  $(a, b, c)$  in Eq. (2.56).

The components  $f_a$ ,  $f_b$  and  $f_c$  satisfy a set of three coupled homogeneous integral equations, in the case where the interaction between particles is described for zero-range potentials. For three identical bosons, only one homogeneous integral equation has to be solved, since  $f_a(\mathbf{q}_a) = f_b(\mathbf{q}_b) = f_c(\mathbf{q}_c)$ . In the same way, for two identical bosons plus a distinct particle, there is a set of two coupled homogeneous integral equations, since  $f_a(\mathbf{q}_a) = f_b(\mathbf{q}_b) \neq f_c(\mathbf{q}_c)$ . In the most general case of three distinguishable particles, the set of coupled equations reads

$$f_a(\mathbf{q}_a) = \tau_a \left( E_3 - \frac{q_a^2}{2m_{bc,a}} \right) \langle \chi_a, \mathbf{q}_a | G_0(E_3) (|\chi_b\rangle |f_b\rangle + |\chi_c\rangle |f_c\rangle), \quad (2.57)$$

$$f_b(\mathbf{q}_b) = \tau_b \left( E_3 - \frac{q_b^2}{2m_{ca,b}} \right) \langle \chi_b, \mathbf{q}_b | G_0(E_3) (|\chi_a\rangle |f_a\rangle + |\chi_c\rangle |f_c\rangle), \quad (2.58)$$

$$f_c(\mathbf{q}_c) = \tau_c \left( E_3 - \frac{q_c^2}{2m_{ab,c}} \right) \langle \chi_c, \mathbf{q}_c | G_0(E_3) (|\chi_a\rangle |f_a\rangle + |\chi_b\rangle |f_b\rangle). \quad (2.59)$$

The matrix elements in Eqs. (2.57) to (2.59) have the same structure, namely

$$\langle \chi_a, \mathbf{q}_a | G_0(E_3) |\chi_b\rangle |f_b\rangle. \quad (2.60)$$

These matrix elements are derived in detail in Appendix C and the result is used to finally write the set of three coupled homogeneous integral equations for the bound state of an  $abc$  system as

$$\begin{aligned} f_a(\mathbf{q}_a) = & \left[ -4\pi \frac{m_b m_c}{m_b + m_c} \ln \left( \sqrt{\frac{\frac{m_a + m_b + m_c}{2m_a(m_b + m_c)} q_a^2 - E_3}{E_{bc}}} \right) \right]^{-1} \times \\ & \times \left[ \int d^2k \frac{f_b(\mathbf{k})}{E_3 - \frac{m_a + m_c}{2m_a m_c} q_a^2 - \frac{m_b + m_c}{2m_b m_c} k^2 - \frac{1}{m_c} \mathbf{k} \cdot \mathbf{q}_a} + \right. \\ & \left. + \int d^2k \frac{f_c(\mathbf{k})}{E_3 - \frac{m_a + m_b}{2m_a m_b} q_a^2 - \frac{m_b + m_c}{2m_b m_c} k^2 - \frac{1}{m_b} \mathbf{k} \cdot \mathbf{q}_a} \right], \quad (2.61) \end{aligned}$$

$$\begin{aligned}
f_b(\mathbf{q}_b) = & \left[ -4\pi \frac{m_a m_c}{m_a + m_c} \ln \left( \sqrt{\frac{\frac{m_a + m_b + m_c}{2m_b(m_a + m_c)} q_b^2 - E_3}{E_{ac}}} \right) \right]^{-1} \times \\
& \times \left[ \int d^2 k \frac{f_a(\mathbf{k})}{E_3 - \frac{m_b + m_c}{2m_b m_c} q_b^2 - \frac{m_a + m_c}{2m_a m_c} k^2 - \frac{1}{m_c} \mathbf{k} \cdot \mathbf{q}_b} + \right. \\
& \left. + \int d^2 k \frac{f_c(\mathbf{k})}{E_3 - \frac{m_a + m_b}{2m_a m_b} q_b^2 - \frac{m_a + m_c}{2m_a m_c} k^2 - \frac{1}{m_a} \mathbf{k} \cdot \mathbf{q}_b} \right], \quad (2.62)
\end{aligned}$$

$$\begin{aligned}
f_c(\mathbf{q}_c) = & \left[ -4\pi \frac{m_a m_b}{m_a + m_b} \ln \left( \sqrt{\frac{\frac{m_a + m_b + m_c}{2m_c(m_a + m_b)} q_c^2 - E_3}{E_{ab}}} \right) \right]^{-1} \times \\
& \times \left[ \int d^2 k \frac{f_a(\mathbf{k})}{E_3 - \frac{m_b + m_c}{2m_b m_c} q_c^2 - \frac{m_a + m_b}{2m_a m_b} k^2 - \frac{1}{m_b} \mathbf{k} \cdot \mathbf{q}_c} + \right. \\
& \left. + \int d^2 k \frac{f_b(\mathbf{k})}{E_3 - \frac{m_a + m_c}{2m_a m_c} q_c^2 - \frac{m_a + m_b}{2m_a m_b} k^2 - \frac{1}{m_a} \mathbf{k} \cdot \mathbf{q}_c} \right]. \quad (2.63)
\end{aligned}$$

The particles  $a$ ,  $b$  and  $c$  have masses  $m_a, m_b, m_c$ , respectively. Also, the two-body bound state energy of each pair, defined as the scale factor of the two-body system for Dirac- $\delta$  potentials (see Eq. (2.22)), is specifically labeled as  $E_{ab}$ ,  $E_{bc}$  and  $E_{ac}$ .

The spectator functions in Eqs. (2.61) to (2.63) compose the three-body bound-state wave function. Using the vertex function defined before Eq. (2.50),  $|\Gamma_B\rangle = V|\Phi_B\rangle$ , it is possible to write that  $(v_a + v_b + v_c)|\Psi_B\rangle = |\Gamma_a\rangle + |\Gamma_b\rangle + |\Gamma_c\rangle$ . Multiplying both sides by the free resolvent results in

$$|\Psi_{abc}\rangle = |\Psi_a\rangle + |\Psi_b\rangle + |\Psi_c\rangle = G_0(E_3)[|\Gamma_a\rangle + |\Gamma_b\rangle + |\Gamma_c\rangle], \quad (2.64)$$

where  $|\Psi_a\rangle = G_0(E_3)v_a|\Psi_B\rangle$  is one of the so-called Faddeev components of the wave function. It is possible to choose any one of the set of Jacobi momenta to project Eq. (2.64). The set  $(\mathbf{q}_a, \mathbf{p}_a)$  gives

$$\langle \mathbf{q}_a, \mathbf{p}_a | \Psi_{abc} \rangle = \langle \mathbf{q}_a, \mathbf{p}_a | G_0(E_3) (|\Gamma_a\rangle + |\Gamma_b\rangle + |\Gamma_c\rangle) \rangle. \quad (2.65)$$

The matrix elements on the right-hand-side of Eq.(2.65) can be handled in a similar way as it is done in Appendix C. Finally, the three-body bound-state wave function is written in term of the spectator functions as

$$\Psi_{abc}(\mathbf{q}_a, \mathbf{p}_a) = \frac{f_a(\mathbf{q}_a) + f_b(\mathbf{q}_b(\mathbf{q}_a, \mathbf{p}_a)) + f_c(\mathbf{q}_c(\mathbf{q}_a, \mathbf{p}_a))}{E_3 - \frac{m_a+m_b+m_c}{2m_a(m_b+m_c)}\mathbf{q}_a^2 - \frac{m_b+m_c}{2m_b m_c}\mathbf{p}_a^2}, \quad (2.66)$$

where the Jacobi momenta  $\mathbf{q}_b$  and  $\mathbf{q}_c$  are linearly related to  $\mathbf{q}_a$  and  $\mathbf{p}_a$  through the relations given in Appendix B.

In a compact notation,  $(\alpha, \beta, \gamma)$  are introduced as cyclic permutations of the labels  $(a, b, c)$  and the wave function is written taking into account the momentum of particle  $\alpha$  with respect to the CM of the  $\beta\gamma$  subsystem as

$$\Psi(\mathbf{q}_\alpha, \mathbf{p}_\alpha) = \frac{f_\alpha(q_\alpha) + f_\beta\left(\left|\mathbf{p}_\alpha - \frac{m_\beta}{m_\beta+m_\gamma}\mathbf{q}_\alpha\right|\right) + f_\gamma\left(\left|\mathbf{p}_\alpha + \frac{m_\gamma}{m_\beta+m_\gamma}\mathbf{q}_\alpha\right|\right)}{-E_3 + \frac{q_\alpha^2}{2m_{\beta\gamma,\alpha}} + \frac{p_\alpha^2}{2m_{\beta\gamma}}}, \quad (2.67)$$

where  $\mathbf{q}_\alpha, \mathbf{p}_\alpha$  are the Jacobi momenta of particle  $\alpha$  with the shifted arguments given in Eqs. (B.31) and (B.32) and  $m_{\beta\gamma,\alpha} = m_\alpha(m_\beta + m_\gamma)/(m_\alpha + m_\beta + m_\gamma)$  and  $m_{\beta\gamma} = (m_\beta + m_\gamma)/(m_\beta + m_\gamma)$  are the reduced masses. In the same way, the spectator functions in Eq. (2.67), i.e.,  $f_{\alpha,\beta,\gamma}(\mathbf{q})$ , fulfill the set of three coupled homogeneous integral equations for the bound state, which in the compact notation are written as

$$f_\alpha(\mathbf{q}) = \left[ 4\pi m_{\beta\gamma} \ln \left( \sqrt{\frac{\frac{q^2}{2m_{\beta\gamma,\alpha}} - E_3}{E_{\beta\gamma}}} \right) \right]^{-1} \quad (2.68)$$

$$\times \int d^2k \left( \frac{f_\beta(\mathbf{k})}{-E_3 + \frac{q^2}{2m_{\alpha\gamma}} + \frac{k^2}{2m_{\beta\gamma}} + \frac{1}{m_\gamma}\mathbf{k} \cdot \mathbf{q}} + \frac{f_\gamma(\mathbf{k})}{-E_3 + \frac{q^2}{2m_{\alpha\beta}} + \frac{k^2}{2m_{\beta\gamma}} + \frac{1}{m_\beta}\mathbf{k} \cdot \mathbf{q}} \right).$$

As the interaction between particles is described for  $s$ -waves potentials and the focus is on states with total zero angular momentum, the spectator functions do not depend on the angle, i.e.,  $f_\alpha(\mathbf{q}) \equiv f_\alpha(q)$ . Then, the angular

integration in Eq. (2.68) is solved using that

$$\int_0^{2\pi} \frac{d\theta}{1 - z \cos \theta} = \frac{1}{\sqrt{1 - z^2}}, \quad (2.69)$$

where the constant  $z$  satisfies  $|z| < 1$ . The result is

$$\begin{aligned} f_\alpha(q) = & 2\pi \left[ 4\pi m_{\beta\gamma} \ln \left( \sqrt{\frac{\frac{q^2}{2m_{\beta\gamma,\alpha}} - E_3}{E_{\beta\gamma}}} \right) \right]^{-1} \\ & \times \int_0^\infty dk \left( \frac{k f_\beta(k)}{\sqrt{\left(-E_3 + \frac{q^2}{2m_{\alpha\gamma}} + \frac{k^2}{2m_{\beta\gamma}}\right)^2 - \left(\frac{kq}{m_\gamma}\right)^2}} \right. \\ & \left. + \frac{k f_\gamma(k)}{\sqrt{\left(-E_3 + \frac{q^2}{2m_{\alpha\beta}} + \frac{k^2}{2m_{\beta\gamma}}\right)^2 - \left(\frac{kq}{m_\beta}\right)^2}} \right), \quad (2.70) \end{aligned}$$

which together with Eq. (2.67) build the  $L_{total} = 0$  bound eigenstate of the Hamiltonian with the zero-range force.

The study of the three-body bound states, in what follows, is based on the numerical solution of the coupled homogeneous integral equations for the spectator functions in Eq. (2.70). Details about the numerical methods are given in Appendix D.

## 2.4 Three-body bound state equation in 3D

The naive attempt to write the three-body bound state integral equation in 3D only by changing the phase factor and the two-body  $T$ -matrix in Eq. (2.68) fails, since the kernel of such equation is non-compact when the interaction between particles is described for Dirac- $\delta$  potentials [Adhikari 1988]. This means that the three-body equations must be renormalized, as it was done for the two-body  $T$ -matrix in Sec. 2.1. A complete discussion about the renormalization method is given in Refs. [Ad-

hikari 1995b, Adhikari 1995a, Frederico 2012], where a discussion of the equivalent method within effective field theory can be found.

### 2.4.1 Renormalization of the 3B transition operator

The Lippmann-Schwinger equation for the transition operator is

$$T(E) = V + VG_0(E)T(E) = V + T(E)G_0(E)V, \quad (2.71)$$

which for the sake of the notation the energy is dropped.

The subtraction point is chosen as  $-\mu_{(3)}^2$  and the transition matrix in this point is  $T(-\mu_{(3)}^2)$ . The potential  $V$  can be expressed as

$$V = \left[ 1 + T(-\mu_{(3)}^2)G_0(-\mu_{(3)}^2) \right]^{-1} T(-\mu_{(3)}^2), \quad (2.72)$$

where  $T(-\mu_{(3)}^2)$  is defined as the sum over the two-body transition matrices in the subtraction point [Adhikari 1995b], namely

$$T(-\mu_{(3)}^2) = \sum_{n=a,b,c} t_n(-\mu_{(3)}^2), \quad (2.73)$$

with  $t_n(E)$  given in Eq. (2.44). Inserting the renormalized potential (2.72) in Eq. (2.71) gives

$$\begin{aligned} T(E) &= \left[ 1 + T(-\mu_{(3)}^2)G_0(-\mu_{(3)}^2) \right]^{-1} T(-\mu_{(3)}^2) [1 + G_0(E)T(E)], \\ \left[ 1 + T(-\mu_{(3)}^2)G_0(-\mu_{(3)}^2) \right] T(E) &= T(-\mu_{(3)}^2) + T(-\mu_{(3)}^2)G_0(E)T(E), \\ T(E) + T(-\mu_{(3)}^2)G_0(-\mu_{(3)}^2)T(E) &= T(-\mu_{(3)}^2) + T(-\mu_{(3)}^2)G_0(E)T(E), \\ T(E) &= T(-\mu_{(3)}^2) + T(-\mu_{(3)}^2)G_1(E, -\mu_{(3)}^2)T(E), \end{aligned} \quad (2.74)$$

where

$$G_1(E, -\mu_{(3)}^2) = G_0(E) - G_0(-\mu_{(3)}^2) = -(\mu_{(3)}^2 + E)G_0(E)G_0(-\mu_{(3)}^2). \quad (2.75)$$

Notice that the matrix form of Eq. (2.74) is given in Eq. (2.45), meaning that each component of the renormalized three-body transition matrix is given by

$$T_a(E_3) = t_a \left( E_3 - \frac{q_a^2}{2m_{bc,a}} \right) \left\{ 1 + G_1 \left( E_3, -\mu_{(3)}^2 \right) \left[ T_b(E_3) + T_c(E_3) \right] \right\}, \quad (2.76)$$

which is analogous to Eq. (2.46), where the only difference arises from the three-body propagator.

## 2.4.2 Three-body bound state integral equation in 3D

Since Eqs. (2.46) and (2.76) are equivalent, the procedure to obtain the three-body bound state equation in 3D is exactly the same followed in Sec. 2.3, only replacing  $G_0(E_3) \rightarrow G_1(E_3, -\mu_{(3)}^2)$ . Then, the homogeneous coupled equations for the spectator function to get the bound state energy are given by

$$f_a(\mathbf{q}_a) = \tau_a \left( E_3 - \frac{q_a^2}{2m_{bc,a}} \right) \langle \chi_a, \mathbf{q}_a | G_1 \left( E_3, -\mu_{(3)}^2 \right) \left( |\chi_b\rangle |f_b\rangle + |\chi_c\rangle |f_c\rangle \right), \quad (2.77)$$

$$f_b(\mathbf{q}_b) = \tau_b \left( E_3 - \frac{q_b^2}{2m_{ca,b}} \right) \langle \chi_b, \mathbf{q}_b | G_1 \left( E_3, -\mu_{(3)}^2 \right) \left( |\chi_a\rangle |f_a\rangle + |\chi_c\rangle |f_c\rangle \right), \quad (2.78)$$

$$f_c(\mathbf{q}_c) = \tau_c \left( E_3 - \frac{q_c^2}{2m_{ab,c}} \right) \langle \chi_c, \mathbf{q}_c | G_1 \left( E_3, -\mu_{(3)}^2 \right) \left( |\chi_a\rangle |f_a\rangle + |\chi_b\rangle |f_b\rangle \right). \quad (2.79)$$

Notice that the matrix elements in Eqs. (2.77) to (2.79) have the same structure as the ones in Eqs. (2.57) to (2.59), namely

$$\langle \chi_a, \mathbf{q}_a | G_1 \left( E_3, -\mu_{(3)}^2 \right) |\chi_b\rangle |f_b\rangle. \quad (2.80)$$

Since the term  $G_1(E_3, -\mu_{(3)}^2)$  can be separated in two terms, as in Eq. (2.75), it turns out that each element in Eqs. (2.77) to (2.79) is identical to the corresponding one in Eqs. (2.57) to (2.59), which are derived in detail in Appendix C. The set of three coupled homogeneous integral equations for the bound state of an  $abc$  system is written in a compact form as

$$f_\alpha(\mathbf{q}) = \left[ 2\pi^2 (2m_{\beta\gamma})^{3/2} \left( \sqrt{\left( \frac{q^2}{2m_{\beta\gamma,\alpha}} - E_3 \right)} - \sqrt{E_{\beta\gamma}} \right) \right]^{-1} \quad (2.81)$$

$$\times \int d^3k \left[ \left( \frac{1}{-E_3 + \frac{q^2}{2m_{\alpha\gamma}} + \frac{k^2}{2m_{\beta\gamma}} + \frac{1}{m_\gamma} \mathbf{k} \cdot \mathbf{q}} - \frac{1}{\mu^2 + \frac{q^2}{2m_{\alpha\gamma}} + \frac{k^2}{2m_{\beta\gamma}} + \frac{1}{m_\gamma} \mathbf{k} \cdot \mathbf{q}} \right) f_\beta(\mathbf{k}) \right.$$

$$\left. + \left( \frac{1}{-E_3 + \frac{q^2}{2m_{\alpha\beta}} + \frac{k^2}{2m_{\beta\gamma}} + \frac{1}{m_\beta} \mathbf{k} \cdot \mathbf{q}} - \frac{1}{\mu^2 + \frac{q^2}{2m_{\alpha\beta}} + \frac{k^2}{2m_{\beta\gamma}} + \frac{1}{m_\beta} \mathbf{k} \cdot \mathbf{q}} \right) f_\gamma(\mathbf{k}) \right].$$

The solutions of Eq.(2.81) with zero total angular momentum are studied, and as the interaction between particles is described for  $s$ -waves potentials, the spectator functions only depends on the momentum modules, i.e.,  $f_\alpha(\mathbf{q}) \equiv f_\alpha(q)$ . Then, the angular integration in Eq. (2.81) is solved by using that

$$\int_{-\pi}^{\pi} \frac{d\theta \sin \theta}{1 - z \cos \theta} = \ln \left( \frac{1+z}{1-z} \right), \quad (2.82)$$

where the constant  $z$  satisfies  $|z| < 1$ . The result is

$$f_\alpha(\mathbf{q}) = \left[ \pi (2m_{\beta\gamma})^{3/2} \left( \sqrt{\left( \frac{q^2}{2m_{\beta\gamma,\alpha}} - E_3 \right)} - \sqrt{E_{\beta\gamma}} \right) \right]^{-1}$$

$$\times \int_0^\infty dk k^2 \left[ \left( \ln \frac{-E_3 + \frac{q^2}{2m_{\alpha\gamma}} + \frac{k^2}{2m_{\beta\gamma}} + \frac{kq}{m_\gamma}}{-E_3 + \frac{q^2}{2m_{\alpha\gamma}} + \frac{k^2}{2m_{\beta\gamma}} - \frac{kq}{m_\gamma}} - \ln \frac{\mu^2 + \frac{q^2}{2m_{\alpha\gamma}} + \frac{k^2}{2m_{\beta\gamma}} + \frac{kq}{m_\gamma}}{\mu^2 + \frac{q^2}{2m_{\alpha\gamma}} + \frac{k^2}{2m_{\beta\gamma}} - \frac{kq}{m_\gamma}} \right) f_\beta(\mathbf{k}) \right.$$

$$\left. + \left( \ln \frac{-E_3 + \frac{q^2}{2m_{\alpha\beta}} + \frac{k^2}{2m_{\beta\gamma}} + \frac{kq}{m_\beta}}{-E_3 + \frac{q^2}{2m_{\alpha\beta}} + \frac{k^2}{2m_{\beta\gamma}} - \frac{kq}{m_\beta}} - \ln \frac{\mu^2 + \frac{q^2}{2m_{\alpha\beta}} + \frac{k^2}{2m_{\beta\gamma}} + \frac{kq}{m_\beta}}{\mu^2 + \frac{q^2}{2m_{\alpha\beta}} + \frac{k^2}{2m_{\beta\gamma}} - \frac{kq}{m_\beta}} \right) f_\gamma(\mathbf{k}) \right]. \quad (2.83)$$

The 3D wave function is also given by Eq. (2.67) and  $(\alpha, \beta, \gamma)$  are cyclic permutations of the labels  $(a, b, c)$ .



# Universal 2D three-body bound states

---

The behavior of three-boson systems changes remarkably from two (2D) to three dimensions (3D), since the dynamics and properties of quantum systems drastically change when the system is restricted to different dimensions. For example, the scattering-length is defined within a constant for 2D systems [Adhikari 1986] and, as it was already pointed out in Chapter 1, the kinetic energy operator gives a negative (attractive) centrifugal barrier for 2D systems with zero total angular momentum, while the centrifugal barrier is always non-negative (zero or repulsive) for 3D systems. This means that any infinitesimal amount of attraction produce a bound state in 2D [Landau 1977], while a finite amount of attraction is necessary for binding a 3D system.

Another important difference between 2D and 3D systems is the occurrence of the Thomas collapse [Thomas 1935] and the Efimov effect [Efimov 1970]. These effects were predicted and measured for three identical bosons in 3D systems, but are absent in 2D. While in 3D the Efimov effect produces an infinite sequence of states when the scattering length diverges, previous studies have shown that the spectrum of three identical bosons in 2D contains exactly one two-body and two three-body bound states in the limit where the range of the force goes to zero [Bruch 1979, Adhikari 1988]. Furthermore, the ratio between the three and two-body energies and radii attain universal values, no matter the detail of the short-range potential used [Nielsen 1997, Nielsen 2001].

Starting from the well-known case of three identical bosons, univer-

sal properties of mass-imbalanced three-body systems in 2D are systematically studied using the zero-range interaction in momentum space [Bellotti 2011, Bellotti 2012]. In this Chapter, the focus is particularly on the dependence of the three-body binding energy with masses and two-body binding energies. The critical values of these parameters (masses and two-body binding energies) allowing a given number of three-particle bound states with zero total angular momentum are determined in a form of boundaries in the multidimensional parametric space. Moreover, it is shown that in extreme asymmetric mass systems, when one of the particles is much lighter than the other two, no bound in the number of weakly three-body bound states is found, as the light particle mass goes to zero [Bellotti 2013b]. This topic is discussed in detail in Chapter 4.

The dependence of the three-particle binding energy on the parameters is highly non-trivial even in the simpler case of two identical particles and a distinct one. This dependence is parametrized for the ground and first excited state in terms of *supercycles* functions [Lamé 1818], even for the most general case of three distinguishable particles [Bellotti 2012].

### 3.1 Symmetry relations

An advantage in the use of two-body energies instead of interaction strengths in the homogeneous integral coupled equations for the bound state Eq. (2.68) is that only mass and energy ratios enter these equations. This means that the three-body energy divided by one of the two-body energies can be expressed as a function of four dimensionless parameters, i.e.,

$$\epsilon_3 = F_n \left( \frac{E_{\beta\gamma}}{E_{\alpha\beta}}, \frac{E_{\alpha\gamma}}{E_{\alpha\beta}}, \frac{m_\beta}{m_\alpha}, \frac{m_\gamma}{m_\alpha} \right) \equiv F_n \left( \epsilon_{\beta\gamma}, \epsilon_{\alpha\gamma}, \frac{m_\beta}{m_\alpha}, \frac{m_\gamma}{m_\alpha} \right), \quad (3.1)$$

where  $\epsilon_3 = E_3/E_{\alpha\beta}$  is the scaled three-body energy,  $\epsilon_{\beta\gamma} = E_{\beta\gamma}/E_{\alpha\beta}$  and  $\epsilon_{\alpha\gamma} = E_{\alpha\gamma}/E_{\alpha\beta}$  are the scaled two-body energies, where  $(\alpha, \beta, \gamma)$  are cyclic permutations of the particle labels  $(a, b, c)$ . The universal functions  $F_n$  are labeled with the subscript  $n$  to distinguish between ground,  $n = 0$ , and

excited states,  $n > 0$ . Interchanging the particle labels, all the universal functions  $F_n$  must obey the symmetry relations

$$\begin{aligned}
 F_n \left( \epsilon_{bc}, \epsilon_{ac}, \frac{m_b}{m_a}, \frac{m_c}{m_a} \right) &= F_n \left( \epsilon_{ac}, \epsilon_{bc}, \frac{m_c}{m_a}, \frac{m_b}{m_a} \right) = \\
 \epsilon_{bc} F_n \left( \frac{1}{\epsilon_{bc}}, \frac{\epsilon_{ac}}{\epsilon_{bc}}, \frac{m_a}{m_b}, \frac{m_c}{m_b} \right) &= \epsilon_{bc} F_n \left( \frac{\epsilon_{ac}}{\epsilon_{bc}}, \frac{1}{\epsilon_{bc}}, \frac{m_c}{m_b}, \frac{m_a}{m_b} \right) = \\
 \epsilon_{ac} F_n \left( \frac{1}{\epsilon_{ac}}, \frac{\epsilon_{bc}}{\epsilon_{ac}}, \frac{m_a}{m_c}, \frac{m_b}{m_c} \right) &= \epsilon_{ac} F_n \left( \frac{\epsilon_{bc}}{\epsilon_{ac}}, \frac{1}{\epsilon_{ac}}, \frac{m_b}{m_c}, \frac{m_a}{m_c} \right).
 \end{aligned} \tag{3.2}$$

The energy and mass scaling reduces the number of unknown parameters from six to four. A straightforward advantage is that the symmetry relations in Eq. (3.2) allow investigations of  $F_n$  to be taken in smaller regions of this four-parameter space, as explained in detail in the following sections.

## 3.2 Survey of mass dependence

The mass dependence of the number of bound states for a three-body system where all the two-body subsystems have the same energy of interaction, i.e.,  $E_{ab} = E_{ac} = E_{bc}$  is shown in Fig. 3.1. In the central region around equal masses only two three-body bound states are available [Bruch 1979]. This region, labeled II, extends in three directions corresponding to one heavy and two rather similar light particles, that is either  $\frac{m_c}{m_a} \geq 1$  and  $\frac{m_b}{m_a} \geq 1$ , or  $m_a \simeq m_b \leq m_c$ . Moving away from these regions in Fig. 3.1, the number of stable bound states increases in all directions. As an example, consider  $\frac{m_b}{m_a} = 10$  and vary  $\frac{m_c}{m_a}$  from small to large value in Fig. 3.1. Perhaps surprisingly, along this line the number of bound states decreases to a minimum of two and subsequently increases again. The reason is that a decreasing mass asymmetry in the three-body system implies less attraction in the effective potential experienced for the light particle due to the two heavy ones (see Chapter 4) and consequently the disappearing states merge into the two-body continuum. A similar behavior is found in three dimensions when the attractive strength is increased and happens the disappearance of the infinitely many Efimov states [Yamashita 2002]. As the mass asymmetry

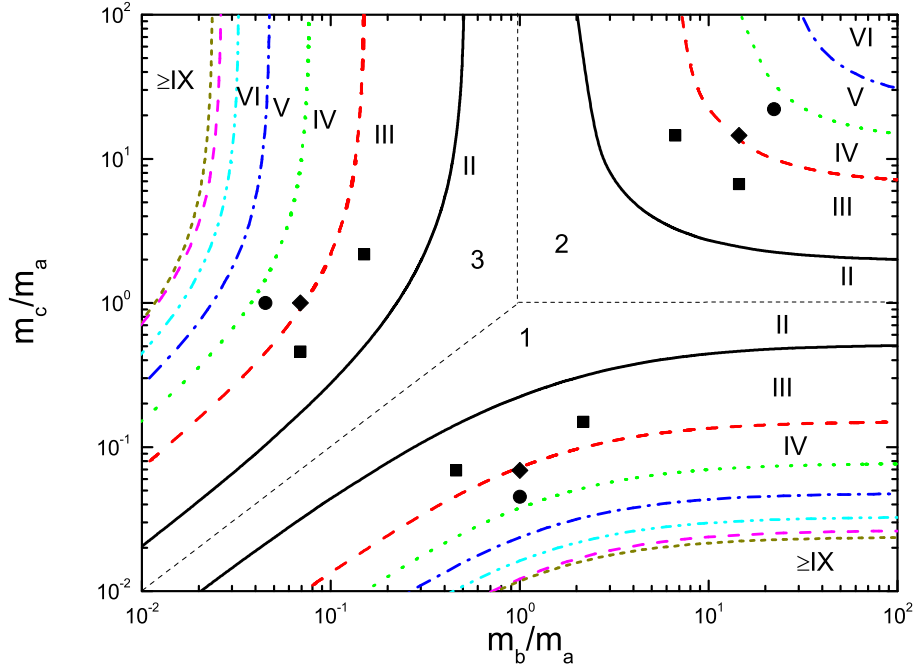


Figure 3.1: Mass diagram of the number of three-body bound states as functions of two mass ratios,  $\frac{m_b}{m_a}$  and  $\frac{m_c}{m_a}$ . The three two-body energies are equal, i.e.,  $E_{ab} = E_{bc} = E_{ac}$ . The Roman numerals indicate the number of bound states in each region. The systems investigated are represented by square ( ${}^6\text{Li}$ - ${}^{40}\text{K}$ - ${}^{87}\text{Rb}$ ), circular ( ${}^6\text{Li}$ - ${}^{133}\text{Cs}$ - ${}^{133}\text{Cs}$ ) and diamond ( ${}^6\text{Li}$ - ${}^{87}\text{Rb}$ - ${}^{87}\text{Rb}$ ) points. The three sets of points are related by the symmetries in Eq. (3.2).

increases again, the strength of effective potential also increases giving room for more bound states.

Variation of the two-body energies from all being equal leads to a distortion of the boundaries in Fig. 3.1, but the main structure remains. The central region still has the smallest number of stable bound states and any variation in the two-body energies expands region II, pushing the other lines away from the center. This result is illustrated in Figs. 3.2 and 3.3 and indicates that the maximum number of bound states supported for any three-body system, no matter the masses, is achieved when all the two-body subsystems interact with the same energy. Therefore, Fig. 3.1 gives the maximum number of stable bound states for any three-body system

composed for particles with different masses.

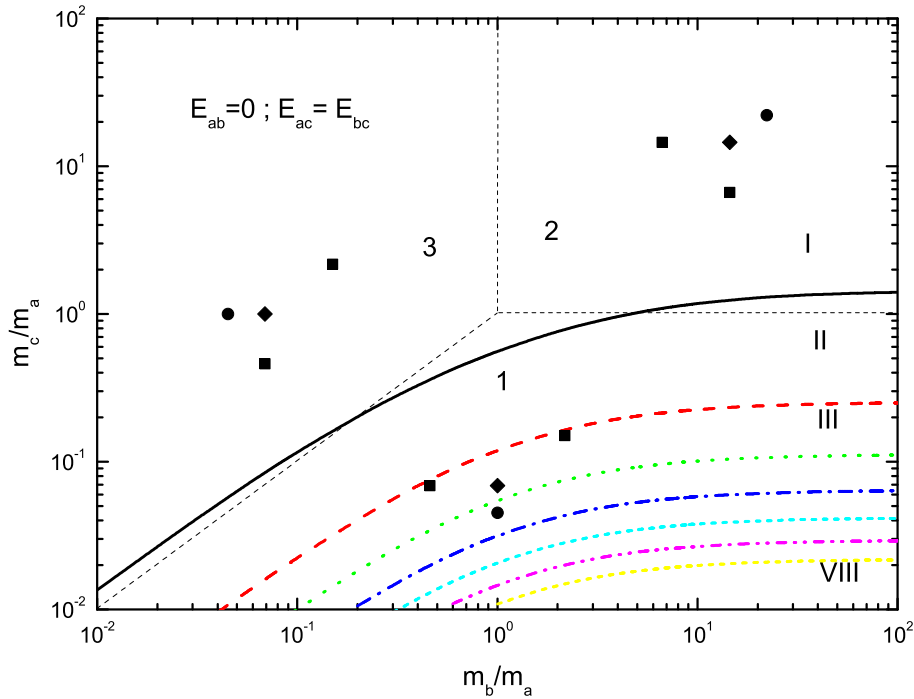


Figure 3.2: Mass diagram of the number of three-body bound states as functions of two mass ratios,  $\frac{m_b}{m_a}$  and  $\frac{m_c}{m_a}$ . The two-body energies are  $E_{ab} = 0$  and  $E_{ac} = E_{bc}$ . The Roman numerals indicate the number of bound states in each region. The systems investigated are represented by square ( ${}^6\text{Li}$ - ${}^{40}\text{K}$ - ${}^{87}\text{Rb}$ ), circular ( ${}^6\text{Li}$ - ${}^{133}\text{Cs}$ - ${}^{133}\text{Cs}$ ) and diamond ( ${}^6\text{Li}$ - ${}^{87}\text{Rb}$ - ${}^{87}\text{Rb}$ ) points. The numbers 1, 2, 3 label three different sectors.

Although presenting the richest energy spectrum, the scenario of three distinct two-body subsystems interacting with the same energy seems hard to be implemented experimentally. However, it was recently reported in Ref. [Repp 2013] that mixtures of  ${}^{133}\text{Cs}$  and  ${}^6\text{Li}$  were successfully trapped with a diverging scattering length of the  ${}^{133}\text{Cs}$ - ${}^{133}\text{Cs}$  subsystem. A system composed of two-heavy particles and a light one is described for instance in the region where  $m_c < m_a$  and  $m_c < m_b$ . Besides, if two particles do not interact in 2D, their energy can be set null. A mass diagram which includes such situation (the  ${}^{133}\text{Cs}$  ${}^{133}\text{Cs}$  ${}^6\text{Li}$  system is represented as circular points in Figs. 3.1 to 3.3) is constructed taking  $E_{ab} = 0$  and keeping  $E_{ac} = E_{bc}$  and is

shown in Fig. 3.2. Region I emerges in the middle of the figure, pushing the other lines away from the center. Excited states are only present in sector 1, where the two non-interacting particles are heavier than the third one (this configuration is studied in detail in Chapter 4).

The symmetries in Eq. (3.2), which clearly appear in Fig. 3.1, can not be seen in Fig. 3.2, but this does not mean that symmetry was broken. This apparent contradiction comes from the way that the mass-diagram is built. In sector 1 the light particle is  $m_c$ , i.e.,  $m_c < m_a$  and  $m_c < m_b$ , so that  $E_{ab} = 0$  means that the two heaviest particles are not interacting. Starting in sector 1 of Fig. 3.2 and moving towards sector 2, after crossing the horizontal dashed line  $E_{ab} = 0$  does not mean that the two heaviest particles are not interacting any more, since in this region the particles  $b$  and  $c$  are the heaviest, i.e.,  $m_a < m_b$  and  $m_a < m_c$  and the effective interaction between the heavy particles is mediated by light one, namely particle  $a$ . The same happens in region 3, where particles  $a$  and  $c$  are the heaviest. In fact, a mass-diagram for imbalanced two-body energies shows information for three different systems. Therefore, each sector in Fig. 3.2 obey the symmetries in Eq. (3.2) itself. For instance, the configuration showed in Fig. 3.2 is also described for  $E_{bc} = 0$  with  $m_a < m_b$  and  $m_a < m_c$  or  $E_{ac} = 0$  with  $m_b < m_a$  and  $m_b < m_c$ . These choices lead to two other plots, where the boundary lines in Fig. 3.2 rotates to sector 2 and 3, respectively. Notice that the symmetries in Eq. (3.2) are not well defined for a non-interacting two-body subsystem, however, it is not hard to extend them for this case.

What about a system where all two-body energies are different from each other? This scenario is shown in Fig. 3.3. In sector 1, where the energy between the two heaviest particles is greater than the other ones, the three distinct systems which are shown in Figs. 3.1 and 3.2 have only one bound state each. In this energy-configuration, region 2 should be the most similar to the previous case, where the heavy-heavy system is not as bound as the other ones. However, sectors 2 and 3 seems to be almost symmetric in Fig. 3.3, showing that both  ${}^6\text{Li}-{}^{133}\text{Cs}-{}^{133}\text{Cs}$  and  ${}^6\text{Li}-{}^{87}\text{Rb}-{}^{87}\text{Rb}$  systems have two bound states each. A small difference is seen for  ${}^6\text{Li}-{}^{40}\text{K}-{}^{87}\text{Rb}$ , which

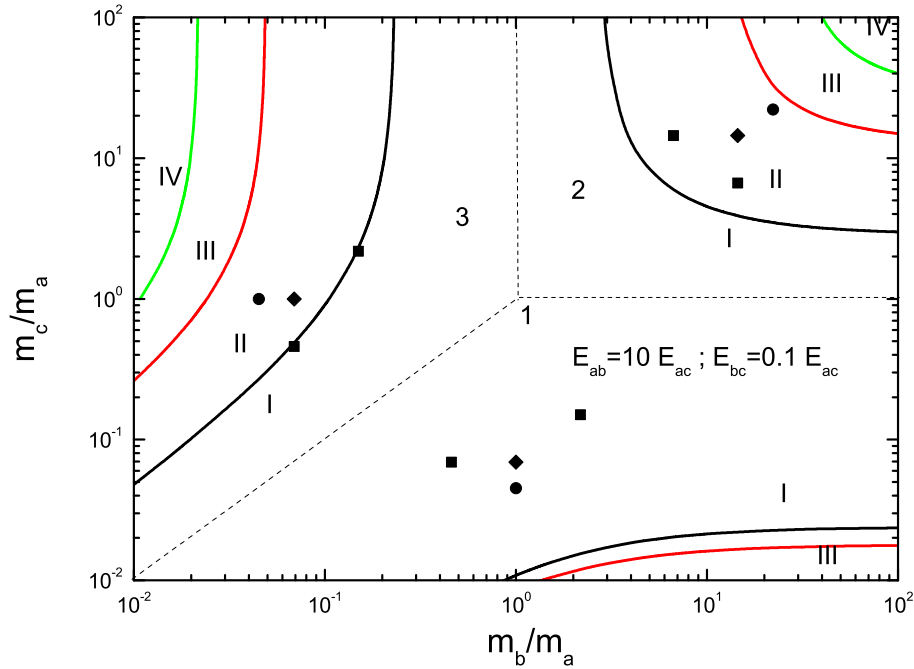


Figure 3.3: Mass diagram of the number of three-body bound states as functions of two mass ratios,  $\frac{m_b}{m_a}$  and  $\frac{m_c}{m_a}$ . The two-body energies are  $E_{ab} = 10E_{ac}$  and  $E_{bc} = 0.1E_{ac}$ . The Roman numerals indicate the number of bound states in each region. The systems investigated are represented by square ( ${}^6\text{Li}$ - ${}^{40}\text{K}$ - ${}^{87}\text{Rb}$ ), circular ( ${}^6\text{Li}$ - ${}^{133}\text{Cs}$ - ${}^{133}\text{Cs}$ ) and diamond ( ${}^6\text{Li}$ - ${}^{87}\text{Rb}$ - ${}^{87}\text{Rb}$ ) points. The numbers 1, 2, 3 label three different sectors.

has two bound states in sector 2, but only one in sector 3. The similarity between sector 1 in Fig. 3.2 and sector 2 in Fig. 3.3 is not clear enough because the strongly bound heavy-light system changes the threshold of binding the three-body system, cutting-out the most weakly three-body bound states. More details about these mass-diagrams and discussion about bound states are found in [Bellotti 2011, Bellotti 2012, Bellotti 2013b].

### 3.3 Three-body energies for given masses

Realistic scenarios correspond to given particles (atoms or molecules) with known masses where in contrast, the interactions are variable through Feshbach resonances [Chin 2010]. Once the constituents are chosen, the di-

agrams from the last section can be powerful guides in the experimental search for 2D three-body bound states, as they indicate how many bound states are expected to exist. However, this number varies for different two-body energies. The dependence in the number of bound states with the two-body energies for a specific system is discussed in this section.

Assuming masses corresponding to the alkali atoms  $^{87}\text{Rb}$ ,  $^{40}\text{K}$  and  $^6\text{Li}$ , the two ratios of two-body energies are left as variables where each set uniquely specifies the three-body energies of ground and possibly excited states. A contour diagram of the scaled three-body energies for the two lowest stable bound states of the chosen system is shown in Fig. 3.4. The log-log plot can be deceiving and on a linear scale the curves of equal scaled three-body energy would be concave for the ground state and almost linear or slightly convex for the first excited state in contrast to the convex contours in Fig. 3.4. The chosen set of masses only allow one, two, or three stable bound states, depending on the two-body energies. The corresponding regions are shown by dotted curves in Fig. 3.4. The true extent of the regions cannot be seen. Both region II and III are closed, namely, region II continues along region III up to energy ratios of about  $10^{\pm 5}$ , and the narrow region III is entirely embedded in region II. Other sets of mass ratios, as  $^6\text{Li}-^{133}\text{Cs}-^{133}\text{Cs}$  or  $^6\text{Li}-^{87}\text{Rb}-^{87}\text{Rb}$ , for instance, could open region III and allow regions inside with more than three stable bound states.

In the log-log plot of Fig. 3.4 the two-body energies vary by five orders of magnitude, whereas the scaled three-body energies for a stable system must be larger than all two-body energies. The three-body energy contours connect minimum and maximum two-body energies, that is zero and maximum two-body energies for the ground state and thresholds boundaries for existence of the excited states [Bellotti 2011]. The contours appear in regular intervals with larger values for increasing two-body energies. Large three-body energies reflect small spatial extension and therefore are less interesting as it presumably is unreachable in the universal limit. The contours pass continuously through the boundaries of the different regions since the ground state exists without knowledge of the excited states. The con-



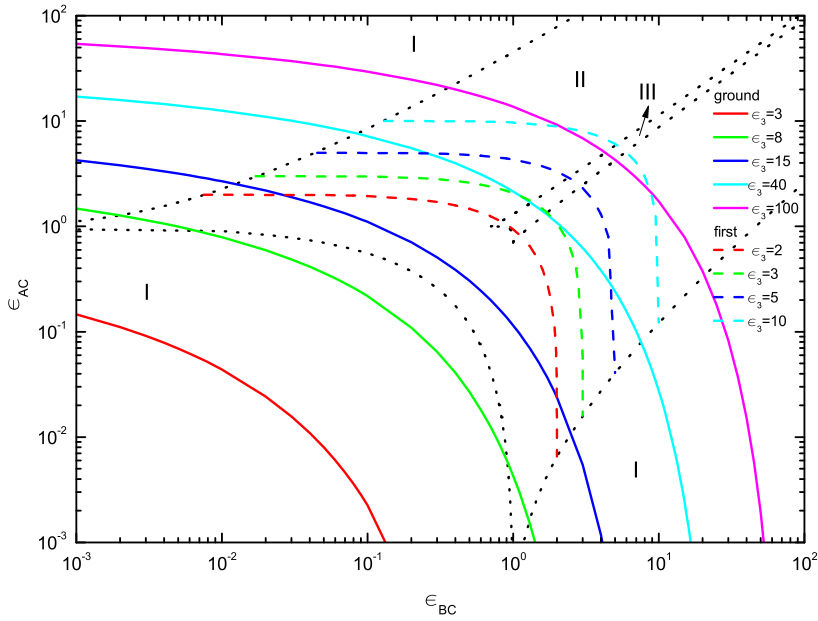


Figure 3.4: Contour diagrams with lines of fixed  $\epsilon_3$  values as function of the two-body energies  $\epsilon_{ac}$  and  $\epsilon_{bc}$ . The solid and dashed curves are for ground and excited states, respectively. Here  $a$  is  $^{87}\text{Rb}$ ,  $b$  is  $^{40}\text{K}$ , and  $c$  is  $^6\text{Li}$ . The dotted curves show where the number of stable bound states change from one (regions most asymmetric for small energies), to two (comparable size of the two-body energies), and to three (equal and large energies). The roman labels I, II, and III are as in Fig. 3.1.

tours in Fig. 3.4 for the excited state can only appear in the regions with two or more stable bound states. These contours therefore must connect points of the boundaries between regions I and II. They may cross continuously through region III precisely as the ground state would cross through boundaries between regions I and II. Similar contours exist within region III but are not exhibited in this narrow strip where they are allowed. The scaled three-body energies are often substantially larger than the initial two-body energies, although both arise from the same two-body interactions.

### 3.4 Parametrization of three-body energies

The universal functions  $F_n$  defined in Eq. (3.1) are not easily found. Their dependence on masses and two-body energies are highly non-trivial, even in a simpler scenario of two identical particles and a distinct one [Bellotti 2011]. However, the contour diagrams in Fig. 3.4 suggest a simple implicit dependence in terms of an extended Lamé curves or *super ellipses* [Lamé 1818]. Note that, despite of the log-log scale in Fig. 3.4, the parametrization in terms of Lamé curves is done with the energies on a linear scale. The three-body energies can be written indirectly by *super circles*, i.e.,

$$\epsilon_{ac}^{t_n} + \epsilon_{bc}^{t_n} = R_n^{t_n} , \quad (3.3)$$

where the radius,  $R_n$ , and the power,  $t_n$ , are functions of  $\epsilon_3$  and both depend on the two mass ratios. The term *super circle* has been adopted since Eq. (3.3) only differs from a circumference of radii  $R_n$  and coordinates  $(\epsilon_{ac}, \epsilon_{bc})$  in the power  $t_n$ , which is not equal two in general. The smallest value of  $\epsilon_3$  is unity corresponding to the two-body threshold of the *ab* system used as the energy unit.

Two sets of alkali atoms ( ${}^6\text{Li}$ - ${}^{40}\text{K}$ - ${}^{87}\text{Rb}$  and  ${}^{40}\text{K}$ - ${}^{87}\text{Rb}$ - ${}^{133}\text{Cs}$ ) and a system of three identical particles are used to validate the parameterization. The fitted radius and exponent functions are respectively shown in Figs. 3.5 and 3.6 for both ground and first excited states.

The radius functions turn out to be surprisingly simple, that is linear functions of  $\epsilon_3$ , which are essentially independent of the masses. For the ground state a slight increase of slope with increasing three-body energy is found. Average estimates are

$$R_0(\epsilon_3) \approx 0.74\epsilon_3 - 2.5 , \quad R_1(\epsilon_3) \approx \epsilon_3 . \quad (3.4)$$

The increasing functions reflect how the contours in Fig. 3.4 are moving to larger two-body energies with increasing  $\epsilon_3$ . This simple linear dependence implies that the three-body energy increases linearly with a kind of

average of the two two-body energy ratios. Notice that the symmetric system, where all particles are identical, has this property where two- and three-body energies are proportional in the universal limit. To approach this limit it is assumed firstly that  $a = b$ , and Eqs. (3.3) and (3.4) imply for the ground states that  $0.74\epsilon_3 \approx 2.5 + \epsilon_{ac}2^{1/t_0}$ . When  $a = b = c$ , the known ratios  $\epsilon_3 \approx (2.5 + 2^{1/t_0})/0.74 = 16.52$  for the ground state and  $\epsilon_3 \approx 2^{1/t_1} = 1.267$  for the excited state are recovered. This is achieved with  $t_0 \approx 0.30$  and  $t_1 \approx 2.93$  and both  $t_0$  and  $t_1$  agree with the ones calculated in Fig. (3.6).

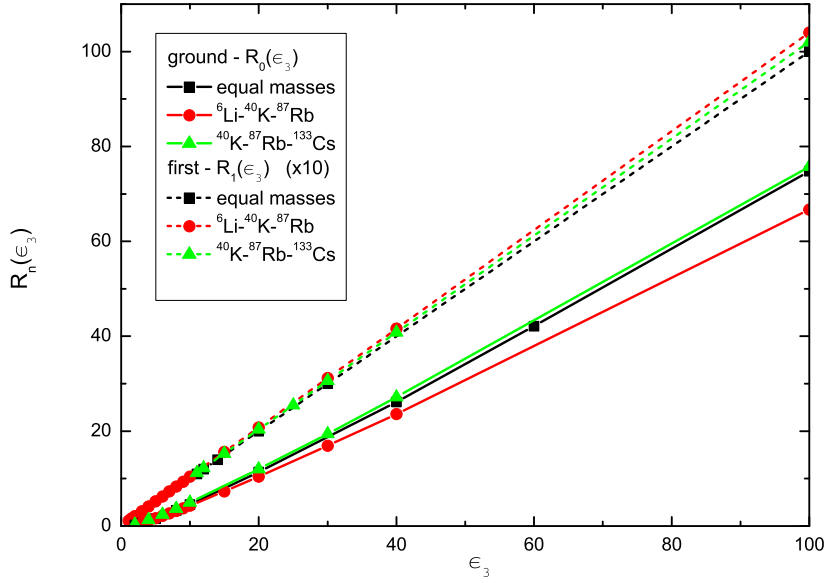


Figure 3.5: The functions,  $R_0$  and  $R_1$ , of the three-body energy  $\epsilon_3$  in the super-ellipse fit for three sets of mass ratios, which are  $(m_\alpha, m_\beta) = (1, 1)$ ,  $(40/87, 6/87)$ ,  $(87/133, 40/133)$  corresponding to three identical molecules,  ${}^6\text{Li}-{}^{40}\text{K}-{}^{87}\text{Rb}$ , and  ${}^{40}\text{K}-{}^{87}\text{Rb}-{}^{133}\text{Cs}$ , respectively. Both axis are scaled up by a factor of 10 for the excited state, where the maximum energy of  $\epsilon_3 = 10$  corresponds to  $R_1 \approx 10$ .

The exponents  $t_n$  are crucial to obtain the correct curvature of the energy contours in Fig. 3.4. In Fig. 3.6 are shown the functions obtained by fitting results for the same sets of masses as in Fig. 3.5. These exponents increase monotonously with  $\epsilon_3$  from small values and the curves bend over at some

point and continue to increase linearly with a smaller slope. Eventually the curves would stop when the states reach a two-body threshold and become unstable. In most cases this only happens for excited states at large energies where the universal properties are, in practice, probably much more unlikely to realize.

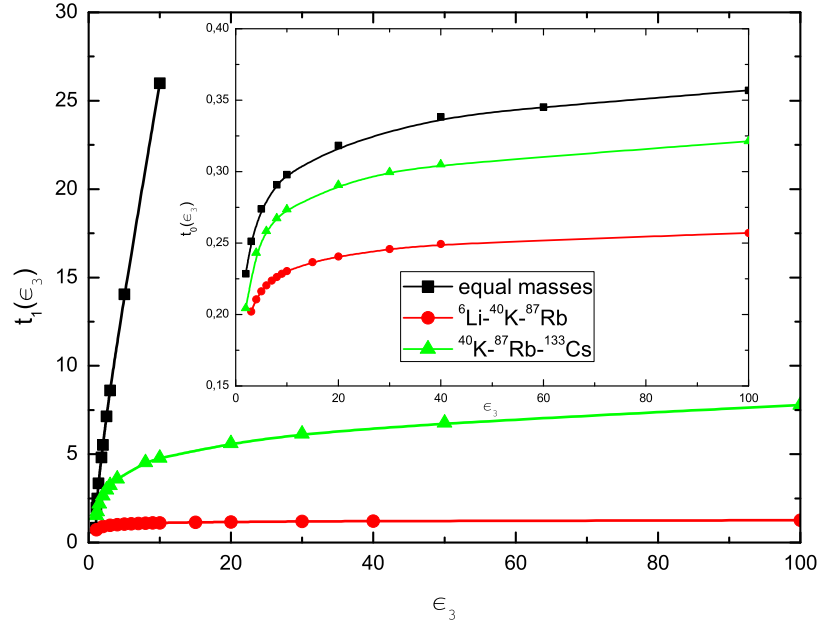


Figure 3.6: The exponents,  $t_0$  and  $t_1$ , in the super-ellipse fit as functions of the three-body energy  $\epsilon_3$  for three sets of mass ratios, which are  $(m_\alpha, m_\beta) = (1, 1)$ ,  $(40/87, 6/87)$  and  $(87/133, 40/133)$  corresponding to identical molecules,  ${}^6\text{Li}-{}^{40}\text{K}-{}^{87}\text{Rb}$ , and  ${}^{40}\text{K}-{}^{87}\text{Rb}-{}^{133}\text{Cs}$ , respectively.

The absolute sizes increase by about an order of magnitude from ground to first excited state. As said before, the role of the exponents in Eq. (3.3) is to adjust to the curvature of the contours in Fig. 3.4. Thus, large  $t$  is necessary for strongly bending curves. This immediately explain the difference between ground and first excited state, but also the overall increase with  $\epsilon_3$ . This is especially pronounced for the excited states which are squeezed in between boundaries defined by stability towards decay to bound two-body

subsystems.

The behavior of the exponents is also surprisingly simple for each set of masses. The relatively fast increase at small energies in Fig. 3.6 slows down and both  $t_0$  and  $t_1$  approach constants at large energy. For the ground state, this can be accurately captured by

$$t_0(\epsilon_3) \approx \alpha_0 \frac{\epsilon_3^{p_0} + \beta_0}{\epsilon_3^{p_0} + \gamma_0}, \quad (3.5)$$

where  $\alpha_0$  is the mass dependent constant approached at large energy (see Fig. 3.6). The parameters,  $(p_0, \alpha_0) \simeq (0.04 - 0.06, 0.3 - 0.5)$ , exhibits a small mass dependence, whereas  $(\beta_0, \gamma_0) \simeq -(0.93 - 0.95), -(0.82 - 0.87)$  are slightly negative but almost mass independent. Remember that stability requires  $\epsilon_3 > 1$ . The value of  $t_0$  for small  $\epsilon_3 \approx 1$  is then in the range of  $t_0 \simeq 0.2 - 0.5$  as required to give the limiting value of  $\epsilon_3 = 16.52$ . A similar parametrization for the exponent corresponding to the excited state can be found.

Combining Eqs. (3.3), (3.4) and (3.5), the parameterized results cannot be distinguished from the computed curves in Fig. 3.4.



# Adiabatic approximation

---

Why does the number of bound states increase as one particle becomes lighter than the other two? This question arises after looking the mass-diagrams in Chapter 3, where an increasing number of bound states was found for decreasing the mass of one of the particles. The situation where one particle is much lighter than the other two is suitably handled in the adiabatic approximation, namely the Born-Oppenheimer (BO) approximation.

The BO approximation considers a system composed of two heavy particles and a light one, where the terms *heavy* and *light* have relative meaning: two particles are heavier than the third one. In this approximation the heavy particles move very slowly while the light particle orbits around them. In fact, for the BO approximation to be valid it is enough to consider the kinetic energy of the heavy particles is much smaller than the light particle one.

A successful implementation of the BO approximation is presented in Ref. [Fonseca 1979], where the Efimov problem is solved in an analytic model. It is shown that the Efimov effect is related to a long-range effective force and it can occur even when the individual pair forces have zero range. This is an example of how long-range forces can arise in the three-body problem in a way unpredictable by two-body intuition. The BO approximation was also implemented in Ref. [Lim 1980], looking for the Efimov effect in 2D mass-imbalanced three-body systems, however the mass-dependence of such systems was not addressed.

The BO approximation of 2D three-body systems is re-visited under the mass-dependence perspective [Bellotti 2013b]. As in the previous Chapter, a 2D three-body system with short-range interactions for general masses

and interaction strengths is considered. The expressions for the adiabatic approximation are derived using separable zero-range potentials and yield a concise adiabatic potential between the two heavy particles in the heavy-heavy-light system when the light particle coordinate is integrated out.

The adiabatic potential, which is found as the solution of a transcendental equation, is mass-dependent and reveals an increasing number of bound states by decreasing the mass of the light. An asymptotic expression for the adiabatic potential is derived and it is shown that this analytic expression faithfully corresponds to the numerically calculated adiabatic potential, even in the non-asymptotic region. The number of bound states for a heavy-heavy-light system is estimated as a function of the light-heavy mass ratio. Infinitely many bound states are expected as this ratio approaches zero. However, for finite masses a finite number of bound states is always expected.

## 4.1 Adiabatic potential

An  $abc$  system where the two heavy particles have masses  $m_a$  and  $m_b$  is considered. These particles are fixed and their centers are separated out by a distance  $\mathbf{R}$ . The light particle has mass  $m_c$  and coordinate  $\mathbf{r}$  relative to the CM of the heavy-heavy subsystem. The interaction between particles is described by zero-range pairwise potentials. The notation for the potential is that  $v_c$  means the interaction between particles  $a$  and  $b$ , with  $v_a, v_b$  analogously defined. The configuration of the three-body system is shown in Fig. 4.1.

The Schrödinger eigenvalue equation of the  $abc$  system is  $H\Psi(\mathbf{r}, \mathbf{R}) = E\Psi(\mathbf{r}, \mathbf{R})$ . The Hamiltonian  $H$  is written in the relative coordinates  $\mathbf{R}, \mathbf{r}$  in the three-body CM frame as

$$H = -\frac{\hbar^2}{2m_{ab}}\nabla_R^2 - \frac{\hbar^2}{2m_{ab,c}}\nabla_r^2 + v_a\left(\mathbf{r} - \frac{m_{ab}}{m_b}\mathbf{R}\right) + v_b\left(\mathbf{r} + \frac{m_{ab}}{m_a}\mathbf{R}\right) + v_c(\mathbf{R}), \quad (4.1)$$



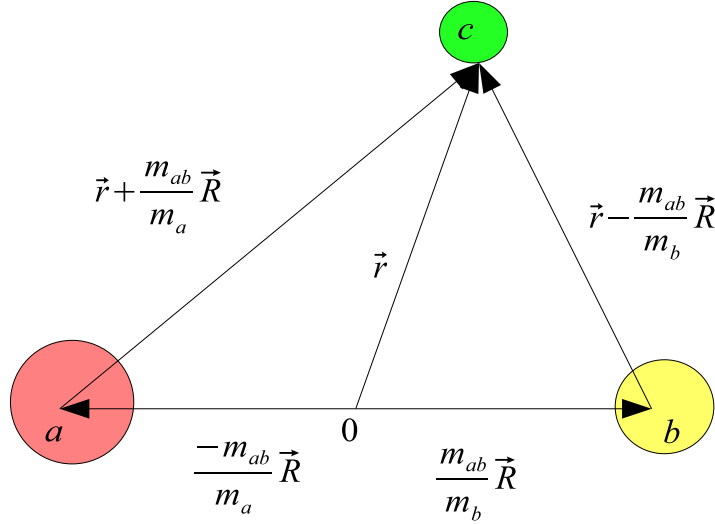


Figure 4.1: Three-body relative coordinates used in the adiabatic approximation.

where the reduced masses are  $m_{ab} = m_a m_b / (m_a + m_b)$  and  $m_{ab,c} = m_c (m_a + m_b) / (m_a + m_b + m_c)$ .

The adiabatic approximation says that it is possible to split the three-body eigenvalue equation into the solution of two two-body problems: the light particle motion is considered with respect to the heavy-heavy system and the heavy-heavy system motion is separated out. These eigenvalue equations are valid whenever the motion of the light particle is rapid compared to the motion of the heavy ones, so that the light particle dynamics can be solved while the heavy particles are instantaneously at rest. The wave function is decomposed as

$$\Psi(\mathbf{r}, \mathbf{R}) = \psi(\mathbf{r}, \mathbf{R})\phi(\mathbf{R}) , \quad (4.2)$$

where  $\psi(\mathbf{r}, \mathbf{R})$  is the wave function describing the state of the light particle for fixed  $\mathbf{R}$  and  $\phi(\mathbf{R})$  is the heavy subsystem wave function. The approximation is valid when the kinetic energy term,  $-\frac{\hbar^2}{2m_{ab}}\nabla_{\mathbf{R}}^2\psi(\mathbf{r}, \mathbf{R})$ , is small compared to the other terms in Eq.(4.1). Using the wave function from

Eq. (4.2), the eigenvalue equation becomes

$$\begin{aligned}
H\psi(\mathbf{r}, \mathbf{R})\phi(\mathbf{R}) &= E\psi(\mathbf{r}, \mathbf{R})\phi(\mathbf{R}), \\
\phi(\mathbf{R}) \left( -\frac{\hbar^2}{2m_{ab,c}} \nabla_{\mathbf{r}}^2 + v_a \left( \mathbf{r} - \frac{m_{ab}}{m_b} \mathbf{R} \right) + v_b \left( \mathbf{r} + \frac{m_{ab}}{m_a} \mathbf{R} \right) \right) \psi(\mathbf{r}, \mathbf{R}) \\
&\quad + \psi(\mathbf{r}, \mathbf{R}) \left( -\frac{\hbar^2}{2m_{ab}} \nabla_{\mathbf{R}}^2 + v_c(\mathbf{R}) \right) \phi(\mathbf{R}) = E\psi(\mathbf{r}, \mathbf{R})\phi(\mathbf{R}), \\
\frac{\left( -\frac{\hbar^2}{2m_{ab,c}} \nabla_{\mathbf{r}}^2 + v_a \left( \mathbf{r} - \frac{m_{ab}}{m_b} \mathbf{R} \right) + v_b \left( \mathbf{r} + \frac{m_{ab}}{m_a} \mathbf{R} \right) \right) \psi(\mathbf{r}, \mathbf{R})}{\psi(\mathbf{r}, \mathbf{R})} \\
&\quad + \frac{\left( -\frac{\hbar^2}{2m_{ab}} \nabla_{\mathbf{R}}^2 + v_c(\mathbf{R}) \right) \phi(\mathbf{R})}{\phi(\mathbf{R})} = E. \tag{4.3}
\end{aligned}$$

The first term on the left-hand-side of Eq. (4.3) is a separation constant,  $\epsilon(R)$ , which does not depend on  $\mathbf{r}$ . Therefore, light particle equation is

$$\left[ -\frac{\hbar^2}{2m_{ab,c}} \nabla_{\mathbf{r}}^2 + v_a \left( \mathbf{r} - \frac{m_{ab}}{m_b} \mathbf{R} \right) + v_b \left( \mathbf{r} + \frac{m_{ab}}{m_a} \mathbf{R} \right) \right] \psi(\mathbf{r}, \mathbf{R}) = \epsilon(R)\psi(\mathbf{r}, \mathbf{R}), \tag{4.4}$$

and the eigenvalue,  $\epsilon(R)$ , plays the role of an effective potential in the equation for the heavy-heavy system. From Eq. (4.3), this equation is

$$\left( -\frac{\hbar^2}{2m_{ab}} \nabla_{\mathbf{R}}^2 + v_c(\mathbf{R}) + \epsilon(R) \right) \phi(\mathbf{R}) = E\phi(\mathbf{R}). \tag{4.5}$$

Assuming that the potentials in Eq.(4.4) are separable and have the same strength, i.e.,  $v_\alpha = \lambda|\chi_\alpha\rangle\langle\chi_\alpha|$ , the wave function of the light particle in momentum space reads

$$\tilde{\psi}(\mathbf{p}) = \lambda \frac{g(\mathbf{p})}{\epsilon(R) - \frac{\hbar^2}{2m_{ab,c}} p^2} \left[ e^{i \frac{m_{ab}}{m_a} \frac{\mathbf{p} \cdot \mathbf{R}}{\hbar}} A_+ + e^{-i \frac{m_{ab}}{m_b} \frac{\mathbf{p} \cdot \mathbf{R}}{\hbar}} A_- \right], \tag{4.6}$$

where

$$A_\pm = \int d^2 r' \tilde{g}^\dagger \left( \mathbf{r}' \pm \frac{m_{ab}}{m_a} \mathbf{R} \right) \Psi(\mathbf{r}') = \int d^2 p' g^\dagger(\mathbf{p}') \frac{e^{\mp i \frac{m_{ab}}{m_a} \frac{\mathbf{p}' \cdot \mathbf{R}}{\hbar}}}{2\pi} \tilde{\psi}(\mathbf{p}') \tag{4.7}$$

and  $g(\mathbf{p})$  is the form factor of the potential.

The formulation of Eq. (4.6) in terms of  $A_{\pm}$  leads to the system of equations

$$A_{\pm} = \lambda \int d^2p \frac{|g(\mathbf{p})|^2}{\epsilon(R) - \frac{\hbar^2}{2m_{ab,c}} p^2} \left( e^{\mp i \frac{\mathbf{p} \cdot \mathbf{R}}{\hbar}} A_{\mp} + A_{\pm} \right). \quad (4.8)$$

The non-trivial solution of Eq.(4.8), i.e.,  $A_{\pm} \neq 0$ , gives a transcendental equation for the effective potential, which reads

$$\frac{1}{\lambda} = \int d^2p \frac{|g(\mathbf{p})|^2}{\epsilon(R) - \frac{\hbar^2}{2m_{ab,c}} p^2} \left[ 1 + \cos\left(\frac{\mathbf{p} \cdot \mathbf{R}}{\hbar}\right) \right]. \quad (4.9)$$

Using the binding energy of the heavy-light subsystem,  $E_2$ , to parameterize  $\lambda$  [Adhikari 1995a], Eq. (4.9) is rewritten as

$$\int d^2p |g(\mathbf{p})|^2 \left[ \frac{1 + \cos\left(\frac{\mathbf{p} \cdot \mathbf{R}}{\hbar}\right)}{\epsilon(R) - \frac{\hbar^2}{2m_{ab,c}} p^2} + \frac{1}{|E_2| + \frac{\hbar^2}{2m_{ab,c}} p^2} \right] = 0. \quad (4.10)$$

Model-independent results are naturally obtained with the use of zero-range potentials and the form factor of such potential in momentum space is a constant, i.e.,  $g(\mathbf{p}) = 1$ . In this case, Eq. (4.10) is finite and the integration of the two terms leads to the transcendental equation for the adiabatic potential

$$\ln \frac{|\epsilon(R)|}{|E_2|} = 2K_0 \left( \sqrt{\frac{2m_{ab,c} |\epsilon(R)|}{\hbar^2}} R \right), \quad (4.11)$$

where  $K_0$  is the modified Bessel function of second kind of order zero.

The effective potential  $\epsilon(R)$  is exactly defined as the solution of Eq. (4.11) and is a powerful tool in understanding mass-imbalanced three-body systems in two dimensions. However, a transcendental equation involving a logarithm and a modified Bessel function of second kind is not intuitive at all. In the next section, two limiting expressions are found by expanding both sides of Eq. (4.11) for small and large  $R$ .

## 4.2 Asymptotic expressions

The asymptotic form for  $|\mathbf{R}| \rightarrow 0$  is found inserting the asymptotic form of  $K_0$  for small arguments [Abramowitz 1965] into Eq. (4.11). The result is a Coulomb-like potential, which up to 2<sup>nd</sup> order reads

$$\frac{|\epsilon_{asymptotic}(R)|}{|E_2|} \rightarrow \frac{2e^{-\gamma}}{s(R)} \left( 1 - \frac{e^{-\gamma}}{2} s(R) \left[ (1 - \gamma) - \frac{1}{2} \ln \left( \frac{e^{-\gamma}}{2} s(R) \right) \right] \right)^{-1}, \quad (4.12)$$

where  $\gamma$  is the constant of Euler and  $s(R) = \sqrt{\frac{2m_{ab,c}|E_2|}{\hbar^2}} R$ .

When the distance  $\mathbf{R}$  between the two heavy particles is large, i.e.,  $|\mathbf{R}| \rightarrow \infty$ , the light particle feels only the interaction from one of the heavy particles. In this limit the three-body problem becomes a two-body problem and is expected that  $|E| = |E_2|$ . Therefore, defining  $\frac{|E(R)|}{|E_2|} = 1 + V(R)$ , this condition is fulfilled when  $V \rightarrow 0$  for  $|\mathbf{R}| \rightarrow \infty$ . Replacing  $|E|/|E_2|$  by  $1 + V(R)$  in Eq. (4.11) and expanding both sides up to first order in  $R$  results in

$$V(R) = \frac{2K_0(s(R))}{1 + s(R) K_1(s(R))}, \quad (4.13)$$

The asymptotic expression of the adiabatic potential for large  $\mathbf{R}$  is then

$$\frac{|\epsilon_{asymptotic}(R)|}{|E_2|} \rightarrow 1 + \frac{2K_0(s(R))}{1 + s(R) K_1(s(R))} \rightarrow 1 + \sqrt{2\pi} \frac{e^{-s(R)}}{\sqrt{s(R)}}. \quad (4.14)$$

Notice that the approximation accuracy increases when higher order terms are included in the expansions. It is possible to go to more precise adiabatic potential representations taken higher order expansions of Eq. (4.11). However, the results of the approximations (4.12) and (4.14) and the adiabatic potential (4.11) are almost indistinguishable in practice. The largest deviations, shown in Fig. 4.2, are found in the region  $0.3 < s < 3$ , where the difference between  $\epsilon_{asymptotic}(s)$  and  $\epsilon_{exact}(s)$  never exceeds 9%.

In spite of the fact that the asymptotic potential in Eqs. (4.12) and (4.14) is valid respectively in the extreme limits  $R \rightarrow 0$  and  $R \rightarrow \infty$ , it perfectly reproduces the effective potential in almost all the range of the

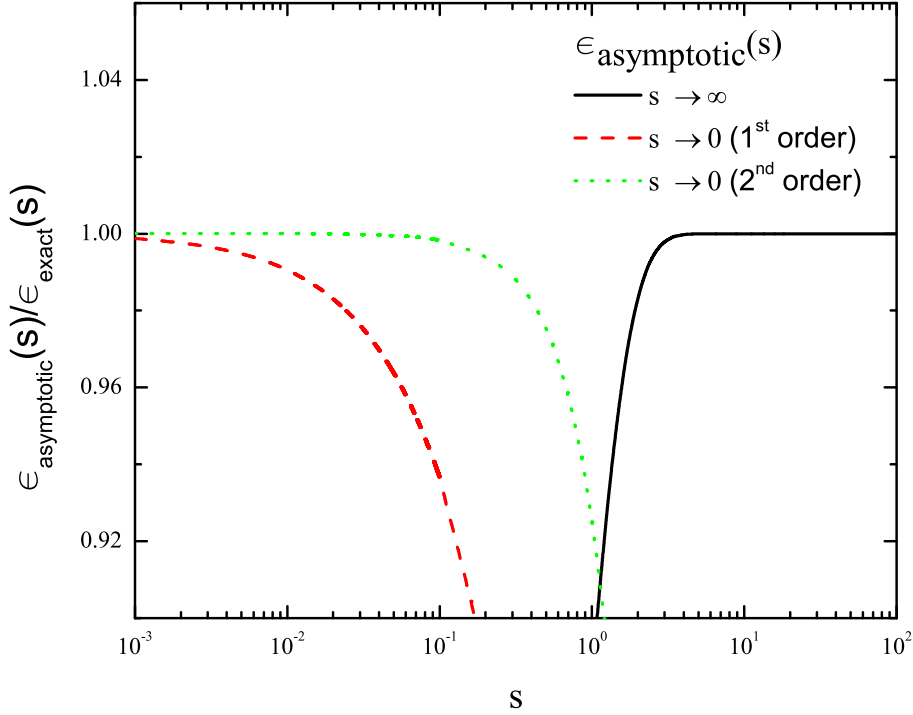


Figure 4.2: Ratio  $\epsilon_{asymptotic}(s)/\epsilon_{exact}(s)$  as function of the dimensionless coordinate  $s$ , showing the validity of asymptotic expressions in Eqs. (4.12) and (4.14). The black-solid and red-dashed curves are the first order expansion of the adiabatic potential at small and large distances, respectively. The green-dotted curve is the second order expansion of the adiabatic potential at small distances.

scaled coordinate  $s(R)$ , since its difference to the potential numerically calculated from Eq. (4.11) is almost imperceptible. These features are shown in Fig.4.3.

For  $R \rightarrow 0$  the first order expansion of the effective potential in Eq. (4.12) resembles a hydrogen atom in 2D, where the pre-factor  $1/\sqrt{m_c}$  makes the energy of the deepest states grow without boundaries when  $m_c \rightarrow 0$ . Furthermore, for  $R \rightarrow \infty$ , the potential in Eq. (4.14) is long-ranged and screened by a factor  $\sqrt{m_c}$ , which becomes less important for  $m_c \rightarrow 0$ . Therefore, an increasing number of bound states is expected when particle  $c$  is much lighter than the other ones, i.e.,  $m_c \rightarrow 0$ , since the adiabatic potential becomes more attractive and less screened in this limit. Still, these states will accumulate

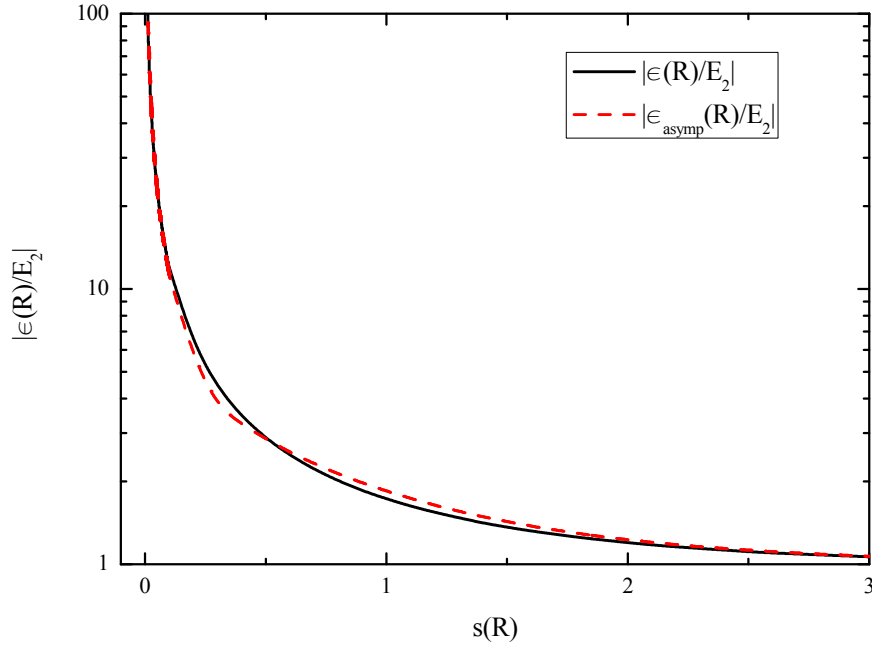


Figure 4.3: Adiabatic potential  $|\epsilon_{asymptotic}(R)/E_2|$  as function of the dimensionless coordinate  $s(R)$ . The solid-black line is the numerical solution of Eq. (4.11) and the dashed-red line is the asymptotic expression in Eqs. (4.12) and (4.14). The limiting expression for  $R \rightarrow 0$  in Eq. (4.12) is plotted in the interval  $0 < s(R) \leq 0.3$  and the expression for  $R \rightarrow \infty$  in Eq. (4.14) is plotted for  $s(R) \geq 0.3$ .

both at  $R \rightarrow 0$ , as the strength of the Coulomb-like potential increases, and at  $R \rightarrow \infty$ , where more states are allowed because the exponential moves to larger distances. However, for finite  $m_c$ , still the number of bound states is finite.

One might argue that the limit  $|E_2| \rightarrow 0$  must produce the same effect as  $m_c \rightarrow 0$  in the asymptotic form of the adiabatic potential in Eqs. (4.12) and (4.14). However, the limit where all subsystems interacting through zero-range interactions are unbound does not support three-body bound states in 2D [Bruch 1979, Lim 1980, Bellotti 2012].

### 4.3 Numerical results

The increasing number of three-body bound states as function of the mass of the particles, presented in Chapter 3, was qualitatively explained in the last section with the asymptotic expressions of the adiabatic potential. In this section, the analytic properties of the asymptotic expressions in Eqs. (4.12) and (4.14) are used in the numerical survey of bound states in the adiabatic limit.

In the following, the analysis is done for a system of two identical heavy particles of masses  $m_a = m_b = M$  in units that  $\hbar^2 = M = E_{ac} = E_{bc} = E_2 = 1$ . The mass ratio between light and heavy particles is defined  $m = \frac{m_c}{M}$ . In this case, the reduced mass  $m_{ab,c}$  is written as

$$m_{ab,c} = \frac{2m}{m+2} \quad \text{and} \quad m_{ab,c} \rightarrow m \quad \text{for} \quad m \rightarrow 0. \quad (4.15)$$

With these units, the asymptotic expression for the effective potential becomes

$$\epsilon(R) \rightarrow -\frac{2e^{-\gamma}}{\sqrt{\frac{4m}{m+2}} R} \left( 1 - \frac{e^{-\gamma}}{2} \sqrt{\frac{4m}{m+2}} R \left[ (1-\gamma) - \frac{1}{2} \ln \left( \frac{e^{-\gamma}}{2} \sqrt{\frac{4m}{m+2}} R \right) \right] \right)^{-1}, \quad (4.16)$$

for  $\sqrt{\frac{4m}{m+2}} R \leq 1.15$  and

$$\epsilon(R) \rightarrow -1 - \sqrt{2\pi} \frac{e^{-\sqrt{\frac{4m}{m+2}} R}}{\sqrt{\left(\sqrt{\frac{4m}{m+2}}\right)^{\frac{1}{2}} R}}, \quad (4.17)$$

for  $\sqrt{\frac{4m}{m+2}} R \geq 1.15$ . Notice that this approximation is very accurate even when  $2R \approx 1.15\sqrt{(1+2/m)}$  where the largest deviation of 9% is reached.

The Schrödinger equation for the heavy-heavy system in Eq. (4.5) is transformed in a Sturm-Liouville eigenvalue equation in a  $L_z = 0$  state. The

wave function  $\phi(R)$  is replaced by  $\frac{\chi(R)}{\sqrt{R}}$  giving

$$\left[ -\left( \frac{d^2}{dR^2} + \frac{1}{4R^2} \right) + v_c(R) + \epsilon(R) \right] \chi(R) = E_3 \chi(R), \quad (4.18)$$

where  $E_3$  is the three-body energy and  $\epsilon(R)$  is given in Eqs. (4.16) and (4.17). Genuinely bound states are present when  $E_3 - E_2 \leq 0$ , or equivalently  $|E_3| \geq |E_2|$ , since bound states have negative energies.

The differential equation (4.18) is numerically solved to estimate the number of bound states ( $N_B$ ) for a system with mass ratio  $m$  when the heavy particles do not interact with each other. Due to the attractive centrifugal barrier in 2D, all the two-body subsystems interact with finite energy. This means that  $E_{ab} = 0$  implies in a non-interacting  $ab$  subsystem. Once the heavy-heavy is not interacting,  $E_{ab} = 0$  is translated to  $v_c = 0$  in Eq. (4.18). If  $v_c$  is attractive and able to support bound states, the three-body system would effectively be reduced to the lightest particle moving around a heavy-heavy dimer. The corresponding additional much deeper-lying bound states are, however, not interesting in the present context.

The method to solve Eq. (4.18) numerically consists in writing this eigenvalue equation in matrix form. The operators, potential, wave function and the radial coordinate in this equation are discretized, which leads to a tridiagonal matrix form. This tridiagonal matrix is then diagonalized to give the eigenvalues of the problem. It is also possible to calculate the number of bound states ( $N_B$ ) by solving the set of homogeneous integral equations (2.68).

Counting the number of bound states, a critical mass ratio ( $m_t$ ) is introduced, above which  $N_B$  bound states are available. These critical values are shown in Fig. 4.4, where a comparison between the solutions of the differential equation (4.18) and homogeneous coupled integral equations (2.68) is made.

The results in Fig. 4.4 show that the adiabatic approximation picks up the small mass behavior very well, even for mass ratios up towards 1. There is a small error in the threshold for the number of available bound states



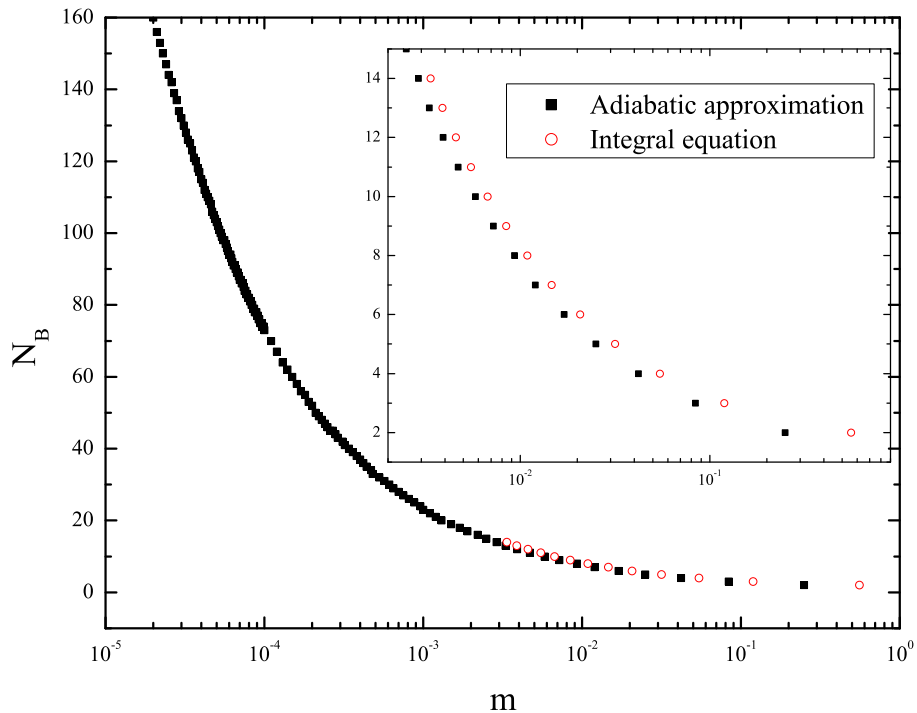


Figure 4.4: Number of possible bound states ( $N_B$ ) for a system with masses  $(1, 1, m)$  and  $E_{ab} = 0$ . The (black) squares represent the mass ratio  $m$  from where  $N_B$  states are bound, calculated through the adiabatic approximation (4.18). The (red) circles represent the solutions of the set of coupled homogeneous integral equations (2.68).

for  $0 \leq N_B \leq 14$ , but it decreases as  $m \rightarrow 0$ . The adiabatic approximation has an accuracy better than 10% for  $m = 0.01$ , as it can be seen in the inset of Fig. 4.4. Due to the numerical difficulties, it is very hard to count the number of bound states for  $N_B > 14$  by solving the set of coupled homogeneous integral equation (2.68). Fortunately, it is very easy to do it with the differential equation (4.18). It is clearly possible to see in Fig. 4.4, that  $N_B \rightarrow \infty$  for  $m \rightarrow 0$  as it was pointed out in the last section.

## 4.4 Estimate of the number of bound states

A fit to the results presented in Fig. 4.4 shows that the dependence of the number of bound states,  $N_B$ , with the mass ratio,  $m$ , is rather well described

by

$$N_B \approx \frac{0.731}{\sqrt{m}} . \quad (4.19)$$

This behavior can be explained by the old quantum mechanics. An usual way to estimate the number of bound states in a semi-classical approximation of the one-dimensional quantum problem is

$$\int p \, dq = N\pi\hbar . \quad (4.20)$$

Taking into account the effective potential in Eq.(4.18) and proper units, the number of bound states with energy up to  $E_3 = 0$  is estimated as

$$N = \frac{1}{\pi\sqrt{2m}} \int_0^\infty dx \sqrt{\frac{m}{2x^2} - V(x)} = \frac{0.733}{\sqrt{m}} , \quad (4.21)$$

where  $V(x)$  is the adiabatic potential (4.16) and (4.17) with  $x = \sqrt{\frac{4m}{m+2}}R$ . One could argue that the integral in Eq.(4.21) diverges in both limits and can not be performed. Introducing a lower and an upper cut-off in the integral, which are the same used in the numerical calculation ( $10^{-2}$  and  $10^5$  respectively), the result is  $N = \frac{0.766}{\sqrt{m}}$ . This result approaches the estimate given in Eq. (4.19) as the diverging term on Eq.(4.21) becomes less important when  $m$  becomes smaller. The integral in Eq.(4.21) is practically  $m$ -independent for  $m \leq 0.001$  with the  $10^{-2}$  cut-off, implying that the term  $m/x^2$  is negligibly small by itself. The apparent divergences are due to the semi-classical estimate, and accurately removed by cut-off at both small and large  $x$ . The true quantum mechanical number of states are then recovered.

The estimate of the number of bound states in (4.19) and (4.21) nicely agree. Besides that, this estimate is less than the upper limit for a two-dimensional system with total angular momentum equal to zero, which is given in [Khuri 2002]. For the adiabatic potential (4.16) and (4.17), this upper limit is given by  $N = \frac{0.5}{m}$ . The difference between both estimates is shown in Fig. 4.5. It was shown in Chapter 3 that any three-body system in two dimensions will achieve its maximum number of bound states when all

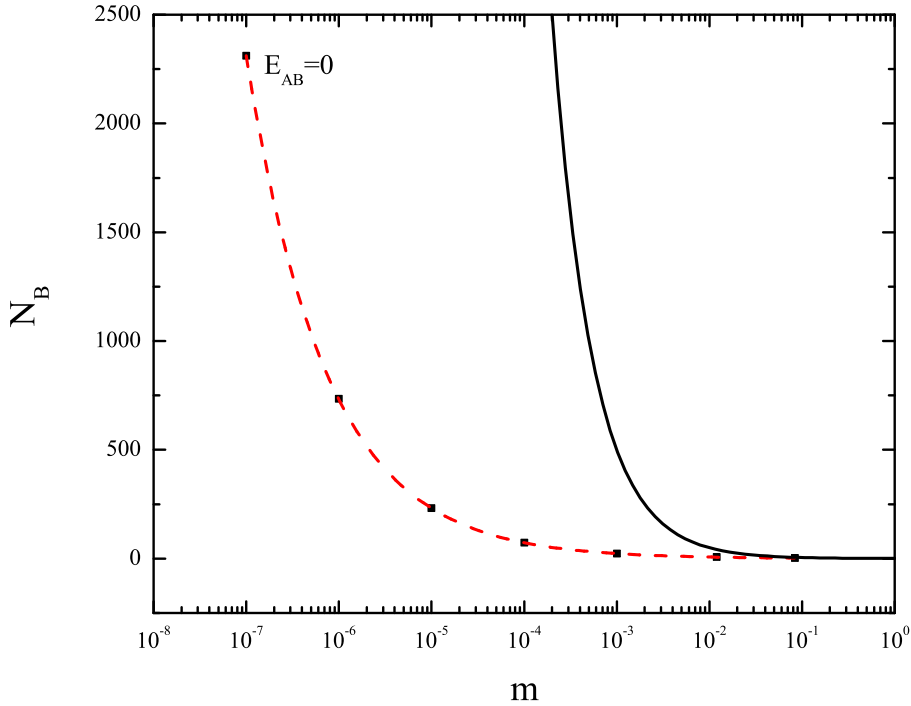


Figure 4.5: Number of possible bound states ( $N_B$ ) for a system with masses  $(1, 1, m)$  for  $E_{ab} = 0$  (red-dashed line) given in Eq. (4.21) and  $E_{ab} = 1$  given in Ref. [Khuri 2002] (black-full line). The black squares represent some of the points from Fig. 4.4.

subsystem are bound with the same energy [Bellotti 2012] (notice that the richest energy spectrum in 2D requires a large mass asymmetry, but on the other hand the energies have to be symmetric). So, it is expected that the estimate given by the solid-black curve in Fig. 4.5 will hold for the adiabatic potential (4.16) and (4.17) when  $E_{ab} = E_2$ , since this situation gives the upper limit in the number of bound states of 2D three-body systems. Also, the number of bound states for a system with  $0 \leq |E_{ab}| \leq E_2$  is in the window between the black-solid curve and the red-dashed curve shown in Fig. 4.5.

As expected, the results confirm that the bound states accumulate in both  $R \rightarrow 0$  and  $R \rightarrow \infty$  as  $m \rightarrow 0$ . The energy of the lowest states seems to increase without boundaries in this limit and the wave function vanishes slower at large distances, allowing more bound states. This can be interpreted as an Efimov-like effect for the two dimensional case, however, an

important distinction between the 2D and 3D case must be done. While the Efimov effect says that three identical particles can have infinitely many bound states when  $E_2 \rightarrow 0$ , in 2D this limit leads to an unbound three-body system. Infinitely many bound states are only expected in 2D when  $m = 0$ . Therefore, finite  $m_c$  leads to a finite number of bound states.

# Momentum distribution in 2D

---

Another important theoretical prediction for cold atomic systems, which was reported in Ref. [Tan 2008], is a parameter that emerges in the study of two-component Fermi gases. This parameter, which is often called Tan's contact or two-body contact parameter and represented by  $C_2$ , connects universal two-body correlations and many-body properties. For instance, the variation in the energy of a two-component Fermi gas of momentum  $k_F$  with the interaction strength (scattering length  $a$ ) is directly proportional to this parameter [Tan 2008], as it can be seen in

$$2\pi \frac{dE}{d[-1/(k_F a)]} = C_2. \quad (5.1)$$

Furthermore, the virial theorem for this atomic gas also relates with  $C_2$  through

$$E - 2V = -\frac{C_2}{4\pi k_F a}. \quad (5.2)$$

These relations were confirmed in experiments with two-component Fermi gases [Kuhle 2010], where each side of Eqs. (5.1) and (5.2) were measured independently and after compared to each other. A later experiment showed that these relations also hold for bosons [Wild 2012].

The quantities in the left-hand-side of Eqs. (5.1) and (5.2) are defined through the many-body properties of the gas, while the contact parameter is defined in the few-body sector. A way to determine this parameter is to find the coefficient in the leading order of the asymptotic one-body large momentum density ( $n(q)$ ) of few-body systems, namely

$$\lim_{q \rightarrow \infty} n(q) \rightarrow \frac{C_2}{q^4} + C_3 F(q). \quad (5.3)$$

The next order in this expansion defines the three-body contact parameter,  $C_3$ , which may be important only for bosonic systems, since the Pauli principle suppresses the short-range correlations for two-component Fermi gases. Notice that the momentum dependence of the leading order term in this expansion is the same for 1D, 2D and 3D systems [Valiente 2012], but the function  $F(q)$ , which is strongly related to the spectator functions, depends on the the dimensionality of the system [Bellotti 2013a].

The spectator functions are the key ingredients for understanding the asymptotic one-body momentum densities of few-body systems. While the large momentum asymptotic behavior of such functions is well-known for 3D systems [Danilov 1961], a striking result presented in this Chapter is the derivation of asymptotic expressions for the spectator functions of three-distinguishable bosons in 2D [Bellotti 2013a, Bellotti 2014]. Using the expression for the large momentum behavior, this asymptotic equation is extended to the full range of the momentum and used to calculate an analytic expression for  $C_2$  in the ground state.

For three identical bosons, the two-body contact parameter is found to be a universal constant, in the sense that  $\frac{C_2}{E_3}$  is the same for both states, each one described for a three-body energy  $E_3$  [Bellotti 2013a]. Furthermore, the three-body contact parameter has a very different behavior in 2D, when compared to 3D systems (the 3D system is discussed in Chapter 6).

It was showed in Chapters 3 and 4 that, in 2D, mixed-species systems have a richer energy spectrum than symmetric mass systems. So, it is important to understand how the asymptotic one-body momentum density changes when dealing with mixed-species systems in 2D. In this case,  $C_2$  is not a universal constant anymore, however the universality is recovered in at least one special case of a three-body system composed for two identical non-interacting particles. The sub-leading order in the asymptotic momentum density presents the same functional form for both equal masses and mixed-species systems [Bellotti 2014].

## 5.1 Asymptotic spectator function

Exhaustive numerical analysis of the spectator function in Eq. (2.70) for three-identical bosons strongly suggests that the large momentum asymptotic behavior of such functions is given by

$$\lim_{q \rightarrow \infty} f(q) \rightarrow \Gamma \frac{\ln q}{q^2}, \quad (5.4)$$

where  $\Gamma$  is a constant of normalization, as it can be seen in Fig. 5.1.

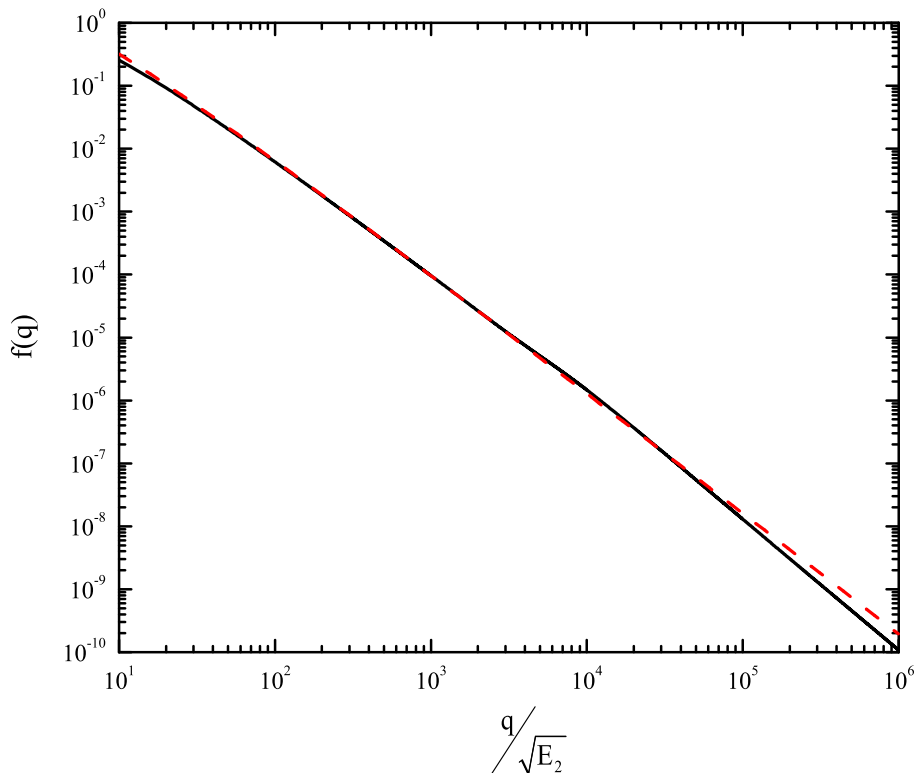


Figure 5.1: Spectator function,  $f(q)$ , for the ground state calculated numerically (black solid line) and using the ansatz  $f(q) = A_0 \frac{\ln q}{q^2}$  (red dashed line). The solid (black) line tends to oscillates around the dashed (red) one as  $q \rightarrow \infty$  due to finite numerical precision.

The ansatz in Eq. (5.4) are, in fact, the exact large momentum asymptotic expression of the spectator function, even for mass-imbalanced systems (within a constant). A system composed of three-distinguishable particles,

when all pairs are bound, have three distinct spectator functions in the wave function expressed by Eq. (2.67). However, their large-momentum asymptotic behavior all remain identical, except for individual proportionality factors. To prove that, Eq.(2.70) is rewritten as

$$f_\alpha(\mathbf{q}) = 2\pi\tau_\alpha(q, E_3) \left[ \int_0^\infty dk \frac{k f_\beta(k)}{\left(-E_3 + \frac{q^2}{2m_{\alpha\gamma}} + \frac{k^2}{2m_{\beta\gamma}}\right) \sqrt{1 - \frac{k^2 q^2 / m_\gamma^2}{\left(-E_3 + \frac{q^2}{2m_{\alpha\gamma}} + \frac{k^2}{2m_{\beta\gamma}}\right)^2}} + \int_0^\infty dk \frac{k f_\gamma(k)}{\left(-E_3 + \frac{q^2}{2m_{\alpha\beta}} + \frac{k^2}{2m_{\beta\gamma}}\right) \sqrt{1 - \frac{k^2 q^2 / m_\beta^2}{\left(-E_3 + \frac{q^2}{2m_{\alpha\beta}} + \frac{k^2}{2m_{\beta\gamma}}\right)^2}} \right], \quad (5.5)$$

with

$$\tau_\alpha(q, E_3) = \left[ 4\pi m_{\beta\gamma} \ln \left( \sqrt{\frac{\frac{q^2}{2m_{\beta\gamma,\alpha}} - E_3}{E_{\beta\gamma}}} \right) \right]^{-1}, \quad (5.6)$$

where  $m_{\beta\gamma,\alpha} = m_\alpha(m_\beta + m_\gamma)/(m_\alpha + m_\beta + m_\gamma)$  and  $m_{\beta\gamma} = (m_\beta + m_\gamma)/(m_\beta + m_\gamma)$  are reduced masses,  $E_{\beta\gamma}$  the two-body energy and  $(\alpha, \beta, \gamma)$  are cyclic permutations of the particle labels  $(a, b, c)$ . The two terms on the right-hand-side of Eq.(5.5) have the same form, and one can be obtained from the other by interchanging labels  $\beta$  and  $\gamma$ . Therefore it suffices to calculate the first integral in Eq.(5.5).

The contribution for large  $q$  can, in principle, be collected from  $k$ -values ranging from zero to infinity. Separating small and large  $k$ -contributions, the integration is divided into two intervals, that is from zero to a large ( $q$ -independent) momentum  $\Lambda \gg \sqrt{E_3}$ , and from  $\Lambda$  to infinity. Thus, Eq. (5.5)



reads

$$f_\alpha(\mathbf{q}) = \tau_\alpha(q, E_3) \left[ \int_0^\Lambda dk \frac{k f_\beta(k)}{\left(E_3 + \frac{q^2}{2m_{\alpha\gamma}} + \frac{k^2}{2m_{\beta\gamma}}\right) \sqrt{1 - \frac{k^2 q^2 / m_\gamma^2}{\left(E_3 + \frac{q^2}{2m_{\alpha\gamma}} + \frac{k^2}{2m_{\beta\gamma}}\right)^2}} + \int_\Lambda^\infty dk \frac{k f_\beta(k)}{\left(\frac{q^2}{2m_{\alpha\gamma}} + \frac{k^2}{2m_{\beta\gamma}}\right) \sqrt{1 - \frac{k^2 q^2 / m_\gamma^2}{\left(E_3 + \frac{q^2}{2m_{\alpha\gamma}} + \frac{k^2}{2m_{\beta\gamma}}\right)^2}} + \dots \right], \quad (5.7)$$

where the dots indicate that the second term in Eq.(5.5) should be added.

For  $q \rightarrow \infty$  the first term,  $f_{\alpha,1}$ , on the right-hand-side of Eq.(5.7) goes to zero as

$$\lim_{q \rightarrow \infty} f_{\alpha,1}(q) \rightarrow \frac{m_{\alpha\gamma} / m_{\beta\gamma}}{q^2 \ln(q)} \int_0^\Lambda dk \frac{k f_\beta(k)}{\sqrt{1 - \frac{k^2 q^2 / m_\gamma^2}{\left(E_3 + \frac{q^2}{2m_{\alpha\gamma}} + \frac{k^2}{2m_{\beta\gamma}}\right)^2}}, \quad (5.8)$$

where  $\lim_{q \rightarrow \infty} \tau_\alpha(q, E_3) \rightarrow [2m_{\beta\gamma} \ln q]^{-1}$ , and both  $E_3$  and  $\frac{k^2}{2m_{\beta\gamma}}$  are much smaller than  $\frac{q^2}{2m_{\alpha\gamma}}$ . The integral in Eq. (5.8) is finite and only weakly  $q$ -dependent for large  $q \gg \Lambda$ .

The asymptotic spectator function in Eq.(5.4) can be inserted in the second term on the right-hand-side of Eq.(5.7),  $f_{\alpha,2}$ , because in the asymptotic limit  $k > \Lambda$ . In the limit of large momentum, i.e.,  $q \rightarrow \infty$ ,  $f_{\alpha,2}$  is

$$\begin{aligned} \lim_{q \rightarrow \infty} f_{\alpha,2}(q) &\rightarrow \frac{\Gamma_\beta}{2m_{\beta\gamma} \ln q} \int_\Lambda^\infty dk \frac{\ln k}{k \left(\frac{q^2}{2m_{\alpha\gamma}} + \frac{k^2}{2m_{\beta\gamma}}\right) \sqrt{1 - \frac{k^2 q^2 / m_\gamma^2}{\left(E_3 + \frac{q^2}{2m_{\alpha\gamma}} + \frac{k^2}{2m_{\beta\gamma}}\right)^2}}, \\ &\rightarrow \frac{\Gamma_\beta}{q^2 \ln q} \int_{\Lambda/q}^\infty dy \frac{\ln y + \ln q}{y \left(\frac{m_{\beta\gamma}}{m_{\alpha\gamma}} + y^2\right)}, \end{aligned} \quad (5.9)$$

with  $k = qy$  in the last expression. Carrying out the two integrals in Eq. (5.9)

results in

$$\begin{aligned} \int_{\Lambda/q}^{\infty} dy \frac{\ln y}{y \left( \frac{m_{\beta\gamma}}{m_{\alpha\gamma}} + y^2 \right)} &= \frac{1}{2} \frac{\ln^2 y}{\left( \frac{m_{\beta\gamma}}{m_{\alpha\gamma}} + y^2 \right)} \Big|_{\Lambda/q}^{\infty} + \int_{\Lambda/q}^{\infty} dy \frac{y \ln^2 y}{\left( \frac{m_{\beta\gamma}}{m_{\alpha\gamma}} + y^2 \right)^2} \\ &\rightarrow -\frac{m_{\alpha\gamma}}{2m_{\beta\gamma}} \ln^2 \left( \frac{\Lambda}{q} \right) \rightarrow -\frac{\ln^2 q}{2 \frac{m_{\beta\gamma}}{m_{\alpha\gamma}}}, \end{aligned} \quad (5.10)$$

$$\begin{aligned} \int_{\Lambda/q}^{\infty} dy \frac{1}{y \left( \frac{m_{\beta\gamma}}{m_{\alpha\gamma}} + y^2 \right)} &= \frac{\ln y}{\left( \frac{m_{\beta\gamma}}{m_{\alpha\gamma}} + y^2 \right)} \Big|_{\Lambda/q}^{\infty} + 2 \int_{\Lambda/q}^{\infty} dy \frac{y \ln y}{\left( \frac{m_{\beta\gamma}}{m_{\alpha\gamma}} + y^2 \right)^2} \\ &\rightarrow -\frac{m_{\alpha\gamma}}{m_{\beta\gamma}} \ln \left( \frac{\Lambda}{q} \right) \rightarrow \frac{\ln q}{\frac{m_{\beta\gamma}}{m_{\alpha\gamma}}}, \end{aligned} \quad (5.11)$$

where it is assumed that the integrals in the right-hand-side of Eqs. (5.10) and (5.11) are finite and their contributions can be neglected when  $q \rightarrow \infty$  in comparison with the terms carrying the log's.

Inserting Eqs. (5.10) and (5.11) in Eq.(5.9), the asymptotic expression of  $f_{\alpha,2}$  reads

$$\begin{aligned} \lim_{q \rightarrow \infty} f_{\alpha,2}(q) &\rightarrow \frac{\Gamma_{\beta}}{q^2 \ln q} \int_{\Lambda/q}^{\infty} dy \frac{\ln y + \ln q}{y \left( \frac{m_{\beta\gamma}}{m_{\alpha\gamma}} + y^2 \right)}, \\ &\rightarrow \frac{\Gamma_{\beta}}{q^2 \ln q} \left( -\frac{m_{\alpha\gamma}}{2m_{\beta\gamma}} \ln^2 q + \ln q \frac{m_{\alpha\gamma}}{m_{\beta\gamma}} \ln q \right), \\ &\rightarrow \frac{m_{\alpha\gamma}}{m_{\beta\gamma}} \Gamma_{\beta} \frac{\ln q}{q^2}. \end{aligned} \quad (5.12)$$

The missing term from Eq. (5.5) is recovered by interchanging the labels  $\gamma$  by  $\beta$  in Eq.(5.12). The large-momentum behavior of the spectator function is therefore

$$\lim_{q \rightarrow \infty} f_{\alpha}(q) \rightarrow \left( \frac{m_{\alpha\gamma}}{2m_{\beta\gamma}} \Gamma_{\beta} + \frac{m_{\alpha\beta}}{2m_{\beta\gamma}} \Gamma_{\gamma} \right) \frac{\ln q}{q^2}. \quad (5.13)$$

Replacing  $f_{\alpha}(q_{\alpha})$  in Eq. (5.13) by its conjectured asymptotic form, Eq. (5.4), results in a system of three linear equations for the three unknown,  $\Gamma_{\alpha} = \frac{m_{\alpha\gamma}}{2m_{\beta\gamma}} \Gamma_{\beta} + \frac{m_{\alpha\beta}}{2m_{\beta\gamma}} \Gamma_{\gamma}$ , which can be rewritten as  $m_{\beta\gamma} \Gamma_{\alpha} = m_{\alpha\gamma} \Gamma_{\beta} = m_{\alpha\beta} \Gamma_{\gamma}$ . The large-momentum asymptotic behavior for the three distinct spectator

functions are then

$$\lim_{q \rightarrow \infty} f_\alpha(q) \rightarrow \frac{\Gamma}{m_{\beta\gamma}} \frac{\ln q}{q^2}. \quad (5.14)$$

This result relates the asymptotic behavior of the three spectator functions for any state. The remaining constant  $\Gamma$  still depends on which excited state is considered, and also on two-body masses, energies and normalization.

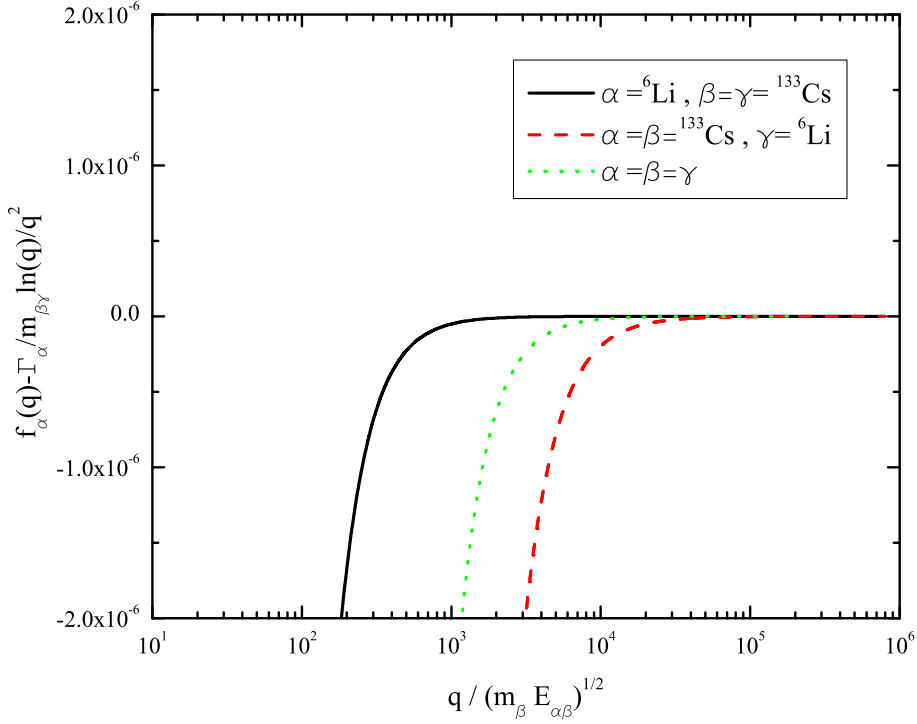


Figure 5.2: The difference  $f_\alpha(q) - \frac{\Gamma}{m_{\beta\gamma}} \frac{\ln q}{q^2}$  as a function of the momentum  $q$ . The solid (black) and dash (red) lines are respectively the spectator function of  ${}^6\text{Li}$  and  ${}^{133}\text{Cs}$  in a  ${}^{133}\text{Cs}$ - ${}^{133}\text{Cs}$ - ${}^6\text{Li}$  system. The dot (green) line is the spectator function of a system composed for three identical bosons. Notice that Eq. (5.14) exactly describes the asymptotic spectator function, up to the numerical accuracy.

The derived large momentum asymptotic expression and the coefficients in Eq.(5.14) beautifully agree with the numerical calculation. In Fig. 5.2, the difference  $f_\alpha(q) - \frac{\Gamma}{m_{\beta\gamma}} \frac{\ln q}{q^2}$  is plotted as function of the momentum  $q$  for the two different spectator functions in the  ${}^{133}\text{Cs}$  ${}^{133}\text{Cs}$  ${}^6\text{Li}$  system. The same difference for a three-body system composed of identical bosons is also

shown. The nice agreement between the analytic derivation and the numerical calculation demonstrate that the large momentum asymptotic behavior is always  $\ln q/q^2$  for any spectator function in  $2D$  three-body systems.

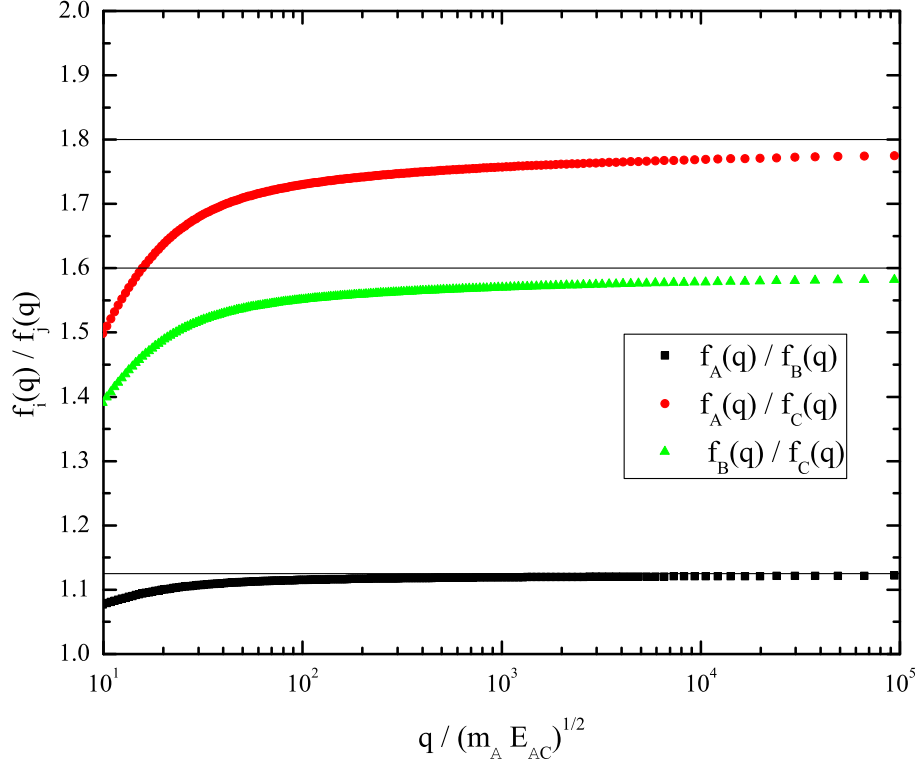


Figure 5.3: Ratios between the three distinct spectator function for a generic case of three distinct particles. Discrete points are the ratios between spectator functions numerically calculated from Eq. (2.70) and full lines are ratios between coefficients in Eq.(5.14).

The general behavior of the large-momentum asymptotic form of the spectator function is further demonstrated in Fig. 5.3 for a system of three distinct particles. The numerically calculated points are compared to the full lines obtained from Eq. (5.14). This comparison is again consistent with the derived asymptotic behavior, and furthermore exhibit the rate and accuracy of the convergence. The limit is reached within 10% and 1% already for  $q \approx 50$  and  $q \approx 10^4$ , respectively.

### 5.1.1 Parameterizing from small to large momenta

The asymptotic spectator function in Eq. (5.14) seems to be a good approximation even for moderate values of  $q$ , e.g.,  $q \approx 3\sqrt{E_3}$ . Information about the large-distance behavior for a given binding energy is also available, that is  $\exp(-\kappa\rho)$ , where  $\kappa$  is related to the binding energy and  $\rho$  is the hyper-radius. Fourier transformation then relates to the small momentum limit with an overall behavior of  $(D + q^2)^{-1}$ , where  $D$  is a constant related to the energy. This perfectly matches Eq. (2.67) when two Jacobi momenta are present as in the three-body system. Therefore, a parametrization combining the expected small momenta with the known large-momentum behavior is attempted. The result is

$$f_\alpha(q) = f_\alpha(0) \frac{E_3}{\ln \sqrt{E_3}} \frac{\ln \left( \sqrt{\frac{q^2}{2m_{\beta\gamma,\alpha}} + E_3} \right)}{\frac{q^2}{2m_{\beta\gamma,\alpha}} + E_3}, \quad (5.15)$$

where  $f_\alpha(0)$  is a normalization constant of the one-body momentum density,  $n(q_\alpha)$ , which satisfies  $\int d^2q_\alpha n(q_\alpha) = 1$ .

Notice that excited states with the same angular structure must have a different number of radial nodes. Therefore the focus here is only on the ground state. The expression in Eq.(5.15) parametrizes the small momentum behavior of the ground state spectator functions in general cases. As an example, a system composed of two-identical bosons and a distinct particle is shown in Fig. 5.4, where the numerical and parametrized solutions are compared. However, when small momenta are reproduced the large-momentum limit deviates in overall normalization, although with the same  $q$ -dependence. Surprisingly, the analytic expression is most successful for the spectator function related to the heaviest particle in the three-body system. This large-momentum mismatch is due to the normalization choice in Eq.(5.15), which is chosen to exactly reproduce the  $q = 0$  limit.

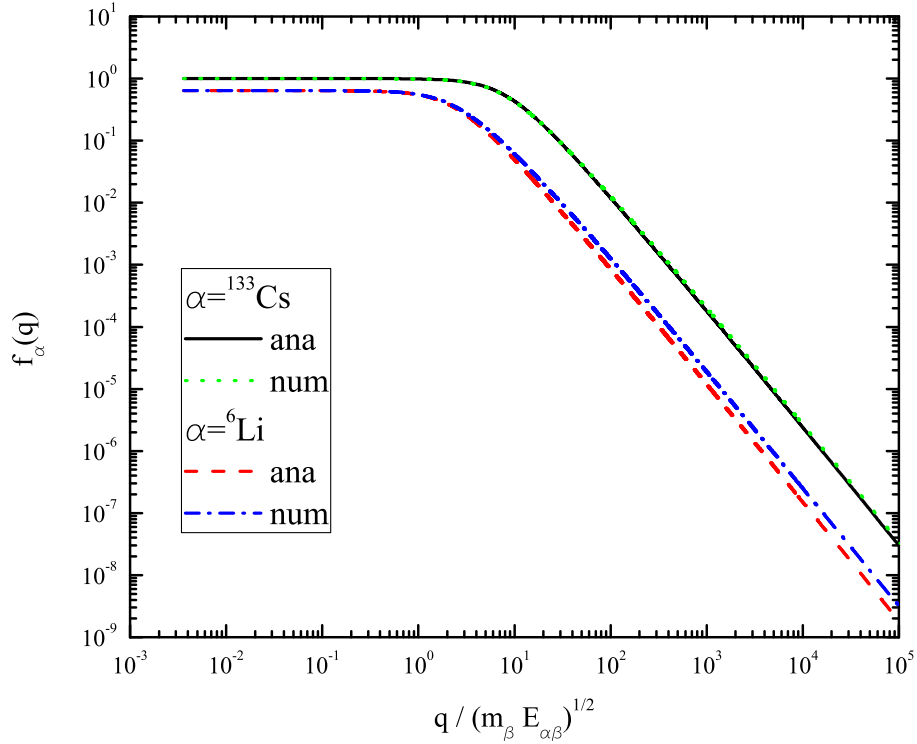


Figure 5.4: Comparison between the analytic spectator function estimated for the ground state given in Eq. (5.15) and the numeric solution of Eq. (2.70), for a  $^{133}\text{Cs}$ - $^{133}\text{Cs}$ - $^6\text{Li}$  system. The solid (black) and dot (green) lines are the analytic estimative and the numeric result for the  $^{133}\text{Cs}$  spectator function. The dash (red) and dash-dot (blue) lines are the analytic estimative and the numeric result for the  $^6\text{Li}$  spectator function.

## 5.2 Asymptotic one-body densities

The one-body density functions are observable quantities and the most directly measurable part is the limit of large momenta, which has already been observed in experiments using time-of-flight and the mapping to momentum space [Stewart 2010], Bragg spectroscopy [Kuhnle 2010] or momentum-resolved photo-emission spectroscopy [Fröhlich 2011]. The one-body momentum density of the particle  $\alpha$  is defined as  $n(q_\alpha) = \int d^2p_\alpha |\Psi(\mathbf{q}_\alpha, \mathbf{p}_\alpha)|^2$ , where  $\Psi(\mathbf{q}_\alpha, \mathbf{p}_\alpha)$  is given in Eq. (2.67). From now on, the normalization is  $\int d^2q_\alpha n(q_\alpha) = 1$ . The nine terms in  $\int d^2p_\alpha |\Psi(\mathbf{q}_\alpha, \mathbf{p}_\alpha)|^2$  are then grouped into four components with distinctly different integrand structure.

The one-body momentum density is expressed as a sum of four terms, i.e.,  $n(q_\alpha) = \sum_{i=1}^4 n_i(q_\alpha)$  [Bellotti 2013a, Bellotti 2014].

A general system of three distinguishable particles, presents three distinct one-body momentum density distributions, each one corresponding to a different particle. The four terms for particle  $\alpha$  are expressed as

$$n_1(q_\alpha) = |f_\alpha(q_\alpha)|^2 \int d^2 p \frac{1}{\left(-E_3 + \frac{q_\alpha^2}{2m_{\beta\gamma,\alpha}} + \frac{p^2}{2m_{\beta\gamma}}\right)^2} = \frac{2\pi m_{\beta\gamma} |f_\alpha(q_\alpha)|^2}{-E_3 + \frac{q_\alpha^2}{2m_{\beta\gamma,\alpha}}}, \quad (5.16)$$

$$n_2(q_\alpha) = \int d^2 k \frac{|f_\beta(k)|^2}{\left(-E_3 + \frac{q_\alpha^2}{2m_{\alpha\gamma}} + \frac{k^2}{2m_{\beta\gamma}} + \frac{\mathbf{k}\cdot\mathbf{q}_\alpha}{m_\gamma}\right)^2} + \int d^2 k \frac{|f_\gamma(k)|^2}{\left(-E_3 + \frac{q_\alpha^2}{2m_{\alpha\beta}} + \frac{k^2}{2m_{\beta\gamma}} - \frac{\mathbf{k}\cdot\mathbf{q}_\alpha}{m_\beta}\right)^2}, \quad (5.17)$$

$$n_3(q_\alpha) = 2f_\alpha(q_\alpha) \left[ \int d^2 k \frac{f_\beta(k)}{\left(-E_3 + \frac{q_\alpha^2}{2m_{\alpha\gamma}} + \frac{k^2}{2m_{\beta\gamma}} + \frac{\mathbf{k}\cdot\mathbf{q}_\alpha}{m_\gamma}\right)^2} + \int d^2 k \frac{f_\gamma(k)}{\left(-E_3 + \frac{q_\alpha^2}{2m_{\alpha\beta}} + \frac{k^2}{2m_{\beta\gamma}} - \frac{\mathbf{k}\cdot\mathbf{q}_\alpha}{m_\beta}\right)^2} \right], \quad (5.18)$$

$$n_4(q_\alpha) = \int d^2 k \frac{f_\beta(k)f_\gamma(|\mathbf{k} + \mathbf{q}_\alpha|)}{\left(-E_3 + \frac{q_\alpha^2}{2m_{\alpha\gamma}} + \frac{k^2}{2m_{\beta\gamma}} + \frac{\mathbf{k}\cdot\mathbf{q}_\alpha}{m_\gamma}\right)^2} + \int d^2 k \frac{f_\gamma(k)f_\beta(|\mathbf{k} + \mathbf{q}_\alpha|)}{\left(-E_3 + \frac{q_\alpha^2}{2m_{\alpha\beta}} + \frac{k^2}{2m_{\beta\gamma}} + \frac{\mathbf{k}\cdot\mathbf{q}_\alpha}{m_\beta}\right)^2}. \quad (5.19)$$

where the integration variable originating from Eq. (2.67) are properly redefined to simplify the arguments of the spectator functions in the integrands. Only  $n_4$  is then left with an angular dependence through the spectator functions. The distributions for the other particles are obtained by cyclic permutations of  $(\alpha, \beta, \gamma)$  in these expressions.

The large-momentum limit of the four terms in Eqs. (5.16) to (5.19) is considered separately. In three dimensions (3D), the similar problem is solved by inserting the correspondent asymptotic spectator function into

each of the four terms in Eqs. (5.16) to (5.19), and evaluating the corresponding integrals [Castin 2011, Yamashita 2013]. This procedure is not guaranteed to work in 2D because smaller than asymptotic momentum values may contribute in the integrands. However, for 3D it was shown that the leading order in the integrands is sufficient to provide both leading and next to leading order of the one-body momentum distributions. The details of these calculation in 3D can be found in [Castin 2011] for three identical bosons and in [Yamashita 2013] for mass-imbalanced systems. The 3D momentum distributions are discussed in Chapter 6.

The large-momentum behavior of the spectator functions changes a lot with dimension, going from  $\sin(\ln(q))/q^2$  in 3D to  $\ln(q)/q^2$  in 2D. Naively proceeding in 2D as successfully done in 3D, the integrals in Eqs. (5.16) to (5.19) diverge. This divergence problem is circumvented by following the procedure used in the derivation of the asymptotic spectator functions. In the following, each of the four momentum components defined in Eqs. (5.16) to (5.19) are worked out. In addition, the next-to-leading order term arising from the dominant  $n_2$ -term must be simultaneously considered, since it has the same order as the leading order of  $n_3$ - and  $n_4$ -terms.

### 5.2.1 Asymptotic contribution from $n_1(q_\alpha)$

This term is straightforward to calculate. The argument of the spectator function in Eq. (5.16) does not depend on the integration variable. The large-momentum limit is then found by replacing the spectator function by its asymptotic form and taking the large  $q$  limit after a simple integration, resulting in

$$\lim_{q_\alpha \rightarrow \infty} n_1(q_\alpha) \rightarrow 4\pi m_{\beta\gamma,\alpha} m_{\beta\gamma} \frac{|f_\alpha(q_\alpha)|^2}{q_\alpha^2} \rightarrow 4\pi \frac{m_{\beta\gamma,\alpha}}{m_{\beta\gamma}} \Gamma^2 \frac{\ln^2(q_\alpha)}{q_\alpha^6}. \quad (5.20)$$

### 5.2.2 Asymptotic contribution from $n_2(q_\alpha)$

Integrating the two terms in Eq. (5.17) over the angle is possible, once the integrand has a simple structure where the spectator function is angle



independent. The result

$$\begin{aligned}
n_2(q_\alpha) = 2\pi \int_0^\infty dk \frac{k |f_\beta(k)|^2 \left(-E_3 + \frac{q_\alpha^2}{2m_{\alpha\gamma}} + \frac{k^2}{2m_{\beta\gamma}}\right)}{\left[\left(-E_3 + \frac{q_\alpha^2}{2m_{\alpha\gamma}} + \frac{k^2}{2m_{\beta\gamma}}\right)^2 - \frac{k^2 q_\alpha^2}{m_\gamma^2}\right]^{3/2}} \\
+ 2\pi \int_0^\infty dk \frac{k |f_\gamma(k)|^2 \left(-E_3 + \frac{q_\alpha^2}{2m_{\alpha\beta}} + \frac{k^2}{2m_{\beta\gamma}}\right)}{\left[\left(-E_3 + \frac{q_\alpha^2}{2m_{\alpha\beta}} + \frac{k^2}{2m_{\beta\gamma}}\right)^2 - \frac{k^2 q_\alpha^2}{m_\beta^2}\right]^{3/2}}
\end{aligned} \tag{5.21}$$

is then expanded for large  $q$ . Since  $\int_0^\infty dk k |f_\alpha(k)|^2$  is finite, the large momentum expansion becomes

$$\begin{aligned}
\lim_{q_\alpha \rightarrow \infty} n_2(q_\alpha) &\rightarrow \frac{8\pi}{q_\alpha^4} \left( m_{\alpha\gamma}^2 \int_0^\infty dk k |f_\beta(k)|^2 + m_{\alpha\beta}^2 \int_0^\infty dk k |f_\gamma(k)|^2 \right) + n_5(q_\alpha), \\
&\equiv \frac{C_{\beta\gamma}}{q_\alpha^4} + n_5(q_\alpha),
\end{aligned} \tag{5.22}$$

where  $C_{\beta\gamma}$  is the so-called two-body contact parameter.

As mentioned before, the second term on the right-hand-side of Eq. (5.22),  $n_5(q_\alpha)$ , which is sub-leading term in the expansion of  $n_2(q_\alpha)$  has the same asymptotic behavior as  $n_3(q_\alpha)$  and  $n_4(q_\alpha)$ . This term is kept and derived later.

It is important to emphasize that the one-body large-momentum leading order term comes only from  $n_2(q_\alpha)$ . The spectator function can not be replaced by its asymptotic expression, because the main contribution to  $\int_0^\infty dk k |f_\alpha(k)|^2$  arises from small  $k$ . This replacement would therefore lead to a completely wrong result. However, this is not always the case, as later shown for  $n_5(q_\alpha)$ .

### 5.2.3 Asymptotic contribution from $n_3(q_\alpha)$

The structure of  $n_3(q_\alpha)$  in Eq. (5.18) is similar to  $n_2(q_\alpha)$  in Eq. (5.17). The only difference is that the spectator function under the integration sign is not squared anymore. This functional difference leads to a completely different

result. The angular integration, which only involves the denominator, can still be carried out as in the previous case. Integrating Eq. (5.18) over the angle gives

$$n_3(q_\alpha) = 4\pi f_\alpha(q_\alpha) \left( \int_0^\infty dk \frac{k f_\beta(k) \left( -E_3 + \frac{q_\alpha^2}{2m_{\alpha\gamma}} + \frac{k^2}{2m_{\beta\gamma}} \right)}{\left[ \left( -E_3 + \frac{q_\alpha^2}{2m_{\alpha\gamma}} + \frac{k^2}{2m_{\beta\gamma}} \right)^2 - \frac{k^2 q_\alpha^2}{m_\gamma^2} \right]^{3/2}} + \int_0^\infty dk \frac{k f_\gamma(k) \left( -E_3 + \frac{q_\alpha^2}{2m_{\alpha\beta}} + \frac{k^2}{2m_{\beta\gamma}} \right)}{\left[ \left( -E_3 + \frac{q_\alpha^2}{2m_{\alpha\beta}} + \frac{k^2}{2m_{\beta\gamma}} \right)^2 - \frac{k^2 q_\alpha^2}{m_\beta^2} \right]^{3/2}} \right). \quad (5.23)$$

Here, the difference between  $n_2$  and  $n_3$  becomes important. Since the integral  $\int_0^\infty dk k f(k)$  is divergent, Eq. (5.23) can not be expanded as done for Eq. (5.21). Instead, the trick is to proceed as done in obtaining the asymptotic spectator function. The integration in Eq. (5.23) is separated a large, but finite, momentum,  $\Lambda \gg \sqrt{E_3}$ , and each term on the right-hand-side is then split in two others. The two terms only differ by simple factors, and therefore details are only given for the first term. Changing variables to  $k = q_\alpha y$ , Eq. (5.23) becomes

$$\lim_{q_\alpha \rightarrow \infty} n_3(q_\alpha) \rightarrow 16\pi m_{\beta\gamma}^2 \frac{f_\alpha(q_\alpha)}{q_\alpha^2} \int_0^{\Lambda/q_\alpha} dy \frac{y f_\beta(q_\alpha y) \left( -\frac{2m_{\beta\gamma} E_3}{q_\alpha^2} + \frac{m_{\beta\gamma}}{m_{\alpha\gamma}} + y^2 \right)}{\left[ \left( -\frac{2m_{\beta\gamma} E_3}{q_\alpha^2} + \frac{m_{\beta\gamma}}{m_{\alpha\gamma}} + y^2 \right)^2 - \frac{4m_{\beta\gamma}^2}{m_\gamma^2} y^2 \right]^{3/2}} + 16\pi m_{\beta\gamma}^2 \frac{f_\alpha(q_\alpha)}{q_\alpha^4} \frac{\Gamma}{m_{\alpha\gamma}} \int_{\Lambda/q_\alpha}^\infty dy \frac{[\ln(q_\alpha) + \ln(y)] \left( \frac{m_{\beta\gamma}}{m_{\alpha\gamma}} + y^2 \right)}{y \left[ \left( \frac{m_{\beta\gamma}}{m_{\alpha\gamma}} + y^2 \right)^2 - \frac{4m_{\beta\gamma}^2}{m_\gamma^2} y^2 \right]^{3/2}} + \dots, \quad (5.24)$$

where  $f_\beta(k)$  is replaced by its asymptotic form and  $E_3$  is neglected in the second term on the right-hand-side, where  $\sqrt{E_3} \ll \Lambda$  and  $k > \Lambda$ . In the limit  $q_\alpha \rightarrow \infty$ , the integral in the first term on the right-hand-side of Eq. (5.24) vanishes and therefore does not contribute to the large-momentum limit.

The integrals in the second term are

$$\begin{aligned} \int_{\Lambda/q_\alpha}^{\infty} dy \frac{\ln(y) h(y)}{y} &= \frac{1}{2} \ln^2(y) h(y) \Big|_{\Lambda/q_\alpha}^{\infty} - \frac{1}{2} \int_{\Lambda/q_\alpha}^{\infty} dy \ln^2(y) g(y) \\ &\rightarrow -\frac{m_{\alpha\gamma}^2}{2m_{\beta\gamma}^2} \ln^2\left(\frac{\Lambda}{q_\alpha}\right) \rightarrow -\frac{m_{\alpha\gamma}^2}{2m_{\beta\gamma}^2} \ln^2(q_\alpha), \end{aligned} \quad (5.25)$$

$$\begin{aligned} \int_{\Lambda/q_\alpha}^{\infty} dy \frac{h(y)}{y} &= \ln(y) h(y) \Big|_{\Lambda/q_\alpha}^{\infty} - \int_{\Lambda/q_\alpha}^{\infty} dy \ln(y) g(y) \\ &\rightarrow -\frac{m_{\alpha\gamma}^2}{m_{\beta\gamma}^2} \ln\left(\frac{\Lambda}{q_\alpha}\right) \rightarrow \frac{m_{\alpha\gamma}^2}{m_{\beta\gamma}^2} \ln(q_\alpha), \end{aligned} \quad (5.26)$$

where

$$h(y) = \left( \frac{m_{\beta\gamma}}{m_{\alpha\gamma}} + y^2 \right) \left[ \left( \frac{m_{\beta\gamma}}{m_{\alpha\gamma}} + y^2 \right)^2 - \frac{4m_{\beta\gamma}^2}{m_\gamma^2} y^2 \right]^{-3/2}, \quad (5.27)$$

$$g(y) = \frac{d h(y)}{dy}, \quad \lim_{y \rightarrow 0} \ln^2(y) g(y) \rightarrow 0, \quad \lim_{y \rightarrow \infty} \ln^2(y) g(y) \rightarrow 0. \quad (5.28)$$

The function  $g(y)$  and its limits ensure that the integrals on the right-hand-side of Eqs. (5.25) and (5.26) are finite and their contributions to the momentum distribution can be neglected when  $q_\alpha \rightarrow \infty$ .

Finally, inserting the results given in Eqs. (5.25) and (5.26) into Eq. (5.24) and replacing the spectator function  $f_\alpha(q_\alpha)$  by its asymptotic form, the  $n_3(q_\alpha)$  leading order term is given by

$$\lim_{q_\alpha \rightarrow \infty} n_3(q_\alpha) \rightarrow 8\pi \left( \frac{m_{\alpha\gamma} + m_{\alpha\beta}}{m_{\beta\gamma}} \right) \Gamma^2 \frac{\ln^3(q_\alpha)}{q_\alpha^6}, \quad (5.29)$$

where the second term in the right-hand-side of Eq. (5.23) is recovered and added by the interchange of  $m_{\alpha\gamma} \rightarrow m_{\alpha\beta}$  in Eqs. (5.24) to (5.26).

Although  $n_2(q_\alpha)$  and  $n_3(q_\alpha)$  have rather similar form, their contributions to the one-body large momentum density are quite different. The sub-leading order,  $n_5(q_\alpha)$ , of  $n_2(q_\alpha)$  is comparable to the  $n_3(q_\alpha)$  leading order, given in Eq. (5.29).

### 5.2.4 Asymptotic contribution from $n_4(q_\alpha)$

This is the most complicated of the four additive terms in the one-body momentum density. The angular dependence in both spectator arguments can not be removed simultaneously by variable change. The formulation in Eq. (5.19) has the advantage that the argument in  $f_\gamma(|\mathbf{k} + \mathbf{q}_\alpha|)$  (or in  $f_\beta(|\mathbf{k} + \mathbf{q}_\alpha|)$ ) is never small in the limit of large  $q_\alpha$ . This is in contrast with the choice of variables where the numerator in the first term of Eq. (5.19) would be  $f_\gamma(k)f_\beta(|\mathbf{k} - \mathbf{q}_\alpha|)$ , and the argument in  $f_\beta$  would consequently be small as soon as  $k$  is comparable to  $q_\alpha$ .

The main contribution to the integrals in Eq. (5.19) arise from small  $k$ . For large  $q_\alpha$ , the approximation,  $f_\gamma(|\mathbf{k} + \mathbf{q}_\alpha|) \approx f_\gamma(q_\alpha)$  (or  $f_\beta(|\mathbf{k} + \mathbf{q}_\alpha|) \approx f_\beta(q_\alpha)$ ) is used and the integrals are then identical to the terms of  $n_3$  in Eq. (5.18). Keeping track of the slightly different mass factors immediately leads the asymptotic limit to be

$$\lim_{q_\alpha \rightarrow \infty} n_4(q_\alpha) \rightarrow 4\pi \left( \frac{m_{\alpha\gamma}}{m_{\alpha\beta}} + \frac{m_{\alpha\beta}}{m_{\alpha\gamma}} \right) \Gamma^2 \frac{\ln^3(q_\alpha)}{q_\alpha^6}. \quad (5.30)$$

### 5.2.5 Asymptotic contribution from $n_5(q_\alpha)$

This is the next-to-leading order contribution from the  $n_2(q_\alpha)$  term. It turns out that this term has the same large-momentum behavior as the leading orders of both  $n_3(q_\alpha)$  and  $n_4(q_\alpha)$ . By definition

$$n_5(q_\alpha) = n_2(q_\alpha) - \lim_{q_\alpha \rightarrow \infty} n_2(q_\alpha) = n_2(q_\alpha) - \frac{C_{\beta\gamma}}{q_\alpha^4} \quad (5.31)$$

which can be rewritten in detail as

$$n_5(q_\alpha) = \lim_{q_\alpha \rightarrow \infty} 2\pi \int_0^\infty dk k |f_\beta(k)|^2 \times \left( \frac{\left( -E_3 + \frac{q_\alpha^2}{2m_{\alpha\gamma}} + \frac{k^2}{2m_{\beta\gamma}} \right)}{\left[ \left( -E_3 + \frac{q_\alpha^2}{2m_{\alpha\gamma}} + \frac{k^2}{2m_{\beta\gamma}} \right)^2 - \frac{k^2 q_\alpha^2}{m_\gamma^2} \right]^{3/2}} - \frac{4m_{\alpha\gamma}^2}{q_\alpha^4} \right) + \dots, \quad (5.32)$$

where the dots denote that the last term in Eq. (5.21) is obtained by interchange of labels  $\beta$  and  $\gamma$ . The tempting procedure is now to expand the integrand around  $q_\alpha = \infty$  assuming that  $q_\alpha$  overwhelms all terms in this expression. This immediately leads to integrals corresponding to the cubic momentum multiplying the spectator function which however is not converging. On the other hand Eq. (5.32) is perfectly well defined due to the large- $k$  cut-off from the denominator. In fact, the spectator function is multiplied by  $k^3$  and  $1/k^3$  at small and large  $k$ -values, respectively. The integrand therefore has a maximum where the main contribution to  $n_5$  arises. This peak in  $k$  moves towards infinity proportional to  $q$ .

Computing  $n_5(q_\alpha)$ , the integration is divided into two intervals, that is from zero to a finite but very large  $k$ -value,  $\Lambda_s$ , and from  $\Lambda_s$  to infinity. The small momentum interval,  $k/q_\alpha \ll 1$ , allows an expansion in  $k/q_\alpha$  leading to the following contribution  $n_{5,1}(q_\alpha)$ :

$$n_{5,1}(q_\alpha) = 8\pi \frac{m_{\alpha\gamma}^2}{q_\alpha^6} \left( 3 \frac{m_{\alpha\gamma}^2}{m_\gamma^2} - \frac{m_{\alpha\gamma}}{m_{\beta\gamma}} \right) \int_0^{\Lambda_s} dk k^3 |f_\beta(k)|^2 + \frac{\omega}{q_\alpha^8} \dots, \quad (5.33)$$

where  $\omega$  is constant. Thus, the contribution from this small momentum integration vanish with the 6'th power of  $q_\alpha$ , which is faster than the sub-leading orders of the other terms kept.

Choosing  $\Lambda_s$  sufficiently large such that the spectator function reaches its asymptotic behavior in Eq. (5.14), the momentum integration over larges values can now be performed by omitting the small  $E_3$ -terms and changing the integration variable to  $y$ , i.e.,  $k^2 = yq_\alpha^2$ , results in

$$n_{5,2}(q_\alpha) = \frac{\pi\Gamma^2}{q_\alpha^6} \int_{\Lambda_s^2/q_\alpha^2}^{\infty} \frac{dy}{y^2} \left[ \ln^2(y) + \ln^2(q_\alpha^2) + 2 \ln y \ln(q_\alpha^2) \right] \\ \times \left( \frac{1 + y m_{\alpha\gamma}/m_{\beta\gamma}}{\left[ (1 + y m_{\alpha\gamma}/m_{\beta\gamma})^2 - 4y m_{\alpha\gamma}^2/m_\gamma^2 \right]^{3/2}} - 1 \right) + \dots, \quad (5.34)$$

where the large  $y$ -limit behaves like  $\ln^2 y/y^4$  and therefore assuring rapid

convergence, whereas the integrand for small  $y$  behaves like  $(\ln^2(y) + \ln^2(q^2) + 2 \ln y \ln(q^2))/y$ . Integration from an arbitrary minimum value,  $y_L$  (independent of  $q_\alpha$ ), of  $y > \Lambda_s^2/q_\alpha^2$  gives a  $q_\alpha$ -independent value except for the logarithmic factors and  $q_\alpha$  in the numerator. Thus the large- $q_\alpha$  dependence is found from very small values of  $y$  close to the lower, and vanishing, limit. Expanding around small  $y$ , the limit for large  $q_\alpha$  approach zero as

$$\lim_{q_\alpha \rightarrow \infty} n_{5,2}(q_\alpha) \rightarrow \frac{16\pi\Gamma^2}{q_\alpha^6} \left( 3 \frac{m_{\alpha\gamma}^2}{m_\gamma^2} - \frac{m_{\alpha\gamma}}{m_{\beta\gamma}} \right) \times \int_{\Lambda_s^2/q_\alpha^2}^{y_L} \frac{dy}{y} [\ln^2(y) + \ln^2(q_\alpha^2) + 2 \ln y \ln(q_\alpha^2)]. \quad (5.35)$$

Together with the missing term from Eq. (5.34), which comes from the interchange of labels  $\beta$  and  $\gamma$  the final result is

$$\lim_{q_\alpha \rightarrow \infty} n_5(q_\alpha) \rightarrow \frac{16\pi}{3} \left[ 3 \left( \frac{m_{\alpha\gamma}^2}{m_\gamma^2} + \frac{m_{\alpha\beta}^2}{m_\beta^2} \right) - \frac{m_{\alpha\gamma} + m_{\alpha\beta}}{m_{\beta\gamma}} \right] \Gamma^2 \frac{\ln^3(q_\alpha)}{q_\alpha^6}. \quad (5.36)$$

## 5.3 Contact parameters

The expressions for the asymptotic one-body densities, which were analytically derived in Eqs. (5.20), (5.22), (5.29), (5.30) and (5.36) are collected and then compared to numerical calculations.

### 5.3.1 Analytic expressions

Two- and three-body contact parameters are defined via the large-momentum one-body density. The two-body contact parameter,  $C_{\beta\gamma}$ , is the proportionality constant of the leading order  $q_\alpha^{-4}$  term, which arises solely from  $n_2(q_\alpha)$  in Eq. (5.22). A system of three distinguishable particles have three contact parameters related to the momentum distribution of each particle. The two-body contact parameter,  $C_{\beta\gamma}$ , is defined in Eq. (5.22), where the momentum distribution of the particle  $\alpha$  is considered with respect to the CM

of the  $(\beta, \gamma)$  subsystem. This parameter reads

$$C_{\beta\gamma} = 8\pi m_{\alpha\gamma}^2 \int_0^\infty dk k |f_\beta(k)|^2 + 8\pi m_{\alpha\beta}^2 \int_0^\infty dk k |f_\gamma(k)|^2. \quad (5.37)$$

In the same way, the two-body parameters related to the momenta of particles  $\beta$  and  $\gamma$  are given by

$$C_{\alpha\gamma} = 8\pi m_{\beta\gamma}^2 \int_0^\infty dk k |f_\alpha(k)|^2 + 8\pi m_{\alpha\beta}^2 \int_0^\infty dk k |f_\gamma(k)|^2, \quad (5.38)$$

$$C_{\alpha\beta} = 8\pi m_{\alpha\gamma}^2 \int_0^\infty dk k |f_\beta(k)|^2 + 8\pi m_{\beta\gamma}^2 \int_0^\infty dk k |f_\alpha(k)|^2, \quad (5.39)$$

and a relation between the three independent parameters is found, from Eqs. (5.37), (5.38) and (5.39), to be

$$C_{\alpha\beta} + C_{\alpha\gamma} = C_{\beta\gamma} + 16\pi m_{\beta\gamma}^2 \int_0^\infty dk k |f_\alpha(k)|^2. \quad (5.40)$$

For a specific system, where two of the particles are non-interacting, both the corresponding two-body energy and spectator function vanish, i.e.,  $E_{\beta\gamma} = 0$  leads to  $f_\alpha(q) = 0$  in Eq. (2.70) [Bellotti 2011, Bellotti 2012]. In this case, Eq. (5.40) becomes a simple relation between the three two-body contact parameters, that is

$$C_{\alpha\beta} + C_{\alpha\gamma} = C_{\beta\gamma} \text{ for } E_{\beta\gamma} = 0. \quad (5.41)$$

Notice that this relation between different two-body parameters does not depend on the system dimension. Although the calculations in this chapter are for 2D systems, the relation in Eq. (5.41) applies as well for 3D systems with a non-interacting subsystem. Note that a non-interacting system and a vanishing two-body energy is not the same in 3D, where attraction is required to provide a state with zero binding energy.

The three-body contact parameter expressed by  $C_{\beta\gamma,\alpha}$ , is the coefficient of the next-to-leading order term in the one-body large-momentum density distribution given by  $\ln^3(q_\alpha)/q_\alpha^6$  (see Ref. [Bellotti 2012] and references therein). For distinguishable particles there are again three of these pa-

rameters, each one related to the momentum distributions of the different particles. The asymptotic behavior,  $\ln^3(q_\alpha)/q_\alpha^6$ , receives contributions from the three terms in Eqs. (5.29), (5.30) and (5.36). In total

$$C_{\beta\gamma,\alpha} = 16\pi \left( \frac{m_{\alpha\gamma} + m_{\alpha\beta}}{6m_{\beta\gamma}} + \frac{m_{\alpha\gamma}}{4m_{\alpha\beta}} + \frac{m_{\alpha\beta}}{4m_{\alpha\gamma}} + \frac{m_{\alpha\gamma}^2}{m_\gamma^2} + \frac{m_{\alpha\beta}^2}{m_\beta^2} \right) \Gamma^2 . \quad (5.42)$$

It is worth emphasizing that only a logarithmic factor distinguishes the behavior of the three-body contact term from the next order one,  $\ln^2(q_\alpha)/q_\alpha^6$  which arises from the leading order of  $n_1$  (see Eq. (5.20)), the next-to-next order of  $n_2$  (see Eq. (5.22)) as well as from next order of  $n_3$ , and  $n_4$  (see Eqs. (5.29) and (5.30)) . In practice, it must be a huge challenge to distinguish between terms differing by only one power of  $\ln(q_\alpha)$  in experiments.

If one of the two-body subsystems is non-interacting, the three-body contact parameter in Eq. (5.42) becomes

$$C_{\beta\gamma,\alpha} = 16\pi \left( -\frac{m_{\alpha\gamma} + m_{\alpha\beta}}{3m_{\beta\gamma}} + \frac{m_{\alpha\gamma}}{4m_{\alpha\beta}} + \frac{m_{\alpha\beta}}{4m_{\alpha\gamma}} + \frac{m_{\alpha\gamma}^2}{m_\gamma^2} + \frac{m_{\alpha\beta}^2}{m_\beta^2} \right) \Gamma^2 , \quad (5.43)$$

which is obtained by collecting contributions only from the non-vanishing  $n_4$  and  $n_5$  terms (since  $f_\alpha(q) = 0$ ,  $n_1$  and  $n_3$  do not contribute). Cyclic permutations of the indices in Eqs. (5.42) and (5.43) show that the three different three-body contact parameters are related by the mass factors in Eqs. (5.42) and (5.43). This conclusion holds for all excited states.

### 5.3.2 Identical Bosons

For three-identical bosons, all the two-body contact parameters in Eq. (5.40) are identical. Introducing the label  $n$  to distinguish between ground,  $n = 0$  and excited  $n > 0$  states, the parameter reads

$$C_2^n = 4\pi \int_0^\infty dk k |f_n(k)|^2 . \quad (5.44)$$



The leading order (LO) behavior of the one-body large-momentum density in Eq. (5.22), which is characterized by  $C_2$ , can be seen in Fig. 5.5 for both ground and first excited states and reads

$$n_3^0(q) \rightarrow \frac{3.71E_2}{q^4} \quad \text{and} \quad n_3^1(q) \rightarrow \frac{0.28E_2}{q^4}. \quad (5.45)$$

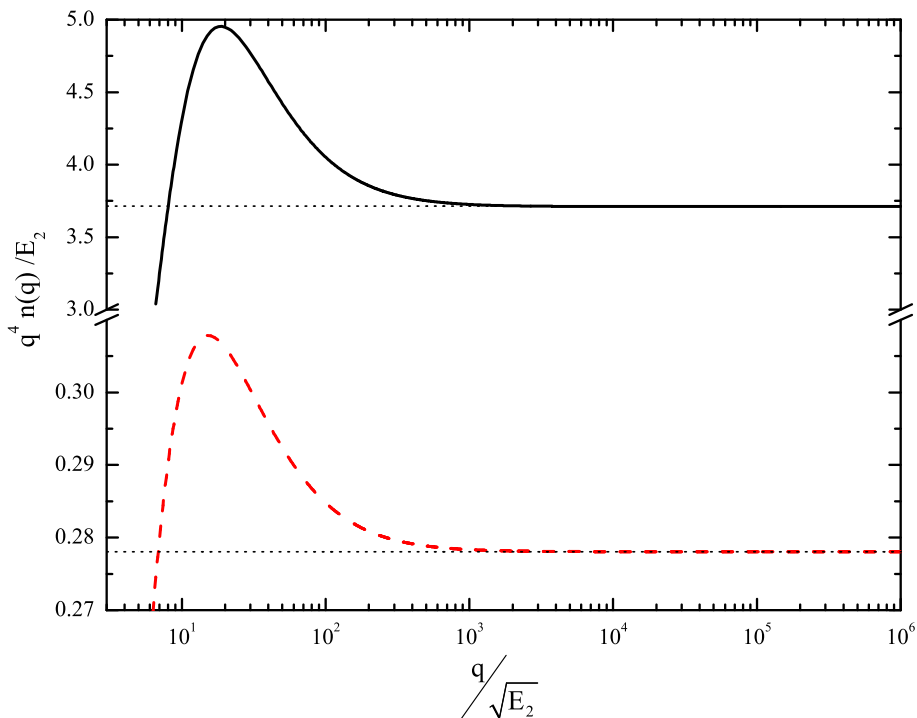


Figure 5.5: LO momentum distribution tail,  $q^4 n(q)$ , for ground (upper solid black line) and excited (lower dashed red line) three-body states. Note that the vertical axis is not uniform. The asymptotic dashed lines are the analytical results given by Eq. (5.45).

Each one of the two states is defined exclusively by its corresponding three-body energy  $E_3$ . Scaling  $C_2$  with  $E_3$  results in  $3.71E_2/16.52E_2 = 0.224$  and  $0.28E_2/1.270E_2 = 0.219$  for ground and excited state respectively. This striking result demonstrates the state-independence of the LO term in 2D to within the numerical accuracy of about 2%. The two-body contact for a bosonic system in 2D with short-range attractive interactions in the limit

of zero range is

$$C_2/E_3 = 0.222 \pm 0.0025, \quad (5.46)$$

where  $E_3$  is the trimer energy.

The universal behavior of the tail of the momentum distribution is far from trivial. In 3D and at unitarity, the discrete scale invariance induced by the ultraviolet sensitivity of the three-body dynamics, implies that the system should behave similarly irrespective of which trimer state is considered. This does not occur in 2D and the universal trimer energies are in some sense magic numbers multiplying the only scale available,  $E_2$ . The above result show that in spite of this major difference, the 2D momentum tail displays universal behavior, i.e.,  $C_2/E_3$  has the same value for both ground and excited states. This should be compared to the 2D relation for the trimer energy  $\frac{dE}{d \ln a} = \pi N C_2$  derived on general grounds in Ref. [Werner 2012]. The factor  $N$  appears due a different normalization and this result nicely agrees with Eq. (5.46).

The same does not happen to the next-to-leading (NLO) order term, where  $C_3^0/E_3^0 \neq C_3^1/E_3^1$ . The three-body contact parameters in Eq. (5.42) for the two states of a system of identical particles are

$$C_3^0 = 52.07 \quad \text{and} \quad C_3^1 = 1.01. \quad (5.47)$$

While the (LO) behavior of the momentum distribution exhibits the same  $\frac{C_2}{k^4}$  tail in 1D, 2D, and 3D, since it derives solely from two-body physics [Valiente 2012],  $C_2$  depends on what system is addressed and whether few-body bound states are present. On the other hand, the functional form of the NLO term also changes when the system is confined to different dimensions. Collecting results from Eqs. (5.46) and (5.47), the 2D tail is

$$n_{2D}(k) \rightarrow \frac{1}{k^4} C_2 + \frac{\ln^3(k)}{k^6} C_3, \quad (5.48)$$

while for bosons in 3D, the tail reads [Castin 2011, Braaten 2011]

$$n_{3D}(k) \rightarrow \frac{1}{k^4} C_2 + \frac{\cos[2s_0 \ln(\sqrt{3}k/\kappa_*) + \phi]}{k^5} C_3, \quad (5.49)$$

where  $s_0 = 1.00624$  and  $\phi = -0.87280$  are constants that can be determined from a full solution of the three-bosons problem in 3D at unitarity (see Chapter 6) with trimer energy  $E_3 = \kappa_*^2$ . The log-periodic three-body NLO term derives from the Efimov effect, whose solution can be used to determine  $C_2 = 53.097/\kappa_*$  and  $C_3 = -89.263/\kappa_*^2$  [Castin 2011].

Expressions in Eqs. (5.48) and (5.49) have the same and expect LO behavior, but vastly different NLO term, as shown in Fig. 5.6. The oscillations seen in Eq. (5.49) can be traced directly to the discrete scaling symmetry and are independent of the state considered. It is known that the condition on the dimension,  $D$ , for this behavior is  $2.3 < D < 3.8$  [Nielsen 1997, Nielsen 2001]. Imagining an interpolation between 2D and 3D [Yamashita 2014], the log-periodic terms would be expected only in this range of  $D$ . The NLO term is therefore a tell-tale sign of effective dimensionality of the system. The dimensional crossover is discussed in Chapter 7.

In experiments that study cold 2D quantum gases, a tight transverse optical lattice potential is used to reduce the motion in this direction (see Ref. [Bloch 2008]). The strength of the transverse optical lattice can be used to interpolate between 2D and 3D behavior of fermionic two-component systems [Dyke 2011, Sommer 2012].

Results here are for bosonic systems, and demonstrate how the NLO part of the momentum distribution can be used as a measure of the effective dimensionality felt by the particles in the system by identifying the presence of log-periodic behavior. The extreme cases of 2D and 3D are shown in Fig. 5.6 where the log-periodic oscillations are clearly seen in the latter, while the former has a smooth behavior. The form of the tail at the crossover is still unknown.

A measurement of the overall functional form of the NLO term is thus

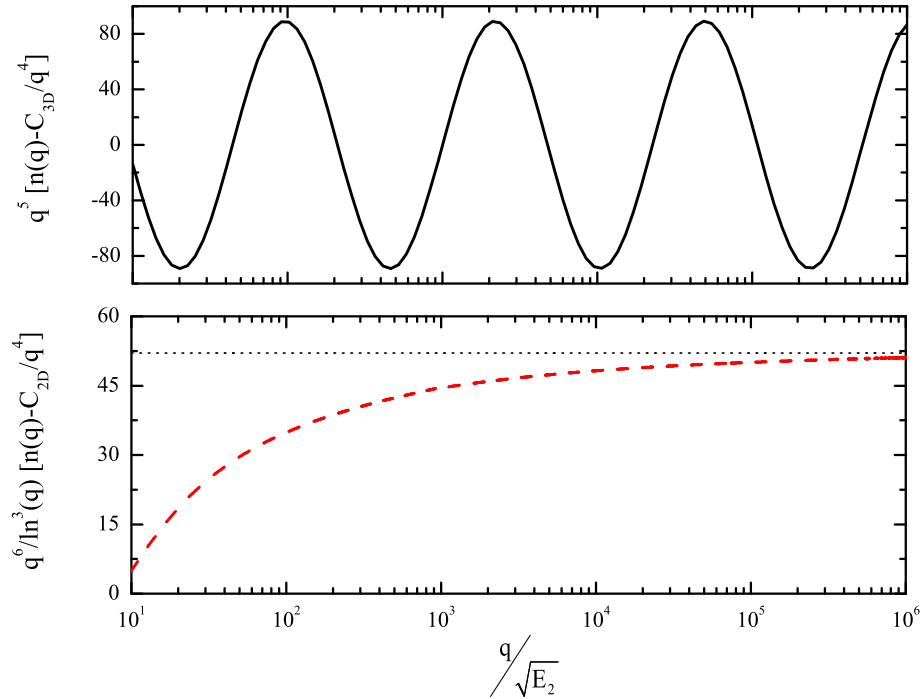


Figure 5.6: NLO momentum distribution comparison of 3D (upper panel) and 2D (lower panel). The 2D momentum distribution is the one of the ground state, but the result is similar for the excited state.

enough to determine the effective dimensionality of the squeezed bosonic gas. Since experiments have shown that it is possible to reach both the extreme 2D and the 3D regime, there must necessarily be a dimensional crossover that can be seen in the NLO behavior. A theoretical formulation of how the dimensionality can be smoothly changed is presented in Chapter 7.

### 5.3.3 Mass-imbalanced systems

#### Two-body contact parameters

The analytical results in this Chapter hold for any mass-imbalanced three-body system. Such a system has six independent parameters, which are reduced to four by choosing one mass and one energy as units [Bellotti 2012] (shown in Chapter 3, see Eq. (3.2)). This simply implies that all results can

be expressed as ratios of masses and energies, and in this way provides very useful scaling relations. However, results depending on four independent parameters are still hard to display and digest.

A systems composed of two identical particles,  $a$ , and a distinct one,  $c$ , has from the beginning four independent parameters, which are reduced to two after the choice of units. From now on,  $E_{ac}$  and  $m_a$  are the energy and mass units, and to simplify the notation, the mass ratio  $m = \frac{m_c}{m_a}$  is defined. In this case, the two-body contact parameters in Eqs.(5.37) to (5.39) are given by

$$C_{aa} = 16\pi \left( \frac{m}{1+m} \right)^2 \int_0^\infty dk k |f_a(k)|^2 , \quad (5.50)$$

$$C_{ac} = \frac{C_{aa}}{2} + 2\pi \int_0^\infty dk k |f_c(k)|^2 , \quad (5.51)$$

As shown in the previous section, for three identical particles where all masses and interactions are the same,  $C_{aa} = C_{ac} = C_2$ , and the quantity  $\frac{C_2}{E_3}$  is a universal constant in 2D [Bellotti 2013a], since it does not depend on the quantum state considered. Maintaining universal conditions for all excited states in mass-imbalanced systems, which have more excited states [Bellotti 2012, Bellotti 2013b], must be more demanding.

Detailed investigations reveal that when the mass-energy symmetry is broken, meaning that particles and two-body energies are not identical, the universality of  $\frac{C_2}{E_3}$  does not hold anymore. The two two-body contact parameters defined in Eqs. (5.50) and (5.51) divided by the three-body energy are not the same for all possible bound states in this general case. However, at least in one special case of two identical non-interacting particles,  $E_{aa} = 0$ , the universality is recovered. This condition leads to  $f_c = 0$  in the set of coupled homogeneous integrals equations (2.70) and two universal two-body contact parameters are related by

$$C_{ac} = \frac{C_{aa}}{2} \text{ for } E_{aa} = 0 . \quad (5.52)$$

The effect of the two-body energy on the contact parameter is shown

in Fig. 5.7 for the  $^{133}\text{Cs}^{133}\text{Cs}^6\text{Li}$  system, where  $a = ^{133}\text{Cs}$  and  $c = ^6\text{Li}$ . This system has four excited states in both cases of  $E_{aa} = E_{ac}$  and  $E_{aa} = 0$  and the coefficients (two-body contact) of the large-momentum limit reach constants in all cases. For  $E_{aa} = 0$ , universality is observed, since all two-body contacts ratios,  $C_{ac}/E_3$ , are equal in units of the three-body energy. This case is rather special because two particles do not interact and the three-body structure is determined by the identical two-body interactions in the identical subsystems. In other words the large-momentum limit of the one-body density for particle  $a$  is determined universally by the properties of the  $ac$  subsystem. The other contact parameter,  $C_{aa}/E_3$ , is also universal and follows from Eq. (5.52).

This picture changes when  $E_{aa} = E_{ac}$ , as seen in Fig. 5.7. Now, in the large-momentum limit, the coefficients  $C_{aa}$  and  $C_{ac}$  of the one-body densities change with the excitation energy. The systematics is that both  $C_{aa}/E_3$  and  $C_{ac}/E_3$  as function of excitation energy move towards the corresponding values for  $E_{aa} = 0$ , one from below and the other from above. First the non-universality of the ratios with the two-body energies is understandable, since the interaction of the two identical particles now must affect the three-body structure at small distances, and hence at large momenta. However, as the three-body binding energy decreases, the size of the system increases and details of the short-distance structure becomes less important.

The quantities  $\frac{C_{aa}}{E_3}$  and  $\frac{2\pi}{E_3} \int_0^\infty dk k |f_c(k)|^2$  are defined by the limit of large- $q$  in  $n_2$  in Eq. (5.22). Plotting the corresponding pieces of  $n_2(q)q^4$  as function of  $q$  lead to figures similar to Fig. 5.7, where the different bound state excitations show distinct results for  $E_{aa} = E_{ac}$ , while they all coincide for  $E_{aa} = 0$ . The ratio of the coefficients  $\frac{C_{ac}}{E_3}$ ,  $\frac{C_{aa}}{E_3}$  and  $\frac{2\pi}{E_3} \int_0^\infty dk k |f_c(k)|^2$  are shown in table 5.1. The results are presented for two different two-body energies and two different systems represented by  $c = ^6\text{Li}$ ,  $a = ^{133}\text{Cs}$  or  $a = ^{40}\text{K}$ . These numerical calculations confirm the systematics described above in complete agreement with Eqs. (5.51) and (5.52).

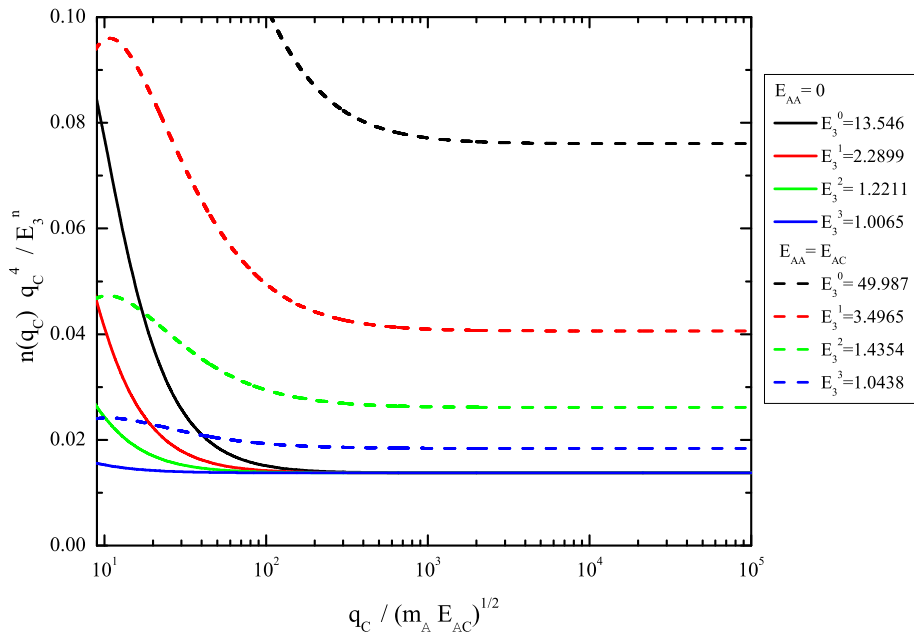


Figure 5.7: The leading order term of the one-body momentum density divided by  $E_3^n$  for each bound state labeled as  $n$  in a system composed of two identical ( $a = {}^{133}\text{Cs}$ ) particles and a distinct one ( $c = {}^6\text{Li}$ ) as a function of the momentum  $q$  for both  $E_{aa} = E_{ac}$  and  $E_{aa} = 0$ .

Table 5.1: The coefficients  $\frac{C_{ac}}{E_3}$ ,  $\frac{C_{aa}}{E_3}$  and  $\frac{2\pi}{E_3} \int_0^\infty dk k |f_c(k)|^2$  defined by Eqs. (5.37) to (5.39), are shown for two different interactions and two different systems represented by  $c = {}^6\text{Li}$  and  $a = {}^{133}\text{Cs}$  or  $a = {}^{40}\text{K}$ . Values in the fifth column are plotted in Fig. 5.7.

system	$\frac{E_{aa}}{E_{ac}}$	state	$\frac{C_{aa}}{E_3}$	$\frac{C_{ac}}{E_3}$	$\frac{2\pi}{E_3} \int_0^\infty dk k  f_c(k) ^2$
$a = {}^{133}\text{Cs}$ $c = {}^6\text{Li}$	1	Ground	0.02210	0.07625	0.06503
		First	0.02495	0.04062	0.02812
		Second	0.02616	0.02612	0.01305
		Third	0.02718	0.01837	0.00478
	0	all	0.02748	0.01374	0
$a = {}^{40}\text{K}$ $c = {}^6\text{Li}$	1	Ground	0.06337	0.11499	0.08372
		First	0.07438	0.08256	0.04727
		Second	0.07934	0.05369	0.01840
	0	all	0.08304	0.04152	0

### Mass-dependence of the two-body contacts

In general, for two identical particles, the two-body contact parameters divided by the three-body energy depend on the mass ratio  $m$ . The de-

pendence change from universal for  $E_{aa} = 0$  to non-universal for  $E_{aa} = E_{ac}$ . The mass dependence for ground states are shown in Fig. 5.8, where the ratio  $\frac{C_{aa}}{C_{ac}} = 2$  in Eq. (5.52) is shown to hold for  $E_{aa} = 0$  in the entire mass interval investigated. It is also possible to see how the second term on the right-hand-side of Eq. (5.51) affects the relation between the two two-body contact parameters. Fig. 5.8 shows that the values rapidly increase from small  $m$  up to 1 and become almost constant above  $m \approx 5$ . This behavior is similar to mass-imbalanced system in 3D [Yamashita 2013].

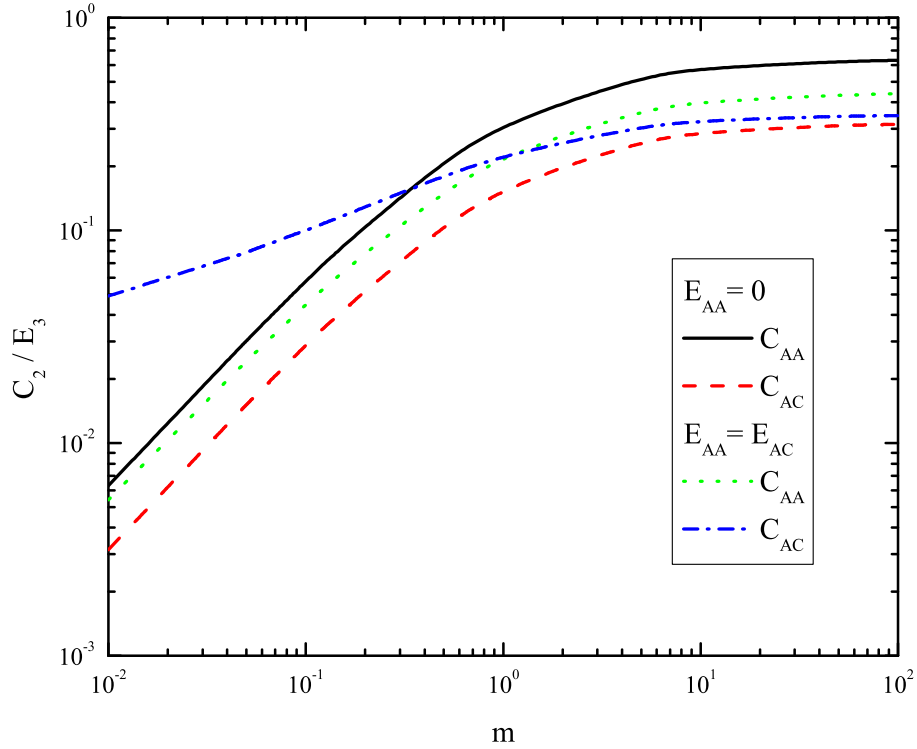


Figure 5.8: The two-body parameters  $C_{aa}$  and  $C_{ac}$  defined in Eqs. (5.50) and (5.51) as function of the mass ratio  $m = \frac{m_c}{m_a}$  for an  $aac$  system in both cases where  $E_{aa} = 0$  and  $E_{aa} = E_{ac}$ .

### Estimate of the two-body contact in the ground state

The parametrization of the ground state spectator function in Eq. (5.15) is used to estimate the dependence of the two-body contact parameter on the



three-body energy. Inserting it in Eq. (5.50) gives

$$\frac{C_{aa}}{E_3} = 16\pi \frac{m^2}{(1+m)(2+m)} f_a^2(0) \left( 1 + \frac{2}{\ln(E_3)} + \frac{2}{\ln^2(E_3)} \right). \quad (5.53)$$

A comparison between this approximation and the numerical results is shown in Fig. 5.9. Notice that Eq. (5.53) provides a fairly good estimate, which is accurate within 5% for small  $m$ , around 10% for  $m > 1$ , and within about 20% deviation in the worst case of  $m = 1$ . The divergence in Eq. (5.53) for  $E_3 \rightarrow 1$  means that the two-body contact parameters diverge when the three-body system approaches the threshold of binding. This does not reveal the full energy dependence since the normalization factor,  $f_a^2(0)$ , also is state and energy dependent.

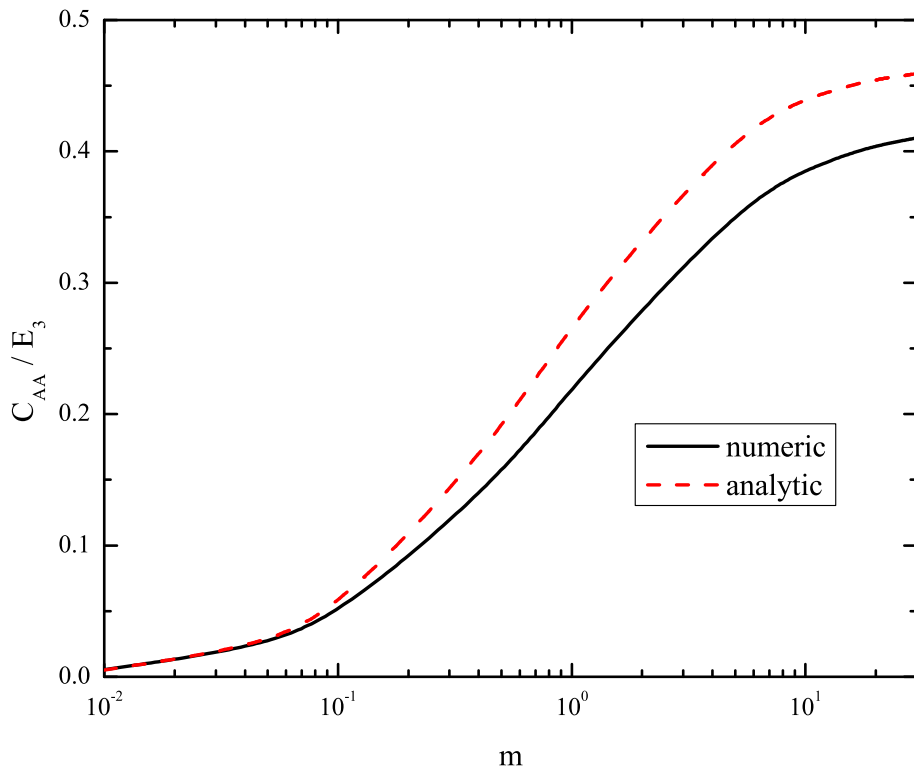


Figure 5.9: Comparison between the analytic estimative of  $C_{aa}$ , given by Eq. (5.53) and the numerical calculation from Eq. (5.50).

### Three-body contact parameters

The non-universality of the two-body contact parameters, and even of the three-body one for identical particles (see Eq. (5.47)), does not encourage to check the universality of the three-body contact parameter in mass-asymmetric systems. However, at least the system with two non-interacting identical particles turned out to be universal and may lead to an interesting large-momentum three-body structure. As before, inserting  $E_{aa} = 0$  in the set of coupled integral equations (2.70) gives  $f_c(q_c) = 0$ . Then Eqs. (5.16) to (5.19) show directly that  $n_1(q_c)$  and  $n_3(q_c)$  vanish when  $f_c(q_c) = 0$ , leaving only contributions from  $n_4(q_c)$  and  $n_5(q_c)$ .

The sub-leading order of the large-momentum distribution multiplied by  $q_c^6/\ln^3(q_c)$  is shown in Fig. 5.10, that is  $C_{aa,c}$ , as functions of  $q_c$  for the four bound states of the system  $a = {}^{133}\text{Cs}$  and  $c = {}^6\text{Li}$  for both  $E_{aa} = E_{ac}$  and  $E_{aa} = 0$ . Only one of these three-body contact parameters is shown, since the other one,  $C_{ac,a}$ , is related state-by-state through the mass factors in Eqs. (5.42) and (5.43). The momentum dependence flattens at much larger  $q_c$  is not shown in figure. The values are divided by the three-body energy and no simple energy scaling were obtained. Not surprisingly, a more complicated and non-universal behavior is present.

However, it is striking to see that this sub-leading order in the large-momentum limit is negligibly small for  $E_{aa} = 0$  compared to the interacting case with  $E_{aa} = E_{ac}$ . This suggests that a negligible three-body contact parameter combined with a universal two-body contact parameter can be taken as a signature of a two-body non-interacting subsystem within a three-body system in 2D.

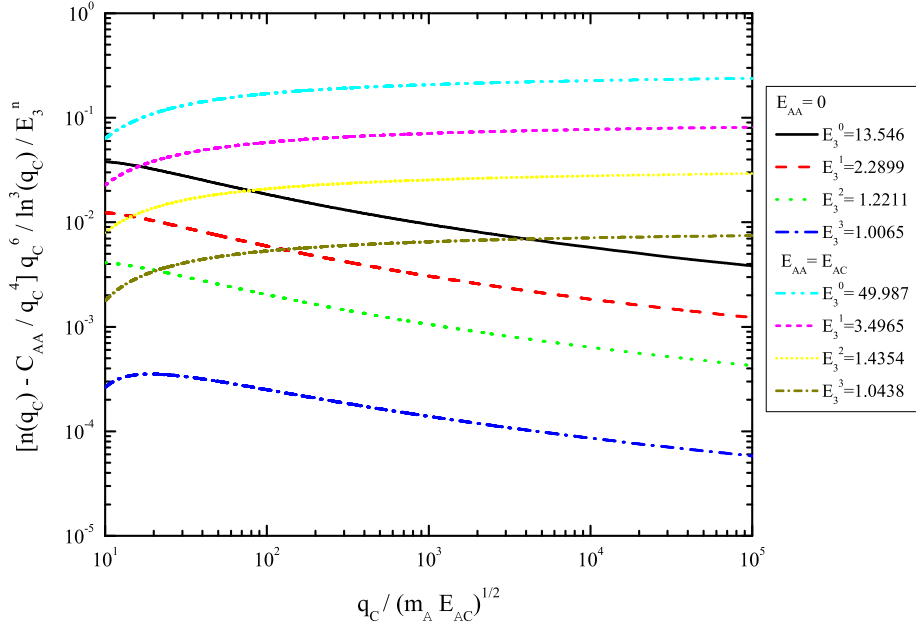


Figure 5.10: The sub-leading order of the one-body momentum density divided by  $E_3^n$  for each bound state labeled as  $n$  in a system composed of two identical particles ( $a = {}^{133}\text{Cs}$ ) and a distinct one ( $c = {}^6\text{Li}$ ) as a function of the momentum  $q$  for both  $E_{aa} = E_{ac}$  and  $E_{aa} = 0$ .

## 5.4 Discussion about possible experiments

As demonstrated in Sec. 5.3.3, the NLO term in the momentum distribution can be used to distinguish whether the two-body subsystems are interacting when three-body systems are being taken into account. Maybe more important, the NLO term also carries a tell-tale signature of the dimensionality of the quantum system under study. The 2D to 3D crossover was studied in Ref. [Dyke 2011, Sommer 2012], and it has been shown that both the 3D and the strict 2D limits are accessible in experiments. The crossover was here discussed by using formalism applicable to either pure 2D or pure 3D without explicit consideration of the external confinement. The results predict that a proof-of-principle experiment is possible by going to the two strict limits. However, the full crossover including the intermediate regime (quasi-2D) where the transverse confinement must be taken explicitly into account, which is experimentally addressable, should be explored theoret-

cally in the future. A first step in this direction is taken in [Yamashita 2014] and discussed in Chapter 7.

The units (the dimer binding energy  $E_2$ ) and the effects of the transverse confinement on this two-body bound state need to be considered when connecting the results to the experiments. The interaction is controlled by Feshbach resonances [Chin 2010]. However, under the confinement, the dimer energy is modified and becomes  $E_2 = B\hbar\omega_z \exp(-\sqrt{2\pi}l_z/|a|)/\pi$  [Petrov 2001]. Here,  $\omega_z$  is the transverse harmonic confinement frequency,  $l_z = \sqrt{\hbar/m\omega_z}$  the trapping length,  $a$  the 3D scattering length associated with the Feshbach resonance and  $B = 0.905$  is a constant. This formula holds for  $a < 0$  and  $|a| \ll l_z$ , while on resonance,  $|a| \rightarrow \infty$  and  $E_2 = 0.244\hbar\omega_z$ . Corrections also arise from the non-harmonic optical lattice, but they are not essential for the discussion which follows. The dimer energy scale can be converted into a momentum scale,  $k_0$ , through  $E_2 = \hbar^2 k_0^2 / 2m$ . Accessing the tail behavior and the 2D-3D crossover, the range  $k \sim 10^1 - 10^3 k_0$  is enough, as shown in Figs. 5.5 and 5.6. Some 2D Bose gas experiments [Hung 2011, Yefsah 2011] use  $l_z \sim 3800a_0$ , where  $a_0$  is the Bohr radius, which implies that  $k_0 \sim 10^{-4}a_0^{-1}$  when  $|a| = \infty$ . For the momentum distribution measurements [Stewart 2010, Kuhnle 2010], the maximum momentum reported is about  $k \sim 10^{-3}a_0^{-1}$ . This implies that an order of magnitude or two beyond the reported capabilities is necessary. However, if  $a$  is tuned away from resonance to the  $a < 0$  side,  $E_2$  will decrease rapidly according to the formulas above, inducing a corresponding rapid decrease of  $k_0$  which should render the physics discussed here within reach of current experimental setups. Notice that the van der Waals length scale of about  $100a_0$  is in the deep tail, so there is no conflict with the universal zero-range description employed here.

# Momentum distribution in 3D

---

A key result in the study of the two-dimensional (2D) one-body density is the analytic expression of the large-momentum asymptotic behavior for the spectator functions. In Chapter 5, mass-imbalanced systems were addressed and it was shown that the spectator functions have the same asymptotic behavior, i.e.,  $\ln(q)/q^2$ , each one having specific normalization constants, irrespective of the quantum state considered, with a relation among them.

Three-dimensional (3D) three-body systems have geometric scaling between consecutive three-body states for  $|a| \rightarrow \infty$ , as predicted in the seventies by V. Efimov [Efimov 1970] and firstly observed in cold atomic gases around 35 years latter [Kraemer 2006]. The experimental verification of the effect has opened a new research direction dubbed Efimov physics [Ferlaino 2010]. In practice, the Efimov effect occurs when the size of the three-body system, given for the scattering length  $|a|$  is much larger than interaction range  $r_0$ , i.e.,  $|a|/r_0 \rightarrow \infty$ . In this limit, a sequence of three-body bound states occurs wherein two successive states always have the same fixed ratio of their binding energies. The scaling of the energy levels implies that some of properties of three-body 3D systems are universal, in the sense that are independent of the state considered once properly rescaled. The focus here is in the two- and three- body contact parameters, defined via the one-body momentum density.

The two- and three-body contact parameters were determined for a 3D system of three identical bosons in Ref. [Castin 2011] and for mixed-species systems in Ref. [Yamashita 2013]. Unlike the 2D analogue, the results show that the influence of non-equal masses in three-body systems goes beyond changing the contact parameters values, i.e., the sub-leading term in the

one-body momentum distribution, which defines  $C_3$ , has a different and mass-dependent functional form in each case.

The study is taken for three-body bound Efimov-like states for systems that contain two identical bosons and a third distinguishable particle. The contact parameters of such systems are addressed when the masses are different and for different strengths of the interaction parameters. For that aim the one-body momentum distributions are computed and its asymptotic behavior is studied. Only the universal regime is considered, since all two-body potentials are described by zero-range interactions. Results are shown for the experimentally relevant cases  ${}^6\text{Li}^{133}\text{Cs}^{133}\text{Cs}$  and  ${}^6\text{Li}^{87}\text{Rb}^{87}\text{Rb}$ , as in Chapter 5.

## 6.1 Formalism and definitions

The  $AAB$  system is constituted by two identical bosons  $A$  and a third particle  $B$  of different kind. The universal limit  $|a| \gg r_0$ , where the range of the two-body potentials can be neglected, is naturally achieved by introducing zero-range interactions between the particles.

The set of 3D homogeneous integral equations are given by Eq. (2.83) for a general system of three distinguishable particles. For the  $AAB$  system, the  $s$ -wave coupled subtracted integral equations for the spectator functions,  $\chi$ , corresponding to a bound state, where  $|E_3|$  is the absolute value of the three-body energy, is written in units of  $\hbar = m_A = 1$  as

$$\chi_{AA}(y) = 2\tau_{AA}(y; |E_3|) \int_0^\infty dx \frac{x}{y} G_1(y, x; |E_3|) \chi_{AB}(x) , \quad (6.1)$$

$$\begin{aligned} \chi_{AB}(y) = \tau_{AB}(y; |E_3|) \int_0^\infty dx \frac{x}{y} [G_1(x, y; |E_3|) \chi_{AA}(x) \\ + \mathcal{A}G_2(y, x; |E_3|) \chi_{AB}(x)] , \end{aligned} \quad (6.2)$$

with

$$\tau_{AA}(y; |E_3|) \equiv \frac{1}{\pi} \left[ \sqrt{|E_3| + \frac{\mathcal{A}+2}{4\mathcal{A}}y^2 \mp \sqrt{E_{AA}}} \right]^{-1}, \quad (6.3)$$

$$\tau_{AB}(y; |E_3|) \equiv \frac{1}{\pi} \left( \frac{\mathcal{A}+1}{2\mathcal{A}} \right)^{3/2} \left[ \sqrt{|E_3| + \frac{\mathcal{A}+2}{2(\mathcal{A}+1)}y^2 \mp \sqrt{E_{AB}}} \right]^{-1}, \quad (6.4)$$

$$G_1(y, x; |E_3|) \equiv \ln \frac{2\mathcal{A}(|E_3| + x^2 + xy) + y^2(\mathcal{A}+1)}{2\mathcal{A}(|E_3| + x^2 - xy) + y^2(\mathcal{A}+1)} - \ln \frac{2\mathcal{A}(\mu^2 + x^2 + xy) + y^2(\mathcal{A}+1)}{2\mathcal{A}(\mu^2 + x^2 - xy) + y^2(\mathcal{A}+1)}, \quad (6.5)$$

$$G_2(y, x; |E_3|) \equiv \ln \frac{2(\mathcal{A}|E_3| + xy) + (y^2 + x^2)(\mathcal{A}+1)}{2(\mathcal{A}|E_3| - xy) + (y^2 + x^2)(\mathcal{A}+1)} - \ln \frac{2(\mathcal{A}\mu^2 + xy) + (y^2 + x^2)(\mathcal{A}+1)}{2(\mathcal{A}\mu^2 - xy) + (y^2 + x^2)(\mathcal{A}+1)}, \quad (6.6)$$

where  $x$  and  $y$  denote dimensionless momenta and  $\mathcal{A}$  is the mass ratio  $\mathcal{A} = m_B/m_A$ . Notice that a slightly different notation is introduced for the study of the 3D system, in order to avoid confusion with the previous 2D case.

The interaction strengths of the  $AA$  and  $AB$  subsystems are parametrized by the energies  $E_{AA}$  and  $E_{AB}$ , and the plus and minus signs in Eqs. (6.3) and (6.4) refer to virtual and bound two-body subsystems, respectively [Yamashita 2002, Bringas 2004, Yamashita 2008].

The universal regime of the  $AB$  system is studied with  $|a_{AB}| \rightarrow \infty$  and/or  $E_{AB} \rightarrow 0$ . In light of the fact that experimental information about mixed systems of the  $AAB$  type is still sparse, the two extreme cases of *i*)  $E_{AA} = 0$  and *ii*) a non-interacting  $AA$  subsystem are considered. Notice that conditions *i*) and *ii*) are equivalent in 2D systems [Bellotti 2014], while they are distinct in 3D.

As before,  $\mathbf{q}_\alpha$  is the Jacobi momentum from  $\alpha$  particle to the center-of-mass of the pair ( $\beta\gamma$ ) and  $\mathbf{p}_\alpha$  the relative momentum of the pair. The four terms in the one-body momentum density for each constituent are defined

in the most general case of three distinguishable particles in Eqs. (5.16) to (5.19). The  $AAB$  system has only two distinct distributions, namely of type  $\alpha = \beta = A$  and type  $\gamma = B$ . Following the notation and units defined in this Chapter, the wave function in Eq. (2.67) is written in terms of the spectator functions in the basis  $|\mathbf{q}_B \mathbf{p}_B\rangle$  as

$$\begin{aligned} \langle \mathbf{q}_B \mathbf{p}_B | \Psi \rangle &= \frac{\chi_{AA}(q_B) + \chi_{AB}(q_A) + \chi_{AB}(q'_A)}{|E_3| + H_0}, \\ &= \frac{\chi_{AA}(q_B) + \chi_{AB}(|\mathbf{p}_B - \frac{\mathbf{q}_B}{2}|) + \chi_{AB}(|\mathbf{p}_B + \frac{\mathbf{q}_B}{2}|)}{|E_3| + H_0}, \end{aligned} \quad (6.7)$$

or in the basis  $|\mathbf{q}_A \mathbf{p}_A\rangle$  as

$$\langle \mathbf{q}_A \mathbf{p}_A | \Psi \rangle = \frac{\chi_{AA}(|\mathbf{p}_A - \frac{A}{A+1} \mathbf{q}_A|) + \chi_{AB}(|\mathbf{p}_A + \frac{1}{A+1} \mathbf{q}_A|) + \chi_{AB}(q_A)}{|E_3| + H'_0}, \quad (6.8)$$

where  $H_0 = \frac{p_B^2}{2m_{AA}} + \frac{q_B^2}{2m_{AA,B}}$  and  $H'_0 = \frac{p_A^2}{2m_{AB}} + \frac{q_A^2}{2m_{AB,A}}$ . The reduced masses are given by  $m_{AA} = \frac{1}{2}$ ,  $m_{AA,B} = \frac{2A}{A+2}$ ,  $m_{AB} = \frac{A}{A+1}$  and  $m_{AB,A} = \frac{A+1}{A+2}$ .

The momentum distributions for the particles  $A$  and  $B$  are

$$n(q_B) = \int d^3 p_B |\langle \mathbf{q}_B \mathbf{p}_B | \Psi \rangle|^2, \quad n(q_A) = \int d^3 p_A |\langle \mathbf{q}_A \mathbf{p}_A | \Psi \rangle|^2 \quad (6.9)$$

and they are normalized such that  $\int d^3 q n(q) = 1$ .

Since the results here are compared to Ref. [Castin 2011], note that the definition of momentum distributions as well as their normalizations differ for factor of  $1/(2\pi)^3$  multiplying the definition of  $n(q)$ , which is normalized to 3, the number of particles, in that reference.

## 6.2 Asymptotic spectator function

The asymptotic behavior of the spectator function is used in deriving some analytic formulas and compare to corresponding numerical results. The large momentum regime  $\sqrt{|E_3|} \ll q$  is accessed by taking the limit  $\mu \rightarrow \infty$  and  $|E_3| = E_{AA} = E_{AB} \rightarrow 0$ . The coupled equations for the spectator



functions in Eqs. (6.1) and (6.2) consequently simplify and become

$$\chi_{AA}(y) = \frac{2}{\pi} \left[ y \sqrt{\frac{\mathcal{A}+2}{4\mathcal{A}}} \right]^{-1} \int_0^\infty dx \frac{x}{y} G_{1a}(y, x) \chi_{AB}(x), \quad (6.10)$$

$$\begin{aligned} \chi_{AB}(y) = \frac{1}{\pi} \left( \frac{\mathcal{A}+1}{2\mathcal{A}} \right)^{3/2} \left[ y \sqrt{\frac{\mathcal{A}+2}{2(\mathcal{A}+1)}} \right]^{-1} \times \\ \int_0^\infty dx \frac{x}{y} [G_{1a}(x, y) \chi_{AA}(x) + \mathcal{A} G_{2a}(y, x) \chi_{AB}(x)], \end{aligned} \quad (6.11)$$

where

$$G_{1a}(y, x) \equiv \ln \frac{2\mathcal{A}(x^2 + xy) + y^2(\mathcal{A}+1)}{2\mathcal{A}(x^2 - xy) + y^2(\mathcal{A}+1)}, \quad (6.12)$$

$$G_{2a}(y, x) \equiv \ln \frac{(y^2 + x^2)(\mathcal{A}+1) + 2xy}{(y^2 + x^2)(\mathcal{A}+1) - 2xy}. \quad (6.13)$$

The coupled equations in Eqs. (6.10) and (6.11) are solved by using the ansatz

$$\chi_{AA}(y) = c_{AA} y^{-2+\imath s} \quad \text{and} \quad \chi_{AB}(y) = c_{AB} y^{-2+\imath s}, \quad (6.14)$$

where  $y$  once again denotes a dimensionless momentum. Inserting the functions (6.14) in the set of coupled equations and performing the scale transformation  $x = yz$  in the integrand of Eqs. (6.10) and (6.11), it is derived the set of equations for the constants  $c_{AA}$  and  $c_{AB}$ , given by

$$c_{AA} = c_{AB} \frac{2}{\pi} \sqrt{\frac{4\mathcal{A}}{\mathcal{A}+2}} \int_0^\infty dz z^{-2+1+\imath s} \ln \frac{2\mathcal{A}(z^2 + z) + (\mathcal{A}+1)}{2\mathcal{A}(z^2 - z) + (\mathcal{A}+1)}, \quad (6.15)$$

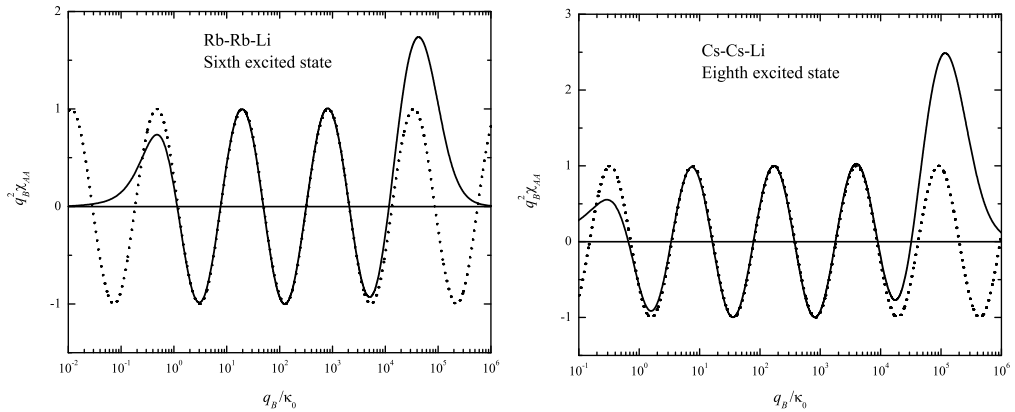
$$\begin{aligned} c_{AB} = \frac{1}{\pi} \left( \frac{\mathcal{A}+1}{2\mathcal{A}} \right)^{3/2} \sqrt{\frac{2(\mathcal{A}+1)}{\mathcal{A}+2}} \int_0^\infty dz z^{-2+1+\imath s} \left[ c_{AA} \ln \frac{2\mathcal{A}(1+z) + z^2(\mathcal{A}+1)}{2\mathcal{A}(1-z) + z^2(\mathcal{A}+1)} \right. \\ \left. + \mathcal{A} c_{AB} \ln \frac{(1+z^2)(\mathcal{A}+1) + 2z}{(1+z^2)(\mathcal{A}+1) - 2z} \right]. \end{aligned} \quad (6.16)$$

Returning to Eqs. (6.10) and (6.11), there are two solutions which are complex conjugates of each other, i.e.,  $z^{\pm \imath s}$ . Apart from an overall normalization, there is still a relative phase between these two independent solutions, which is determined by requiring the wave function to be zero at

a certain momentum denoted  $q^*$ . This parameter is known as the three-body parameter [Nielsen 2001, Braaten 2006]. This is the momentum-space equivalent of the coordinate-space three-body parameter which is now believed to be simply related to the van der Waals two-body interaction of the atoms in question [Berninger 2011a, Schmidt 2012b, Sørensen 2013]. In this case the asymptotic form of the spectator functions becomes

$$\chi_{AA}(q) = c_{AA} q^{-2} \sin(s \ln q/q^*) \quad \text{and} \quad \chi_{AB}(q) = c_{AB} q^{-2} \sin(s \ln q/q^*), \quad (6.17)$$

where  $q$  denotes momentum and the boundary condition  $\chi(q^*) = 0$  is fulfilled.



(a) Sixth excited state,  $E_3 = -8.6724 \times 10^{-12}$  for a Rb-Rb-Li molecule. (b) Eighth excited state,  $E_3 = -8.9265 \times 10^{-13}$  for a Cs-Cs-Li molecule.

Figure 6.1: The spectator function  $\chi_{AA}(q)$  of a high excited state for  $E_{AA} = E_{AB} = 0$ , solution of the coupled equations (6.1) and (6.2) (solid line), compared with the asymptotic formula (6.14) (dotted line).  $E_3$  energies are given in arbitrary units.

The asymptotic form of the spectator function should be compared with the solutions of the subtracted equations in the limit of large momentum, constrained by the window  $\kappa_0 \ll q_B \ll \mu$ , where  $\kappa_0 \equiv \sqrt{|E_3|}$ . The spectator functions  $\chi_{AA}(q)$  for Rb-Rb-Li and Cs-Cs-Li compared to the respective asymptotic formula are shown in Fig. 6.1. The difference between the numerical calculation and the analytic behavior is easily understood. While

the limit  $\mu \rightarrow \infty$  is taken in the analytical derivations,  $\mu^2 = 1$  is used for the subtraction point in the numerical calculation (see for instance Ref. [Frederico 2012] for a detailed discussion and references therein). Notice that this subtraction method is basically equivalent to the procedure employed by Danilov [Danilov 1961] to regularize the original three-body Skorniakov-Ter-Martirosian equation [Skornyakov 1956]. A very detailed discussion of these issues is given by Pricoupenko [Pricoupenko 2010, Pricoupenko 2011]. Therefore, the two curves would coincide in the idealized limit where  $\kappa_0 = 0$  and  $\mu \rightarrow \infty$  and the effect of finite value of these two quantities is seen on each end of both plots. The window of validity for the use of the asymptotic formulas, i.e.,  $\sqrt{|E_3|} \ll q \ll \mu$  can be clearly seen in these figures.

### 6.2.1 Scaling parameter

Although the asymptotic expression in Eq. (6.17) is already known, the procedure of using it to solve the coupled integral equations in Eqs. (6.10) and (6.11) leads to an expression for the scaling parameter  $s$  of an  $AAB$  system. Inserting Eq. (6.15) into Eq. (6.16), the set of coupled equations can be written as a single transcendental equation

$$\frac{1}{\pi} \left( \frac{\mathcal{A} + 1}{2\mathcal{A}} \right)^{3/2} \sqrt{\frac{2(\mathcal{A} + 1)}{\mathcal{A} + 2}} \left( \mathcal{A} I_1(s) + \frac{2}{\pi} \sqrt{\frac{4\mathcal{A}}{\mathcal{A} + 2}} I_2(s) I_3(s) \right) = 1, \quad (6.18)$$

where

$$I_1(s) = \int_0^\infty dz z^{-1+is} \ln \left[ \frac{(z^2 + 1)(\mathcal{A} + 1) + 2z}{(z^2 + 1)(\mathcal{A} + 1) - 2z} \right] = \frac{2\pi \sinh(\theta_1 s - \frac{\pi}{2}s)}{s \cosh(\frac{\pi}{2}s)}, \quad (6.19)$$

$$I_2(s) = \int_0^\infty dz z^{-1+is} \ln \left[ \frac{2\mathcal{A}(z^2 + z) + \mathcal{A} + 1}{2\mathcal{A}(z^2 - z) + \mathcal{A} + 1} \right] \\ = \frac{2\pi \sinh(\theta_2 s - \frac{\pi}{2}s)}{s \cosh(\frac{\pi}{2}s)} \left( \frac{\mathcal{A} + 1}{2\mathcal{A}} \right)^{is/2}, \quad (6.20)$$

$$\begin{aligned}
I_3(s) &= \int_0^\infty dz z^{-1+is} \ln \left[ \frac{2\mathcal{A}(1+z) + (\mathcal{A}+1)z^2}{2\mathcal{A}(1-z) + (\mathcal{A}+1)z^2} \right] \\
&= \frac{2\pi \sinh(\theta_2 s - \frac{\pi}{2}s)}{s \cosh(\frac{\pi}{2}s)} \left( \frac{\mathcal{A}+1}{2\mathcal{A}} \right)^{-is/2}. \quad (6.21)
\end{aligned}$$

The angles are given by  $\tan^2 \theta_1 = \mathcal{A}(\mathcal{A}+2)$  and  $\tan^2 \theta_2 = (\mathcal{A}+2)/\mathcal{A}$  with the conditions  $\pi/2 < \theta_1$  and  $\theta_2 < \pi$ . For the special case of equal masses, i.e.,  $\mathcal{A} = 1$ ,  $\theta_1 = \theta_2$ ,  $I_1 = I_2 = I_3$  and

$$\left( \frac{1}{\pi} \sqrt{\frac{4}{3}} I_1(s) \right) + 2 \left( \frac{1}{\pi} \sqrt{\frac{4}{3}} I_1(s) \right)^2 - 1 = 0, \quad (6.22)$$

for which the physically relevant solution is seen to be

$$\frac{1}{\pi} \sqrt{\frac{4}{3}} I_1(s) = \frac{1}{2}. \quad (6.23)$$

The Efimov equation for the scaling parameter  $s$  in a system of identical bosons is then recovered from Eqs. (6.19) and (6.23) [Efimov 1970, Nielsen 2001]. Another very interesting and relevant case is when there is no interaction between the two  $A$  particles, in which case  $c_{AA} = 0$  in Eq. (6.16). The equation for the scale factor, Eq. (6.18), now simplifies and gives

$$\frac{\mathcal{A}}{\pi} \left( \frac{\mathcal{A}+1}{2\mathcal{A}} \right)^{3/2} \sqrt{\frac{2(\mathcal{A}+1)}{\mathcal{A}+2}} I_1(s) = 1. \quad (6.24)$$

The scaling factors,  $\exp(\pi/s)$ , are plotted in Fig. 6.2 for the cases when all three subsystems have resonant interaction, which is the expression in Eq. (6.18) valid for  $E_{AA} = E_{AB} = 0$  (solid line) and when there is no interaction in the  $AA$  subsystem, which is the expression in Eq. (6.24) valid for  $E_{AB} = 0$  (dashed line).

What is important to notice is that for  $m_A \gg m_B$  ( $\mathcal{A} \ll 1$ ), the scaling factors are very similar, and both are much smaller than the equal mass case where  $\mathcal{A} = 1$ . Therefore, it is expected that the  $AAB$  system with heavy  $A$  and light  $B$ , would have many universal three-body bound states ( $s$  large or

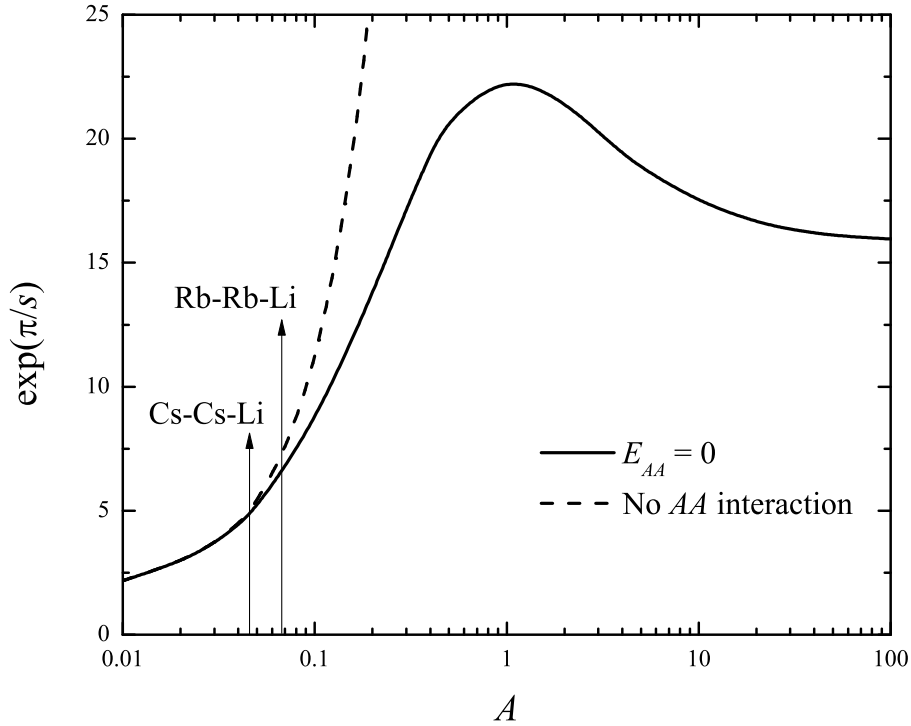


Figure 6.2: Scaling parameter  $s$  as a function of  $\mathcal{A} = m_B/m_A$  for  $E_{AA} = 0$  and  $E_{AB} = 0$  (resonant interactions), solid line, and for the situation where  $E_{AB} = 0$  but with no interaction between AA, dashed line. The arrows show the corresponding mass ratios for  $^{133}\text{Cs}$ - $^{133}\text{Cs}$ - $^6\text{Li}$  and  $^{87}\text{Rb}$ - $^{87}\text{Rb}$ - $^6\text{Li}$ .

equivalently  $e^{\pi/s}$  small) *irrespective* of whether the heavy-heavy subsystem is weakly or strongly interacting. This feature is similar to the 2D case and recent experiments with mixtures of  $^6\text{Li}$  and  $^{133}\text{Cs}$  indicate that there could be a resonance of the  $^6\text{Li}$ - $^{133}\text{Cs}$  subsystem at a point where the scattering length in the  $^{133}\text{Cs}$ - $^{133}\text{Cs}$  system is close to zero, i.e., weak interaction in the AA subsystem [Repp 2013, Tung 2013].

### 6.3 Asymptotic one-body densities

The large-momentum one-body density  $n(q_B)$ , i.e., the single-particle momentum distribution for particle  $B$  is calculated similarly to the procedure used for the 2D case. From Eqs. (6.7) and (6.9) it is possible to split the

momentum density into nine terms, which can be reduced to four considering the symmetry between the two identical particles  $A$ . This simplifies the computation of the momentum density to the form  $n(q_B) = \sum_{i=1}^4 n_i(q_B)$ , where

$$n_1(q_B) = |\chi_{AA}(q_B)|^2 \int d^3 p_B \frac{1}{(|E_3| + p_B^2 + q_B^2 \frac{A+2}{4A})^2} = \pi^2 \frac{|\chi_{AA}(q_B)|^2}{\sqrt{|E_3| + q_B^2 \frac{A+2}{4A}}}, \quad (6.25)$$

$$n_2(q_B) = 2 \int d^3 p_B \frac{|\chi_{AB}(|\mathbf{p}_B - \frac{\mathbf{q}_B}{2}|)|^2}{(|E_3| + p_B^2 + q_B^2 \frac{A+2}{4A})^2}, \quad (6.26)$$

$$n_3(q_B) = 2 \chi_{AA}^*(q_B) \int d^3 p_B \frac{\chi_{AB}(|\mathbf{p}_B - \frac{\mathbf{q}_B}{2}|)}{(|E_3| + p_B^2 + q_B^2 \frac{A+2}{4A})^2} + c.c., \quad (6.27)$$

$$n_4(q_B) = \int d^3 p_B \frac{\chi_{AB}^*(|\mathbf{p}_B - \frac{\mathbf{q}_B}{2}|) \chi_{AB}(|\mathbf{p}_B + \frac{\mathbf{q}_B}{2}|)}{(|E_3| + p_B^2 + q_B^2 \frac{A+2}{4A})^2} + c.c.. \quad (6.28)$$

Going to the large momentum domain,  $q \gg \sqrt{|E_3|}$ , the limit  $|E_3| \rightarrow 0$  is taken, i.e., the three-body energy is assumed to be negligible, since the focus is the imprint of excited Efimov states on the momentum distribution. These states are very extended and do not feel any short-range effects besides those encoded in the three-body parameter,  $q^*$ , discussed above.

The asymptotic forms for the spectator functions are used in the integrals of Eqs. (6.25) to (6.28), where the integration is being performed from 0 to  $\infty$ . This may a priori cause problems at small momenta. However, a numerical check shows that the different behavior of the spectator functions at low momenta contributes only at next-to-next-to-leading order (NNLO). This procedure is the same as the one used in Ref. [Castin 2011].

The large momentum limit of the four terms in Eqs. (6.25) to (6.28) is worked out in Appendix E, which is supplemented by Appendix F. The derivation of the large momentum contributions of the terms  $n_3(q_B)$  (see Eq. (6.27)) and  $n_4(q_B)$  (see Eq. (6.28)) require several non-trivial mathematical steps, which let them too long and make the presentation lengthy in the bulk of the Chapter. However, it is worth to emphasize that the equa-

tions derived in Appendix E are the basis of the following discussion and their tricky derivation deserves to be looked out. Then, the large momentum contribution of the four terms in Eqs. (6.25) to (6.28) up to next-to-leading order (NLO) is found to be

$$\langle n_1(q_B) \rangle = \frac{\pi^2}{q_B^5} |c_{AA}|^2 \sqrt{\frac{\mathcal{A}}{\mathcal{A}+2}}, \quad (6.29)$$

$$\langle n_2(q_B) \rangle = \frac{8\mathcal{A}^2}{q_B^4 (\mathcal{A}+1)^2} \int d^3q_A |\chi_{AB}(q_A)|^2 - \frac{8\pi^2 |c_{AB}|^2}{q_B^5} \frac{\mathcal{A}^3 (\mathcal{A}+3)}{(\mathcal{A}+1)^3 \sqrt{\mathcal{A}(\mathcal{A}+2)}}, \quad (6.30)$$

$$\langle n_3(q_B) \rangle = \frac{4\pi^2 c_{AA} c_{AB}}{q_B^5 \cosh\left(\frac{s\pi}{2}\right)} \left\{ \sqrt{\frac{\mathcal{A}}{\mathcal{A}+2}} \cos\left(s \ln \sqrt{\frac{\mathcal{A}+1}{2\mathcal{A}}}\right) \cosh\left[s\left(\frac{\pi}{2} - \theta_3\right)\right] + \sin\left(s \ln \sqrt{\frac{\mathcal{A}+1}{2\mathcal{A}}}\right) \sinh\left[s\left(\frac{\pi}{2} - \theta_3\right)\right] \right\}, \quad (6.31)$$

$$\langle n_4(q_B) \rangle = \frac{8\pi^2 |c_{AB}|^2 \mathcal{A}^2}{s q_B^5 \sqrt{\mathcal{A}(\mathcal{A}+2)} \cosh\left(\frac{s\pi}{2}\right)} \left\{ \sqrt{\mathcal{A}(\mathcal{A}+2)} \sinh\left[s\left(\frac{\pi}{2} - \theta_4\right)\right] - \frac{s \mathcal{A}}{\mathcal{A}+1} \cosh\left[s\left(\frac{\pi}{2} - \theta_4\right)\right] \right\}, \quad (6.32)$$

where  $\tan \theta_3 = \sqrt{\frac{\mathcal{A}+2}{\mathcal{A}}}$  for  $0 \leq \theta_3 \leq \pi/2$  and  $\tan \theta_4 = \sqrt{\mathcal{A}(\mathcal{A}+2)}$  for  $0 \leq \theta_4 \leq \pi/2$ .

## 6.4 Leading and sub-leading terms

As discussed in Sec. 5.3.2, the leading order term  $\frac{C}{q_B^4}$  has the same functional form as in 2D and comes only from  $n_2$ , i.e., the first term on the right-hand-side of Eq. (6.30). The constant  $C$  is simply given by  $C = \frac{8\mathcal{A}^2}{(\mathcal{A}+1)^2} \int d^3q_A |\chi_{AB}(q_A)|^2$ , which gives  $C/\kappa_0 = 0.0274$  for  $^{133}\text{Cs}$ - $^{133}\text{Cs}$ - $^6\text{Li}$  and  $C/\kappa_0 = 0.0211$  for  $^{87}\text{Rb}$ - $^{87}\text{Rb}$ - $^6\text{Li}$ . For  $\mathcal{A} = 1$ , the value  $3(2\pi)^3 C/\kappa_0 = 52.8$  is close to the exact value 53.097, obtained in Ref. [Castin 2011]. The factor  $3(2\pi)^3$  comes from the different choice of normalization.

The small discrepancy from both values of the contact parameter for a

system composed for identical bosons arises from numerical issues. While the numerical value obtained here is calculated for the second excited state, the exact value in Ref. [Castin 2011] is calculated for an arbitrary highly excited state.

In Fig. 6.3 is shown the value of  $C/\kappa_0$  for mass ratios in the range  $6/133 \leq \mathcal{A} \leq 25$ . The increase is very rapid until  $A \approx 5$ , beyond which an almost constant value is reached. A similar behavior is found in 2D, as shown in Fig. 5.8.

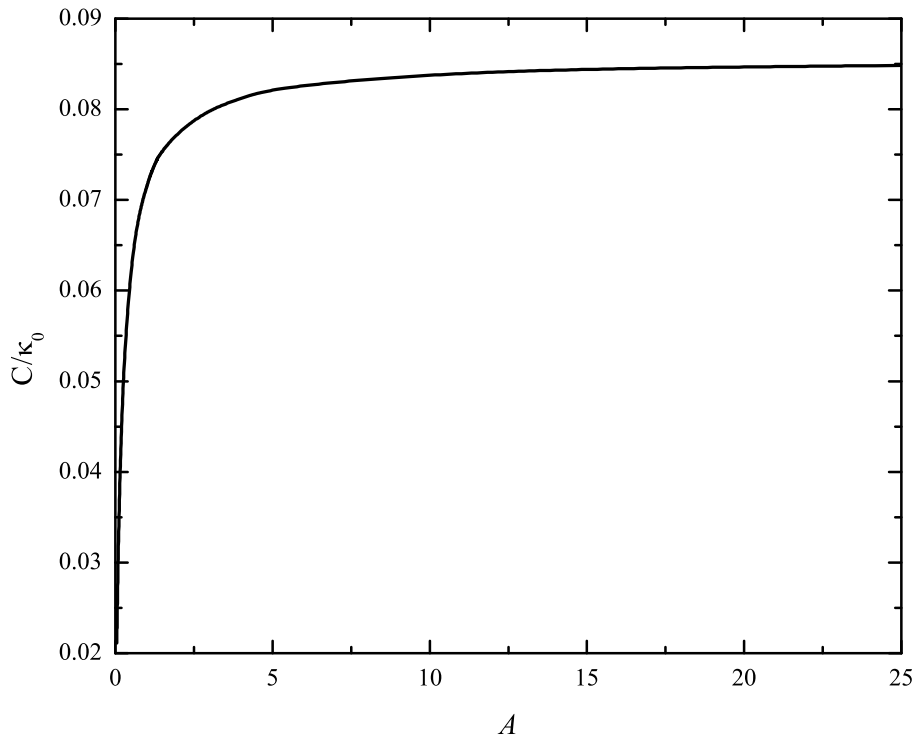


Figure 6.3:  $C/\kappa_0$  for mass ratios in the range  $6/133 \leq \mathcal{A} \leq 25$ .

In Ref. [Castin 2011] it is shown that the non-oscillatory term of order  $q_B^{-5}$  coming from  $n_1$  to  $n_4$  exactly cancels for  $\mathcal{A} = 1$ . However, this conclusion does not hold in the general case  $\mathcal{A} \neq 1$ , as demonstrated bellow.

The four analytic expressions derived for each of the components of the one-body momentum distribution in Sec. 6.3 are defined apart the coefficients  $c_{aa}$  and  $c_{ab}$ . The ratio between these coefficients is given by Eq. (6.15),



which can be used to eliminate one of these factors. The other one can be determined from the overall normalization of the wave function. As the study is focused on the general behavior of the momentum distribution, the normalization is not relevant and the remaining coefficient is set to unit from now on, i.e.,  $c_{AB} = 1$ .

The contribution  $-(n_1+n_2+n_3)$  and  $n_4$  are shown in Fig. 6.4 as a function of mass ratio  $\mathcal{A}$  (each individual component  $n_i$  as function of the mass ratio  $\mathcal{A}$  is shown in Fig. 6.5). What is immediately seen is that for  $\mathcal{A} = 1$  the result of Ref. [Castin 2011] is reproduced, i.e., that the  $q_B^{-5}$  non-oscillatory term cancels. However, for general  $\mathcal{A}$  this does not hold and a  $q_B^{-5}$  term in the asymptotic momentum distribution should also be expected for systems with two identical and a third particle.

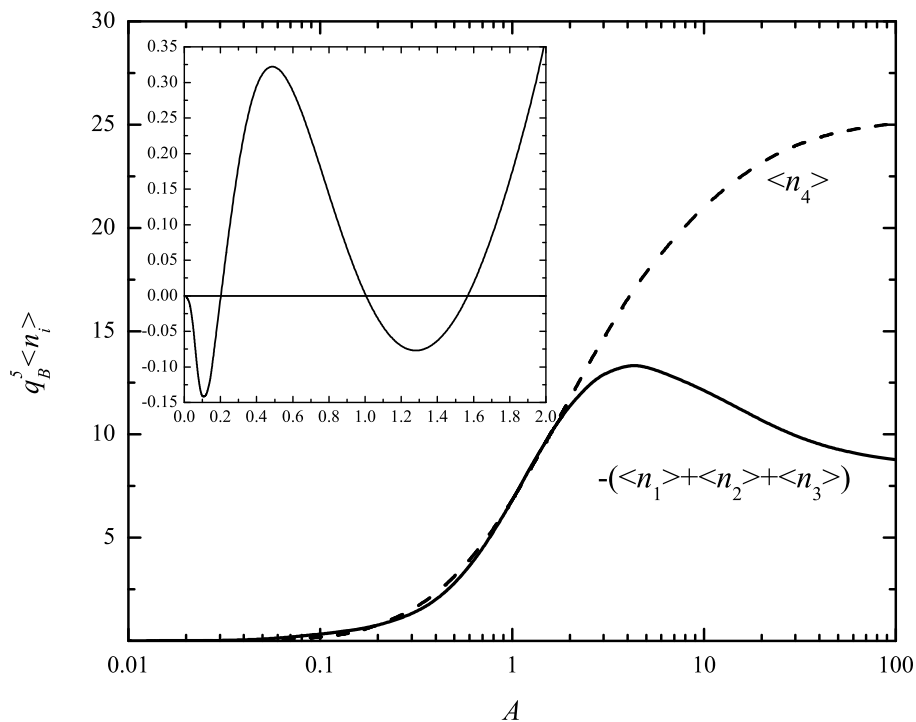


Figure 6.4: Non-oscillatory contributions for  $n_1$ ,  $n_2$ ,  $n_3$  and  $n_4$  as a function of the mass ratio  $\mathcal{A}$ . Their sum, showed in the inset, cancels exactly for  $\mathcal{A} = 0.2, 1$  and  $1.57$ .

This demonstrates that non-equal masses will generally influence not

only the value of the contact parameter attributed to three-body bound states but also the functional form of the asymptotic momentum tail. Another important difference between 2D and 3D system arises here. Remember that systems of non-equal masses have the same functional form of the next-order contribution to the momentum distribution (see Sec. 5.2). Curiously, there is an oscillatory behavior around  $\mathcal{A} \sim 1$  from the sum of all contributions. This is shown in the inset of Fig. 6.4 where zero-crossings are seen at  $\mathcal{A} = 0.2, 1,$  and  $1.57$ . It seems quite clear that all the oscillatory terms, which depend on the scale factor  $s$ , are the reason for this interesting behavior, but a physical explanation for it was not found yet.

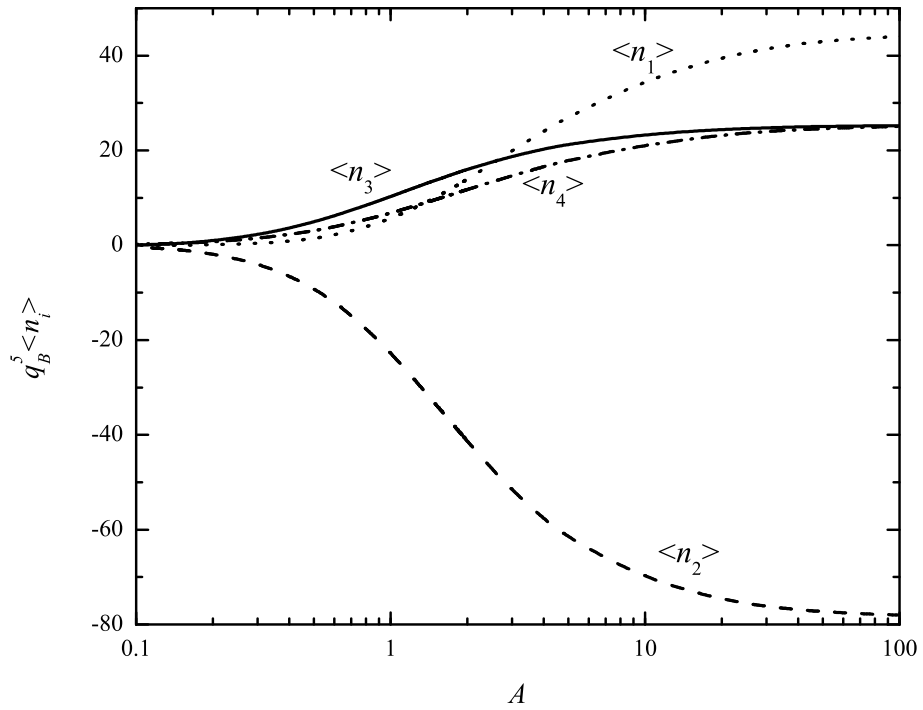


Figure 6.5: Individual non-oscillatory contributions for  $n_1$ ,  $n_2$ ,  $n_3$  and  $n_4$  as a function of the mass ratio  $\mathcal{A}$ .

However, what makes this interesting is the fact that if ratios of typical isotopes of alkali atoms like Li, Na, K, Rb, and Cs are taken, then one can get rather close to 0.2 or 1.57. For instance, taking one  $^{133}\text{Cs}$  and two  $^{85}\text{Rb}$  yields  $\mathcal{A} = 1.565$ , while one  $^7\text{Li}$  atom and two  $^{39}\text{K}$  atoms yields  $\mathcal{A} = 0.179$ . These interesting ratios are thus close to experimentally accessible species.

## 6.5 Numerical examples

Some numerical examples of momentum distributions for the experimentally interesting systems with large mass ratios are now provided. Focus is on  $^{133}\text{Cs}$ - $^{133}\text{Cs}$ - $^6\text{Li}$  and  $^{87}\text{Rb}$ - $^{87}\text{Rb}$ - $^6\text{Li}$  systems, where two extreme possibilities are investigated: (i) the heavy-heavy subsystems, i.e.,  $^{133}\text{Cs}$ - $^{133}\text{Cs}$  and  $^{87}\text{Rb}$ - $^{87}\text{Rb}$ , have a two-body bound state at zero energy and (ii) the opposite limit where they do not interact. In the first case the heavy atoms are at a Feshbach resonance with infinite scattering length, while in the second case they are far from resonance and a negligible background scattering length is assumed. As it was recently demonstrated for the  $^{133}\text{Cs}$ - $^6\text{Li}$  mixture, there are Feshbach resonances in the Li-Cs subsystem at positions where the Cs-Cs scattering length is non-resonant [Repp 2013, Tung 2013]. While this does not automatically imply that the Cs-Cs channel can be neglected, the assumption (ii) is made here. The formalism can be modified in a straightforward manner to also include interaction in the heavy-heavy subsystem.

As before the focus is on the  $AAB$  system, where  $A$  refers to the identical (bosonic) atoms,  $^{133}\text{Cs}$  or  $^{87}\text{Rb}$ , and  $B$  to  $^6\text{Li}$ . By solving Eq. (6.18), the scaling factors are  $s(6/133) = 2.00588$  and  $s(6/87) = 1.68334$  when assuming that all three subsystems have large scattering lengths (solid line in Fig. 6.2). The situation where the interaction between the two identical particles is turned off is shown by the dashed line in Fig. 6.2. In this case,  $s(\mathcal{A})$  is calculated from Eq. (6.16) by setting  $c_{AA} = 0$ . This yields  $s(6/133) = 1.98572$  and  $s(6/87) = 1.63454$ .

Firstly the binding energies are considered. Assuming that the Cs-Cs and Rb-Rb two-body energies are zero, a system satisfying the universality condition  $|a| \gg r_0$  implies that any observable should be a function of the remaining two- and three-body scales, which can be conveniently chosen as  $|E_3|^{(N)}$  and  $E_{AB}$  (the Cs-Li or Rb-Li two-body energy). Here  $N$  denotes the  $N$ th consecutive three-body bound state with  $N = 0$  being the lowest one. Thus, the energy of an  $N + 1$  state can be plotted in terms of a scaling func-

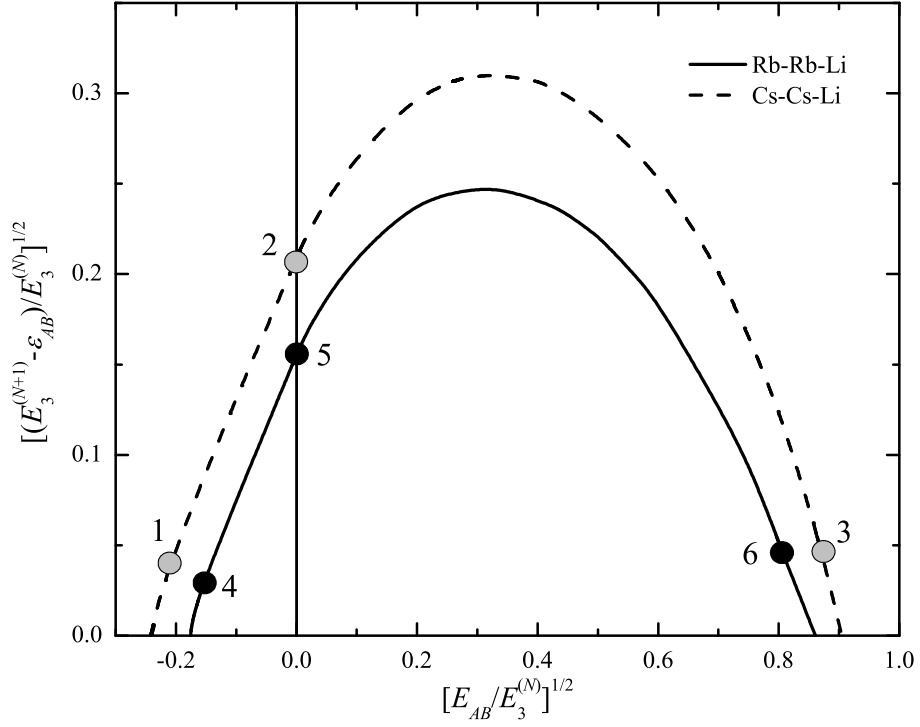


Figure 6.6:  $E_{AB}$  is the Cs-Li or Rb-Li two-body energy (Cs-Cs and Rb-Rb two-body energies are zero). The negative and positive parts refer, respectively, to virtual and bound  $AB$  states, such that  $\epsilon_{AB} = 0$  and  $\epsilon_{AB} \equiv E_{AB}$ , respectively, on the negative and positive sides. The circles labeled from 1 to 6 mark the points where the momentum distributions have been calculated.

tion relating only  $E_{AB}$  and the energy of previous state. The limit cycle, which should be in principle reached for  $N \rightarrow \infty$ , is achieved pretty fast such that the curve in Fig. 6.6 is constructed using  $N = 2$  [Yamashita 2002, Federico 2012]. In this figure, the negative and positive parts of the horizontal axis refer, respectively, to virtual and bound two-body  $AB$  states. The circles labeled from 1 to 6 mark the points where the momentum distributions have been calculated. The points 1 and 4 represent the Borromean case, the points 2 and 5 are the “Efimov situation” and in points 3 and 6  $AB$  is bound.

Fig. 6.7(a) and 6.7(b) give the momentum distributions of the second excited states for the energy ratio  $\sqrt{|E_{AB}|/|E_3|}$  given by the points labeled from

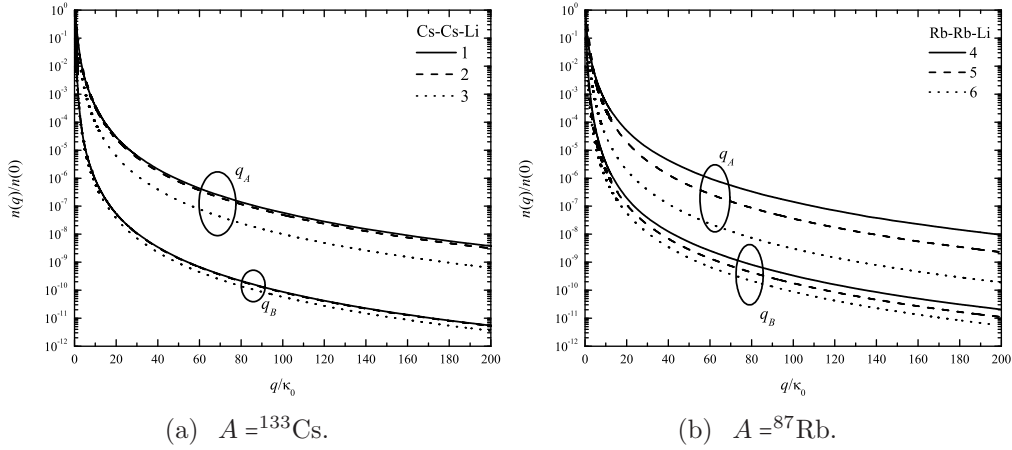


Figure 6.7: Momentum distribution for the second excited state as a function of the relative momentum of one  $A$ -particle,  $q_A$ , or  ${}^6\text{Li}$ ,  $q_B$ , to the center-of-mass of the remaining pair  $A$ - ${}^6\text{Li}$  or  $A$ - $A$ . The solid, dashed and dotted lines were calculated for the two- and three-body energies satisfying the ratios indicated by the points 1 to 3 ( $A = {}^{133}\text{Cs}$ ) and 4 to 6 ( $A = {}^{87}\text{Rb}$ ) in Fig. 6.6. The circles show the set of curves related to  $q_A$  or  $q_B$ .

1 to 6 in Fig. 6.6. According to previous calculations [Yamashita 2004a], for fixed three-body energy the size of the system increases as the number of bound two-body subsystems increase. Thus, it seems reasonable that the Borromean case decreases slower. This behavior is clearly seen in Figs. 6.7(a) and 6.7(b). The distance of one atom to the center-of-mass of the other two is much larger for  ${}^6\text{Li}$  than for  ${}^{133}\text{Cs}$  or  ${}^{87}\text{Rb}$ , due to the large difference of the masses. Therefore, the momentum distribution for the heavier atom,  $q_A$  set, decreases much slower than that for the lighter one,  $q_B$  set.

Figs. 6.8(a) and 6.8(b) show the rescaled momentum distributions for the ground, first and second excited states. In these figures, the subsystem energies are chosen to zero, corresponding to the transition point to a Borromean configuration. In this situation, the only low-energy scale is  $|E_3|$  (remember that the high-momentum scale is  $\mu = 1$ ). Therefore, in units in which  $|E_3| = 1$ , to achieve a universal regime, in principle, to wash-out the effect of the subtraction scale,  $\mu$ , it is necessary to go to a highly excited state. However, a universal low-energy regime of  $n(q_B)/n(q_B = 0)$  is seen

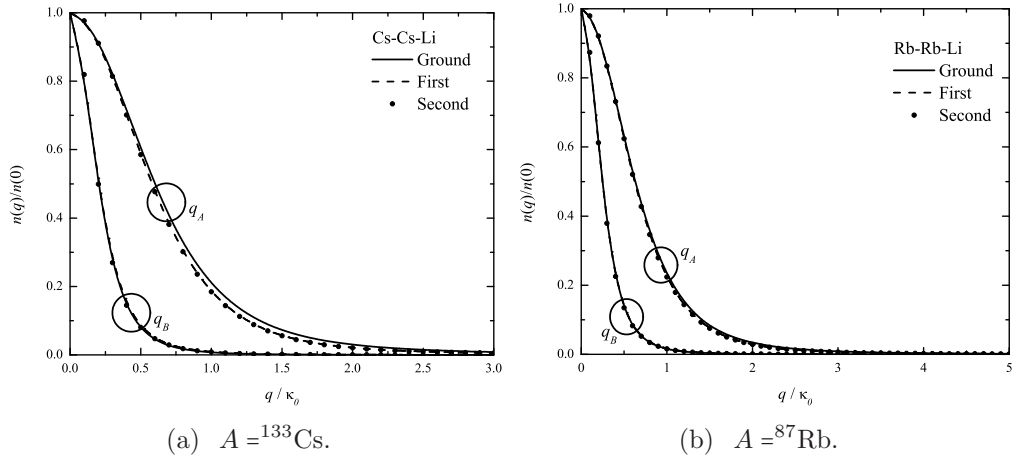


Figure 6.8: Rescaled momentum distribution for the ground, first and second excited states as a function of the relative momenta of the  $A$ -particle to the center-of-mass of the pair  ${}^6\text{Li}-A$ ,  $q_A$ , and of  ${}^6\text{Li}$  to the center-of-mass of the pair  $A-A$ ,  $q_B$ . The subsystem binding energies are all set to zero. Normalization to unity at zero momentum.

for momentum of the order of  $\sqrt{|E_3|}$ , even for the ground state which is smaller than excited states. Then, in practice, the universal behavior of the momentum distribution is approached rapidly.

# Dimensional crossover

---

Examples of how the dimensionality affects the properties of physical system have been recently attracting great interest, since the possibility of probing lower dimensional systems has been continuously increasing. One recent and famous example is graphene, which is itself an effective two-dimensional (2D) structure with good mechanical and electrical properties [Novoselov 2004]. Besides that, the experimental study of one-dimensional (1D) systems, which is an useful theoretical laboratory to study physical problems, has also been recently reported [Serwane 2011, Zürn 2012]. Following this line, maybe the most surprisingly achievement is the study of the so-called quantum dots [Ramos 2011], which are approached as zero-dimensional systems.

Dimensionality also plays an important role in the behavior of few- and many-body quantum systems. As it was discussed in Chapters 3 and 6, the Efimov effect [Efimov 1970], where a geometric series of three-body bound states of three bosons occurs at the threshold for binding the two-body subsystems, is present in 3D systems but absent when the dimension is reduced to two. A straightforward consequence discussed in Chapters 5 and 6 is that systems restricted to different dimensions have very distinct two- and three-body contact parameters and asymptotic forms of the momentum distribution at the next-to-leading order. The contact parameters can be defined via the one-body large momentum density and relate few- and many-body properties of quantum atomic gases [Tan 2008].

Cold atomic gases have proven their ability to be excellent quantum simulators due to the tunability of interactions, geometry and inter-particle statistical properties. At the few-body level, three-body states linked to

the Efimov effect have been observed in three dimensions (see for example Ref. [Kraemer 2006, Berninger 2011b]) using a variety of different atomic species and two-body Feshbach resonances [Chin 2010].

In spite of the tunability of the external trapping geometry of cold atomic systems, there has been little study of how the three-boson bound state problem undergoes its dramatic change from displaying the Efimov effect in three dimensions, yet in two dimensions the systems only holds two bound states [Bruch 1979]. A key question is whether it is possible to interpolate these limits in simple theoretical terms and subsequently explore this in simulations using both more involved numerical methods and experimental setups.

A model that has the ability to interpolate geometrically between two and three spatial dimensions and thus study this crossover for both two- and three-body bound states of identical bosons is proposed. A “squeezed” dimension whose size can be varied to interpolate the two limits is employed with periodic boundary conditions (PBC). This model has the unique feature that it can be regularized analytically which is a great advantage for its numerical implementation allowing to go smoothly between both limits.

The theoretical elegance and tractability of calculations in the three-body system is itself a strong incentive for pursuing this geometry, but in spite of this elegance, a direct connection between experiments and the parameter that dials between different dimensions with PBC in this model was not found yet. On the other hand, it is also possible to formulate the problem with open boundary conditions (OBC). While for many experimental setups in cold atoms the transverse confining geometry is given by a harmonic trapping potential and a recent theoretical study [Levinsen 2014] has considered the properties of three-boson states under strong transverse confinement, the recent successful production of box potential traps with bosons [Gaunt 2013, Schmidutz 2014] means that OBC (hard wall) are now accessible. Besides that, the formulation of the problem with OBC is left for a future consideration.

The method allows to study the dimensional crossover transitions of



strongly interacting two- and three-bosons systems by continuously “squeezing” one of the dimensions. The motion of the particles is separated into two directions, namely a flat surface plus a transverse direction (compact dimension) which has the position/momentum discretized accordingly to the chosen type of boundary conditions. Notice that, unless in the pure 2D limit, the problem is always 3D (Quasi- 2D). In the following, the case of periodic boundary condition (PBC) is considered.

## 7.1 Renormalization with a compact dimension

Effects of a compact dimension are investigated in a system of three-identical bosons with zero-range pairwise interactions. The formal expression of the two- and three-body transition operators is the same as the one presented in Chapter 2, which reads

$$T(E) = V + VG_0(E)T(E) . \quad (7.1)$$

However, the matrix elements are not the same now, due to the restriction of the momentum in the transverse direction, that arises from the boundary condition from which the system is subjected. Being  $\mathbf{k}$  and  $\mathbf{k}'$  respectively the momenta of the incoming and outgoing waves, the matrix elements of Eq. (7.1) are given by

$$\langle \mathbf{k}' | T(E) | \mathbf{k} \rangle = \langle \mathbf{k}' | V | \mathbf{k} \rangle + \int d\mathbf{q} d\mathbf{q}' \langle \mathbf{k}' | V | \mathbf{q} \rangle \langle \mathbf{q} | G_0(E) | \mathbf{q}' \rangle \langle \mathbf{q}' | T(E) | \mathbf{k} \rangle , \quad (7.2)$$

where the symbol  $\int$  indicates that all momenta are being taken into account, i.e., there is an integration over the continuum momentum in the plane ( $p_\perp$ ) and a sum over the discrete perpendicular momentum ( $p_z$ ). The particular form of  $\int$  depends on the type of boundary conditions that are being addressed.

Once more, the interaction between particles is described by Dirac- $\delta$  potentials. As it is discussed in Sec. 2.1, the matrix element for this kind of potential is  $\langle \mathbf{k}' | V | \mathbf{q} \rangle = V(\mathbf{k}', \mathbf{q}) = \lambda$  and therefore Eq. (7.2) has also to be renormalized. Following the procedure from Refs. [Adhikari 1995b, Adhikari 1995a], which is briefly presented in Sec. 2.4.1, the renormalized transition matrix for two- and three-body systems subjected to a compact dimension are given by

$$\langle \mathbf{k}' | T(E) | \mathbf{k} \rangle = T(-\mu^2) - T(-\mu^2)(\mu^2 + E) \int d\mathbf{q} G_0(\mathbf{q}, E) G_0(\mathbf{q}, -\mu^2) T(\mathbf{q}, \mathbf{k}, E), \quad (7.3)$$

where in the two-body sector  $T(-\mu^2)$  is a constant, namely  $T(-\mu^2) = \lambda$  and in the three-body sector  $T(-\mu^2)$  is the sum over the renormalized two-body  $T$ -matrix given in Eq. (2.73).

In the two-body sector, since the right-hand-side of Eq. (7.3) is independent of  $\mathbf{k}'$  and  $\mathbf{k}$ , it is possible to define  $T(\mathbf{q}, \mathbf{k}, E) = \langle \mathbf{q} | T(E) | \mathbf{k} \rangle = \langle \mathbf{k}' | T(E) | \mathbf{k} \rangle = \tau(E)$ . The two-body  $T$ -matrix becomes

$$\begin{aligned} \tau(E) &= \lambda - \lambda(\mu^2 + E) \tau(E) \int d\mathbf{q} G_0(\mathbf{q}, E) G_0(\mathbf{q}, -\mu^2) . \\ &= \frac{\lambda}{1 + \lambda(\mu^2 + E) \int d\mathbf{q} G_0(\mathbf{q}, E) G_0(\mathbf{q}, -\mu^2)} . \end{aligned} \quad (7.4)$$

In the three-body sector, the renormalized  $T$ -matrix in Eq. (7.3) is given by

$$T(E) = T(-\mu^2) + T(-\mu^2) [G_0(E) - G_0(-\mu^2)] T(E), \quad (7.5)$$

is the sum over the renormalized two-body  $T$ -matrix given in Eq. (2.73). Notice that Eq. (7.5) is identical to Eq. (2.74), meaning that the derivation of the coupled homogeneous integral equations for the three-body bound state is the same as in Sec. (2.4.2). The only difference now is that the momentum  $\mathbf{q}$  and the phase factor  $d\mathbf{q}$  are restricted by the boundary conditions.

## 7.2 3D - 2D transition with PBC

Periodic boundary conditions (PBC) are assumed to be valid for the relative distance between the particles in the compact dimension, chosen to be  $z$ . Then, the relative momentum is given by  $\mathbf{p}_\perp = (p_x, p_y)$  in the flat 2D surface and by

$$p_z = \frac{2\pi n}{L} = \frac{n}{R}, \quad n = 0, \pm 1, \pm 2, \dots, \quad (7.6)$$

in the transverse direction, with  $L = 2\pi R$  being the size of the compact dimension corresponding to a radius  $R$ , which is the parameter that dials between two and three-dimensions. When  $R \rightarrow 0$  it selects the 2D case and in the opposite limit, i.e.,  $R \rightarrow \infty$ , the 3D case is selected. The momentum  $\mathbf{q}$  and its corresponding phase factor  $d\mathbf{q}$  in Eq. (7.4) are, with PBC, given by

$$q^2 = p_\perp^2 + \frac{n^2}{R^2} \quad \text{and} \quad d\mathbf{q} = \frac{1}{R} d^2 p_\perp. \quad (7.7)$$

The symbol  $\oint$ , which indicates an integration over the continuum momentum in the plane ( $p_\perp$ ) and a sum over the discrete perpendicular momentum ( $p_z = \frac{n}{R}$ ) in this case reads

$$\oint d\mathbf{q} \equiv \sum_{n=-\infty}^{\infty} \int \frac{1}{R} d^2 p_\perp. \quad (7.8)$$

### 7.2.1 Two-body scattering amplitude

Replacing  $q^2 = p_\perp^2 + \frac{n^2}{R^2}$  and  $d\mathbf{q} = \frac{1}{R} d^2 p_\perp$ , Eq. (7.4) becomes

$$R^{-1}\tau(E) = \left[ \lambda^{-1}R - (\mu^2 + E) \oint d^2 p_\perp \frac{1}{(E - p_\perp^2 - \frac{n^2}{R^2} + i\epsilon)(\mu^2 + p_\perp^2 + \frac{n^2}{R^2})} \right]^{-1}. \quad (7.9)$$

The choice of  $-\mu^2 = E_2$  leads to  $\lambda^{-1} = 0$  (see Sec. 2.1) and the matrix

elements in Eq. (7.9) are given by

$$R^{-1}\tau_p(E) = [I_R(E)]^{-1}, \quad (7.10)$$

where the subscript  $p$  distinguish between the matrix elements of systems restricted purely to 2D or 3D to the compacted dimension (quasi-2D) with PBC discussed here and the function  $I_R(E)$  is given by

$$I_R(E) = \oint d^2p_\perp \frac{-(E - E_2)}{(E - p_\perp^2 - \frac{n^2}{R^2} + i\epsilon)(-E_2 + p_\perp^2 + \frac{n^2}{R^2})}. \quad (7.11)$$

For  $E < 0$  the function in Eq. (7.11) reads

$$\begin{aligned} I_R(E) &= - \oint d^2p_\perp \left[ \frac{1}{|E_2| + p_\perp^2 + \frac{n^2}{R^2}} - \frac{1}{|E| + p_\perp^2 + \frac{n^2}{R^2}} \right], \\ &= -\pi \sum_{n=-\infty}^{\infty} \lim_{\Lambda \rightarrow \infty} \left[ \ln \left( |E_2| + p_\perp^2 + \frac{n^2}{R^2} \right) \Big|_{p_\perp=0}^{\Lambda} - \ln \left( |E| + p_\perp^2 + \frac{n^2}{R^2} \right) \Big|_{p_\perp=0}^{\Lambda} \right], \\ &= -\pi \sum_{n=-\infty}^{\infty} \lim_{\Lambda \rightarrow \infty} \left[ \ln \left( \frac{|E_2| + \Lambda^2 + \frac{n^2}{R^2}}{|E| + \Lambda^2 + \frac{n^2}{R^2}} \right) + \ln \left( \frac{|E| + \frac{n^2}{R^2}}{|E_2| + \frac{n^2}{R^2}} \right) \right], \\ &= -\pi \sum_{n=-\infty}^{\infty} \ln \left( \frac{|E| + \frac{n^2}{R^2}}{|E_2| + \frac{n^2}{R^2}} \right) = -\pi \sum_n \ln \left( \frac{-E + \frac{n^2}{R^2}}{|E_2| + \frac{n^2}{R^2}} \right). \end{aligned} \quad (7.12)$$

On the other hand, for  $E > 0$  the analytic extension of Eq. (7.12) must be

$$\begin{aligned} I_R(E) &= -\pi \sum_{n=-\infty}^{\infty} \left\{ \ln \left( \frac{-E + \frac{n^2}{R^2}}{|E_2| + \frac{n^2}{R^2}} \right) \Theta \left( \frac{n^2}{R^2} - E \right) \right. \\ &\quad \left. + \left[ \ln \left( \frac{E - \frac{n^2}{R^2}}{|E_2| + \frac{n^2}{R^2}} \right) - i\pi \right] \Theta \left( E - \frac{n^2}{R^2} \right) \right\}. \end{aligned} \quad (7.13)$$

The sum over  $n$  in Eq. (7.13) can be performed analytically for  $E < 0$ , noticing that

$$\sum_{n=-\infty}^{\infty} \ln \left( \frac{a^2 + n^2}{b^2 + n^2} \right) = 2 \ln \left[ \frac{\sinh(\pi a)}{\sinh(\pi b)} \right]. \quad (7.14)$$

Then, the function  $I_R(E)$  becomes

$$I_R(E) = -2\pi \ln \left[ \frac{\sinh(\pi R \sqrt{|E|})}{\sinh(\pi R \sqrt{|E_2|})} \right], \quad (7.15)$$

and the matrix elements of the transition operator for two-body systems restricted to a compact dimension with PBC are given by

$$\tau_p(E)^{-1} = R^{-1} I_R(E) = -\frac{2\pi}{R} \ln \left[ \frac{\sinh(\pi R \sqrt{|E|})}{\sinh(\pi R \sqrt{|E_2|})} \right]. \quad (7.16)$$

Notice that  $\tau_p(E)$  recovers the matrix elements of 3D and 2D systems in the limits  $R \rightarrow \infty$  and  $R \rightarrow 0$ , respectively. The first case is straightforward and reads

$$\tau_{3D}^{-1}(E) = \lim_{R \rightarrow \infty} \tau_p^{-1}(E) = -2\pi^2 \left( \sqrt{|E|} - \sqrt{|E_2|} \right), \quad (7.17)$$

which is identical to Eq. (2.28).

Before going to the 2D limit, it is important to notice that, as it was said before, a quasi-2D system is in practice a 3D system. Then, the units of  $\tau_{3D}^{-1}(E)$  and  $\tau_p^{-1}(E)$  are exactly the same and reads  $[E].[L]^3$ , as it can be easily seen in from Eq. (7.2), where

$$\langle \mathbf{k}' | T(E) | \mathbf{k} \rangle = \int \frac{d^3x}{(2\pi)^3} e^{i\mathbf{k}' \cdot \mathbf{x}} e^{-i\mathbf{k} \cdot \mathbf{x}} \langle \mathbf{x} | V | \mathbf{x} \rangle. \quad (7.18)$$

On the other hand, the unit of  $\tau_{2D}^{-1}(E)$  is  $[E].[L]^2$ , which gives  $\frac{[\tau_{2D}^{-1}(E)]}{[\tau_p^{-1}(E)]} = [L]^{-1}$ . Taking into account the correct units, the 2D limit of Eq. (7.15) reads

$$\tau_{2D}^{-1}(E) = \lim_{R \rightarrow 0} R \tau_p^{-1}(E) = -2\pi \ln \left( \sqrt{\frac{|E|}{|E_2|}} \right), \quad (7.19)$$

which is identical to Eq. (2.25).

### 7.2.2 Dimer binding energy

Up to this point, the energy of the dimer,  $E_2$ , was considered unchanged during the squeezing of the trap. In this subsection it is shown how  $E_2$  changes as the parameter  $R$ , which controls the size of the trap, is continuously tuned from 3D to 2D when the squeezing is performed with PBC. The analysis starts with the denominator of Eq. (7.9) in the limit of  $\mu \rightarrow \infty$ , which reads

$$R^{-1}\tau_p(E) = \left[ R\lambda^{-1}(\mu \rightarrow \infty) - \rlap{-}\int \frac{d^2p_\perp}{E - \mathbf{p}_\perp^2 - \frac{n^2}{R^2} + i\epsilon} \right]^{-1}. \quad (7.20)$$

Therefore, the ultraviolet divergence has to be removed by  $\lambda^{-1}(\mu \rightarrow \infty)$ , which can be chosen as

$$\lambda^{-1}(\mu \rightarrow \infty) = \int \frac{d^3p}{E_2^{3D} - \mathbf{p}^2}, \quad (7.21)$$

where the limit  $R \rightarrow \infty$  leads to the bound-state pole at the dimer energy in 3D, namely  $\tau_p^{-1}(E) = 0$  at  $E = E_2^{3D}$ . The renormalized scattering amplitude becomes

$$R^{-1}\tau_p(E) = \left[ R \int \frac{d^3p}{E_2^{3D} - \mathbf{p}^2} - \rlap{-}\int \frac{d^2p_\perp}{E - \mathbf{p}_\perp^2 - \frac{n^2}{R^2} + i\epsilon} \right]^{-1}, \quad (7.22)$$

and to get a finite value for  $\tau_p(E)$  the ultraviolet cutoffs in both divergent terms have to be chosen consistently to keep the correct 3D limit. It is enough to regularize the momentum integral in the plane, namely  $d^2p_\perp$ , in both terms of Eq. (7.22) with an UV cutoff  $\Lambda$  and then perform the limit  $\Lambda \rightarrow \infty$ . The integration in  $d^2p_\perp$  in Eq. (7.22) was already done in Eq. (7.12) and changing variables to  $y \equiv R p$ , the renormalized  $T$ -matrix is given by

$$R\tau_p^{-1}(E) = \pi \lim_{\Lambda \rightarrow \infty} \left[ \int_{-\infty}^{\infty} dy \ln \left( \frac{-E_2^{3D} R^2 + y^2}{-E_2^{3D} R^2 + y^2 + (\Lambda R)^2} \right) - \sum_{n=-\infty}^{\infty} \ln \left( \frac{-E R^2 + n^2 - i\epsilon}{-E R^2 + n^2 + (\Lambda R)^2 + i\epsilon} \right) \right]. \quad (7.23)$$

The sum and the integral of the terms in the right-hand-side of Eq. (7.23) are respectively given by Eq. (7.14) and by

$$\int_{-\infty}^{\infty} dy \ln \left( \frac{a^2 + y^2}{b^2 + y^2} \right) = 2\pi \left( \frac{a^2}{|a|} - \frac{b^2}{|b|} \right). \quad (7.24)$$

For negative energies, Eq. (7.23) becomes

$$\begin{aligned} R\tau_p^{-1}(E) &= 2\pi \lim_{\Lambda \rightarrow \infty} \left\{ \pi R \left( \sqrt{-E_2^{3D}} - \sqrt{-E_2^{3D} + \Lambda^2} \right) \right. \\ &\quad \left. - \ln \left[ \frac{\sinh(\pi R \sqrt{-E})}{\sinh(\pi R \sqrt{-E + \Lambda^2})} \right] \right\}, \\ &= 2\pi \left\{ \pi R \sqrt{-E_2^{3D}} - \ln \left[ \sinh(\pi R \sqrt{-E}) \right] + L(\Lambda) \right\}, \end{aligned} \quad (7.25)$$

where

$$\begin{aligned} L(\Lambda) &\rightarrow \lim_{\Lambda \rightarrow \infty} \left\{ -\pi R \sqrt{-E_2^{3D} + \Lambda^2} + \ln \left[ \sinh(\pi R \sqrt{-E + \Lambda^2}) \right] \right\}, \\ &\rightarrow \ln \lim_{\Lambda \rightarrow \infty} \frac{1}{2} e^{-\pi R \sqrt{-E_2^{3D} + \Lambda^2}} \left( e^{\pi R \sqrt{-E + \Lambda^2}} - e^{-\pi R \sqrt{-E + \Lambda^2}} \right), \\ &\rightarrow \ln \frac{1}{2} \lim_{\Lambda \rightarrow \infty} \left( 1 - e^{-2\pi R \Lambda \sqrt{1 - E/\Lambda^2}} \right) \rightarrow -\ln 2, \end{aligned} \quad (7.26)$$

in the limit  $\Lambda \rightarrow \infty$  gives a finite result. The two-body  $T$ -matrix is finally written as

$$R^{-1}\tau_p(E) = (2\pi)^{-1} \left\{ \pi R \sqrt{-E_2^{3D}} - \ln \left[ 2 \sinh(\pi R \sqrt{-E}) \right] \right\}^{-1}. \quad (7.27)$$

The formula in Eq. (7.27) for the 2B scattering amplitude can be generalized to allow negative scattering lengths by recognizing that  $\sqrt{-E_2^{3D}} \rightarrow 1/a$  in the zero-range limit. Therefore, the energy of the bound dimer in quasi-2D for positive or negative 3D scattering lengths is the solution of

$$\tau_p^{-1}(E) = (2\pi) \left\{ \pi a^{-1} - R^{-1} \ln \left[ 2 \sinh(\pi R \sqrt{-E}) \right] \right\} = 0, \quad (7.28)$$

and can be written as

$$\sqrt{-E} = \frac{1}{\pi R} \sinh^{-1} \frac{e^{\pi R/a}}{2}, \quad (7.29)$$

For  $R \rightarrow 0$  it goes to  $\sqrt{-E} \sim (\pi R)^{-1} \sinh^{-1} \frac{1}{2} = 0.153174 R^{-1}$ , which does not depend on the scattering length. Therefore, for any 3D two-body subsystem - bound or virtual - a strong deformation of the trap towards 2D always binds the dimer.

### 7.2.3 Trimer bound state equation

Considering the momentum  $\mathbf{q}$  and the phase factor  $d\mathbf{q}$  as given in Eq. (7.7), where  $\mathbf{q} = \mathbf{q}_\perp + \mathbf{q}_z$  and  $d\mathbf{q} = \frac{1}{R} d^2 q_\perp$ , the three-body free Hamiltonian (see Eq. (2.32)) becomes

$$\begin{aligned} H_0^p(\mathbf{q}, \mathbf{k}) &= (\mathbf{q}_\perp + \mathbf{q}_z)^2 + (\mathbf{k}_\perp + \mathbf{k}_z)^2 + (\mathbf{q}_\perp + \mathbf{q}_z) \cdot (\mathbf{k}_\perp + \mathbf{k}_z), \\ &= q_\perp^2 + k_\perp^2 + \mathbf{q}_\perp \cdot \mathbf{k}_\perp + \frac{n^2}{R^2} + \frac{m^2}{R^2} + \frac{n m}{R^2}. \end{aligned} \quad (7.30)$$

Considering the proper two-body  $T$ -matrix and  $H_0^p$  respectively from Eqs. (7.16) and (7.30), the three-body bound state equation for a compact dimension with PBC is found to be

$$f(\mathbf{q}) = -\frac{2}{R} \tau_c \left( \frac{3}{4} q^2 - E_3 \right) \rlap{-}\int d\mathbf{k} \left( \frac{f(\mathbf{k})}{-E_3 + H_0^p(\mathbf{q}, \mathbf{k})} - \frac{f(\mathbf{k})}{\mu^2 + H_0^p(\mathbf{q}, \mathbf{k})} \right), \quad (7.31)$$

which after introducing the discrete momentum is written as

$$\begin{aligned} f(\mathbf{q}_\perp, n) &= -\frac{2}{R} \tau_c \left[ \frac{3}{4} \left( q_\perp^2 + \frac{n^2}{R^2} \right) - E_3 \right] \\ &\times \sum_{m=-\infty}^{\infty} \int d^2 k_\perp \left( \frac{f(\mathbf{k}_\perp, m)}{-E_3 + H_0^p(\mathbf{q}, \mathbf{k})} - \frac{f(\mathbf{k}_\perp, m)}{\mu^2 + H_0^p(\mathbf{q}, \mathbf{k})} \right). \end{aligned} \quad (7.32)$$

Note that the subtraction is kept even after the discretization because the Thomas collapse is always present for any finite compact radius, no



matter how small.

As the interaction between the particles corresponds to  $s$ -waves potentials and the focus is on states with zero angular momentum, the spectator functions do not depend on the angle, i.e.,  $f(\mathbf{q}) \equiv f(q)$  and the angular integration in Eq. (7.32) is solved using Eq. (2.69). Then, introducing dimensionless variables,  $\epsilon_3 = E_3/\mu^2$ ,  $\epsilon_2 = E_2/\mu^2$ ,  $r = R/\mu$ ,  $y_\perp = q_\perp/\sqrt{\mu}$  and  $x_\perp = k_\perp/\sqrt{\mu}$ , the subtracted equation for the three-body bound state with a compact dimension subjected to PBC is written as

$$f(y_\perp, n) = \left\{ \pi \ln \left[ \frac{\sinh \left( \pi r \sqrt{\frac{3}{4} \left( y_\perp^2 + \frac{n^2}{r^2} \right) - \epsilon_3} \right)}{\sinh(\pi r \sqrt{\epsilon_2})} \right] \right\}^{-1} \\ \times \sum_{m=-\infty}^{\infty} \int_0^\infty dx_\perp x_\perp f(x_\perp, m) \left( \frac{1}{\sqrt{\left( -\epsilon_3 + y_\perp^2 + x_\perp^2 + \frac{n^2}{r^2} + \frac{m^2}{r^2} + \frac{n m}{r^2} \right)^2 - y_\perp^2 x_\perp^2}} \right. \\ \left. - \frac{1}{\sqrt{\left( 1 + y_\perp^2 + x_\perp^2 + \frac{n^2}{r^2} + \frac{m^2}{r^2} + \frac{n m}{r^2} \right)^2 - x_\perp^2 y_\perp^2}} \right). \quad (7.33)$$

It is worthwhile to remind that Eq. (7.33) for  $R \rightarrow \infty$  returns precisely Eq. (6.1) for the spectator function in the 3D case.

### 7.3 2D - 1D with PBC

Periodic boundary conditions (PBC) are assumed to be valid for the relative distance between the particles in the compact dimension, chosen to be  $y$ . The relative momentum is given by  $\mathbf{p} = (p_x)$  in the linear dimension and by

$$p_y = \frac{\pi n}{L} = \frac{n}{R}, \quad n = 0, \pm 1, \pm 2, \pm 3, \dots, \quad (7.34)$$

in the transverse direction, with  $L = 2\pi R$  being the size of the compact dimension corresponding to a radius  $R$ , that is again the parameter that dials between two and three-dimensions. The limit  $R \rightarrow 0$  selects the 1D

case and in the opposite limit  $R \rightarrow \infty$ , the 2D one is selected.

Now, the momentum  $\mathbf{q}$  and its corresponding phase factor  $d\mathbf{q}$  in Eq. (7.4) are, with PBC, given by

$$q^2 = p_x^2 + \frac{n^2}{R^2} \quad \text{and} \quad d\mathbf{q} = \frac{1}{R} dp_x. \quad (7.35)$$

The symbol  $\oint$  indicates that all momenta are being taken into account, i.e., there is an integration over the continuum momentum in the linear coordinate ( $p_x$ ) and a sum over the discrete perpendicular momentum ( $p_y = \frac{n}{R}$ ). In other words

$$\oint d\mathbf{q} \equiv \sum_{n=-\infty}^{\infty} \int \frac{1}{R} dp_x. \quad (7.36)$$

### 7.3.1 Two-body scattering amplitude

Replacing  $q^2 = p_x^2 + \frac{n^2}{R^2}$  and  $d\mathbf{q} = \frac{1}{R} dp_x$ , Eq. (7.4) becomes

$$R^{-1} \bar{\tau}_p(E) = \left[ \lambda^{-1} R - (\mu^2 + E) \oint dp_x \frac{1}{\left(E - p_x^2 - \frac{n^2}{R^2} + i\epsilon\right) \left(\mu^2 + p_x^2 + \frac{n^2}{R^2}\right)} \right]^{-1}. \quad (7.37)$$

which leads to the renormalized scattering amplitude written as

$$R^{-1} \bar{\tau}_p(E) = \left[ R \int \frac{d^2 p}{E_2^{2D} - \mathbf{p}^2} - \oint \frac{dp}{E - \mathbf{p}^2 - \frac{n^2}{R^2} + i\epsilon} \right]^{-1}. \quad (7.38)$$

In order to get a finite value for  $\tau_p(E)$  the ultraviolet cutoffs in both divergent terms have to be chosen consistently to keep the correct 2D limit. Using that

$$\sum_{n=-\infty}^{\infty} \frac{1}{n^2 + a^2} = \frac{\pi \coth(\pi a)}{a}, \quad (7.39)$$

the  $T$ -matrix in Eq. (7.38) is worked for negative energies, which is enough for bound trimer calculations and reads

$$\begin{aligned}
 R^{-1}\bar{\tau}_p(E) &= (R\pi)^{-1} \lim_{\Lambda \rightarrow \infty} \left[ - \int_{-\Lambda}^{\Lambda} dp \frac{1}{\sqrt{-E_2^{2D} + p^2}} \right. \\
 &\quad \left. + \int_{-\Lambda}^{\Lambda} dp \frac{\coth(\pi R\sqrt{-E + p^2})}{\sqrt{-E + p^2}} \right]^{-1}, \\
 \bar{\tau}_p(E) &= \pi^{-1} \left[ \int_{-\infty}^{\infty} dp \left( \frac{\coth(\pi R\sqrt{-E + p^2})}{\sqrt{-E + p^2}} - \frac{1}{\sqrt{-E_2^{2D} + p^2}} \right) \right]^{-1}.
 \end{aligned} \tag{7.40}$$

The energy of the bound dimer in the quasi 1D situation is given by the pole of Eq. (7.40) at negative energies and it is found to be

$$\int_{-\infty}^{\infty} dp \left( \frac{\coth(\pi R\sqrt{-E_2 + p^2})}{\sqrt{-E_2 + p^2}} - \frac{1}{\sqrt{-E_2^{2D} + p^2}} \right) = 0, \tag{7.41}$$

which for  $R \rightarrow \infty$  gives correctly that  $E_2 \rightarrow E_2^{2D}$  as in this limit  $\coth R \rightarrow 1$ . For  $R \rightarrow 0$  it should happen that  $-E_2 \rightarrow \infty$  as given in Ref. [Delfino 2011].

### 7.3.2 Trimer bound state equation

Considering the momentum  $\mathbf{q}$  and the phase factor  $d\mathbf{q}$  as given in Eq. (7.35), where  $\mathbf{q} = \mathbf{q}_x + \mathbf{q}_y$  and  $d\mathbf{q} = \frac{1}{R}dq_x$ , the three-body free Hamiltonian (see Eq. (2.32)) becomes

$$\begin{aligned}
 \bar{H}_0^p(\mathbf{q}, \mathbf{k}) &= (\mathbf{q}_x + \mathbf{q}_y)^2 + (\mathbf{k}_x + \mathbf{k}_y)^2 + (\mathbf{q}_x + \mathbf{q}_y) \cdot (\mathbf{k}_x + \mathbf{k}_y), \\
 &= q_x^2 + k_x^2 + \mathbf{q}_x \cdot \mathbf{k}_x + \frac{n^2}{R^2} + \frac{m^2}{R^2} + \frac{n m}{R^2}.
 \end{aligned} \tag{7.42}$$

Considering the proper two-body  $T$ -matrix and  $H_0^p$  respectively from Eqs. (7.40) and (7.42), the three-body bound state equation for a compact

dimension with PBC is found to be

$$f(q_x, n) = R^{-1} \bar{\tau}_p \left[ E_3 - \frac{3}{4} \left( q_x^2 + \frac{n^2}{R^2} \right) \right] \sum_{m=-\infty}^{\infty} \int_{-\infty}^{\infty} dk_x \frac{f(k_x, m)}{E_3 - \bar{H}_0^p(\mathbf{q}, \mathbf{k})}. \quad (7.43)$$

In this case of quasi-1D there is no need of UV regularization of the integral equations as the Thomas collapse of the trimer in quasi-2D is absent in 2D and, therefore, in quasi-1D.

## 7.4 Trimer at 3D - 2D crossover with PBC

The results for the trimer binding energy shown in Fig. 7.1 are obtained from the numerical solution of the integral bound state equation for the spectator function in quasi-2D (see Eq. (7.33)). In order to explore the dimensional crossover transition, Fig. 7.1 shows the ratios  $\epsilon_3/\epsilon_2$  as a function of the compact dimension radius  $r$ , for the ground, first, and second excited states. Note that the last state goes into the continuum before the 2D limit is reached.

The computations were performed for two fixed two-body energies  $\epsilon_2 = 10^{-6}$  (empty circles/dashed lines) and  $10^{-7}$  (full circles/solid lines). In a pure 3D calculation these parameters are on the  $a > 0$  side of the resonance and only three three-body bound states are found from the solution of the integral equation (2.83), such that the well known Efimov ratio between two consecutive three-body states,  $\sim 515$ , is still far if the second and first excited states are considered. The points at which the energies are calculated are shown explicitly, while the curves are guides to the eye. For the largest radius ( $r = 1000$ ) the energies are obtained from the pure 3D equation given in Eq. (2.83). The plot shows a very interesting dimensional crossover result, where only one sharp transition is present for the ground state while there are two for the first excited state. This behavior can be understood by considering the size of the trimer given roughly by  $\bar{r} \sim 1/\sqrt{\epsilon_3}$ .

For  $\epsilon_2 = 10^{-7}$ , the ground state plateau for  $\epsilon_3/\epsilon_2 = 93330$  is placed at  $\bar{r} = 10.35$  and first excited state plateau for  $\epsilon_3/\epsilon_2 = 211.79$  at  $\bar{r} = 217.29$ .

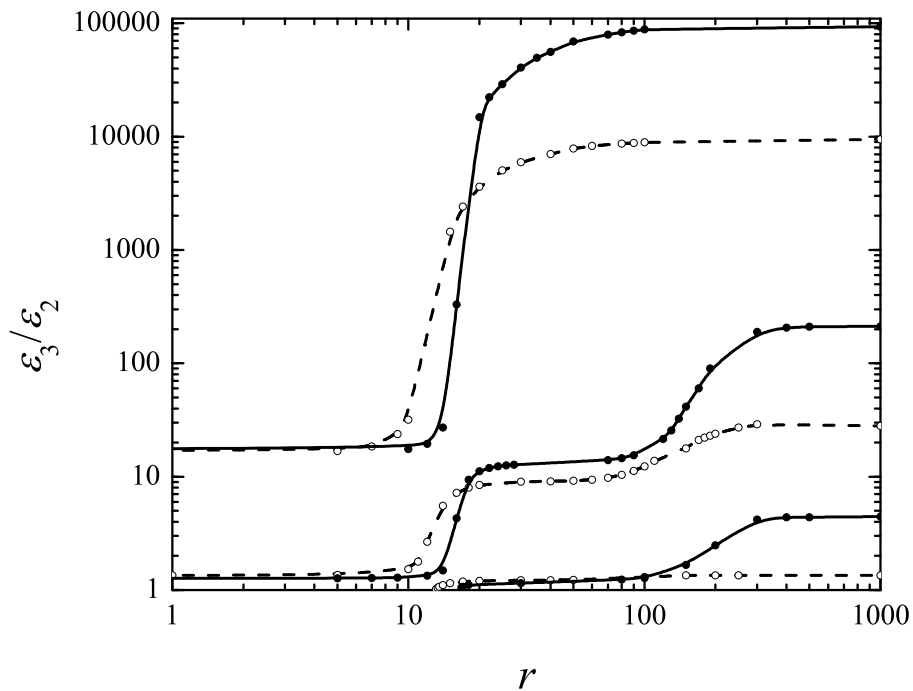


Figure 7.1:  $\epsilon_3/\epsilon_2$  as a function of  $r$ , for  $\epsilon_2 = 10^{-7}$  (full circles) and  $10^{-6}$  (empty circles). The solid and dashed lines are guides to the eye. As the 2D limit ( $r \rightarrow 0$ ) is approached, higher excited states disappear and only the ground and first excited states remain.

These  $\bar{r}$  values give approximately the region of the jumps signaling that the 3D limit, represented by the plateau, is reached once the trimer size matches the size of the squeezed dimension,  $r$ . The same analysis can be made for  $\epsilon_2 = 10^{-6}$  with  $\bar{r} = 10.27$  and  $\bar{r} = 188.98$ , respectively, for the ground and first excited state. Varying  $r$  from large to small values, the 3D $\rightarrow$ 2D transition occurs for  $r \sim 10$ , where it is possible to notice the disappearance of the higher excited states in order to reproduce the well known 2D results with two trimer bound state energies proportional to  $\epsilon_2$  with the ratios  $\epsilon_3/\epsilon_2 = 16.52$  and  $\epsilon_3/\epsilon_2 = 1.27$  [Bruch 1979].

From the experimental point of view it may be difficult to keep the dimer energy constant. However, the transition observed in Fig. 7.1 will not disappear due to a variation of  $\epsilon_2$  with  $r$ . The increase of the dimer energy will merely move the beginning of the jumps towards smaller  $r$ . The

optimal way to probe these jumps is to start from a two-body energy in the unitary limit ( $a \rightarrow \infty$ ) where the 2D plateaus are fixed. Larger dimer energies will cause the 3D plateau to move to lower  $\epsilon_3/\epsilon_2$  ratio and push the beginning of the transition to smaller  $r$ , thus making the transition region broader.

In the case where the dimer energy is not tuned to be fixed and runs with  $r$ , it is possible to estimate with Eq. (7.29) that for the small values of  $r \sim 10 - 20$ , when compared to the 3D scattering length of  $a \sim 10^3$ ,  $\epsilon_2 \sim 0.02346/r^2$  is a reasonable approximation. In the case of  $\epsilon_2^{3D} = 10^{-6}$ , one has for  $r = 10$ ,  $\epsilon_2 \sim 2.3 \times 10^{-4}$  and  $\epsilon_2/\epsilon_2^{3D} = 230$ . For  $r = 20$ ,  $\epsilon_2 \sim 5.1 \times 10^{-5}$  one get the ratio  $\epsilon_2/\epsilon_2^{3D} = 51$ . The results shown in Figure 7.1 for fixed  $\epsilon_2 = 10^{-6}$ , are expected to have some changes, as  $r = 10$ , where  $\epsilon_3/\epsilon_2^{3D}$  is comparable to  $\epsilon_2/\epsilon_2^{3D} = 230$ , while for  $r = 20$ ,  $\epsilon_3/\epsilon_2^{3D}$  is quite large compared to  $\epsilon_2/\epsilon_2^{3D} = 51$ . Therefore, one expects that while some changes in the above picture will be expected for small radius, for  $r > 20$  it will be quite unaffected.

# Summary and outlook

---

Quantum few-body systems composed of two and three particles with attractive zero range pairwise interactions for general masses and interaction strengths were considered in two and three dimensions. In order to have the methods clearly stated, the Faddeev decomposition was used to write the set of homogeneous coupled integral equations for the bound state as well as the momentum-space wave function, which are the starting points for the analytical and numerical investigations of the universal properties in few-body systems.

The universal properties are those that any potential with similar constraints (observables) are able to describe in a model-independent form. They occur when the system is large compared to the range of the potential and in this case the details of the basic two-body ingredients are unimportant. Then, zero-range interaction models introduced through Dirac- $\delta$  potential are useful, since all properties are determined at distances outside the potential [Frederico 2012].

A considerable simplification in the 2D three-body problem comes by defining scaling functions and choosing appropriate energy and mass scales. This reduces the number of unknown parameters in the set of coupled homogeneous integral equations for the bound state and simplifies the presentation of the results [Bellotti 2012].

It was shown in Chapter 3 that the number of three-body bound states in 2D varies from one and up depending on mass ratios and two-body subsystem energies, with symmetric mass system having the fewest and the most for two heavy particles and a light one. An upper limit for the number of bound states in any  $abc$  system was found when all the subsystems interact

with the same energy, namely  $E_{ab} = E_{ac} = E_{bc}$  [Bellotti 2012]. Since this configuration seems still hard to be experimentally implemented, a feasible situation corresponds to three-body systems composed for a heavy-heavy non-interacting subsystem, i.e.  $m_c \ll m_a = m_b$  and  $E_{ab} = 0; E_{ac} = E_{bc}$ , which has also a rich energy spectrum [Bellotti 2013b].

For example, 2D mixtures of  $^{87}\text{Rb}$ - $^{87}\text{Rb}$ - $^6\text{Li}$  and  $^{133}\text{Cs}$ - $^{133}\text{Cs}$ - $^6\text{Li}$  are expected to have respectively 3 and 4 three-body universal bound states [Bellotti 2013b]. It is very important to note that these numbers do not depend on the exact two-body energy in the  $^6\text{Li}$ - $^{133}\text{Cs}$  subsystem. These two-body energies in the 2D setup are functions of the 3D low-energy scattering length of the particular Feshbach resonance that is used in experiment to tune the interaction [Bloch 2008]. However, as long as there is such a resonance, the results should hold when the system is squeezed into a two-dimensional geometry. The possibility of tuning the binding energy of each pair and performing experiments mixing molecules and atoms should open new avenues for even richer two-dimensional three-body spectra.

One of these promising configurations was recently reported as the experimental realization of  $^{133}\text{Cs}$ - $^6\text{Li}$  systems [Repp 2013, Tung 2013], where it even looks as if three-body bound states can be expected when the subsystem  $^{133}\text{Cs}$ - $^{133}\text{Cs}$  is almost non-interacting. Therefore, the system  $^{133}\text{Cs}$ - $^{133}\text{Cs}$ - $^6\text{Li}$  seems to be the most promising realistic combination to experimentally achieve a rich three-body energy spectrum in 2D. Some other mixtures with large mass imbalances under study at the moment are Lithium-Ytterbium [Hansen 2013] and Helium-Rubidium [Knoop 2012]. Cases of layered systems with long-range dipolar interactions are also extremely promising for finding bound states [Armstrong 2012, Volosniev 2012], since that some of these are expected to have a universal low-energy character.

The three-body ground and first excited state energies in 2D have been successfully parameterized by universal functions that are so-called *super circles* (powers different from two) where the coordinates are the independent two-body energy ratios and the radius parameter is the three-body energy. The latter is an approximately linear function of the three-body



energy, independent of masses, while the powers of the coordinates are functions of both mass and three-body energy. This result can be used to estimate three-body energies and the number of bound states, and as a measure of the deviation from the universal zero-range limit [Bellotti 2012].

The interesting scenario in 2D where a particle is much lighter than the other two ( $m_c \ll m_a \approx m_b$ ) presents a rich energy spectrum even for non-interacting heavy particles ( $E_{ab} = 0$ ) and was analyzed in the Born-Oppenheimer (BO) approximation, where the light particle coordinate is integrated out from the Schrödinger equation leading to an effective adiabatic potential between the heavy particles in the heavy-heavy-light system, as presented in Chapter 4.

The adiabatic potential, which was found as the solution of a transcendental equation, is mass-dependent and reveals an increasing number of bound states for the decreasing mass of one of the particles. An asymptotic expression for the adiabatic potential was derived and was shown that this analytic expression faithfully corresponds to the numerically calculated adiabatic potential, even in the non-asymptotic region where the biggest deviation is still less than 9% [Bellotti 2013b]. This means that the asymptotic expression can be directly applied in 2D three-body system calculations, even in the non-asymptotic regions.

An estimate of the number of bound states as a function of the light-heavy mass ratio  $m$  for a heavy-heavy-light system in 2D was done using the analytic expression in the JWKB approximation. Infinitely many bound states are expected as this ratio approaches zero since the number of states is proportional to  $1/\sqrt{m}$  [Bellotti 2013b]. However, for finite masses a finite number of bound states is always expected. The explicitly mass-dependence of the asymptotic expression shows that the adiabatic potential becomes more attractive and less screened as one particle is much lighter than the other two ( $m \rightarrow 0$ ). This behavior explains the increasing number of bound states when the mass of the light particle is decreased. Besides, being  $R$  the distance between the heavy particles, the bound states accumulate both at  $R \rightarrow 0$  and  $R \rightarrow \infty$ . While particles with finite mass always produce a

finite number of bound states, an Efimov-like effect is expected only for  $m = 0$  [Bellotti 2013b].

In order to experimentally observe the presence of these three-body bound states in 2D one should be able to use similar techniques to those used for the study of Efimov states in 3D, i.e. loss measurements [Kraemer 2006] and photo-association [Lompe 2010]. It may also be possible to use RF techniques as in experiments that studied two-body bound states and many-body pairing in two-dimensional Fermi gases [Fröhlich 2011, Sommer 2012]. Another possible experimental signature of 2D three-body systems is through the momentum distribution and the two- and three-body contact parameters which appears as coefficients [Werner 2012, Bellotti 2012, Bellotti 2014]. These coefficients depends sensitively on the presence of bound two- and three-body states.

Important ingredients in the study of the momentum distribution are the Faddeev components, also called spectator functions, that compose the wave-function in momentum space. A key result shown in Chapter 5 was the finding of an exact analytic expression for the spectator functions in 2D of any generic  $abc$  system in the large momentum regime [Bellotti 2013a, Bellotti 2014], where the normalization of three distinct spectator functions relates to each other through a constant, properly weighted by reduced masses. These analytical results are supported by accurate numerical computations, which confirmed both the asymptotic behavior and the relation between the asymptotic expressions for different spectator functions in a generic case of three distinguishable particles.

The spectator functions and their asymptotic behavior define both the two- and the three- body contact parameters,  $C_2$  and  $C_3$ . The parameter  $C_2$  arises from integration of the spectator functions over all momenta, so that both small and large momenta contribute. The three two-body parameters in a system of three distinguishable particles in 2D are related by simple mass scaling, however they are in general not universal in the sense of being independent of the state when more than one excited state is present, or at least the energy scaling is more complicated than the corresponding one for

identical bosons, where the three-body energy was used as the measuring unit [Bellotti 2014]. This non-universal behavior was expected, since unlike for 3D systems, 2D three-body states does not present any geometric scaling. Then, the surprisingly and interesting result also showed in Chapter 5 is that the two-body parameter scales with the three-body energy and becomes independent of the quantum state considered for three-body systems composed of one distinguishable and two identical and non-interacting particles, and also in the case of three-identical bosons [Bellotti 2013a, Bellotti 2014]. In these cases the third particle apparently does not disturb the short-distance structure arising from the other two particles and therefore the two-body contact parameter turn out to be universal. This is similar to the 3D case with three identical bosons where  $C_2$  is universal in the scaling or Efimov limit where the binding energy is negligible.

The three-body contact parameter  $C_3$  depends only on the large-momentum asymptotic behavior of the spectator function and was fully determined due to the analytic expression found for the spectator function in 2D for the large momentum regime [Bellotti 2014]. Unlike  $C_2$ , the three-body contact parameters do not turn out to be universal in any of the investigated cases. This parameter is highly sensitive to the large-momentum asymptotic spectator function. Indeed, the proportionality coefficient determined in the asymptotic region, appears explicitly in the expression for  $C_3$ . It was found that  $C_3$  drastically change from the cases of two interacting and non-interacting identical particles. The values of  $C_3$  for any state in the non-interacting scenario are always less than 10% of the values obtained for interacting identical particles. The "absence" of a significant  $C_3$ , combined with universal  $C_2$  parameters, is then a signature of a non-interacting subsystem within the three-body system [Bellotti 2014].

It is of interest to know the spectator functions in 2D for all, both small and large, momenta, since the two-body contact parameters are integral quantities. The knowledge about the asymptotic spectator functions was used to guess an analytic structure describing approximately the ground state. This analytic form of the spectator function was used to derive an

expression for the two-body contact parameter between the two identical non-interacting particles in the ground state. The mass ratio,  $m$ , and energy,  $E_3$ , dependences then appear explicitly in addition to a more hidden, but much weaker, dependence in a normalization constant. The derived expression deviates from the exact value of  $C_2$  about 10% for  $m \gg 1$ , about 20% when  $m = 1$  and less than 5% for  $m \ll 1$ . Although the exact value is not fully reproduced, this formula presents a powerful way to determine the two-body contact parameter as function of  $m$  within percents [Bellotti 2014].

The single-particle momentum distribution was also calculated for 3D systems consisting of two identical bosons and a third particle of a different kind. Zero-range interaction was considered in the regime of a finite number of three-body bound states and also in the Efimov limit. Again, the asymptotic momentum distribution was analytically calculated as a function of the mass ratio and it was shown in Chapter 6 that the corresponding functional form is sensitive to this mass ratio [Yamashita 2013]. In the case of equal masses the results of Ref. [Castin 2011] were reproduced. The leading term has a  $q^{-4}$  tail while the sub-leading contribution is  $q^{-5}$  times a log-periodic function that is a characteristic of the Efimov limit. In particular, it was shown that for general mass ratios there is a non-oscillatory  $q^{-5}$  contribution which happens to vanish (and leave the oscillatory contribution behind) when the mass ratio is 0.2, 1, or 1.57 [Yamashita 2013].

Exemplifying the study above, the coefficient of the  $q^{-4}$  tail, which is the two-body contact parameter, was numerically determined for the systems  $^{133}\text{Cs}$ - $^{133}\text{Cs}$ - $^6\text{Li}$  and  $^{87}\text{Rb}$ - $^{87}\text{Rb}$ - $^6\text{Li}$ . For these cases, the momentum distributions of excited Efimov trimers for both the heavy and light components were also calculated. The numerical results demonstrate that the momentum distributions of ground, first, and second excited Efimov trimers approach a universal form at large but also at small momentum, indicating that one does not need to go to highly excited (and numerically challenging) three-body states in order to study the universal behavior of Efimov states in momentum space [Yamashita 2013].

As a brief parenthesis, it is worth to highlight that the steps employed

in the challenging analytical derivation of the sub-leading terms  $n_3$  and  $n_4$  would be used as a complete and exciting example in a course of complex analysis (see Chapter 6 and Appendix F).

In 3D systems, the two-body contact has been observed in experiments using time-of-flight and the mapping to momentum space [Stewart 2010], Bragg spectroscopy [Kuhnle 2010] or momentum-resolved photo-emission spectroscopy [Fröhlich 2011]. Measuring the sub-leading term and thus accessing  $C_3$  requires more precision, which has so far only produced the upper limits for the particular case of  $^{87}\text{Rb}$  [Wild 2012]. In 2D systems the functional form of the sub-leading term is different from the 3D case, so it is difficult to compare with the 3D case. However, given that the precision improves continuously it should be possible to also probe the 2D case when tightly squeezing a 3D sample. As it was shown here, the mass ratio can change the values of the contact parameters significantly. It is thus expected that mixtures of different atoms is the most promising direction to make a measurement of a 2D contact parameter.

A first step in the study of higher-order correlations and dimensional 3D - 2D crossover was taken by demonstrating how trimer observables in strongly-interacting quantum gases can be used to probe dimensionality [Bellotti 2013a]. Specifically, the breakdown of scale-invariance due to the Efimov effect is directly seen in the functional form of the tail of the momentum distribution. A clear direction of study is a full inclusion of the transverse direction and the discrete spectrum that it brings, since it was shown that a crossover with fundamental influence on the momentum tail will happen. A first try to mapping the dimensional crossover out in a system that would be squeezed by optical lattice(s) is shown in Chapter 7 (see also Ref. [Yamashita 2014]). For that aim, periodic boundary conditions were used to change from 3D to quasi-2D the trimer physics.

Squeezing the transverse direction with periodic boundary conditions, a sharp transition was found in the energy spectrum of the trimer as the compact dimension changes from a 3D to a 2D situation [Yamashita 2014]. This is an ongoing project and more studies are still necessary in order to

relate the parameter which dials between the different dimensions to real experiments. Only the transition in the trimer energy spectrum was still studied and another interesting topic is to follow the dimensional crossover transition of the wave function, since it was shown that the spectator function drastically changes with the dimensionality. An intriguing point is to identify what is the form of the spectator function in the sharp crossover region, where the system is clearly neither 2D or 3D.

Another ongoing project is the study of the two-dimensional three-body systems containing one fermion that is identical to the ones of a Fermi sea background. So far, our studies in 2D have concerned mass-imbalanced three-body systems of different nature in the vacuum. In the Fermi sea background, the dynamics of the shallow molecules having in its components fermions have to also account for the Pauli-blocking effect. Furthermore, the boson self-energy has to be treated as it has been done for two-body systems in, for example, Refs. [Meera 2011, Sascha 2011, Schmidt 2012a]. It is open the question on the effects of Pauli-Blocking and self-energies corrections for the three-body systems. The numerical solution of this problem is much more time-demanding and more technically challenging, but worth while to solve in view of the experimental possibility of squeezing systems with bosons immersed in cold atomic Fermi gases.

Further projects are the study of range-corrections in the universal properties presented in this thesis and the investigation of four-body systems in 2D. For real applications it is necessary to care about details of the short-range interaction, as the universal limit in which the range of the interaction is zero is an idealization. Therefore, it is necessary to study how the introduction of real potentials with a given range make the few-particle properties deviate from the results obtained in the universal regime. The need for details of the interaction must be significant when the system is probed at wavelengths close to the potential range, while for low energies the range effect can be possibly studied by a systematic expansion, as has been done, e.g. for three- [Platter 2009] and four-boson [Hadizadeh 2013] systems in 3D. Therefore, the corrections in the binding and structure of three- and

four-body systems due to a finite interaction range in 2D will be investigated for several different possibilities of constituents, paying attention to the implications of the four-body scale [Hadizadeh 2011].

The three-particle system for large mass asymmetries can have a large number of bound states in two-dimensions, as shown in Chapters 3 and 4 (see Ref. [Bellotti 2011, Bellotti 2012, Bellotti 2013b]). It will be interesting to find how the interwoven three- and four-body spectra come with different possibilities of particles masses. In such case, it is expected that some of these four-body states will be resonances in the atom plus triatomic molecule continuum, as has been seen in 3D calculations in traps [Thøgersen 2008] and without traps [von Stecher 2009, Deltuva 2010]. In the case of the formulation in momentum space, to obtain the position of the four-body resonances a rotation to the complex momentum plane of the integral equation will be required, as has been done in the case of the calculation of three-boson resonances in 3D [Bringas 2004].





# Revision of the scattering theory

## A.1 Brief presentation of the quantum scattering

The two-body problem is much simpler than the three-body one, since there are only two possibilities for the two-body systems: a scattering state or a bound state with structureless constituents. In the quantum regime, the particles can be described as waves (see for example Ref. [de Toledo Piza 2002, Landau 1977]). In this scenario, two colliding particles are described by an incoming wave and a scattered one as shown in Fig. A.1.

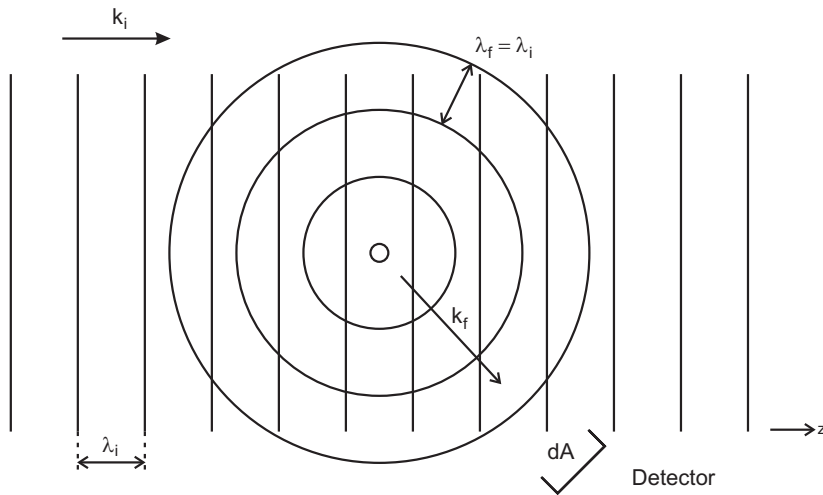


Figure A.1: Schematic figure showing the quantum scattering process.  $\mathbf{k}$  and  $\lambda$  are respectively the relative momentum and corresponding wavelength. The subscripts  $i$  and  $f$  means initial and final.

The Hamiltonian for two particles that interact through a generic potential  $V$  is written as

$$H' = \frac{\mathbf{k}_1^2}{2m_1} + \frac{\mathbf{k}_2^2}{2m_2} + V, \quad (\text{A.1})$$

where  $\mathbf{k}_i$  and  $m_i$  are respectively the momentum and mass of the particle  $i$  in the laboratory frame. If the potential  $V$  is translational invariant, the Hamiltonian is given by

$$H = \frac{\mathbf{k}^2}{2(m_1 + m_2)} + \frac{\mathbf{p}^2}{2m_{12}} + V, \quad (\text{A.2})$$

where  $\mathbf{k} = \mathbf{k}_1 + \mathbf{k}_2$  is the total momentum and  $\mathbf{p} = \frac{m_2\mathbf{k}_1 - m_1\mathbf{k}_2}{m_1 + m_2}$  the relative one. The reduced mass of the system is  $m_{12} = \frac{m_1 m_2}{m_1 + m_2}$ . As there are no external forces, the CM motion is free and just the relative motion has to be considered. The Hamiltonian for the relative motion is

$$H = \frac{\mathbf{p}^2}{2m_{12}} + V \equiv H_0 + V. \quad (\text{A.3})$$

The solution of the Schrödinger equation for the scattered outgoing wave,  $(H_0 + V)\psi^+ = E\psi^+$  is formulated as

$$\psi^+ = \psi_0^+ + g_0(E)V\psi^+, \quad (\text{A.4})$$

where  $\psi_0^+$  is the solution of the homogeneous equation and the free resolvent  $g_0(E)$  is given by

$$g_0(E) \equiv \frac{1}{E - H_0 + i\epsilon}. \quad (\text{A.5})$$

Analogously, the resolvent (or Green's function) is defined as

$$g(E) \equiv \frac{1}{E - H + i\epsilon}. \quad (\text{A.6})$$

Relations between the free and full propagators, respectively in Eqs. (A.5)

and (A.6), are found by noticing that

$$V = H - H_0 = g_0^{-1}(E) - g^{-1}(E). \quad (\text{A.7})$$

Multiplying Eq. (A.7) for  $g_0$  from left and  $g$  from right gives

$$g_0^{-1} - g^{-1} = V, \quad 1 - g_0 g^{-1} = g_0 V, \quad g - g_0 = g_0 V g, \quad g = g_0 + g_0 V g. \quad (\text{A.8})$$

On the other hand, multiplying Eq. (A.7) for  $g$  from left and  $g_0$  from right results in

$$g_0^{-1} - g^{-1} = V, \quad g g_0^{-1} - 1 = g V, \quad g - g_0 = g V g_0, \quad g = g_0 + g V g_0. \quad (\text{A.9})$$

Then, the two-body transition matrix  $t(E)$  is found by inserting Eq. (A.8) into Eq. (A.9). The result is

$$\begin{aligned} g &= g_0 + g_0 V (g_0 + g V g_0) = g_0 + g_0 V g_0 + g_0 V g V g_0 = g_0 + g_0 [V + V g V] g_0 \\ &\equiv g_0 + g_0 t g_0, \end{aligned} \quad (\text{A.10})$$

where the transition matrix ( $T$ -matrix),  $t(E)$ , is defined as

$$t = V + V g V. \quad (\text{A.11})$$

Notice that the  $T$ -matrix, as well as the free and full propagators, depends explicitly on the energy, i.e.,  $t \equiv t(E)$ ,  $g \equiv g(E)$  and  $g_0 \equiv g_0(E)$ , however, this dependence is not shown in Eqs. (A.8) to (A.11) in order to let the visualization of such equations clearer.

The transition matrix is a key ingredient in the study of quantum systems, since it relates directly to the main observable in the scattering problem: the connection between theory and measurable data is made through the scattering phase-shifts and cross-section. While the study of the scattering phase-shift and cross-section is broadly made for three-dimensional systems in several text books, the analogous two-dimensional (2D) problem

is beautifully described in Ref. [Adhikari 1993].

## A.2 Scattering equation for the two-body T-matrix

The  $T$ -matrix plays a central role in the scattering problem and, it is the base of the mathematical framework used to describe quantum few-body problems. An integral equation for this operator is found by combining the two expressions for the full propagator in Eqs. (A.8) and (A.10). Inserting the latter in the former one gives:

$$g = g_0 + g_0 V (g_0 + g_0 t g_0) = g_0 + g_0 V g_0 + g_0 V g_0 t g_0 = g_0 + g_0 [V + V g_0 t] g_0 . \quad (\text{A.12})$$

Comparing the two forms of the resolvent as written in Eqs. (A.10) and (A.12), the scattering integral equation comes as

$$t = V + V g_0 t . \quad (\text{A.13})$$

Alternatively, it is possible to insert the resolvent in Eq. (A.10) into Eq. (A.9), which results in

$$t = V + t g_0 V . \quad (\text{A.14})$$

The integral equation for the  $T$ -matrix, Eq. (A.13), can in principle be solved for any potential  $V$ , however, more complex the potential more difficult to solve the equation. Hopefully, there is a class of potentials which allows the algebraic manipulation of Eq. (A.13). These potentials are called separable and have the operator form

$$V = \lambda |\chi\rangle \langle \chi| , \quad (\text{A.15})$$

where  $\lambda$  is the potential strength.

Inserting the potential given in Eq. (A.15), in the two-body scattering

integral equation from Eq. (A.13) leads to

$$t(E) = \lambda |\chi\rangle \langle \chi| + \lambda |\chi\rangle \langle \chi| g_0(E) t(E) . \quad (\text{A.16})$$

In order to find the term  $\langle \chi| g_0(E) t(E)$ , Eq. (A.16) is multiplied by  $\langle \chi| g_0(E)$  from the left, which gives

$$\begin{aligned} \langle \chi| g_0(E) t(E) &= \lambda \langle \chi| g_0(E) |\chi\rangle \langle \chi| + \lambda \langle \chi| g_0(E) |\chi\rangle \langle \chi| g_0(E) t(E) , \\ \langle \chi| g_0(E) t(E) &= \frac{\lambda \langle \chi| g_0(E) |\chi\rangle \langle \chi|}{1 - \lambda \langle \chi| g_0(E) |\chi\rangle} . \end{aligned} \quad (\text{A.17})$$

Inserting Eq. (A.17) back in Eq. (A.16), the two-body  $T$ -matrix becomes

$$t(E) = |\chi\rangle \left( \frac{1}{\lambda^{-1} - \langle \chi| g_0(E) |\chi\rangle} \right) \langle \chi| , \quad (\text{A.18})$$

which in a compact form becomes

$$t(E) = |\chi\rangle \tau(E) \langle \chi| , \quad (\text{A.19})$$

where the matrix element  $\tau(E)$  is given by

$$\tau(E) = \left( \lambda^{-1} - \langle \chi| g_0(E) |\chi\rangle \right)^{-1} . \quad (\text{A.20})$$

Introducing the identity  $\hat{\mathbf{1}} = \int d^D p |\mathbf{p}\rangle \langle \mathbf{p}|$  in Eq. (A.20), the integral form of the  $T$ -matrix is

$$\begin{aligned} \tau(E) &= \left( \lambda^{-1} - \iint d^D p' d^D p \langle \chi| \mathbf{p}'\rangle \langle \mathbf{p}'| g_0(E) |\mathbf{p}\rangle \langle \mathbf{p}| \chi\rangle \right)^{-1} , \\ &= \left( \lambda^{-1} - \int d^D p \frac{g(p)^2}{E - \frac{p^2}{2m_{red}} + i\epsilon} \right)^{-1} , \end{aligned} \quad (\text{A.21})$$

where  $m_{red}$  is the two-body reduced mass and  $g(p) \equiv \langle \mathbf{p}| \chi\rangle$  is the form factor of the potential  $V$ .



# Jacobi relative momenta

---

## B.1 Classical three-body problem

The physical attributes of the three particles are labeled as  $\alpha = i, j, k$ . Their masses are  $m_\alpha$ , and their positions and velocities in the laboratory frame are respectively given by  $\mathbf{r}_\alpha$  and  $\mathbf{v}_\alpha = \frac{d\mathbf{r}_\alpha}{dt}$ . The momentum of each particle is  $\mathbf{K}_\alpha = m_\alpha \mathbf{v}_\alpha$ . The total momentum  $\mathbf{K}$  and the free Hamiltonian  $H_0$  of the three-body system are written as

$$\mathbf{K} = m_i \mathbf{v}_i + m_j \mathbf{v}_j + m_k \mathbf{v}_k = \mathbf{K}_i + \mathbf{K}_j + \mathbf{K}_k, \quad (\text{B.1})$$

$$H_0 = \frac{\mathbf{K}_i^2}{2m_i} + \frac{\mathbf{K}_j^2}{2m_j} + \frac{\mathbf{K}_k^2}{2m_k}. \quad (\text{B.2})$$

The center-of-mass (CM) position and velocity are found to be

$$\mathbf{R}_{cm} = \frac{m_i \mathbf{r}_i + m_j \mathbf{r}_j + m_k \mathbf{r}_k}{M}, \quad (\text{B.3})$$

$$\mathbf{V}_{cm} = \frac{d\mathbf{R}_{cm}}{dt} = \frac{m_i \mathbf{v}_i + m_j \mathbf{v}_j + m_k \mathbf{v}_k}{M}, \quad (\text{B.4})$$

where the total mass is  $M = m_i + m_j + m_k$ . The relative coordinate and velocity between each particle  $\alpha$  and the CM of the system are shown in Fig. B.1 and read

$$\mathbf{R}_\alpha = \mathbf{r}_\alpha - \mathbf{R}_{cm}, \quad (\text{B.5})$$

$$\mathbf{V}_\alpha = \frac{d\mathbf{R}_\alpha}{dt} = \mathbf{v}_\alpha - \mathbf{V}_{cm}. \quad (\text{B.6})$$

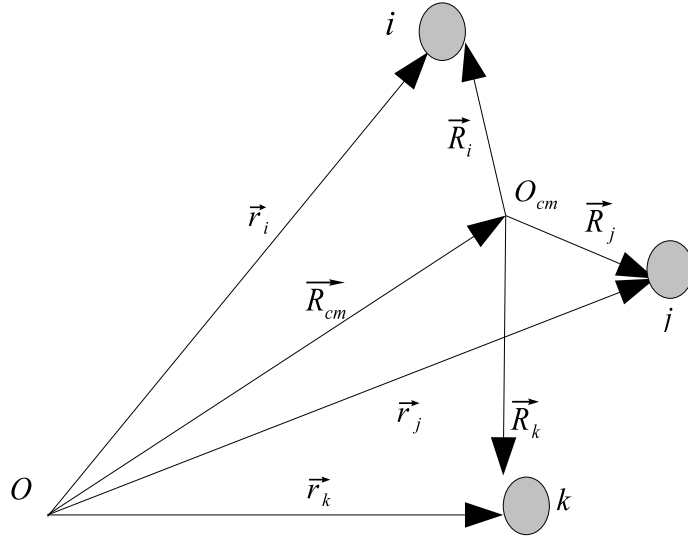


Figure B.1: Three-body coordinates in laboratory frame.

In the CM frame, the momentum of particle  $\alpha$  is written as

$$\mathbf{k}_\alpha = m_\alpha \mathbf{V}_\alpha , \quad (\text{B.7})$$

where  $V_\alpha$  is given in Eq. (B.6). Besides, at the CM frame the three momenta must fulfill

$$\mathbf{k}_i + \mathbf{k}_j + \mathbf{k}_k = 0. \quad (\text{B.8})$$

Inserting the CM velocity from Eq. (B.4) and the relative velocity of particle  $\alpha$  from Eq. (B.6) into Eq. (B.7), the momentum of particle  $\alpha$  in the CM frame becomes

$$\begin{aligned} \mathbf{k}_\alpha &= m_\alpha \left( \mathbf{v}_\alpha - \frac{m_\alpha \mathbf{v}_\alpha + m_\beta \mathbf{v}_\beta + m_\gamma \mathbf{v}_\gamma}{M} \right) , \\ &= \frac{m_\alpha}{m_\alpha + m_\beta + m_\gamma} \left[ (m_\alpha + m_\beta + m_\gamma) \mathbf{v}_\alpha - m_\alpha \mathbf{v}_\alpha + m_\beta \mathbf{v}_\beta + m_\gamma \mathbf{v}_\gamma \right] , \\ &= \frac{m_\alpha (m_\beta + m_\gamma)}{m_\alpha + m_\beta + m_\gamma} \left( \mathbf{v}_\alpha - \frac{m_\beta \mathbf{v}_\beta + m_\gamma \mathbf{v}_\gamma}{m_\beta + m_\gamma} \right) , \end{aligned} \quad (\text{B.9})$$



Remembering that  $(\alpha, \beta, \gamma)$  represent cyclic permutations of  $(i, j, k)$ , the momentum of each particle in the CM frame is

$$\mathbf{k}_i = \frac{m_i(m_j + m_k)}{m_i + m_j + m_k} \left( \mathbf{v}_i - \frac{m_j \mathbf{v}_j + m_k \mathbf{v}_k}{m_j + m_k} \right), \quad (\text{B.10})$$

$$\mathbf{k}_j = \frac{m_j(m_i + m_k)}{m_i + m_j + m_k} \left( \mathbf{v}_j - \frac{m_i \mathbf{v}_i + m_k \mathbf{v}_k}{m_i + m_k} \right), \quad (\text{B.11})$$

$$\mathbf{k}_k = \frac{m_k(m_i + m_j)}{m_i + m_j + m_k} \left( \mathbf{v}_k - \frac{m_i \mathbf{v}_i + m_j \mathbf{v}_j}{m_i + m_j} \right). \quad (\text{B.12})$$

Notice that the momenta given in Eqs. (B.10) to (B.12) fulfill the relation in Eq. (B.8).

## B.2 Jacobi relative momenta

As it was stated in Chapter 2, an advantage in the use of the Jacobi momenta in the study of the three-body problem is that the motion of the CM can be separated out. The Jacobi momenta are illustrated in Fig. 2.1, where  $\mathbf{q}_\alpha$  is identified as the momentum of the particle  $\alpha$  with respect to  $cm_\alpha$ , the CM of particles  $(\beta, \gamma)$ . Also,  $\mathbf{p}_\alpha$  is the relative momentum of the two-body system  $(\beta, \gamma)$ . In order to identify all these relative momenta, the three-body motion is split out in the motion of one particle  $\alpha$  plus the motion of the CM of the remaining pair,  $cm_\alpha$ . Considering  $cm_\alpha$  as a particle, the problem is roughly reduced to a two-body problem, as shown in Fig. B.2.

In Fig. B.2, the relative coordinate  $\rho$  and velocity  $\sigma$  are

$$\rho_\alpha = \mathbf{r}_\alpha - \mathbf{R}_{cm_\alpha}, \quad (\text{B.13})$$

$$\sigma_\alpha = \mathbf{v}_\alpha - \mathbf{V}_{cm_\alpha}. \quad (\text{B.14})$$

The mass of the particle  $cm_\alpha$  is given by

$$M_{cm_\alpha} = m_\beta + m_\gamma. \quad (\text{B.15})$$

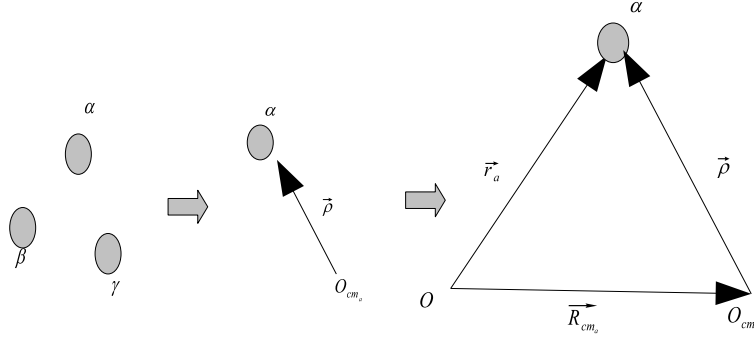


Figure B.2: Relation of the new coordinates with the coordinates in frame of the laboratory for a system composed of an  $\alpha$  particle and  $cm_\alpha$ .

In the same way, its position and velocity in the laboratory frame are

$$\mathbf{R}_{cm_\alpha} = \frac{m_\beta \mathbf{r}_\beta + m_\gamma \mathbf{r}_\gamma}{m_\beta + m_\gamma}, \quad (\text{B.16})$$

$$\mathbf{V}_{cm_\alpha} = \frac{m_\beta \mathbf{v}_\beta + m_\gamma \mathbf{v}_\gamma}{m_\beta + m_\gamma}. \quad (\text{B.17})$$

From the classical two-body problem, it must not be hard to identify the relative momentum between particles  $\alpha$  and  $cm_\alpha$  as

$$\mathbf{q}_\alpha = \mu_\alpha \boldsymbol{\sigma}_\alpha, \quad (\text{B.18})$$

where the reduced mass  $\mu_\alpha$  reads

$$\mu_\alpha = \frac{m_\alpha M_{cm_\alpha}}{m_\alpha + M_{cm_\alpha}} = \frac{m_\alpha (m_\beta + m_\gamma)}{m_\alpha + m_\beta + m_\gamma}. \quad (\text{B.19})$$

Inserting the relative velocity from Eq. (B.14) and the reduced mass (B.19) in Eq. (B.18), the relative momentum between particle  $\alpha$  and the CM of the  $(\beta, \gamma)$  subsystem is found to be

$$\mathbf{q}_\alpha = \frac{m_\alpha (m_\beta + m_\gamma)}{m_\alpha + m_\beta + m_\gamma} \left( \mathbf{v}_\alpha - \frac{m_\beta \mathbf{v}_\beta + m_\gamma \mathbf{v}_\gamma}{m_\beta + m_\gamma} \right). \quad (\text{B.20})$$

Notice the Jacobi momentum in Eq. (B.20) is identical to the momentum in Eq. (B.9), meaning that

$$\mathbf{q}_i = \mathbf{k}_i, \quad \mathbf{q}_j = \mathbf{k}_j, \quad \mathbf{q}_k = \mathbf{k}_k \quad . \quad (\text{B.21})$$

The relative momentum between particles  $\beta$  and  $\gamma$ ,  $\mathbf{p}_\alpha$ , is

$$\mathbf{p}_\alpha = \frac{m_\beta m_\gamma}{m_\beta + m_\gamma} \mathbf{v}_{\beta\gamma} = \frac{m_\beta m_\gamma}{m_\beta + m_\gamma} (\mathbf{v}_\beta - \mathbf{v}_\gamma) = \frac{m_\gamma \mathbf{k}_\beta - m_\beta \mathbf{k}_\gamma}{m_\beta + m_\gamma} , \quad (\text{B.22})$$

and using Eq. (B.21) it becomes

$$\mathbf{p}_i = \frac{m_k \mathbf{q}_j - m_j \mathbf{q}_k}{m_j + m_k} , \quad (\text{B.23})$$

$$\mathbf{p}_j = \frac{m_i \mathbf{q}_k - m_k \mathbf{q}_i}{m_i + m_k} , \quad (\text{B.24})$$

$$\mathbf{p}_k = \frac{m_j \mathbf{q}_i - m_i \mathbf{q}_j}{m_j + m_i} . \quad (\text{B.25})$$

Writing the momentum of each particle as function of the Jacobi momenta ( $\mathbf{q}_\alpha, \mathbf{p}_\alpha$ ), the free Hamiltonian in Eq. (B.2) becomes

$$H_0 = \frac{\mathbf{q}_\alpha^2}{2m_{\beta\gamma,\alpha}} + \frac{\mathbf{p}_\alpha^2}{2m_{\beta\gamma}} + \frac{Q^2}{m_\alpha + m_\beta + m_\gamma} , \quad (\text{B.26})$$

where  $\mathbf{Q} = \sum_\alpha \mathbf{k}_\alpha = \sum_\alpha \mathbf{q}_\alpha$  is the total momentum and the reduced masses are

$$m_{\beta\gamma,\alpha} = \frac{m_\alpha (m_\beta + m_\gamma)}{m_\alpha + m_\beta + m_\gamma} , \quad (\text{B.27})$$

$$m_{\beta\gamma} = \frac{m_\beta m_\gamma}{m_\beta + m_\gamma} . \quad (\text{B.28})$$

The shifted arguments of the spectator functions in the wave-function from Eq. (2.66) are found by manipulating Eqs. (B.8), (B.21), (B.23), (B.24) and (B.25). The momentum  $\mathbf{q}_j(\mathbf{q}_i, \mathbf{p}_i)$  reads

$$\mathbf{q}_j(\mathbf{q}_i, \mathbf{p}_i) = \frac{m_j + m_k}{m_k} \mathbf{p}_i + \frac{m_j}{m_k} \mathbf{q}_k = \frac{m_j + m_k}{m_k} \mathbf{p}_i + \frac{m_j}{m_k} (-\mathbf{q}_i - \mathbf{q}_j) ,$$

$$\begin{aligned} \left(1 + \frac{m_j}{m_k}\right) \mathbf{q}_j(\mathbf{q}_i, \mathbf{p}_i) &= \frac{m_j + m_k}{m_k} \mathbf{p}_i - \frac{m_j}{m_k} \mathbf{q}_i, \\ \mathbf{q}_j(\mathbf{q}_i, \mathbf{p}_i) &= \mathbf{p}_i + \frac{m_j}{m_j + m_k} \mathbf{q}_i. \end{aligned} \quad (\text{B.29})$$

In the same way, momentum  $\mathbf{q}_k(\mathbf{q}_i, \mathbf{p}_i)$  is found to be

$$\begin{aligned} \mathbf{q}_k(\mathbf{q}_i, \mathbf{p}_i) &= -\frac{m_j + m_k}{m_j} \mathbf{p}_i + \frac{m_k}{m_j} \mathbf{q}_j = -\frac{m_j + m_k}{m_j} \mathbf{p}_i + \frac{m_k}{m_j} (-\mathbf{q}_i - \mathbf{q}_k), \\ \left(1 + \frac{m_k}{m_j}\right) \mathbf{q}_k(\mathbf{q}_i, \mathbf{p}_i) &= -\frac{m_j + m_k}{m_j} \mathbf{p}_i - \frac{m_k}{m_j} \mathbf{q}_i, \\ \mathbf{q}_k(\mathbf{q}_i, \mathbf{p}_i) &= -\left(\mathbf{p}_i + \frac{m_k}{m_j + m_k} \mathbf{q}_i\right). \end{aligned} \quad (\text{B.30})$$

The same manipulation can be made for the momenta  $\mathbf{q}_i(\mathbf{q}_j, \mathbf{p}_j)$ ,  $\mathbf{q}_k(\mathbf{q}_j, \mathbf{p}_j)$ ,  $\mathbf{q}_i(\mathbf{q}_k, \mathbf{p}_k)$  and  $\mathbf{q}_j(\mathbf{q}_k, \mathbf{p}_k)$ . Introducing the variables  $(\alpha, \beta, \gamma)$  as cyclic permutation of the particle labels  $(i, j, k)$ , the six combinations needed can be simply written as

$$\mathbf{q}_\beta(\mathbf{q}_\alpha, \mathbf{p}_\alpha) = \mathbf{p}_\alpha - \frac{m_\beta}{m_\beta + m_\gamma} \mathbf{q}_\alpha, \quad (\text{B.31})$$

$$\mathbf{q}_\gamma(\mathbf{q}_\alpha, \mathbf{p}_\alpha) = -\left(\mathbf{p}_\alpha + \frac{m_\gamma}{m_\beta + m_\gamma} \mathbf{q}_\alpha\right). \quad (\text{B.32})$$

# Matrix elements of the three-body resolvent

---

The six matrix elements which appear in Eqs. (2.57) to (2.59) are calculated in detail in this Appendix. These elements have the same structure as given in Eq. (2.60), namely

$$ME = \langle \chi_\alpha, \mathbf{q}_\alpha | G_0(E) | \chi_\beta \rangle | f_\beta \rangle . \quad (\text{C.1})$$

Defining two resolutions of the unit as

$$\hat{1} = \int d^2 q_\beta | \mathbf{q}_\beta \rangle \langle \mathbf{q}_\beta | \quad \text{and} \quad \hat{1} = \int d^2 p_\alpha | \mathbf{p}_\alpha \rangle \langle \mathbf{p}_\alpha | , \quad (\text{C.2})$$

the matrix element in Eq. (C.1) becomes

$$\begin{aligned} ME &= \int d^2 q_\beta \langle \chi_\alpha, \mathbf{q}_\alpha | G_0(\epsilon) | \mathbf{q}_\beta \rangle \langle \mathbf{q}_\beta | \chi_\beta \rangle | f_\beta \rangle , \\ &= \int d^2 q_\beta d^2 p_\alpha d^2 p_\beta \langle \chi_\alpha, \mathbf{q}_\alpha | \mathbf{p}_\alpha \rangle \langle \mathbf{p}_\alpha | G_0(\epsilon) | \mathbf{p}_\beta \rangle \langle \mathbf{p}_\beta | \chi_\beta, \mathbf{q}_\beta \rangle f_\beta(\mathbf{q}_\beta) , \\ &= \int d^2 q_\beta d^2 p_\alpha d^2 p_\beta \frac{g_\alpha(\mathbf{p}_\alpha) g_\beta(\mathbf{p}_\beta)}{E - \frac{\mathbf{q}_\alpha^2}{2m_{\beta\gamma,\alpha}} - \frac{\mathbf{p}_\alpha^2}{2m_{\beta\gamma}}} \langle \mathbf{q}_\alpha, \mathbf{p}_\alpha | \mathbf{p}_\beta, \mathbf{q}_\beta \rangle f_\beta(\mathbf{q}_\beta) , \end{aligned} \quad (\text{C.3})$$

where  $(\alpha, \beta, \gamma)$  are cyclic permutations of the particle labels  $(i, j, k)$ .

The matrix element  $\langle \mathbf{q}_\alpha, \mathbf{p}_\alpha | \mathbf{p}_\beta, \mathbf{q}_\beta \rangle$  is written as [Schmid 1974]

$$\langle \mathbf{q}_\alpha, \mathbf{p}_\alpha | \mathbf{p}_\beta, \mathbf{q}_\beta \rangle = \delta(\mathbf{p}_\alpha - \mathbf{p}'_\alpha(\mathbf{p}_\beta, \mathbf{q}_\beta)) \delta(\mathbf{q}_\alpha - \mathbf{q}'_\alpha(\mathbf{p}_\beta, \mathbf{q}_\beta)). \quad (\text{C.4})$$

The six possibilities in Eqs. (2.57) to (2.59) come from permutation of particles label in Eq. (C.1). Handling Eq. (C.4) requires some manipulation

of the Jacobi relative momenta in Eqs. (B.21) and (B.22) and  $\mathbf{p}'_\alpha$  is written as function of the others momenta as

$$\begin{aligned}\mathbf{p}'_\alpha(\mathbf{p}_\beta, \mathbf{q}_\beta) &= \frac{m_\gamma \mathbf{q}_\beta - m_\beta \mathbf{q}_\gamma}{m_\gamma + m_\beta}, \\ &= \frac{m_\gamma}{m_\gamma + m_\beta} \mathbf{q}_\beta - \frac{m_\beta}{m_\gamma + m_\beta} (-\mathbf{q}_\alpha - \mathbf{q}_\beta), \\ &= \mathbf{q}_\beta + \frac{m_\beta}{m_\gamma + m_\beta} \mathbf{q}_\alpha,\end{aligned}\tag{C.5}$$

and the first term on the right-hand-side of Eq.(C.4) is

$$\delta(\mathbf{p}_\alpha - \mathbf{p}'_\alpha(\mathbf{p}_\beta, \mathbf{q}_\beta)) = \delta\left(\mathbf{p}_\alpha - \mathbf{q}_\beta - \frac{m_\beta}{m_\gamma + m_\beta} \mathbf{q}_\alpha\right).\tag{C.6}$$

In the same way,  $\mathbf{q}'_\alpha$  reads

$$\begin{aligned}\mathbf{q}'_\alpha(\mathbf{p}_\beta, \mathbf{q}_\beta) &= -\frac{m_\gamma + m_\alpha}{m_\gamma} \mathbf{p}_\beta + \frac{m_\alpha}{m_\gamma} \mathbf{q}_\gamma, \\ &= -\frac{m_\gamma + m_\alpha}{m_\gamma} \mathbf{p}_\beta + \frac{m_\alpha}{m_\gamma} (-\mathbf{q}_\alpha - \mathbf{q}_\beta),\end{aligned}\tag{C.7}$$

and the second term on the right-hand-side of Eq.(C.4) is

$$\begin{aligned}\delta(\mathbf{q}_\alpha - \mathbf{q}'_\alpha(\mathbf{p}_\beta, \mathbf{q}_\beta)) &= \delta\left(\mathbf{q}_\alpha + \frac{m_\gamma + m_\alpha}{m_\gamma} \mathbf{p}_\beta + \frac{m_\alpha}{m_\gamma} (\mathbf{q}_\alpha + \mathbf{q}_\beta)\right), \\ &= \delta\left(\frac{m_\gamma + m_\alpha}{m_\gamma} \mathbf{p}_\beta + \frac{m_\gamma + m_\alpha}{m_\gamma} \mathbf{q}_\alpha + \mathbf{q}_\beta\right), \\ &\equiv \delta\left(\mathbf{p}_\beta + \mathbf{q}_\alpha + \frac{m_\alpha}{m_\gamma + m_\alpha} \mathbf{q}_\beta\right).\end{aligned}\tag{C.8}$$

The matrix element  $\langle \mathbf{q}_\alpha, \mathbf{p}_\alpha | \mathbf{p}_\beta, \mathbf{q}_\beta \rangle$  is written as

$$\langle \mathbf{q}_\alpha, \mathbf{p}_\alpha | \mathbf{p}_\beta, \mathbf{q}_\beta \rangle = \delta\left(\mathbf{p}_\alpha - \mathbf{q}_\beta - \frac{m_\beta}{m_\gamma + m_\beta} \mathbf{q}_\alpha\right) \delta\left(\mathbf{p}_\beta + \mathbf{q}_\alpha + \frac{m_\alpha}{m_\gamma + m_\alpha} \mathbf{q}_\beta\right)\tag{C.9}$$

and remembering that it was shown in Sec. 2.1 that the form factor of the

Dirac- $\delta$  potential is  $g(\mathbf{p}) = 1$ , Eq. (C.3) becomes

$$\begin{aligned}
 ME &= \int d^2q_\beta d^2p_\alpha d^2p_\beta \frac{\delta\left(\mathbf{p}_\alpha - \mathbf{q}_\beta - \frac{m_\beta}{m_\beta+m_\gamma}\mathbf{q}_\alpha\right) \delta\left(\mathbf{p}_\beta + \mathbf{q}_\alpha + \frac{m_\alpha}{m_\alpha+m_\gamma}\mathbf{q}_\beta\right)}{E - \frac{\mathbf{q}_\alpha^2}{2m_{\beta\gamma,\alpha}} - \frac{\mathbf{p}_\alpha^2}{2m_{\beta\gamma}}} f_\beta(\mathbf{q}_\beta) , \\
 &= \int d^2q_\beta \frac{f_\beta(\mathbf{q}_\beta)}{E - \frac{\mathbf{q}_\alpha^2}{2m_{\beta\gamma,\alpha}} - \frac{\left(\mathbf{q}_\beta + \frac{m_\beta}{m_\beta+m_\gamma}\mathbf{q}_\alpha\right)^2}{2m_{\beta\gamma}}} . \tag{C.10}
 \end{aligned}$$

Finally, the matrix element which appears in Eqs. (2.61) to (2.63) are given by

$$\langle \chi_\alpha, \mathbf{q}_\alpha | G_0(E) | \chi_\beta \rangle | f_\beta \rangle = \int d^2q_\beta \frac{f_\beta(\mathbf{q}_\beta)}{E - \frac{q_\alpha^2}{2m_{\alpha\gamma}} - \frac{q_\beta^2}{2m_{\beta\gamma}} - \frac{1}{m_\gamma} \mathbf{q}_\beta \cdot \mathbf{q}_\alpha} , \tag{C.11}$$

where  $(\alpha, \beta, \gamma)$  are cyclic permutations of the particle labels  $(i, j, k)$ .





# Numerical methods

---

The set of integral homogeneous coupled equations in Eq. (2.70) does not have analytic solution in general and then, it has to be numerically solved. There are several well established methods available in the literature to solve integral equations as given, for example, in Ref. [Press 2007]. Besides, classical techniques as Gauss-Legendre quadratures are used for the numerical discretization of the integral equations, the Newton-Raphson method is used to find zeros of functions and the Gauss decomposition method is used to find the determinant of a matrix. Optimized routines which implement these techniques are available in the libraries of the programming languages as C, C++ and Fortran and are also described in Ref. [Press 2007].

The three-body problem studied in this thesis consists, basically, of an eigenvalue - eigenvector problem, where the determination of the energy (eigenvalue) leads to the determination of the spectator, and consequently, the wave function (eigenvector).

## D.1 Three-body energy (eigenvalue)

In order to illustrate the methods employed in the numerical solution of Eq. (2.70), the symmetric mass case is considered, i.e.,  $m_a = m_b = m_c = m$  and  $E_{ab} = E_{ac} = E_{bc} = E_2$ . This means that only one integral equation has to be solved and choosing  $E_2$  and  $m$  as the energy and mass units, the three-body energy  $E_3$  and the momenta  $q$  and  $k$  in Eq. (2.70) are rewritten

as  $E_3 \equiv \frac{E_3}{E_2}$  and  $q \equiv \frac{q}{\sqrt{mE_2}}$ . In units of  $E_2 = m = 1$ , Eq. (2.70) becomes

$$f(q) = 2 \left[ \ln \left( \sqrt{\frac{3}{4}q^2 - E_3} \right) \right]^{-1} \int_0^\infty dk \frac{k f(k)}{\sqrt{(-E_3 + q^2 + k^2)^2 - (kq)^2}}, \quad (\text{D.1})$$

which in a compact form reads

$$f(q) = \int_0^\infty K(E_3, q, q') f(q') dq', \quad (\text{D.2})$$

where  $\mathbf{k} \equiv \mathbf{q}'$  and the kernel  $K(E_3, q, q')$  is defined by

$$K(E_3, q, q') = 2 \left[ \ln \left( \sqrt{\frac{3}{4}q^2 - E_3} \right) \right]^{-1} \frac{q'}{\sqrt{(-E_3 + q^2 + q'^2)^2 - (q'q)^2}}. \quad (\text{D.3})$$

The Gauss-Legendre mesh-points are used for the discretization of the kernel in Eq. (D.3), where the discrete momentum  $q \equiv x_i$  correspond to one set of points with the respective Gauss-Legendre weights  $dq \equiv \omega_i$ . The Gauss-Legendre mesh points and weights are generated, in general, to calculate integrals in the interval  $[-1, 1]$ . Since the kernel has to be discretized in the interval  $[0, \infty[$ , a possible transformation of the set of mesh points and weights is

$$\begin{aligned} q_i &= \frac{1 + x_i}{1 - x_i} \\ w_i &= \frac{2}{(1 - x_i)^2} \omega_i. \end{aligned} \quad (\text{D.4})$$

Therefore, the discretization of the homogeneous integral equation in

Eq. (D.2) is written as

$$\begin{aligned} f(q_i) &= \sum_{j=1}^N K(E_3, q_i, q_j) f(q_j) w_j , \\ f(q_i) - \sum_{j=1}^N K(E_3, q_i, q_j) f(q_j) w_j &= 0 , \\ \left( \delta_{ij} - \sum_{j=1}^N K(E_3, q_i, q_j) w_j \right) f(q_j) &= 0 , \end{aligned} \quad (\text{D.5})$$

where  $\delta_{ij}$  is the Kronecker's delta,  $1 \leq i \leq N$  and  $K(E_3, q_i, q_j)$  reads

$$K(E_3, q_i, q_j) = 2 \left[ \ln \left( \sqrt{\frac{3}{4} q_i^2 - E_3} \right) \right]^{-1} \frac{q_j}{\sqrt{(-E_3 + q_i^2 + q_j^2)^2 - (q_i q_j)^2}} . \quad (\text{D.6})$$

The matrix form of Eq. (D.5) is given by

$$HF = 0 \quad (\text{D.7})$$

whit

$$H = \begin{pmatrix} 1 - K(E_3, q_1, q_1)w_1 & -K(E_3, q_1, q_2)w_2 & \cdots & -K(E_3, q_1, q_N)w_N \\ -K(E_3, q_2, q_1)w_1 & 1 - K(E_3, q_2, q_2)w_2 & \cdots & -K(E_3, q_2, q_N)w_N \\ \vdots & \vdots & \ddots & \vdots \\ -K(E_3, q_N, q_1)w_1 & -K(E_3, q_N, q_2)w_2 & \cdots & 1 - K(E_3, q_N, q_N)w_N \end{pmatrix} \quad (\text{D.8})$$

and

$$F = \begin{pmatrix} f(q_1) \\ f(q_2) \\ \vdots \\ f(q_N) \end{pmatrix} . \quad (\text{D.9})$$

The matrix equation (D.7) only admits non-trivial solution for

$$\det H = \det \left( \delta_{ij} - \sum_{j=1}^N K(E_3, q_i, q_j) w_j \right) = 0 . \quad (\text{D.10})$$

The determinant of  $H$  is a function of the three-body energy  $E_3$ , namely

$$F(E_3) = \det \left( \delta_{ij} - \sum_{j=1}^N K(E_3, q_i, q_j) w_j \right), \quad (\text{D.11})$$

and it is calculated, for instance with the Gauss method or the QR-decomposition [Press 2007]. When  $E_3$  corresponds to a three-body bound state energy,  $E_3^n$ , the determinant of  $H$  must be null. In other words,

$$F(E_3^n) = 0, \quad (\text{D.12})$$

where the superscript  $n$  labels the three-body energy for the  $n^{\text{th}}$  bound state. which satisfies Eqs. (D.1) and (D.10).

The Newton-Raphson method is used in order to find  $E_3^n$  from Eq. (D.11). Expanding Eq. (D.12) up to first order around  $E_3$  gives

$$\begin{aligned} F(E_3^n) &= F(E_3) + (E_3^n - E_3)F'(E_3) = 0, \\ E_3^n &= E_3 - \frac{F(E_3)}{F'(E_3)}, \end{aligned} \quad (\text{D.13})$$

where  $F'(E_3) = \frac{dF(E_3)}{dE_3} |_{E_3^n=E_3}$ . The three-body bound-state energy is found by successively iterations of Eq. (D.13), where the output of the  $m^{\text{th}}$  iteration,  $E_m$ , is used as thin input of the consecutive one. This means that

$$E_m = E_{m-1} - \frac{F(E_{m-1})}{F'(E_{m-1})} \quad \text{for } m = 1, 2, 3 \dots, \quad (\text{D.14})$$

Notice that an appropriate guess is needed for  $E_0$ . A good guess can be found by plotting  $F(E)$  vs.  $E$  and taking  $E_0$  as the point where  $F(E_0) \approx 0$ . However, the kernel in Eq. (D.3) presents the so-called well of attraction, which means that even bad guesses for  $E_0$  would lead to the right final result. The iterative process in Eq. (D.14) must be repeated until

$$\left| \frac{E_m - E_{m-1}}{E_{m-1}} \right| \leq acc, \quad (\text{D.15})$$

where  $acc$  is the desired accuracy.

Unfortunately, the functions  $F$  and  $F'$  in Eq. (D.14) does not have an analytical form. While  $F(E_m)$  can be easily calculated from Eq. (D.11), its derivative is found from the definition of derivative

$$F'(E) = \lim_{\Delta E \rightarrow 0} \frac{F(E + \Delta E) - F(E)}{\Delta E}, \quad (\text{D.16})$$

where the discrete version reads

$$F'(E_m) = \frac{F(E_m) - F(E_{m-1})}{E_m - E_{m-1}}, \quad (\text{D.17})$$

Finally, inserting the derivative (D.17) in Eq. (D.14), the iterative equation for the three-body energy becomes

$$E_m = E_{m-1} - F(E_{m-1}) \frac{E_{m-1} - E_{m-2}}{F(E_{m-1}) - F(E_{m-2})} \quad \text{for } m \geq 2, \quad (\text{D.18})$$

where now  $E_1$  has also to be guessed. A good try is  $E_1 = 1.1E_0$ .

It is straight forward to extended the method above for the case of three distinguishable particles, since only the matrix  $H$  in Eq. (D.8) and  $F$  in Eq. (D.9) have to be redefined. The set of coupled integral equations is given in Eq. (2.70). These equations read

$$f_\alpha(q) = 2\pi \left[ 4\pi m_{\beta\gamma} \ln \left( \sqrt{\frac{\frac{q^2}{2m_{\beta\gamma,\alpha}} - E_3}{E_{\beta\gamma}}} \right) \right]^{-1} \\ \times \int_0^\infty dk \left( \frac{k f_\beta(k)}{\sqrt{\left(-E_3 + \frac{q^2}{2m_{\alpha\gamma}} + \frac{k^2}{2m_{\beta\gamma}}\right)^2 - \left(\frac{kq}{m_\gamma}\right)^2}} \right. \\ \left. + \frac{k f_\gamma(k)}{\sqrt{\left(-E_3 + \frac{q^2}{2m_{\alpha\beta}} + \frac{k^2}{2m_{\beta\gamma}}\right)^2 - \left(\frac{kq}{m_\beta}\right)^2}} \right), \quad (\text{D.19})$$

or in a more compact form

$$f_\alpha(q) = \int_0^\infty K_{\alpha\beta}(E_3, q, k) f_\beta(k) dk + \int_0^\infty K_{\alpha\gamma}(E_3, q, k) f_\gamma(k) dk , \quad (\text{D.20})$$

where, writing the labels of each particle explicitly results in three equations, namely

$$f_a(q) = \int_0^\infty K_{12}(E_3, q, k) f_b(k) dk + \int_0^\infty K_{13}(E_3, q, k) f_c(k) dk , \quad (\text{D.21})$$

$$f_b(q) = \int_0^\infty K_{21}(E_3, q, k) f_a(k) dk + \int_0^\infty K_{23}(E_3, q, k) f_c(k) dk , \quad (\text{D.22})$$

$$f_c(q) = \int_0^\infty K_{31}(E_3, q, k) f_a(k) dk + \int_0^\infty K_{32}(E_3, q, k) f_b(k) dk , \quad (\text{D.23})$$

with the kernels defined as

$$K_{12}(E_3, q, k) = \frac{\left[ 2m_{bc} \ln \left( \sqrt{\frac{q^2 - E_3}{2m_{bc,a}}} \right) \right]^{-1} k}{\sqrt{\left( -E_3 + \frac{q^2}{2m_{ac}} + \frac{k^2}{2m_{bc}} \right)^2 - \left( \frac{kq}{m_c} \right)^2}} , \quad (\text{D.24})$$

$$K_{13}(E_3, q, k) = \frac{\left[ 2m_{bc} \ln \left( \sqrt{\frac{q^2 - E_3}{2m_{bc,a}}} \right) \right]^{-1} k}{\sqrt{\left( -E_3 + \frac{q^2}{2m_{ab}} + \frac{k^2}{2m_{bc}} \right)^2 - \left( \frac{kq}{m_b} \right)^2}} , \quad (\text{D.25})$$

$$K_{21}(E_3, q, k) = \frac{\left[ 2m_{ac} \ln \left( \sqrt{\frac{q^2 - E_3}{2m_{ac,b}}} \right) \right]^{-1} k}{\sqrt{\left( -E_3 + \frac{k^2}{2m_{ac}} + \frac{q^2}{2m_{bc}} \right)^2 - \left( \frac{kq}{m_c} \right)^2}} , \quad (\text{D.26})$$

$$K_{23}(E_3, q, k) = \frac{\left[ 2m_{ac} \ln \left( \sqrt{\frac{q^2 - E_3}{2m_{ac,b}}} \right) \right]^{-1} k}{\sqrt{\left( -E_3 + \frac{q^2}{2m_{ab}} + \frac{k^2}{2m_{ac}} \right)^2 - \left( \frac{kq}{m_a} \right)^2}} , \quad (\text{D.27})$$

$$K_{31}(E_3, q, k) = \frac{\left[ 2m_{ab} \ln \left( \sqrt{\frac{q^2 - E_3}{2m_{ab,c} E_{ab}}} \right) \right]^{-1} k}{\sqrt{\left(-E_3 + \frac{k^2}{2m_{ab}} + \frac{q^2}{2m_{bc}}\right)^2 - \left(\frac{kq}{m_b}\right)^2}}, \quad (\text{D.28})$$

$$K_{32}(E_3, q, k) = \frac{\left[ 2m_{ab} \ln \left( \sqrt{\frac{q^2 - E_3}{2m_{ab,c} E_{ab}}} \right) \right]^{-1} k}{\sqrt{\left(-E_3 + \frac{k^2}{2m_{ab}} + \frac{q^2}{2m_{ac}}\right)^2 - \left(\frac{kq}{m_a}\right)^2}}. \quad (\text{D.29})$$

Therefore, the discretization of the homogeneous integral equation in Eq. (D.20) is written as

$$\begin{aligned} f_\alpha(q_i) &= \sum_{j=1}^N K_{\alpha\beta}(E_3, q_i, q_j) f_\beta(q_j) w_j + \sum_{j=1}^N K_{\alpha\gamma}(E_3, q_i, q_j) f_\gamma(q_j) w_j, \\ f_\alpha(q_i) - \sum_{j=1}^N K_{\alpha\beta}(E_3, q_i, q_j) f_\beta(q_j) w_j - \sum_{j=1}^N K_{\alpha\gamma}(E_3, q_i, q_j) f_\gamma(q_j) w_j &= 0, \\ \left( \delta_{ij} - \sum_{j=1}^N K_{\alpha\beta}(E_3, q_i, q_j) w_j - \sum_{j=1}^N K_{\alpha\gamma}(E_3, q_i, q_j) w_j \right) \begin{pmatrix} f_\alpha(q_i) \\ f_\beta(q_i) \\ f_\gamma(q_i) \end{pmatrix} &= 0, \end{aligned} \quad (\text{D.30})$$

where  $\delta_{ij}$  is the Kronecker's delta,  $1 \leq i \leq N$  and  $K_{\alpha\beta}$  and  $K_{\alpha\gamma}$  are defined in Eqs. (D.24) to (D.29). The matrix equation of the discretized kernel is in fact a so-called matrix by blocks and reads

$$\begin{pmatrix} \mathbb{1} & H_{12} & H_{13} \\ H_{21} & \mathbb{1} & H_{23} \\ H_{31} & H_{32} & \mathbb{1} \end{pmatrix} \begin{pmatrix} f_a \\ f_b \\ f_c \end{pmatrix} = 0, \quad (\text{D.31})$$

where  $\mathbb{1}$  is the identity matrix and the matrix blocks  $H_{\alpha\beta}$  and  $f_\alpha$  are given by

$$H_{\alpha\beta} = \sum_{j=1}^N K_{\alpha\beta}(E_3, q_i, q_j) w_j \quad \text{for } 1 \leq i \leq N, \quad (\text{D.32})$$

$$f_\alpha = f_\alpha(q_i) \quad \text{for } 1 \leq i \leq N. \quad (\text{D.33})$$

Or, in matrix form

$$f_\alpha = \begin{pmatrix} f_\alpha(q_1) \\ f_\alpha(q_2) \\ \vdots \\ f_\alpha(q_N) \end{pmatrix} \quad (\text{D.34})$$

and, in the same way, the matrix blocks  $H_{\alpha\beta}$  are

$$H_{\alpha\beta} = \begin{pmatrix} K_{\alpha\beta}(E_3, q_1, q_1)w_1 & K_{\alpha\beta}(E_3, q_1, q_2)w_2 & \cdots & K_{\alpha\beta}(E_3, q_1, q_N)w_N \\ K_{\alpha\beta}(E_3, q_2, q_1)w_1 & K_{\alpha\beta}(E_3, q_2, q_2)w_2 & \cdots & K_{\alpha\beta}(E_3, q_2, q_N)w_N \\ \vdots & \vdots & \ddots & \vdots \\ K_{\alpha\beta}(E_3, q_N, q_1)w_1 & K_{\alpha\beta}(E_3, q_N, q_2)w_2 & \cdots & K_{\alpha\beta}(E_3, q_N, q_N)w_N \end{pmatrix}. \quad (\text{D.35})$$

Finally, Eq. (D.31) can be written as Eq. (D.7), i.e.,  $HF = 0$  and the steps between Eqs. (D.10) and (D.18) are the same, giving the three-body energy for a system composed for three-distinguishable particles.

## D.2 Spectator functions (eigenvector)

The method is illustrated for the case of identical particles, since it allows a simpler notation. However, the procedure is general and easily extended to the case of three-distinguishable particles, as it was done in the calculation of the three-body energy in Sec. D.1.

Once the three-bode energy  $E_3$  is calculated, it should be inserted again in Eq. (D.5) in order to once more generate the matrix  $H$ , as given in Eq. (D.8). Now, the matrix equation  $HF = 0$  (see Eq. (D.7)) is simply a set of  $N$  equations for  $N$  unknown, namely, each value of the spectator function  $f(q_n)$  has to be determined in a point  $q_n$ , with  $1 \leq n \leq N$ .

The set of  $N$  equations is given by

$$\sum_{j=1}^N H_{ij}(E_3, q_i, q_j)f(q_j) = 0 \quad \text{for } 1 \leq i \leq N. \quad (\text{D.36})$$



Notice, however, that the three-body energy calculated in the last section is the one which fulfills  $\det H = 0$ . This means that one of the equations from the set is redundant and that the system in Eq. (D.36) can not be unequivocally determined. In other words,  $N - 1$  variables will be given in terms of an arbitrary value. This freedom in the system is utilized to set, for instance,  $f(q_1) = 1$ . Then, eliminating a line and a column in Eq.(D.7), the system of equations becomes

$$\sum_{j=2}^N H_{ij}(E_3, q_i, q_j) f(q_j) = -H_{i1} f(q_1) = -H_{i1} \quad \text{for } 2 \leq i \leq N, \quad (\text{D.37})$$

or in the matrix form

$$\left[ \begin{array}{c} \left[ \begin{array}{c} \left[ \begin{array}{c} \tilde{H}_{(N-1) \times (N-1)} \end{array} \right] \end{array} \right] \begin{array}{c} 1 \\ f(q_2) \\ \vdots \\ \vdots \\ f(q_N) \end{array} \end{array} \right] = 0,$$

where all the unknown  $f(q_n)$  with  $2 \leq n \leq N$  are determined in term of  $f(q_1) = 1$ . There is no problem in choosing an arbitrary value for  $f(q_1)$ , since the wave-function is defined unless a normalization constant. The Gauss-Jordan elimination method is then used to solve the set algebraic equations in Eq. (D.37). Besides, this method still holds in the case of three-distinguishable particles, where the only difference arises from the matrix  $H$  and  $F$  which have to be respectively defined as in Eqs. (D.32) and (D.33), whose matrix form is given in Eq. (D.31).



# Asymptotic one-body density in 3D

---

The large momentum limit of the four terms in Eqs. (6.25) to (6.28) is worked out in this Appendix.

## E.0.1 Asymptotic contribution from $n_1(q_B)$

As in the 2D case, this is also the simplest term. The asymptotic form of the spectator function from Eq. (6.17) is inserted in Eq. (6.25), the first out of the four terms of the momentum distribution. Taking the large momentum limit results in

$$\begin{aligned} n_1(q_B) &\rightarrow 2\pi^2 \sqrt{\frac{\mathcal{A}}{\mathcal{A}+2}} \frac{|\chi_{AA}(q_B)|^2}{q_B} \rightarrow 2\pi^2 |c_{AA}|^2 \sqrt{\frac{\mathcal{A}}{\mathcal{A}+2}} \frac{|\sin(s \ln q_B/q^*)|^2}{q_B^5}, \\ &\rightarrow \frac{\pi^2}{q_B^5} |c_{AA}|^2 \sqrt{\frac{\mathcal{A}}{\mathcal{A}+2}}, \end{aligned} \quad (\text{E.1})$$

where the  $1/2$  came from the average of the oscillating part.

## E.0.2 Asymptotic contribution from $n_2(q_B)$

For large  $q_B$ , Eq. (6.26) becomes

$$\begin{aligned} n_2(q_B) &= 2 \int d^3 q_A \frac{|\chi_{AB}(q_A)|^2}{(q_A^2 + \mathbf{q}_A \cdot \mathbf{q}_B + q_B^2 \frac{\mathcal{A}+1}{2\mathcal{A}})^2}, \\ &= \frac{8\mathcal{A}^2}{q_B^4 (\mathcal{A}+1)^2} \int d^3 q_A |\chi_{AB}(q_A)|^2 + n_{2s}(q_B), \end{aligned} \quad (\text{E.2})$$

where a sub-leading part,  $n_{2s}(q_B)$ , is retained since it is of the same order as the leading order of the other terms. It is important to emphasize that the one-body large-momentum leading order comes only from  $n_2(q_B)$ . The spectator function can not be replaced by its asymptotic expression, because the main contribution to  $\int_0^\infty dq_A q_A^2 |\chi_{AB}(q_A)|^2$  arises from small  $q_A$ . This replacement would therefore lead to a completely wrong result. However, this is not always the case, as shown below for  $n_{2s}(q_B)$ .

The sub-leading term is

$$\begin{aligned}
n_{2s}(q_B) &= \int d^3q_A |\chi_{AB}(q_A)|^2 \left[ \frac{2}{(q_A^2 + \mathbf{q}_A \cdot \mathbf{q}_B + q_B^2 \frac{A+1}{2A})^2} - \frac{8A^2}{(A+1)^2} \frac{1}{q_B^4} \right], \\
&= |c_{AB}|^2 \int \frac{d^3q_A}{q_A^4} \left[ \frac{1}{(q_A^2 + \mathbf{q}_A \cdot \mathbf{q}_B + q_B^2 \frac{A+1}{2A})^2} - \frac{4A^2}{(A+1)^2} \frac{1}{q_B^4} \right], \\
&= \frac{2\pi |c_{AB}|^2}{q_B^5} \int_{-\infty}^{\infty} \frac{dx}{x^2} \left[ \frac{1}{x^4 + \frac{1}{A}x^2 + (\frac{A+1}{2A})^2} - \frac{1}{(\frac{A+1}{2A})^2} \right], \tag{E.3}
\end{aligned}$$

where it was used in the second line the asymptotic form of  $|\chi_{AB}(q_A)|^2 = |c_{AB}|^3 q_A^{-4}/2$  obtained after averaging over the oscillatory term in Eq. (6.17). Next, the angular integral was solved and the variable  $q_A = q_B x$  introduced. Since the integrand is even the integration can be extended to the entire real axis.

The function under the integral,

$$f(x) = \frac{1}{x^2} \left[ \frac{1}{x^4 + \frac{1}{A}x^2 + (\frac{A+1}{2A})^2} - \frac{1}{(\frac{A+1}{2A})^2} \right], \tag{E.4}$$

falls off faster than  $1/x$  for  $|x| \rightarrow \infty$ . Therefore, it is extended to the complex domain, where a contour in the upper-half plane that includes the real axis and a semi-circle of large radius in a counterclockwise orientation is considered. The poles of  $f(x)$  have to be determined in order to use the Cauchy residue theorem. Since  $f(x)$  is regular at  $x = 0$ , the four poles are

out in the complex plane and are given by

$$x_1 = re^{i\theta_1/2}, \quad x_2 = re^{i(\pi-\theta_1/2)}, \quad x_3 = re^{i(\pi+\theta_1/2)}, \quad x_4 = re^{-i\theta_1/2}, \quad (\text{E.5})$$

where  $r = \sqrt{\frac{\mathcal{A}+1}{2\mathcal{A}}}$  and  $\tan^2 \theta_1 = \mathcal{A}(\mathcal{A}+2)$ . Following the convention from Eqs. (6.19) to (6.21), where  $\pi/2 < \theta_1 < \pi$ , then  $x_1$  and  $x_2$  are the poles in the upper-half plane. The sum of the two residues is

$$\text{Res}(f, x_1) + \text{Res}(f, x_2) = -\frac{1}{ir^3} \frac{\mathcal{A}(\mathcal{A}+3)}{(\mathcal{A}+1)^2} \frac{\cos(\frac{\theta_1}{2})}{\sin(\theta_1)}. \quad (\text{E.6})$$

Using the residue theorem, the sub-leading term in Eq. (E.3) becomes

$$n_{2s}(q_B) = -\frac{4\pi^2 |c_{AB}|^2}{q_B^5 2 \sin(\frac{\theta_1}{2})} \frac{\mathcal{A}(\mathcal{A}+3)}{(\mathcal{A}+1)^2} \left( \frac{2\mathcal{A}}{\mathcal{A}+1} \right)^{3/2}, \quad (\text{E.7})$$

where, from the definition of  $\theta_1$ ,  $\cos\theta_1 = -\frac{1}{\mathcal{A}+1}$  and  $[2 \sin(\frac{\theta_1}{2})]^{-1} = \sqrt{\frac{\mathcal{A}+1}{2(\mathcal{A}+2)}}$ . Finally, the sub-leading term in  $n_2$  is given by

$$\langle n_2(q_B) \rangle = -\frac{8\pi^2 |c_{AB}|^2}{q_B^5} \frac{\mathcal{A}^3(\mathcal{A}+3)}{(\mathcal{A}+1)^3 \sqrt{\mathcal{A}(\mathcal{A}+2)}}, \quad (\text{E.8})$$

where the special case  $\mathcal{A} = 1$  yields  $\langle n_2(q_B) \rangle = -4\pi^2 |c_{AB}|^2 / (\sqrt{3}q_B^5)$ . The sub-index  $s$  was dropped, since this term has the same order as the leading-order of the  $n_3(q_B)$  and  $n_4(q_B)$  terms.

### E.0.3 Asymptotic contribution from $n_3(q_B)$

The structure of  $n_3(q_B)$  in Eq. (6.27) is similar to  $n_2(q_B)$  in Eq. (6.26). The only difference is that the spectator function under the integration sign is not squared anymore. This small functional difference leads to a completely different result. Neglecting the three-body energy and changing variables

to  $\mathbf{q}_A = \mathbf{p}_B - \frac{\mathbf{q}_B}{2}$  in Eq. (6.27) results in

$$\begin{aligned}
n_3(q_B) &= 2\chi_{AA}^*(q_B) \int d^3q_A \frac{\chi_{AB}(q_A)}{\left(q_A^2 + q_B^2 \frac{A+1}{2A} + \mathbf{q}_A \cdot \mathbf{q}_B\right)^2} + c.c. , \\
&= 2\chi_{AA}^*(q_B) \int d^3y q_B^3 \frac{\chi_{AB}(q_B y)}{\left(y^2 q_B^2 + q_B^2 \frac{A+1}{2A} + y q_B^2 \cos \theta\right)^2} + c.c. , \\
&= \frac{2\chi_{AA}^*(q_B)}{q_B} \int d^3y \frac{\chi_{AB}(q_B y)}{\left(y^2 + \frac{A+1}{2A} + y \cos \theta\right)^2} + c.c. , \\
&= 4\pi \frac{\chi_{AA}^*(q_B)}{q_B} \int_0^\infty dy y^2 \int_0^\pi \frac{d\theta \sin \theta \chi_{AB}(q_B y)}{\left(y^2 + \frac{A+1}{2A} + y \cos \theta\right)^2} + c.c. . \quad (\text{E.9})
\end{aligned}$$

where in the second line it was defined  $\mathbf{q}_A = q_B \mathbf{y}$ .

The angular integral is

$$\begin{aligned}
\int_0^\pi \frac{d\theta \sin \theta}{\left(y^2 + \frac{A+1}{2A} + y \cos \theta\right)^2} &= \int_{-1}^1 \frac{dx}{(A+Bx)^2} = \frac{-1}{B} \int_{A-B}^{A+B} \frac{dz}{z^2} = \frac{-1}{B} \frac{1}{z} \Big|_{A-B}^{A+B} , \\
&= \frac{2}{A^2 - B^2} = \frac{2}{\left(y^2 + \frac{A+1}{2A}\right)^2 - y^2} , \\
&= \frac{2}{y^4 + \frac{1}{A}y^2 + \left(\frac{A+1}{2A}\right)^2} . \quad (\text{E.10})
\end{aligned}$$

Besides, replacing the spectator functions  $\chi_{AA}$  and  $\chi_{AB}$  by their asymptotic form, as given in Eq. (6.17), results in

$$\begin{aligned}
\chi_{AA}^*(q_B) &= \frac{c_{AA}^*}{q_B^2} \sin\left(s \ln \frac{q_B}{q^*}\right), \quad (\text{E.11}) \\
\chi_{AB}(q_B y) &= \frac{c_{AB}}{y^2 q_B^2} \sin\left[s \ln\left(\frac{q_B y}{q^*}\right)\right], \\
&= \frac{c_{AB}}{y^2 q_B^2} \sin\left(s \ln \frac{q_B}{q^*} + s \ln y\right), \\
&= \frac{c_{AB}}{y^2 q_B^2} \left[ \sin\left(s \ln \frac{q_B}{q^*}\right) \cos(s \ln y) + \sin(s \ln y) \cos\left(s \ln \frac{q_B}{q^*}\right) \right]. \quad (\text{E.12})
\end{aligned}$$

Inserting Eqs. (E.10) to (E.12) into Eq. (E.9) gives

$$\begin{aligned}
n_3(q_B) &= 8\pi \frac{c_{AA}^* c_{AB}}{q_B^5} \sin^2(s \ln q_B/q^*) \int_0^\infty \frac{\cos(s \ln y) dy}{y^4 + \frac{1}{\mathcal{A}}y^2 + \left(\frac{\mathcal{A}+1}{2\mathcal{A}}\right)^2} \\
&+ 8\pi \frac{c_{AA}^* c_{AB}}{q_B^5} \sin(s \ln q_B/q^*) \cos(s \ln q_B/q^*) \int_0^\infty \frac{\sin(s \ln y) dy}{y^4 + \frac{1}{\mathcal{A}}y^2 + \left(\frac{\mathcal{A}+1}{2\mathcal{A}}\right)^2} + c.c. .
\end{aligned} \tag{E.13}$$

Averaging out the oscillatory terms, only the first term of Eq. (E.13) gives a non-vanishing result

$$\langle n_3(q_B) \rangle = 4\pi \frac{c_{AA}^* c_{AB}}{q_B^5} \int_0^\infty \frac{\cos(s \ln y) dy}{y^4 + \frac{1}{\mathcal{A}}y^2 + \left(\frac{\mathcal{A}+1}{2\mathcal{A}}\right)^2} + c.c. . \tag{E.14}$$

Expressing cosine in the complex exponential form

$$\cos(s \ln y) = \frac{e^{is \ln y} + e^{-is \ln y}}{2} = \frac{e^{\ln y^{is}} + e^{\ln y^{-is}}}{2} = \frac{y^{is} + y^{-is}}{2}, \tag{E.15}$$

the integral in Eq. (E.14) becomes

$$I(s) = \int_0^\infty \frac{\cos(s \ln y) dy}{y^4 + \frac{1}{\mathcal{A}}y^2 + \left(\frac{\mathcal{A}+1}{2\mathcal{A}}\right)^2} = \frac{1}{2} \int_0^\infty dy \frac{y^{is} + y^{-is}}{y^4 + \frac{1}{\mathcal{A}}y^2 + \left(\frac{\mathcal{A}+1}{2\mathcal{A}}\right)^2}. \tag{E.16}$$

In order to extend the integration to the full real axis, the variables are changed to  $y = e^\alpha$ , where  $dy = e^\alpha d\alpha$  and the integral  $I(s)$  is expressed as

$$I(s) = \frac{1}{2} \int_{-\infty}^\infty \frac{d\alpha e^\alpha (e^{is\alpha} + e^{-is\alpha})}{e^{4\alpha} + \frac{1}{\mathcal{A}}e^{2\alpha} + \left(\frac{\mathcal{A}+1}{2\mathcal{A}}\right)^2} = \text{Re } I_\alpha(s), \tag{E.17}$$

where  $\text{Re}$  denotes the real part and the integral  $I_\alpha(s)$  is explicitly rewritten in terms of its poles as

$$I_\alpha(s) = \int_{-\infty}^\infty \frac{e^{\alpha(1+is)} d\alpha}{(e^\alpha - e^{\alpha_1})(e^\alpha - e^{\alpha_2})(e^\alpha - e^{\alpha_3})(e^\alpha - e^{\alpha_4})}. \tag{E.18}$$

The integral (E.17) is solved using the residues theorem. The next steps are

about finding the poles of the integrand  $f(\alpha)$  and evaluating the residues of the poles. In order to simplify the calculation of the roots in the denominator of  $f(\alpha)$ , the variable  $x = y^2 = e^{2\alpha}$  is introduced. The zeros of the denominator in Eq. (E.17) are found from  $x^2 + \frac{1}{\mathcal{A}}x + \left(\frac{\mathcal{A}+1}{2\mathcal{A}}\right)^2 = 0$  and are given by

$$x_{\pm} = -\frac{1}{2\mathcal{A}} \pm \frac{1}{2} \sqrt{\frac{1}{\mathcal{A}^2} - \left(\frac{\mathcal{A}+1}{2\mathcal{A}}\right)^2} = \frac{1}{2\mathcal{A}} \left(-1 \pm i\sqrt{\mathcal{A}(\mathcal{A}+2)}\right). \quad (\text{E.19})$$

In the variable  $y = \pm\sqrt{x}$  these roots read

$$y_1 = +\sqrt{\frac{1}{2\mathcal{A}} \left(-1 + i\sqrt{\mathcal{A}(\mathcal{A}+2)}\right)^{1/2}} = +\frac{1}{2} + i\sqrt{\frac{\mathcal{A}+2}{4\mathcal{A}}} = r e^{i\theta_3}, \quad (\text{E.20})$$

$$y_2 = -\sqrt{\frac{1}{2\mathcal{A}} \left(-1 + i\sqrt{\mathcal{A}(\mathcal{A}+2)}\right)^{1/2}} = -\frac{1}{2} - i\sqrt{\frac{\mathcal{A}+2}{4\mathcal{A}}} = r e^{-i(\pi-\theta_3)} = -r e^{i\theta_3}, \quad (\text{E.21})$$

$$y_3 = +\sqrt{\frac{1}{2\mathcal{A}} \left(-1 - i\sqrt{\mathcal{A}(\mathcal{A}+2)}\right)^{1/2}} = +\frac{1}{2} - i\sqrt{\frac{\mathcal{A}+2}{4\mathcal{A}}} = r e^{-i\theta_3}, \quad (\text{E.22})$$

$$y_4 = -\sqrt{\frac{1}{2\mathcal{A}} \left(-1 - i\sqrt{\mathcal{A}(\mathcal{A}+2)}\right)^{1/2}} = -\frac{1}{2} + i\sqrt{\frac{\mathcal{A}+2}{4\mathcal{A}}} = r e^{i(\pi-\theta_3)} = -r e^{-i\theta_3}. \quad (\text{E.23})$$

Finally, the roots in the variable  $\alpha = \ln y$  are

$$\alpha_1 = \ln y_1 = \ln r + i\theta_3, \quad (\text{E.24})$$

$$\alpha_2 = \ln y_2 = \ln r - i(\pi - \theta_3), \quad (\text{E.25})$$

$$\alpha_3 = \ln y_3 = \ln r - i\theta_3, \quad (\text{E.26})$$

$$\alpha_4 = \ln y_4 = \ln r + i(\pi - \theta_3), \quad (\text{E.27})$$

showing that all of them are in the complex plane, out of the real axis. The quantities  $r$  and  $\theta_3$  are defined as

$$r = \sqrt{\frac{\mathcal{A}+1}{2\mathcal{A}}}, \quad (\text{E.28})$$



$$\tan \theta_3 = \sqrt{\frac{\mathcal{A}+2}{\mathcal{A}}} \quad \text{for } 0 \leq \theta_3 \leq \frac{\pi}{2}. \quad (\text{E.29})$$

A rectangle of vertices  $-R$ ,  $+R$ ,  $+R+i\pi$  and  $-R+i\pi$  molds a closed path in a complex plane, as shown in Fig. E.1. Due to the restriction of  $\theta_3$ , given in Eq. (E.29), this closed path encompasses the poles  $\alpha_1$  and  $\alpha_4$  in the upper-half plane and then, four integrals have to be worked out, namely  $J_1$  which extends along the real axis from  $-R$  to  $+R$ ,  $J_2$  from  $+R$  to  $+R+i\pi$ ,  $J_3$  from  $+R+i\pi$  to  $-R+i\pi$  and  $J_4$  from  $-R+i\pi$  to  $-R$ .

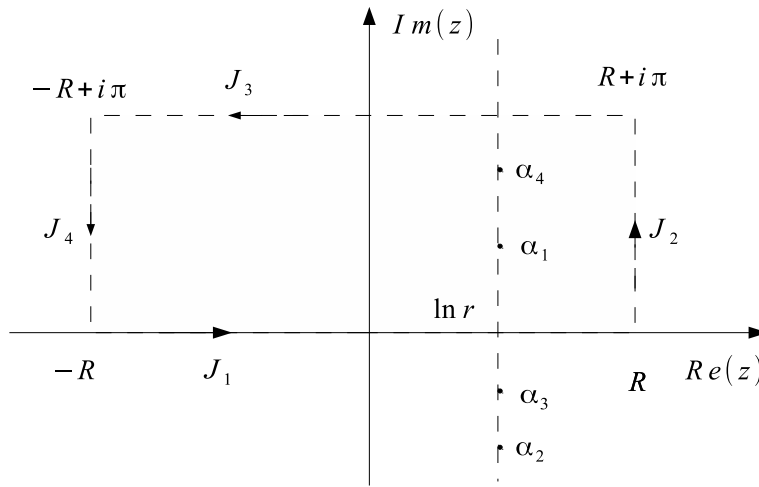


Figure E.1: A rectangle of vertices  $-R$ ,  $+R$ ,  $+R+i\pi$  and  $-R+i\pi$ , which molds the closed path in a complex plane of  $z$ . The poles  $\alpha_1$  and  $\alpha_4$  are encompassed in the upper-half plane. The the direction of integration of the four integrals  $J_1$ ,  $J_2$ ,  $J_3$  and  $J_4$  are indicated by the arrows.

The residues theorem is used to calculate  $I_\alpha(s)$ . The integral in the closed path reads

$$\oint \frac{dz e^z e^{isz}}{e^{4z} + \frac{1}{\mathcal{A}} e^{2z} + \left(\frac{\mathcal{A}+1}{2\mathcal{A}}\right)^2} = J_1 + J_2 + J_3 + J_4 = 2\pi i \left[ \text{Res}(f, \alpha_1) + \text{Res}(f, \alpha_4) \right], \quad (\text{E.30})$$

where changing variables to the  $z = \alpha + i 0$ , the integral  $J_1$  reads

$$J_1 = \lim_{R \rightarrow \infty} \int_{-R}^R \frac{d\alpha e^\alpha e^{i s \alpha}}{e^{4\alpha} + \frac{1}{\mathcal{A}} e^{2\alpha} + \left(\frac{\mathcal{A}+1}{2\mathcal{A}}\right)^2} \rightarrow I_\alpha(s). \quad (\text{E.31})$$

Analogously, setting  $z = R + i y$  gives  $dz = i dy$  and the integral  $J_2$  becomes

$$\begin{aligned} J_2 &= \lim_{R \rightarrow \infty} \int_R^{R+i\pi} \frac{dz e^z e^{i s z}}{e^{4z} + \frac{1}{\mathcal{A}} e^{2z} + \left(\frac{\mathcal{A}+1}{2\mathcal{A}}\right)^2}, \\ &= \lim_{R \rightarrow \infty} i \int_0^\pi \frac{dy e^{R+iy} e^{i s (R+iy)}}{e^{4(R+iy)} + \frac{1}{\mathcal{A}} e^{2(R+iy)} + \left(\frac{\mathcal{A}+1}{2\mathcal{A}}\right)^2}, \\ &= \lim_{R \rightarrow \infty} \frac{e^R}{e^{4R}} i \int_0^\pi \frac{dy e^{iy} e^{i s (R+iy)}}{e^{4iy} + \frac{1}{\mathcal{A}} e^{2iy} \frac{1}{e^{2R}} + \left(\frac{\mathcal{A}+1}{2\mathcal{A}}\right)^2 \frac{1}{e^{4R}}} \rightarrow 0. \end{aligned} \quad (\text{E.32})$$

The integral  $J_3$  is similar to  $J_1$  and changing variables to  $z = \alpha + i\pi$  it reads

$$\begin{aligned} J_3 &= \lim_{R \rightarrow \infty} \int_{R+i\pi}^{-R+i\pi} \frac{dz e^z e^{i s z}}{e^{4z} + \frac{1}{\mathcal{A}} e^{2z} + \left(\frac{\mathcal{A}+1}{2\mathcal{A}}\right)^2}, \\ &= \lim_{R \rightarrow \infty} \int_R^{-R} \frac{d\alpha e^{\alpha+i\pi} e^{i s (\alpha+i\pi)}}{e^{4(\alpha+i\pi)} + \frac{1}{\mathcal{A}} e^{2(\alpha+i\pi)} + \left(\frac{\mathcal{A}+1}{2\mathcal{A}}\right)^2}, \\ &= \lim_{R \rightarrow \infty} \int_{-R}^R \frac{d\alpha e^\alpha e^{i s \alpha} e^{-s\pi}}{e^{4\alpha} + \frac{1}{\mathcal{A}} e^{2\alpha} + \left(\frac{\mathcal{A}+1}{2\mathcal{A}}\right)^2} \rightarrow e^{-s\pi} J_1 = e^{-s\pi} I_\alpha(s), \end{aligned} \quad (\text{E.33})$$

where  $e^{\alpha+i\pi} = e^\alpha e^{i\pi} = -e^\alpha$ . Then, performing the same transformation as in  $J_2$ , the last term becomes

$$\begin{aligned} J_4 &= \lim_{R \rightarrow \infty} \int_{-R+i\pi}^{-R} \frac{d\alpha e^\alpha e^{i s \alpha}}{e^{4\alpha} + \frac{1}{\mathcal{A}} e^{2\alpha} + \left(\frac{\mathcal{A}+1}{2\mathcal{A}}\right)^2}, \\ &= \lim_{R \rightarrow \infty} i \int_\pi^0 \frac{dy e^{R+iy} e^{i s (R+iy)}}{e^{4(R+iy)} + \frac{1}{\mathcal{A}} e^{2(R+iy)} + \left(\frac{\mathcal{A}+1}{2\mathcal{A}}\right)^2}, \\ &= - \lim_{R \rightarrow \infty} J_2 \rightarrow 0, \end{aligned} \quad (\text{E.34})$$

Summarizing, in the limit  $R \rightarrow \infty$ , the integrals are  $J_1 = I_\alpha(s)$ ,  $J_3 =$

$e^{-s\pi}I_\alpha(s)$  and  $J_2, J_4 \rightarrow 0$ . Then, from Eq. (E.30) the integral  $I_\alpha(s)$  reads

$$I_\alpha(s) = \frac{2\pi i}{1 + e^{-\pi s}} \left[ \text{Res}(f, \alpha_1) + \text{Res}(f, \alpha_4) \right]. \quad (\text{E.35})$$

In order to calculate the residues of the poles  $\alpha_1$  and  $\alpha_4$ , it is necessary to expand the  $n^{\text{th}}$  root, in the limit  $\alpha \rightarrow \alpha_n$ , as

$$\begin{aligned} e^\alpha - e^{\alpha_n} &= e^\alpha (1 - e^{\alpha_n - \alpha}) = e^\alpha \left( 1 - 1 - (\alpha_n - \alpha) - \frac{(\alpha_n - \alpha)^2}{2!} - \dots \right), \\ &= e^\alpha (\alpha - \alpha_n) \left( 1 + \frac{(\alpha - \alpha_n)}{2!} - \dots \right). \end{aligned} \quad (\text{E.36})$$

Besides, notice that the exponential of each root  $\alpha_n$  in Eqs. (E.24) to (E.27) is already given in Eqs. (E.20) to (E.23). Taking the first order in the expansion, the residues are given by

$$\begin{aligned} \text{Res}(f, \alpha_1) &= \lim_{\alpha \rightarrow \alpha_1} (\alpha - \alpha_1) \frac{e^{\alpha(1+i s)}}{e^\alpha (\alpha - \alpha_1) (e^\alpha - e^{\alpha_2}) (e^\alpha - e^{\alpha_3}) (e^\alpha - e^{\alpha_4})}, \\ &= \frac{e^{\alpha_1}}{e^{\alpha_1} e^{i s \alpha_1}} \frac{e^{\alpha_1(1+i s)}}{e^{\alpha_1} (e^{\alpha_1} - e^{\alpha_2}) (e^{\alpha_1} - e^{\alpha_3}) (e^{\alpha_1} - e^{\alpha_4})}, \\ &= \frac{1}{8 i r^3 \sin \theta_3 \cos \theta_3 e^{i \theta_3}}, \\ &= \frac{1}{2i} \sqrt{\frac{\mathcal{A}}{\mathcal{A} + 2}} \frac{1}{\cos \theta_3} e^{i s (\ln r + i \theta_3) - i \theta_3}, \end{aligned} \quad (\text{E.37})$$

and

$$\begin{aligned} \text{Res}(f, \alpha_4) &= \lim_{\alpha \rightarrow \alpha_4} (\alpha - \alpha_4) \frac{e^{\alpha(1+i s)}}{e^\alpha (\alpha - \alpha_4) (e^\alpha - e^{\alpha_1}) (e^\alpha - e^{\alpha_2}) (e^\alpha - e^{\alpha_3})}, \\ &= \frac{e^{\alpha_4}}{e^{\alpha_4} e^{i s \alpha_4}} \frac{e^{\alpha_4(1+i s)}}{e^{\alpha_4} (e^{\alpha_4} - e^{\alpha_1}) (e^{\alpha_4} - e^{\alpha_2}) (e^{\alpha_4} - e^{\alpha_3})}, \\ &= \frac{1}{8 i r^3 \sin \theta_3 \cos \theta_3 e^{-i \theta_3}}, \\ &= \frac{1}{2i} \sqrt{\frac{\mathcal{A}}{\mathcal{A} + 2}} \frac{1}{\cos \theta_3} e^{i s [\ln r + i (\pi - \theta_3)] + i \theta_3}, \end{aligned} \quad (\text{E.38})$$

Inserting the residues of the poles from Eqs. (E.37) and (E.38) into

Eq. (E.35) gives

$$\begin{aligned}
I_\alpha(s) &= \frac{\pi}{1+e^{-\pi s}} \sqrt{\frac{\mathcal{A}}{\mathcal{A}+2}} \frac{1}{\cos \theta_3} \left( e^{\imath s(\ln r + \imath \theta_3) - \imath \theta_3} + e^{\imath s[\ln r + \imath(\pi - \theta_3)] + \imath \theta_3} \right), \\
&= \frac{2\pi e^{-s\pi/2}}{1+e^{-\pi s}} \sqrt{\frac{\mathcal{A}}{\mathcal{A}+2}} \frac{1}{\cos \theta_3} e^{\imath s \ln r} \cosh \left[ s \left( \theta_3 - \frac{\pi}{2} \right) + \imath \theta_3 \right], \\
&= \frac{\pi}{\cosh \left( s \frac{\pi}{2} \right)} \sqrt{\frac{\mathcal{A}}{\mathcal{A}+2}} \frac{1}{\cos \theta_3} \left[ \cos(s \ln r) + \imath \sin(s \ln r) \right] \\
&\quad \times \left\{ \cos \theta_3 \cosh \left[ s \left( \frac{\pi}{2} - \theta_3 \right) \right] - \imath \sin \theta_3 \sinh \left[ s \left( \frac{\pi}{2} - \theta_3 \right) \right] \right\}, \\
&= \frac{\pi}{\cosh \left( s \frac{\pi}{2} \right)} \sqrt{\frac{\mathcal{A}}{\mathcal{A}+2}} \frac{1}{\cos \theta_3} \\
&\quad \times \left\{ \cos \theta_3 \cos(s \ln r) \cosh \left[ s \left( \frac{\pi}{2} - \theta_3 \right) \right] \right. \\
&\quad \quad \left. + \sin \theta_3 \sin(s \ln r) \sinh \left[ s \left( \frac{\pi}{2} - \theta_3 \right) \right] \right\} \\
&\quad \times -\imath \left\{ \sin \theta_3 \cos(s \ln r) \sinh \left[ s \left( \frac{\pi}{2} - \theta_3 \right) \right] \right. \\
&\quad \quad \left. + \cos \theta_3 \sin(s \ln r) \cosh \left[ s \left( \frac{\pi}{2} - \theta_3 \right) \right] \right\}, \\
&= \frac{\pi}{\cosh \left( s \frac{\pi}{2} \right)} \left\{ \sqrt{\frac{\mathcal{A}}{\mathcal{A}+2}} \cos(s \ln r) \cosh \left[ s \left( \frac{\pi}{2} - \theta_3 \right) \right] \right. \\
&\quad \quad \left. + \sin(s \ln r) \sinh \left[ s \left( \frac{\pi}{2} - \theta_3 \right) \right] \right\} \\
&\quad \times -\imath \left\{ \cos(s \ln r) \sinh \left[ s \left( \frac{\pi}{2} - \theta_3 \right) \right] \right. \\
&\quad \quad \left. + \sqrt{\frac{\mathcal{A}}{\mathcal{A}+2}} \sin(s \ln r) \cosh \left[ s \left( \frac{\pi}{2} - \theta_3 \right) \right] \right\}, \quad (\text{E.39})
\end{aligned}$$

where the the real, Re, and imaginary, Im, parts of  $I_\alpha(s)$  are explicitly given by

$$\begin{aligned}
\text{Re } I_\alpha(s) &= \frac{\pi}{\cosh \left( \frac{s\pi}{2} \right)} \left\{ \sqrt{\frac{\mathcal{A}}{\mathcal{A}+2}} \cos(s \ln r) \cosh \left[ s \left( \frac{\pi}{2} - \theta_3 \right) \right] \right. \\
&\quad \left. + \sin(s \ln r) \sinh \left[ s \left( \frac{\pi}{2} - \theta_3 \right) \right] \right\}, \quad (\text{E.40})
\end{aligned}$$

$$\text{Im } I_\alpha(s) = \frac{-\pi}{\cosh\left(\frac{s\pi}{2}\right)} \left\{ \sqrt{\frac{\mathcal{A}}{\mathcal{A}+2}} \sin(s \ln r) \cosh\left[s\left(\frac{\pi}{2} - \theta_3\right)\right] + \cos(s \ln r) \sinh\left[s\left(\frac{\pi}{2} - \theta_3\right)\right] \right\}, \quad (\text{E.41})$$

with  $r$  and  $\theta_3$  defined respectively in Eqs. (E.28) and (E.29).

Finally, from equations (E.14), (E.17) and (E.40), the non-oscillating part of  $n_3(q_B)$  is given by

$$\langle n_3(q_B) \rangle = \frac{4\pi^2 c_{AA} c_{AB}}{q_B^5 \cosh\left(\frac{s\pi}{2}\right)} \left\{ \sqrt{\frac{\mathcal{A}}{\mathcal{A}+2}} \cos\left(s \ln \sqrt{\frac{\mathcal{A}+1}{2\mathcal{A}}}\right) \cosh\left[s\left(\frac{\pi}{2} - \theta_3\right)\right] + \sin\left(s \ln \sqrt{\frac{\mathcal{A}+1}{2\mathcal{A}}}\right) \sinh\left[s\left(\frac{\pi}{2} - \theta_3\right)\right] \right\}, \quad (\text{E.42})$$

where  $\tan \theta_3 = \sqrt{\frac{\mathcal{A}+2}{\mathcal{A}}}$  for  $0 \leq \theta_3 \leq \pi/2$ . The special case  $\mathcal{A} = 1$  yields  $\theta_3 = \pi/3$  and  $\langle n_3(q_B) \rangle = 4\pi^2 |c_{AA}|^2 \cosh\left(\frac{s\pi}{6}\right) / (q_B^5 \sqrt{3} \cosh\left(\frac{s\pi}{2}\right))$ .

#### E.0.4 Asymptotic contribution from $n_4(q_B)$

As in the 2D case, this is also the most complicated out of the four additive terms in the one-body momentum density, since the angular dependence in both spectator arguments of Eq. (6.28) can not be removed simultaneously by a change in variables. Then, although Eqs. (6.27) and (6.28) are similar, it is not possible to extend the results from the previous case,  $n_3(q_B)$ , to obtain the non-oscillating part of  $n_4(q_B)$ . Defining  $\mathbf{p}_B = \frac{q_B}{2} \mathbf{y}$  and dropping the three-body energy, Eq. (6.28) becomes

$$n_4(q_B) = \frac{4\pi}{q_B} \int_0^\infty \frac{y^2 dy}{\left(y^2 + \frac{\mathcal{A}+2}{\mathcal{A}}\right)^2} \int_{-1}^{+1} dx \chi_{AB}^*(q_B x_-) \chi_{AB}(q_B x_+) + c.c., \quad (\text{E.43})$$

where  $x_{\pm} = \frac{1}{2}\sqrt{1 + y^2 \pm 2yx}$ . The asymptotic spectator function for a shifted argument is given in Eq. (E.12) and  $\chi_{AB}(q_B x_{\pm})$  reads

$$\chi_{AB}(q_B x_{\pm}) = \frac{c_{AB}}{x_{\pm}^2 q_B^2} \left[ \sin\left(s \ln \frac{q_B}{q^*}\right) \cos(s \ln x_{\pm}) + \sin(s \ln x_{\pm}) \cos\left(s \ln \frac{q_B}{q^*}\right) \right]. \quad (\text{E.44})$$

The spectator function in Eq. (E.43) are replaced by their asymptotic form from Eq. (E.44). The integral is then separated in three terms, namely

$$\begin{aligned} n_4(q_B) = & \frac{8\pi |c_{AB}|^2 \sin^2\left(s \ln \frac{q_B}{q^*}\right)}{q_B^5} \\ & \times \int_0^{\infty} \frac{y^2 dy}{\left(y^2 + \frac{A+2}{A}\right)^2} \int_{-1}^{+1} \frac{dx}{x_+^2 x_-^2} \cos(s \ln x_+) \cos(s \ln x_-) \\ & + \frac{8\pi |c_{AB}|^2 \cos^2\left(s \ln \frac{q_B}{q^*}\right)}{q_B^5} \\ & \times \int_0^{\infty} \frac{y^2 dy}{\left(y^2 + \frac{A+2}{A}\right)^2} \int_{-1}^{+1} \frac{dx}{x_+^2 x_-^2} \sin(s \ln x_+) \sin(s \ln x_-) \\ & + \frac{4\pi |c_{AB}|^2 \sin\left(s \ln \frac{q_B}{q^*}\right) \cos\left(s \ln \frac{q_B}{q^*}\right)}{q_B^5} \\ & \times \int_0^{\infty} \frac{y^2 dy}{\left(y^2 + \frac{A+2}{A}\right)^2} \int_{-1}^{+1} \frac{dx}{x_+^2 x_-^2} \sin[s \ln(x_+ x_-)]. \quad (\text{E.45}) \end{aligned}$$

As it was done for  $n_3(q_B)$ , averaging out the oscillatory term, only the two first terms on the right-hand-side of Eq. (E.45) give a non-vanishing contribution. The angular integration is performed using that

$$\int dx \left( \frac{\beta + x}{\beta - x} \right)^{\pm i s/2} (\beta^2 - x^2)^{-1} = \pm \left( \frac{\beta + x}{\beta - x} \right)^{\pm i s/2} (i\beta s)^{-1}. \quad (\text{E.46})$$

Then, the angular part of Eq. (E.45) has to be written as Eq. (E.46). The denominator in the integrand of the first two terms on the right hand side

of Eq. (E.45) is

$$\begin{aligned} x_+^2 x_-^2 &= \frac{1}{4} (1 + y^2 - 2yx) \frac{1}{4} (1 + y^2 + 2yx) \\ &= \frac{1}{16} (\alpha - v) (\alpha + v) = \frac{1}{16} (\alpha^2 - v^2), \end{aligned} \quad (\text{E.47})$$

where  $\alpha = 1 + y^2$  and  $v = 2yx$ . In the same notation, the numerator in the integrand of the first two terms on the right hand side of Eq. (E.45) are given by

$$\begin{aligned} D1 &= \cos(s \ln x_+) \cos(s \ln x_-) \\ &= \frac{1}{4} \left[ \left( \frac{\alpha + v}{4} \right)^{is/2} + \left( \frac{\alpha + v}{4} \right)^{-is/2} \right] \left[ \left( \frac{\alpha - v}{4} \right)^{is/2} + \left( \frac{\alpha - v}{4} \right)^{-is/2} \right], \\ &= \frac{1}{4} \left[ \left( \frac{\alpha^2 - v^2}{16} \right)^{is/2} + \left( \frac{\alpha + v}{\alpha - v} \right)^{is/2} + \left( \frac{\alpha + v}{\alpha - v} \right)^{-is/2} + \left( \frac{\alpha^2 - v^2}{16} \right)^{-is/2} \right], \end{aligned} \quad (\text{E.48})$$

and

$$\begin{aligned} D2 &= \sin(s \ln x_+) \sin(s \ln x_-) \\ &= \frac{-1}{4} \left[ \left( \frac{\alpha + v}{4} \right)^{is/2} - \left( \frac{\alpha + v}{4} \right)^{-is/2} \right] \left[ \left( \frac{\alpha - v}{4} \right)^{is/2} - \left( \frac{\alpha - v}{4} \right)^{-is/2} \right], \\ &= \frac{-1}{4} \left[ \left( \frac{\alpha^2 - v^2}{16} \right)^{is/2} - \left( \frac{\alpha + v}{\alpha - v} \right)^{is/2} - \left( \frac{\alpha + v}{\alpha - v} \right)^{-is/2} + \left( \frac{\alpha^2 - v^2}{16} \right)^{-is/2} \right]. \end{aligned} \quad (\text{E.49})$$

Collecting Eqs. (E.47), (E.48) and (E.49) together and inserting them into Eq. (E.45), the non-oscillating part of  $n_4(q_B)$  is given by

$$n_4(q_B) = \frac{4\pi |c_{AB}|^2}{q_B^5} \int_0^\infty \frac{y^2 dy}{\left(y^2 + \frac{A+2}{A}\right)^2} I_x(y), \quad (\text{E.50})$$

where the angular integral  $I_x(y)$  reads

$$\begin{aligned}
I_x(y) &= \int_{-1}^{+1} \frac{dx}{x_+^2 x_-^2} \left[ \cos(s \ln x_+) \cos(s \ln x_-) + \sin(s \ln x_+) \sin(s \ln x_-) \right], \\
&= \int_{-1}^{+1} \frac{dx}{2} \left[ \left( \frac{1+y^2+2yx}{1+y^2-2yx} \right)^{is/2} + \left( \frac{1+y^2+2yx}{1+y^2-2yx} \right)^{-is/2} \right] \frac{16}{(1+y^2)^2 - 4x^2 y^2}, \\
&= \frac{8}{4y^2} \int_{-1}^{+1} dx \left[ \left( \frac{\frac{1+y^2}{2y} + x}{\frac{1+y^2}{2y} - x} \right)^{is/2} + \left( \frac{\frac{1+y^2}{2y} - x}{\frac{1+y^2}{2y} - x} \right)^{-is/2} \right] \left[ \left( \frac{1+y^2}{2y} \right)^2 - x^2 \right]^{-1},
\end{aligned} \tag{E.51}$$

which looks like the expression in Eq. (E.46). Then, the result is

$$\begin{aligned}
I_x(y) &= \frac{2}{y^2} \frac{2y}{is(1+y^2)} \left\{ \left[ \left( \frac{\frac{1+y^2}{2y} + x}{\frac{1+y^2}{2y} - x} \right)^{is/2} \right]_{x=-1}^1 - \left[ \left( \frac{\frac{1+y^2}{2y} + x}{\frac{1+y^2}{2y} - x} \right)^{-is/2} \right]_{x=-1}^1 \right\}, \\
&= \frac{8}{isy(1+y^2)} \left[ \left( \frac{\frac{1+y^2}{2y} + 1}{\frac{1+y^2}{2y} - 1} \right)^{is/2} - \left( \frac{\frac{1+y^2}{2y} + 1}{\frac{1+y^2}{2y} - 1} \right)^{-is/2} \right], \\
&= \frac{8}{isy(1+y^2)} \left[ \left( \sqrt{\frac{(y+1)^2}{(y-1)^2}} \right)^{is} - \left( \sqrt{\frac{(y+1)^2}{(y-1)^2}} \right)^{-is} \right].
\end{aligned} \tag{E.52}$$

Combining the expressions in Eqs. (E.50) and (E.52), the non-oscillating part of  $n_4(q_B)$  reads

$$\begin{aligned}
\langle n_4(q_B) \rangle &= \frac{32\pi |c_{AB}|^2}{is q_B^5} \int_0^\infty \frac{y dy}{\left(y^2 + \frac{A+2}{A}\right)^2 (1+y^2)} \left[ \left( \frac{y+1}{|y-1|} \right)^{is} - \left( \frac{y+1}{|y-1|} \right)^{-is} \right], \\
&= \frac{64\pi |c_{AB}|^2}{s q_B^5} \int_0^\infty \frac{y dy}{\left(y^2 + \frac{A+2}{A}\right)^2 (1+y^2)} \sin \left( s \ln \left( \frac{y+1}{|y-1|} \right) \right),
\end{aligned} \tag{E.53}$$

however the absolute value complicates the calculation of the integral. Circumventing this problem, the integral is split in two pieces:  $y \in [0, 1]$  and  $y \in [1, \infty[$  and a new variable is introduced in each piece, i.e., the variable transformation  $y = \frac{x-1}{x+1}$  is made in the first piece and  $y = \frac{x+1}{x-1}$  in the second



one [Castin 2011]. Notice that in both cases  $x \in [1, \infty[$ . In detail

$$\langle n_A(q_B) \rangle = \frac{64\pi |c_{AB}|^2}{s q_B^5} [I_<(s) + I_>(s)], \quad (\text{E.54})$$

where

$$\begin{aligned} I_<(s) &= \int_0^1 \frac{y dy}{\left(y^2 + \frac{\mathcal{A}+2}{\mathcal{A}}\right)^2 (1+y^2)} \sin\left(s \ln\left(\frac{y+1}{|y-1|}\right)\right), \\ &= \int_1^\infty \frac{2 dx}{(x+1)^2} \frac{x-1}{x+1} \sin(s \ln x) \left/ \left\{ \left[ \left(\frac{x-1}{x+1}\right)^2 + \frac{\mathcal{A}+2}{\mathcal{A}} \right]^2 \left[ \left(\frac{x-1}{x+1}\right)^2 + 1 \right] \right\} \right., \\ &= \int_1^\infty \frac{2(x-1) dx}{(x+1)^3} \frac{\sin(s \ln x) (x+1)^6}{\left[ \left(\frac{\mathcal{A}+2}{\mathcal{A}} + 1\right) (x^2+1) + \left(\frac{\mathcal{A}+2}{\mathcal{A}} - 1\right) 2x \right]^2 2(x^2+1)}, \\ &= \int_1^\infty dx \frac{(x-1)(x+1)^3 \sin(s \ln x)}{\left[ \frac{2}{\mathcal{A}} (\mathcal{A}+1) (x^2+1) + \frac{4}{\mathcal{A}} x \right]^2 (x^2+1)}, \end{aligned} \quad (\text{E.55})$$

and

$$\begin{aligned} I_>(s) &= \int_1^\infty \frac{y dy}{\left(y^2 + \frac{\mathcal{A}+2}{\mathcal{A}}\right)^2 (1+y^2)} \sin\left(s \ln\left(\frac{y+1}{|y-1|}\right)\right), \\ &= - \int_\infty^1 \frac{2 dx}{(x-1)^2} \frac{x+1}{x-1} \sin(s \ln x) \left/ \left\{ \left[ \left(\frac{x+1}{x-1}\right)^2 + \frac{\mathcal{A}+2}{\mathcal{A}} \right]^2 \left[ \left(\frac{x+1}{x-1}\right)^2 + 1 \right] \right\} \right., \\ &= \int_1^\infty \frac{2(x+1) dx}{(x-1)^3} \frac{\sin(s \ln x) (x-1)^6}{\left[ \left(\frac{\mathcal{A}+2}{\mathcal{A}} + 1\right) (x^2+1) - \left(\frac{\mathcal{A}+2}{\mathcal{A}} - 1\right) 2x \right]^2 2(x^2+1)}, \\ &= \int_1^\infty dx \frac{(x+1)(x-1)^3 \sin(s \ln x)}{\left[ \frac{2}{\mathcal{A}} (\mathcal{A}+1) (x^2+1) - \frac{4}{\mathcal{A}} x \right]^2 (x^2+1)}. \end{aligned} \quad (\text{E.56})$$

The sum of the two integrals in Eqs. (E.55) and (E.56),  $I_+(s)$ , is found to be

$$\begin{aligned} I_+(s) &= \int_1^\infty dx \frac{(x+1)(x-1) \sin(s \ln x)}{x^2+1} \\ &\quad \times \left\{ \frac{(x+1)^2}{\left[ \frac{2}{\mathcal{A}} (\mathcal{A}+1) (x^2+1) + \frac{4}{\mathcal{A}} x \right]^2} + \frac{(x-1)^2}{\left[ \frac{2}{\mathcal{A}} (\mathcal{A}+1) (x^2+1) - \frac{4}{\mathcal{A}} x \right]^2} \right\}, \end{aligned}$$

$$\begin{aligned}
&= \frac{16}{\mathcal{A}^2} \int_1^\infty dx \sin(s \ln x) \frac{x^2 - 1}{x^2 + 1} \\
&\quad \times \frac{2(x^2 + 1) \left[ \frac{(\mathcal{A}+1)^2}{4} x^4 + \left( \frac{(\mathcal{A}+1)^2}{2} + 1 \right) x^2 + 1 \right] + 4x \left[ (\mathcal{A} + 1) (x^3 + x) \right]}{\left[ \frac{4}{\mathcal{A}^2} (\mathcal{A} + 1)^2 (x^2 + 1)^2 - \frac{16}{\mathcal{A}^2} x^2 \right]^2}, \\
&= \mathcal{A}^2 \int_1^\infty dx \sin(s \ln x) \frac{x^2 - 1}{x^2 + 1} \\
&\quad \times \frac{\frac{(\mathcal{A}+1)^2}{2} x^6 + \left( \frac{3}{2} \mathcal{A}^2 + 7\mathcal{A} + \frac{15}{2} \right) x^4 + (\mathcal{A} + 3)^2 x^2 + 2}{\left\{ (\mathcal{A} + 1)^2 x^4 + [2(\mathcal{A}^2 + 1)^2 - 4] x^2 + (\mathcal{A}^2 + 1)^2 \right\}^2}, \\
&= \frac{\mathcal{A}^2}{2(\mathcal{A} + 1)^4} \int_1^\infty dx \sin(s \ln x) \frac{x^2 - 1}{x^2 + 1} \\
&\quad \times \frac{(\mathcal{A} + 1)^2 (x^6 + 1) + (3\mathcal{A}^2 - 2\mathcal{A} - 1)(x^4 + x^2)}{\left[ x^4 + \left( 2 - \frac{4}{(\mathcal{A}+1)^2} \right) x^2 + 1 \right]^2}.
\end{aligned} \tag{E.57}$$

From Eq. (E.54),  $\langle n_4(q_B) \rangle$  becomes

$$\begin{aligned}
\langle n_4(q_B) \rangle &= \frac{32\pi |c_{AB}|^2}{s q_B^5} \frac{\mathcal{A}^2}{(\mathcal{A} + 1)^4} \\
&\quad \times \int_1^\infty dx \sin(s \ln x) \frac{x^2 - 1}{x^2 + 1} \frac{(\mathcal{A} + 1)^2 (x^6 + 1) + (3\mathcal{A}^2 - 2\mathcal{A} - 1)(x^4 + x^2)}{\left[ x^4 + \left( 2 - \frac{4}{(\mathcal{A}+1)^2} \right) x^2 + 1 \right]^2}.
\end{aligned} \tag{E.58}$$

The residue theorem is used to calculate the non-oscillating part of  $n_4(q_B)$ . The poles of Eq. (E.58) are given by

$$x_1 = \frac{1}{\mathcal{A} + 1} \left( 1 + i\sqrt{\mathcal{A}(\mathcal{A} + 1)} \right) = \sqrt{\frac{1 + \mathcal{A}^2 + 2\mathcal{A}}{(\mathcal{A} + 1)^2}} e^{i\theta_4} = e^{i\theta_4}, \tag{E.59}$$

$$x_2 = \frac{1}{\mathcal{A} + 1} \left( -1 + i\sqrt{\mathcal{A}(\mathcal{A} + 1)} \right) = e^{i(\pi - \theta_4)} = -e^{-i\theta_4}, \tag{E.60}$$

$$x_3 = \frac{1}{\mathcal{A} + 1} \left( 1 - i\sqrt{\mathcal{A}(\mathcal{A} + 1)} \right) = e^{-i\theta_4}, \tag{E.61}$$

$$x_4 = \frac{1}{\mathcal{A} + 1} \left( -1 - i\sqrt{\mathcal{A}(\mathcal{A} + 1)} \right) = e^{-i(\pi - \theta_4)} = -e^{i\theta_4}, \tag{E.62}$$

$$x_5 = i = e^{i\frac{\pi}{2}}, \tag{E.63}$$

$$x_6 = -i = e^{-i\frac{\pi}{2}}, \quad (\text{E.64})$$

with

$$\tan \theta_4 = \sqrt{\mathcal{A}(\mathcal{A} + 2)} \quad \text{for } 0 \leq \theta_4 \leq \frac{\pi}{2}. \quad (\text{E.65})$$

Notice that the roots  $x_n$  with  $1 \leq n \leq 4$  are of order two. Changing variables to  $x = e^\alpha$ , the domain of integration is now to the entire real axis, namely

$$\begin{aligned} \langle n_4(q_B) \rangle &= \frac{32\pi |c_{AB}|^2}{s q_B^5} \frac{\mathcal{A}^2}{(\mathcal{A} + 1)^4} \int_0^\infty d\alpha e^\alpha \sin(s\alpha) \frac{e^{2\alpha} - 1}{e^{2\alpha} + 1} \\ &\quad \times \frac{(\mathcal{A} + 1)^2 (e^{6\alpha} + 1) + (3\mathcal{A}^2 - 2\mathcal{A} - 1)(e^{4\alpha} + e^{2\alpha})}{\left[ e^{4\alpha} + \left( 2 - \frac{4}{(\mathcal{A} + 1)^2} \right) e^{2\alpha} + 1 \right]^2}, \\ &= \frac{16\pi |c_{AB}|^2}{s q_B^5} \frac{\mathcal{A}^2}{(\mathcal{A} + 1)^4} \text{Im } I_\alpha(s), \end{aligned} \quad (\text{E.66})$$

where the integral  $I_\alpha(s)$  is given by

$$I_\alpha(s) = \int_{-\infty}^\infty d\alpha e^{\alpha(1+i s)} \frac{e^{2\alpha} - 1}{e^{2\alpha} + 1} \frac{(\mathcal{A} + 1)^2 (e^{6\alpha} + 1) + (3\mathcal{A}^2 - 2\mathcal{A} - 1)(e^{4\alpha} + e^{2\alpha})}{\left[ e^{4\alpha} + \left( 2 - \frac{4}{(\mathcal{A} + 1)^2} \right) e^{2\alpha} + 1 \right]^2}. \quad (\text{E.67})$$

Writing the integrand  $f(\alpha)$  explicitly in terms of its poles gives

$$f(\alpha) = \frac{e^{\alpha(1+i s)} (e^{2\alpha} - 1) \left[ (\mathcal{A} + 1)^2 (e^{6\alpha} + 1) + (3\mathcal{A}^2 - 2\mathcal{A} - 1)(e^{2\alpha} + e^{4\alpha}) \right]}{(e^\alpha - e^{\alpha_5})(e^\alpha - e^{\alpha_6}) \left[ (e^\alpha - e^{\alpha_1})(e^\alpha - e^{\alpha_2})(e^\alpha - e^{\alpha_3})(e^\alpha - e^{\alpha_4}) \right]^2}. \quad (\text{E.68})$$

It is possible to see, from Eqs. (E.59) to (E.64) that all of the roots on the denominator of the integrand  $f(\alpha)$  are on the imaginary axis. They are given by

$$\alpha_1 = i\theta_4, \quad \alpha_2 = i(\pi - \theta_4), \quad \alpha_3 = -i\theta_4, \quad \alpha_4 = -i(\pi - \theta_4), \quad \alpha_5 = i\frac{\pi}{2}, \quad \alpha_6 = -i\frac{\pi}{2}, \quad (\text{E.69})$$

where  $\theta_4$  is given in Eq. (E.65). Notice that  $\alpha_5$  and  $\alpha_6$  are simple poles in Eq. (E.67), while  $\alpha_1$ ,  $\alpha_2$ ,  $\alpha_3$ , and  $\alpha_4$  are poles of second order.

Evaluating the contour integral, the same closed path used in the calculation of  $n_3(q_B)$  (see in Fig. E.1) is chosen, namely a rectangle of vertices  $-R$ ,  $+R$ ,  $+R + i\pi$  and  $-R + i\pi$ , which now, due to the restriction of  $\theta_4$  in Eq. (E.65), encompasses the poles  $\alpha_1$ ,  $\alpha_2$  and  $\alpha_5$  in the upper-half plane. Once more, four integrals have to be worked out, i.e.,  $J_1$  which extends along the real axis from  $-R$  to  $+R$ ,  $J_2$  from  $+R$  to  $+R + i\pi$ ,  $J_3$  from  $+R + i\pi$  to  $-R + i\pi$  and  $J_4$  from  $-R + i\pi$  to  $-R$ . The integral in the closed path reads

$$\oint f(z) dz = J_1 + J_2 + J_3 + J_4 = 2\pi i \left[ \text{Res}(f, \alpha_1) + \text{Res}(f, \alpha_2) + \text{Res}(f, \alpha_5) \right], \quad (\text{E.70})$$

with  $f(z)$  defined in Eq. (E.68). The four integrals are worked out as in Eqs. (E.31) to (E.34) and it turns out that  $J_1 = I_\alpha(s)$ ,  $J_3 = e^{-s\pi} I_\alpha(s)$  and  $J_2, J_4 \rightarrow 0$ . In this way, the integral  $I_\alpha(s)$  from Eq. (E.67) reads

$$I_\alpha(s) = \frac{2\pi i}{1 + e^{-\pi s}} \left[ \text{Res}(f, \alpha_1) + \text{Res}(f, \alpha_2) + \text{Res}(f, \alpha_5) \right]. \quad (\text{E.71})$$

Calculating the residues is laborious and the details about the calculation of  $I_\alpha(s)$  are given in Appendix F. The real and imaginary part of  $I_\alpha(s)$  are given by

$$\text{Re } I_\alpha(s) = \frac{\pi(\mathcal{A} + 1)^3 \mathcal{A}}{2\sqrt{\mathcal{A}(\mathcal{A} + 2)} \cosh\left(\frac{s\pi}{2}\right)} \cosh\left[s\left(\frac{\pi}{2} - \theta_4\right)\right], \quad (\text{E.72})$$

$$\begin{aligned} \text{Im } I_\alpha(s) &= \frac{\pi(\mathcal{A} + 1)^4}{2\sqrt{\mathcal{A}(\mathcal{A} + 2)} \cosh\left(\frac{s\pi}{2}\right)} \\ &\times \left\{ \sqrt{\mathcal{A}(\mathcal{A} + 2)} \sinh\left[s\left(\frac{\pi}{2} - \theta_4\right)\right] - \frac{s\mathcal{A}}{\mathcal{A} + 1} \cosh\left[s\left(\frac{\pi}{2} - \theta_4\right)\right] \right\}. \quad (\text{E.73}) \end{aligned}$$

Finally, combining Eqs. (E.66) and (E.73), the non-oscillating part of

$n_4(q_B)$  reads

$$\begin{aligned} \langle n_4(q_B) \rangle &= \frac{8\pi^2 |c_{AB}|^2 \mathcal{A}^2}{s q_B^5 \sqrt{\mathcal{A}(\mathcal{A}+2)} \cosh\left(\frac{s\pi}{2}\right)} \\ &\times \left\{ \sqrt{\mathcal{A}(\mathcal{A}+2)} \sinh\left[s\left(\frac{\pi}{2} - \theta_4\right)\right] - \frac{s\mathcal{A}}{\mathcal{A}+1} \cosh\left[s\left(\frac{\pi}{2} - \theta_4\right)\right] \right\}, \quad (\text{E.74}) \end{aligned}$$

where  $\tan \theta_4 = \sqrt{\mathcal{A}(\mathcal{A}+2)}$  for  $0 \leq \theta_4 \leq \pi/2$ . The special case  $\mathcal{A} = 1$  yields  $\theta_4 = \pi/3$  and  $\langle n_4(q_B) \rangle = 8\pi^2 |c_{AA}|^2 \left[ \sinh\left(\frac{s\pi}{6}\right) - s/(2\sqrt{3}) \cosh\left(\frac{s\pi}{6}\right) \right] / \left[ s q_B^5 \cosh\left(\frac{s\pi}{2}\right) \right]$ .



# Detailed calculation of the residue

It is not expected that the reader try to reproduce the calculation in this Appendix. The purpose here is just to let registered all the steps made in some very inspired days of work.

The integral  $I_\alpha(s)$  in Eq. (E.71) is given by

$$I_\alpha(s) = \frac{2\pi i}{1 + e^{-\pi s}} \left[ Res(f, \alpha_1) + Res(f, \alpha_2) + Res(f, \alpha_5) \right], \quad (\text{F.1})$$

where  $f(\alpha)$  is given in Eq. (E.68) and  $\alpha_1, \alpha_2$  and  $\alpha_5$  in Eq. (E.69). Remember that  $\alpha_5$  is a simple pole, while  $\alpha_1$  and  $\alpha_2$  are poles of second order.

Starting with the simplest case and using the pole expansion from Eq. (E.36), the last term on the right-hand-side of Eq. (F.1) reads

$$\begin{aligned} Res(f, \alpha_5) &= \lim_{\alpha \rightarrow \alpha_5} (\alpha - \alpha_5) \frac{e^{\alpha(1+i s)} (e^{2\alpha} - 1)}{e^\alpha (\alpha - \alpha_5) (e^\alpha - e^{\alpha_6})} \\ &\quad \times \frac{(\mathcal{A} + 1)^2 (e^{6\alpha} + 1) + (3\mathcal{A}^2 - 2\mathcal{A} - 1) (e^{4\alpha} + e^{2\alpha})}{\left[ (e^\alpha - e^{\alpha_1}) (e^\alpha - e^{\alpha_2}) (e^\alpha - e^{\alpha_3}) (e^\alpha - e^{\alpha_4}) \right]^2}, \\ &= \frac{e^{\alpha_5} e^{i s \alpha_5} (e^{2\alpha_5} - 1) (\mathcal{A} + 1)^2 (e^{6\alpha_5} + 1) + (3\mathcal{A}^2 - 2\mathcal{A} - 1) (e^{4\alpha_5} + e^{2\alpha_5})}{e^{\alpha_5} (e^{\alpha_5} - e^{\alpha_6}) \left[ (e^{\alpha_5} - e^{\alpha_1}) (e^{\alpha_5} - e^{\alpha_2}) (e^{\alpha_5} - e^{\alpha_3}) (e^{\alpha_5} - e^{\alpha_4}) \right]^2}, \\ &= \frac{-2e^{s\pi/2}}{-2i} \frac{(\mathcal{A} + 1)^2 (-1 + 1) + (3\mathcal{A}^2 - 2\mathcal{A} - 1) (1 - 1)}{\left[ (e^{\alpha_5} - e^{\alpha_1}) (e^{\alpha_5} - e^{\alpha_2}) (e^{\alpha_5} - e^{\alpha_3}) (e^{\alpha_5} - e^{\alpha_4}) \right]^2} = 0, \end{aligned} \quad (\text{F.2})$$

where in the first line it was used that

$$\begin{aligned} e^{2\alpha} + 1 &= (e^\alpha - e^{\alpha_5})(e^\alpha - e^{\alpha_6}) = e^{2\alpha} - e^\alpha e^{\alpha_5} - e^\alpha e^{\alpha_6} + e^{\alpha_5 + \alpha_6}, \\ &= e^{2\alpha} - \imath e^\alpha + \imath e^\alpha + 1 = e^{2\alpha} + 1. \end{aligned} \quad (\text{F.3})$$

Since  $\alpha_1$  and  $\alpha_2$  are poles of second order, the pole expansion of the  $n^{\text{th}}$  root, in the limit  $\alpha \rightarrow \alpha_n$ , from Eq. (E.36) is modified to

$$\begin{aligned} (e^\alpha - e^{\alpha_n})^2 &= e^{2\alpha} (1 - e^{\alpha_n - \alpha})^2 = e^{2\alpha} \left( 1 - 1 - (\alpha_n - \alpha) - \frac{(\alpha_n - \alpha)^2}{2!} - \dots \right)^2, \\ &= e^{2\alpha} (\alpha - \alpha_n)^2 \left( 1 + \frac{(\alpha - \alpha_n)}{2!} - \dots \right)^2. \end{aligned} \quad (\text{F.4})$$

Utilizing the pole expansion in Eq. (F.4) and a software of algebraic computation, the first term on the right-hand-side of Eq. (F.1) is given by

$$\begin{aligned} \text{Res}(f, \alpha_1) &= \lim_{\alpha \rightarrow \alpha_1} \frac{d}{d\alpha} \left\{ (\alpha - \alpha_1)^2 \frac{e^{\alpha(1+\imath s)} (e^{2\alpha} - 1)}{e^{2\alpha} (\alpha - \alpha_1)^2 (e^{2\alpha} + 1)} \right. \\ &\quad \times \left. \frac{(\mathcal{A} + 1)^2 (e^{6\alpha} + 1) + (3\mathcal{A}^2 - 2\mathcal{A} - 1) (e^{2\alpha} + e^{4\alpha})}{\left[ (e^\alpha - e^{\alpha_2}) (e^\alpha - e^{\alpha_3}) (e^\alpha - e^{\alpha_4}) \right]^2} \right\}, \\ &= \frac{e^{\imath\theta_4 - s\theta_4}}{4(-1 + e^{2\imath\theta_4})(1 + e^{2\imath\theta_4})^3} \left[ \imath\mathcal{A}^2 (1 + e^{2\imath\theta_4})^2 (2\imath + s + e^{2\imath\theta_4} s) + (-1 + e^{2\imath\theta_4}) \right. \\ &\quad \times \left. (2 + 6e^{2\imath\theta_4} - \imath s + \imath e^{4\imath\theta_4} s) + 2\mathcal{A}(-1 + e^{2\imath\theta_4})(2 + 6e^{2\imath\theta_4} - \imath s + \imath e^{4\imath\theta_4} s) \right]. \end{aligned} \quad (\text{F.5})$$

In the same way, the second term on the right-hand-side of Eq. (F.1) reads

$$\begin{aligned} \text{Res}(f, \alpha_2) &= \lim_{\alpha \rightarrow \alpha_2} \frac{d}{d\alpha} \left\{ (\alpha - \alpha_2)^2 \frac{e^{\alpha(1+\imath s)} (e^{2\alpha} - 1)}{e^{2\alpha} (\alpha - \alpha_2)^2 (e^{2\alpha} + 1)} \right. \\ &\quad \times \left. \frac{(\mathcal{A} + 1)^2 (e^{6\alpha} + 1) + (3\mathcal{A}^2 - 2\mathcal{A} - 1) (e^{2\alpha} + e^{4\alpha})}{\left[ (e^\alpha - e^{\alpha_1}) (e^\alpha - e^{\alpha_3}) (e^\alpha - e^{\alpha_4}) \right]^2} \right\}, \end{aligned}$$



$$\begin{aligned}
 &= \frac{-e^{i\theta_4+s\theta_4-\pi s}}{4(-1+e^{2i\theta_4})(1+e^{2i\theta_4})^3} \left\{ (1+\mathcal{A})^2 e^{6i\theta_4} (2-\imath s) + e^{4i\theta_4} [4+\mathcal{A}(8+2\imath s) \right. \\
 &\quad \left. + \mathcal{A}^2(4-3\imath s) + \imath s] - \imath(1+\mathcal{A})^2 s + e^{2i\theta_4} [-6+\mathcal{A}^2(2-3\imath s) + \imath s \right. \\
 &\quad \left. + 2\imath\mathcal{A}(6\imath+s)] \right\}. \quad (\text{F.6})
 \end{aligned}$$

Inserting the residues from Eqs. (F.2), (F.5) and (F.6) into Eq. (F.1), the integral  $I_\alpha(s)$  becomes

$$\begin{aligned}
 I_\alpha(s) &= \frac{2\pi\imath}{e^{-\pi s/2}(e^{\pi s/2}+e^{-\pi s/2})} \frac{e^{i\theta_4-s(\pi+\theta_4)}}{4(-1+e^{2i\theta_4})(1+e^{2i\theta_4})^3} \left\{ \imath(1+\mathcal{A})^2 e^{\pi s+6i\theta_4} s \right. \\
 &\quad \left. + \imath(1+\mathcal{A})^2 e^{2s\theta_4} s + \imath(1+\mathcal{A})^2 e^{\pi s} (2\imath+s) + \imath(1+\mathcal{A})^2 e^{2(3\imath+s)\theta_4} (2\imath+s) \right. \\
 &\quad \left. + e^{\pi s+4i\theta_4} [6-2(-6+\mathcal{A})\mathcal{A} + \imath(-1+\mathcal{A})(1+3\mathcal{A})s] + e^{2\theta_4(\imath+s)} \right. \\
 &\quad \times [6-2(-6+\mathcal{A})\mathcal{A} + \imath(-1+\mathcal{A})(1+3\mathcal{A})s] + \imath(e^{\pi s+2i\theta_4} + e^{2(2\imath+s)\theta_4}) \\
 &\quad \left. \times [4\imath(1+\mathcal{A})^2 + (-1+\mathcal{A})(1+3\mathcal{A})s] \right\}, \quad (\text{F.7})
 \end{aligned}$$

which no software of algebraic computation is able to simplify. Manually manipulating Eq. (F.7),  $I_\alpha(s)$  is found to be

$$\begin{aligned}
 I_\alpha(s) &= \frac{2\pi\imath e^{\pi s/2}}{2 \cosh\left(\frac{\pi s}{2}\right)} \frac{e^{i\theta_4-s(\pi+\theta_4)}}{4(-1+e^{2i\theta_4})(1+e^{2i\theta_4})^3} \\
 &\quad \times \left\{ \imath(1+\mathcal{A})^2 [s e^{\pi s+6i\theta_4} + s e^{2s\theta_4} + (e^{\pi s} + e^{2\theta_4(3\imath+s)}) (2\imath+s)] \right. \\
 &\quad \left. + (e^{\pi s+4i\theta_4} + e^{2\theta_4(\imath+s)}) [6-2(-6+\mathcal{A})\mathcal{A} + \imath(-1+\mathcal{A})(1+3\mathcal{A})s] \right. \\
 &\quad \left. + \imath(e^{\pi s+2i\theta_4} + e^{2\theta_4(2\imath+s)}) [4\imath(1+\mathcal{A})^2 + (-1+\mathcal{A})(1+3\mathcal{A})s] \right\}, \quad (\text{F.8})
 \end{aligned}$$

$$\begin{aligned}
 I_\alpha(s) &= \frac{\pi\imath e^{-\pi s/2} e^{i\theta_4} e^{-s\theta_4}}{4 \cosh\left(\frac{\pi s}{2}\right) e^{i\theta_4} (e^{i\theta_4} - e^{-i\theta_4}) e^{3i\theta_4} (e^{i\theta_4} + e^{-i\theta_4})^3} \\
 &\quad \times \left\{ \imath(1+\mathcal{A})^2 [s e^{\pi s} e^{6i\theta_4} + s e^{2s\theta_4} + 2\imath e^{\pi s} + 2\imath e^{6i\theta_4} e^{2\theta_4 s} + s e^{\pi s} + s e^{6i\theta_4} e^{2\theta_4 s}] \right. \\
 &\quad \left. + (e^{\pi s+2i\theta_4+2i\theta_4} + e^{2\theta_4(\imath+s)}) [6+12\mathcal{A}-2\mathcal{A}^2 + \imath s(-1-2\mathcal{A}+3\mathcal{A}^2)] \right. \\
 &\quad \left. + \imath(e^{\pi s+2i\theta_4} + e^{2\theta_4(\imath+s+\imath)}) [s(-1-2\mathcal{A}+3\mathcal{A}^2) + \imath(4+8\mathcal{A}+4\mathcal{A}^2)] \right\}, \quad (\text{F.9})
 \end{aligned}$$

$$\begin{aligned}
I_\alpha(s) &= \frac{\pi \imath e^{-\pi s/2} e^{-s\theta_4} e^{-3\imath\theta_4}}{64 \imath \cosh\left(\frac{\pi s}{2}\right) \sin \theta_4 \cos^3 \theta_4} \\
&\times \left\{ \imath (1 + \mathcal{A})^2 \left[ s \left( e^{\pi s} e^{6\imath\theta_4} + e^{2s\theta_4} + e^{\pi s} + e^{6\imath\theta_4} e^{2\theta_4 s} \right) + 2\imath \left( e^{\pi s} + e^{6\imath\theta_4} e^{2\theta_4 s} \right) \right] \right. \\
&+ e^{\pi s/2} e^{s\theta_4} e^{3\imath\theta_4} \left( e^{\pi s/2 + \imath\theta_4 - s\theta_4} + e^{-\pi s/2 - \imath\theta_4 + s\theta_4} \right) \\
&\quad \times \left[ 6 + 12\mathcal{A} - 2\mathcal{A}^2 + \imath s \left( -1 - 2\mathcal{A} + 3\mathcal{A}^2 \right) \right] \\
&+ e^{\pi s/2} e^{s\theta_4} e^{3\imath\theta_4} \left( e^{\pi s/2 - \imath\theta_4 - s\theta_4} + e^{-\pi s/2 + \imath\theta_4 + s\theta_4} \right) \\
&\quad \left. \times \left[ \left( -4 - 8\mathcal{A} - 4\mathcal{A}^2 \right) + \imath s \left( -1 - 2\mathcal{A} + 3\mathcal{A}^2 \right) \right] \right\}, \tag{F.10}
\end{aligned}$$

$$\begin{aligned}
I_\alpha(s) &= \frac{\pi}{64 \cosh\left(\frac{\pi s}{2}\right) \sin \theta_4 \cos^3 \theta_4} \\
&\times \left\{ \imath (1 + \mathcal{A})^2 \left[ s \left( e^{\pi s/2 - s\theta_4 + 3\imath\theta_4} + e^{-\pi s/2 + s\theta_4 - 3\imath\theta_4} + e^{\pi s/2 - s\theta_4 - 3\imath\theta_4} + e^{-\pi s/2 + s\theta_4 + 3\imath\theta_4} \right) \right. \right. \\
&+ 2\imath \left( e^{\pi s/2 - s\theta_4 - 3\imath\theta_4} + e^{-\pi s/2 + s\theta_4 + 3\imath\theta_4} \right) \left. \right] \\
&+ \left( e^{\pi s/2 + \imath\theta_4 - s\theta_4} + e^{-\pi s/2 - \imath\theta_4 + s\theta_4} \right) \left[ 6 + 12\mathcal{A} - 2\mathcal{A}^2 + \imath s \left( -1 - 2\mathcal{A} + 3\mathcal{A}^2 \right) \right] \\
&+ \left. \left( e^{\pi s/2 - \imath\theta_4 - s\theta_4} + e^{-\pi s/2 + \imath\theta_4 + s\theta_4} \right) \left[ -4 - 8\mathcal{A} - 4\mathcal{A}^2 + \imath s \left( -1 - 2\mathcal{A} + 3\mathcal{A}^2 \right) \right] \right\}, \tag{F.11}
\end{aligned}$$

$$\begin{aligned}
I_\alpha(s) &= \frac{\pi}{64 \cosh\left(\frac{\pi s}{2}\right) \sin \theta_4 \cos^3 \theta_4} \\
&\times \left\{ \imath (1 + \mathcal{A})^2 \left[ s \left( e^{3\imath\theta_4} \left( e^{\pi s/2 - s\theta_4} + e^{-(\pi s/2 - s\theta_4)} \right) + e^{-3\imath\theta_4} \left( e^{\pi s/2 - s\theta_4} + e^{-(\pi s/2 - s\theta_4)} \right) \right) \right. \right. \\
&+ 2\imath \left( e^{\pi s/2 - s\theta_4 - 3\imath\theta_4} + e^{-(\pi s/2 - s\theta_4 - 3\imath\theta_4)} \right) \left. \right] + \imath s \left( -1 - 2\mathcal{A} + 3\mathcal{A}^2 \right) \\
&\times \left[ e^{\imath\theta_4} \left( e^{\pi s/2 - s\theta_4} + e^{-(\pi s/2 - s\theta_4)} \right) + e^{-\imath\theta_4} \left( e^{\pi s/2 - s\theta_4} + e^{-(\pi s/2 - s\theta_4)} \right) \right] \\
&+ \left( e^{\pi s/2 + \imath\theta_4 - s\theta_4} + e^{-\pi s/2 - \imath\theta_4 + s\theta_4} \right) \left( 6 + 12\mathcal{A} - 2\mathcal{A}^2 \right) \\
&+ \left. \left( e^{\pi s/2 - \imath\theta_4 - s\theta_4} + e^{-\pi s/2 + \imath\theta_4 + s\theta_4} \right) \left( -4 - 8\mathcal{A} - 4\mathcal{A}^2 \right) \right\}, \tag{F.12}
\end{aligned}$$

$$\begin{aligned}
 I_\alpha(s) &= \frac{\pi}{64 \cosh\left(\frac{\pi s}{2}\right) \sin \theta_4 \cos^3 \theta_4} \\
 &\times \left\{ \imath (1 + \mathcal{A})^2 \left\{ 4s \cosh \left[ s \left( \frac{\pi}{2} - \theta_4 \right) \right] \cos(3\theta_4) + 4\imath \cosh \left[ s \left( \frac{\pi}{2} - \theta_4 \right) - 3\imath\theta_4 \right] \right\} \right. \\
 &\quad \left. + 4\imath s (-1 - 2\mathcal{A} + 3\mathcal{A}^2) \cosh \left[ s \left( \frac{\pi}{2} - \theta_4 \right) \right] \cos(\theta_4) + 2(6 + 12\mathcal{A} - 2\mathcal{A}^2) \right. \\
 &\quad \left. \times \cosh \left[ s \left( \frac{\pi}{2} - \theta_4 \right) + \imath\theta_4 \right] - 8(1 + \mathcal{A})^2 \cosh \left[ s \left( \frac{\pi}{2} - \theta_4 \right) - \imath\theta_4 \right] \right\}, \tag{F.13}
 \end{aligned}$$

$$\begin{aligned}
 I_\alpha(s) &= \frac{\pi}{64 \cosh\left(\frac{\pi s}{2}\right) \sin \theta_4 \cos^3 \theta_4} \\
 &\times \left\{ \imath (1 + \mathcal{A})^2 \left\{ 4s \cosh \left[ s \left( \frac{\pi}{2} - \theta_4 \right) \right] \cos(3\theta_4) + 4\imath \left\{ \cosh \left[ s \left( \frac{\pi}{2} - \theta_4 \right) \right] \cos(3\theta_4) \right. \right. \right. \\
 &\quad \left. \left. - \imath \sinh \left[ s \left( \frac{\pi}{2} - \theta_4 \right) \right] \sin(3\theta_4) \right\} \right\} + 4\imath s (-1 - 2\mathcal{A} + 3\mathcal{A}^2) \cosh \left[ s \left( \frac{\pi}{2} - \theta_4 \right) \right] \right. \\
 &\quad \times \cos(\theta_4) + 2(6 + 12\mathcal{A} - 2\mathcal{A}^2) \left\{ \cosh \left[ s \left( \frac{\pi}{2} - \theta_4 \right) \right] \cos(\theta_4) + \imath \sinh \left[ s \left( \frac{\pi}{2} - \theta_4 \right) \right] \right. \\
 &\quad \times \sin(\theta_4) \left. \right\} - 8(1 + \mathcal{A})^2 \left\{ \cosh \left[ s \left( \frac{\pi}{2} - \theta_4 \right) \right] \cos(\theta_4) - \imath \sinh \left[ s \left( \frac{\pi}{2} - \theta_4 \right) \right] \right. \\
 &\quad \left. \left. \times \sin(\theta_4) \right\} \right\}, \tag{F.14}
 \end{aligned}$$

where it was used that

$$\begin{aligned}
 \cosh(x \pm \imath y) &= \cosh(x) \cosh(\imath y) + \sinh(x) \sinh(\pm \imath y), \\
 &= \cosh(x) \cos(y) \pm \sinh(x) \sin(y). \tag{F.15}
 \end{aligned}$$

Then, continuing to calculate,  $I_\alpha(s)$  reads

$$\begin{aligned}
I_\alpha(s) = & \frac{\pi}{64 \cosh\left(\frac{\pi s}{2}\right) \sin \theta_4 \cos^3 \theta_4} \left\{ 4\iota s (1 + \mathcal{A})^2 \cosh\left[s\left(\frac{\pi}{2} - \theta_4\right)\right] \cos(3\theta_4) \right. \\
& - 4(1 + \mathcal{A})^2 \cosh\left[s\left(\frac{\pi}{2} - \theta_4\right)\right] \cos(3\theta_4) + 4\iota \sinh\left[s\left(\frac{\pi}{2} - \theta_4\right)\right] \sin(3\theta_4) \\
& + 4\iota s (-1 - 2\mathcal{A} + 3\mathcal{A}^2) \cosh\left[s\left(\frac{\pi}{2} - \theta_4\right)\right] \cos(\theta_4) \\
& + 4(3 + 6\mathcal{A} - \mathcal{A}^2) \cosh\left[s\left(\frac{\pi}{2} - \theta_4\right)\right] \cos(\theta_4) \\
& + 4\iota(3 + 6\mathcal{A} - \mathcal{A}^2) \sinh\left[s\left(\frac{\pi}{2} - \theta_4\right)\right] \sin(\theta_4) \\
& - 8(1 + \mathcal{A})^2 \cosh\left[s\left(\frac{\pi}{2} - \theta_4\right)\right] \cos(\theta_4) \\
& \left. + 8\iota(1 + \mathcal{A})^2 \sinh\left[s\left(\frac{\pi}{2} - \theta_4\right)\right] \sin(\theta_4) \right\}, \tag{F.16}
\end{aligned}$$

$$\begin{aligned}
I_\alpha(s) = & \frac{\pi}{64 \cosh\left(\frac{\pi s}{2}\right) \sin \theta_4 \cos^3 \theta_4} \left\{ \left\{ -4(1 + \mathcal{A})^2 \cos(3\theta_4) + [4(3 + 6\mathcal{A} - \mathcal{A}^2) \right. \right. \\
& \left. \left. - 8(1 + \mathcal{A})^2] \cos(\theta_4) \right\} \cosh\left[s\left(\frac{\pi}{2} - \theta_4\right)\right] \right. \\
& + \iota \left\{ 4s(1 + \mathcal{A})^2 \cosh\left[s\left(\frac{\pi}{2} - \theta_4\right)\right] \cos(3\theta_4) + 4 \sinh\left[s\left(\frac{\pi}{2} - \theta_4\right)\right] \sin(3\theta_4) \right. \\
& + 4s(-1 - 2\mathcal{A} + 3\mathcal{A}^2) \cosh\left[s\left(\frac{\pi}{2} - \theta_4\right)\right] \cos(\theta_4) \\
& + 4(3 + 6\mathcal{A} - \mathcal{A}^2) \sinh\left[s\left(\frac{\pi}{2} - \theta_4\right)\right] \sin(\theta_4) \\
& \left. \left. + 8\iota(1 + \mathcal{A})^2 \sinh\left[s\left(\frac{\pi}{2} - \theta_4\right)\right] \sin(\theta_4) \right\} \right\}, \tag{F.17}
\end{aligned}$$

$$\begin{aligned}
 I_\alpha(s) &= \frac{\pi}{64 \cosh\left(\frac{\pi s}{2}\right) \sin \theta_4 \cos^3 \theta_4} \\
 &\times \left\{ 4 \cosh \left[ s \left( \frac{\pi}{2} - \theta_4 \right) \right] \left[ - (1 + \mathcal{A})^2 \cos(3\theta_4) + (-3\mathcal{A}^2 + 2\mathcal{A} + 1) \cos(\theta_4) \right] \right. \\
 &+ i \left\{ 4s \cosh \left[ s \left( \frac{\pi}{2} - \theta_4 \right) \right] \left[ (1 + \mathcal{A})^2 \cos(3\theta_4) + (3\mathcal{A}^2 - 2\mathcal{A} - 1) \cos(\theta_4) \right] \right. \\
 &\left. \left. + 4 \sinh \left[ s \left( \frac{\pi}{2} - \theta_4 \right) \right] \left[ (1 + \mathcal{A})^2 \sin(3\theta_4) + (\mathcal{A}^2 + 10\mathcal{A} + 5) \sin(\theta_4) \right] \right\} \right\}.
 \end{aligned} \tag{F.18}$$

Using that

$$\sin(3x) = 3 \sin(x) - 4 \sin^3(x), \tag{F.19}$$

$$\cos(3x) = 4 \cos^3(x) - 3 \cos(x), \tag{F.20}$$

the integral  $I_\alpha(s)$  becomes

$$\begin{aligned}
 I_\alpha(s) &= \frac{\pi}{64 \cosh\left(\frac{\pi s}{2}\right) \sin \theta_4 \cos^3 \theta_4} \\
 &\times \left\{ 16 \cosh \left[ s \left( \frac{\pi}{2} - \theta_4 \right) \right] \left[ - (1 + \mathcal{A})^2 \cos^3(\theta_4) + (1 + 2\mathcal{A}) \cos(\theta_4) \right] \right. \\
 &+ i \left\{ 16s \cosh \left[ s \left( \frac{\pi}{2} - \theta_4 \right) \right] \left[ (1 + \mathcal{A})^2 \cos^3(\theta_4) - (1 + 2\mathcal{A}) \cos(\theta_4) \right] \right. \\
 &\left. \left. + 16 \sinh \left[ s \left( \frac{\pi}{2} - \theta_4 \right) \right] \left[ - (1 + \mathcal{A})^2 \sin^3(\theta_4) + (\mathcal{A}^2 + 4\mathcal{A} + 2) \sin(\theta_4) \right] \right\} \right\}.
 \end{aligned} \tag{F.21}$$

It is possible to deduce from Eq. (E.65) that

$$\sin(\theta_4) = \frac{\sqrt{\mathcal{A}(\mathcal{A} + 2)}}{\mathcal{A} + 1} \quad \text{and} \quad \cos(\theta_4) = \frac{1}{\mathcal{A} + 1}, \tag{F.22}$$

and  $I_\alpha(s)$  is

$$\begin{aligned}
I_\alpha(s) = & \frac{\pi(\mathcal{A}+1)^4}{64 \cosh\left(\frac{\pi s}{2}\right) \sqrt{\mathcal{A}(\mathcal{A}+2)}} \left\{ 16 \cosh\left[s\left(\frac{\pi}{2} - \theta_4\right)\right] \left(-\frac{1}{1+\mathcal{A}} + \frac{1+2\mathcal{A}}{1+\mathcal{A}}\right) \right. \\
& + i \left\{ 16s \cosh\left[s\left(\frac{\pi}{2} - \theta_4\right)\right] \left(\frac{1}{1+\mathcal{A}} - \frac{1+2\mathcal{A}}{1+\mathcal{A}}\right) \right. \\
& \left. \left. + 16 \sinh\left[s\left(\frac{\pi}{2} - \theta_4\right)\right] \frac{\sqrt{\mathcal{A}(\mathcal{A}+2)}}{1+\mathcal{A}} [-\mathcal{A}(\mathcal{A}+2) + \mathcal{A}^2 + 4\mathcal{A} + 2] \right\} \right\}. \quad (\text{F.23})
\end{aligned}$$

$$\begin{aligned}
I_\alpha(s) = & \frac{\pi(\mathcal{A}+1)^4}{2 \cosh\left(\frac{\pi s}{2}\right) \sqrt{\mathcal{A}(\mathcal{A}+2)}} \left\{ \frac{\mathcal{A}}{1+\mathcal{A}} \cosh\left[s\left(\frac{\pi}{2} - \theta_4\right)\right] \right. \\
& \left. + i \left\{ \sqrt{\mathcal{A}(\mathcal{A}+2)} \sinh\left[s\left(\frac{\pi}{2} - \theta_4\right)\right] - \frac{s\mathcal{A}}{1+\mathcal{A}} \cosh\left[s\left(\frac{\pi}{2} - \theta_4\right)\right] \right\} \right\}. \quad (\text{F.24})
\end{aligned}$$

Finally, the real and imaginary part of  $I_\alpha(s)$  are given by

$$\text{Re } I_\alpha(s) = \frac{\pi(\mathcal{A}+1)^3 \mathcal{A}}{2\sqrt{\mathcal{A}(\mathcal{A}+2)} \cosh\left(\frac{s\pi}{2}\right)} \cosh\left[s\left(\frac{\pi}{2} - \theta_4\right)\right], \quad (\text{F.25})$$

$$\begin{aligned}
\text{Im } I_\alpha(s) = & \frac{\pi(\mathcal{A}+1)^4}{2\sqrt{\mathcal{A}(\mathcal{A}+2)} \cosh\left(\frac{s\pi}{2}\right)} \\
& \times \left\{ \sqrt{\mathcal{A}(\mathcal{A}+2)} \sinh\left[s\left(\frac{\pi}{2} - \theta_4\right)\right] - \frac{s\mathcal{A}}{\mathcal{A}+1} \cosh\left[s\left(\frac{\pi}{2} - \theta_4\right)\right] \right\}. \quad (\text{F.26})
\end{aligned}$$

# Bibliography

- [Abramowitz 1965] M. Abramowitz and I. A. Stegun. Handbook of mathematical functions with formulas, graphs, and mathematical tables. 1965.
- [Adhikari 1986] Sadhan K. Adhikari. *Quantum scattering in two dimensions*. American Journal of Physics, vol. 54, page 362, 1986.
- [Adhikari 1988] S. K. Adhikari, A. Delfino, T. Frederico, I. D. Goldman and L. Tomio. *Efimov and Thomas effects and the model dependence of three-particle observables in two and three dimensions*. Physical Review A, vol. 37, pages 3666–3673, May 1988.
- [Adhikari 1993] S. K. Adhikari, A. Delfino, T. Frederico and L. Tomio. *Model independence of scattering of three identical bosons in two dimensions*. Physical Review A, vol. 47, pages 1093–1100, February 1993.
- [Adhikari 1995a] S. K. Adhikari and T. Frederico. *Renormalization Group in Potential Scattering*. Physical Review Letters, vol. 74, pages 4572–4575, June 1995.
- [Adhikari 1995b] Sadhan K. Adhikari, T. Frederico and I. D. Goldman. *Perturbative Renormalization in Quantum Few-Body Problems*. Phys. Rev. Lett., vol. 74, pages 487–491, Jan 1995.
- [Armstrong 2010] J. R. Armstrong, N. T. Zinner, D. V. Fedorov and A. S. Jensen. *Bound states and universality in layers of cold polar molecules*. Europhysics Letters, vol. 91, page 16001, July 2010.
- [Armstrong 2012] J. R. Armstrong, N. T. Zinner, D. V. Fedorov and A. S. Jensen. *Layers of cold dipolar molecules in the harmonic approximation*. European Physical Journal D, vol. 66, page 85, March 2012.
- [Bellotti 2011] F F Bellotti, T Frederico, M T Yamashita, D V Fedorov, A S Jensen and N T Zinner. *Scaling and universality in two dimensions: three-body bound states with short-ranged interactions*. Journal of Physics B, vol. 44, no. 20, page 205302, 2011.
- [Bellotti 2012] F F Bellotti, T Frederico, M T Yamashita, D V Fedorov, A S Jensen and N T Zinner. *Supercircle description of universal three-body states in two dimensions*. Phys. Rev. A, vol. 85, page 025601, February 2012.

- [Bellotti 2013a] F. F. Bellotti, T. Frederico, M. T. Yamashita, D. V. Fedorov, A. S. Jensen and N. T. Zinner. *Dimensional effects on the momentum distribution of bosonic trimer states*. Physical Review A, vol. 87, no. 1, page 013610, January 2013.
- [Bellotti 2013b] F. F. Bellotti, T. Frederico, M. T. Yamashita, D. V. Fedorov, A. S. Jensen and N. T. Zinner. *Mass-imbalanced three-body systems in two dimensions*. Journal of Physics B Atomic Molecular Physics, vol. 46, no. 5, page 055301, March 2013.
- [Bellotti 2014] F. F. Bellotti, T. Frederico, M. T. Yamashita, D. V. Fedorov, A. S. Jensen and N. T. Zinner. *Contact parameters in two dimensions for general three-body systems*. New Journal of Physics, vol. 16, no. 1, page 013048, 2014.
- [Berninger 2011a] M. Berninger, A. Zenesini, B. Huang, W. Harm, H.-C. Nägerl, F. Ferlaino, R. Grimm, P. S. Julienne and J. M. Hutson. *Universality of the Three-Body Parameter for Efimov States in Ultracold Cesium*. Physical Review Letters, vol. 107, no. 12, page 120401, September 2011.
- [Berninger 2011b] M. Berninger, A. Zenesini, B. Huang, W. Harm, H.-C. Nägerl, F. Ferlaino, R. Grimm, P. S. Julienne and J. M. Hutson. *Universality of the Three-Body Parameter for Efimov States in Ultracold Cesium*. Physical Review Letters, vol. 107, no. 12, page 120401, September 2011.
- [Bloch 2008] I. Bloch, J. Dalibard and W. Zwerger. *Many-body physics with ultracold gases*. Reviews of Modern Physics, vol. 80, pages 885–964, July 2008.
- [Braaten 2006] E. Braaten and H.-W. Hammer. *Universality in few-body systems with large scattering length*. Physics Reports, vol. 428, pages 259–390, June 2006.
- [Braaten 2011] E. Braaten, D. Kang and L. Platter. *Universal Relations for Identical Bosons from Three-Body Physics*. Physical Review Letters, vol. 106, no. 15, page 153005, April 2011.
- [Bringas 2004] F. Bringas, M. T. Yamashita and T. Frederico. *Triatomic continuum resonances for large negative scattering lengths*. Physical Review A, vol. 69, no. 4, page 040702, April 2004.



- [Bruch 1979] L. W. Bruch and J. A. Tjon. *Binding of three identical bosons in two dimensions*. Physical Review A, vol. 19, pages 425–432, February 1979.
- [Burger 2002] S. Burger, F. S. Cataliotti, C. Fort, P. Maddaloni, F. Minardi and M. Inguscio. *Quasi-2D Bose-Einstein condensation in an optical lattice*. Europhysics Letters, vol. 57, pages 1–6, January 2002.
- [Castin 2011] Y. Castin and F. Werner. *Single-particle momentum distribution of an Efimov trimer*. Physical Review A, vol. 83, no. 6, page 063614, June 2011.
- [Chin 2010] Cheng Chin, Rudolf Grimm, Paul Julienne and Eite Tiesinga. *Feshbach resonances in ultracold gases*. Rev. Mod. Phys., vol. 82, pages 1225–1286, April 2010.
- [Danilov 1961] G. S. Danilov. Zh. Eksp. Teor. Fiz, vol. 40, page 698, 1961.
- [de Miranda 2011] M. H. G. de Miranda, A. Chotia, B. Neyenhuis, D. Wang, G. Quéméner, S. Ospelkaus, J. L. Bohn, J. Ye and D. S. Jin. *Controlling the quantum stereodynamics of ultracold bimolecular reactions*. Nature Physics, vol. 7, pages 502–507, June 2011.
- [de Toledo Piza 2002] A. F. R. de Toledo Piza. Mecnica Quntica. Edusp, So Paulo, 2002.
- [Delfino 2011] A. Delfino, V. S. Timoteo, T. Frederico, Lauro Tomio and C. E. Cordeiro. *Dimensional compactification and two-particle binding*. International Journal of Quantum Chemistry, vol. 111, no. 7-8, pages 1458–1465, 2011.
- [Deltuva 2010] A. Deltuva. *Efimov physics in bosonic atom-trimer scattering*. Physical Review A, vol. 82, no. 4, page 040701, October 2010.
- [Dyke 2011] P. Dyke, E. D. Kuhnle, S. Whitlock, H. Hu, M. Mark, S. Hoinka, M. Lingham, P. Hannaford and C. J. Vale. *Crossover from 2D to 3D in a Weakly Interacting Fermi Gas*. Physical Review Letters, vol. 106, no. 10, page 105304, March 2011.
- [Efimov 1970] V. N. Efimov. *Weakly-bound states of three resonantly-interacting particles*. Yad. Fiz, vol. 12, page 1080, 1970.
- [Faddeev 1965] L. D. Faddeev. Mathematical Aspects of the Three-body Problem in the Quantum Scattering Theory. Israel program for Scientific Translations, 1965.

- [Ferlaino 2010] F. Ferlaino and R. Grimm. *Forty years of Efimov physics: How a bizarre prediction turned into a hot topic*. Physics Online Journal, vol. 3, page 9, January 2010.
- [Fonseca 1979] A. C. Fonseca, E. F. Redish and P. E. Shanley. *Efimov effect in an analytically solvable model*. Nuclear Physics A, vol. 320, pages 273–288, 1979.
- [Frederico 2012] T. Frederico, A. Delfino, L. Tomio and M. T. Yamashita. *Universal aspects of light halo nuclei*. Progress in Particle and Nuclear Physics, vol. 67, pages 939–994, October 2012.
- [Fröhlich 2011] B. Fröhlich, M. Feld, E. Vogt, M. Koschorreck, W. Zwerger and M. Köhl. *Radio-Frequency Spectroscopy of a Strongly Interacting Two-Dimensional Fermi Gas*. Physical Review Letters, vol. 106, no. 10, page 105301, March 2011.
- [Gaunt 2013] A. L. Gaunt, T. F. Schmidutz, I. Gotlibovych, R. P. Smith and Z. Hadzibabic. *Bose-Einstein Condensation of Atoms in a Uniform Potential*. Physical Review Letters, vol. 110, no. 20, page 200406, May 2013.
- [Görlitz 2001] A. Görlitz, J. M. Vogels, A. E. Leanhardt, C. Raman, T. L. Gustavson, J. R. Abo-Shaeer, A. P. Chikkatur, S. Gupta, S. Inouye, T. Rosenband and W. Ketterle. *Realization of Bose-Einstein Condensates in Lower Dimensions*. Physical Review Letters, vol. 87, no. 13, page 130402, September 2001.
- [Günter 2005] K. Günter, T. Stöferle, H. Moritz, M. Köhl and T. Esslinger. *p-Wave Interactions in Low-Dimensional Fermionic Gases*. Physical Review Letters, vol. 95, no. 23, page 230401, December 2005.
- [Hadizadeh 2011] M. R. Hadizadeh, M. T. Yamashita, L. Tomio, A. Delfino and T. Frederico. *Scaling Properties of Universal Tetramers*. Physical Review Letters, vol. 107, no. 13, page 135304, September 2011.
- [Hadizadeh 2013] M. R. Hadizadeh, M. T. Yamashita, Lauro Tomio, A. Delfino and T. Frederico. *Effective range from tetramer-dissociation data for cesium atoms*. Phys. Rev. A, vol. 87, page 013620, Jan 2013.
- [Hammes 2003] M. Hammes, D. Rychtarik, B. Engeser, H.-C. Nägerl and R. Grimm. *Evanescent-Wave Trapping and Evaporative Cooling of an Atomic Gas at the Crossover to Two Dimensions*. Physical Review Letters, vol. 90, no. 17, page 173001, April 2003.

- [Hansen 2013] A. H. Hansen, A. Y. Khramov, W. H. Dowd, A. O. Jamison, B. Plotkin-Swing, R. J. Roy and S. Gupta. *Production of quantum-degenerate mixtures of ytterbium and lithium with controllable interspecies overlap*. Physical Review A, vol. 87, no. 1, page 013615, January 2013.
- [Hung 2011] C.-L. Hung, X. Zhang, N. Gemelke and C. Chin. *Observation of scale invariance and universality in two-dimensional Bose gases*. Nature Physics, vol. 470, pages 236–239, February 2011.
- [Khuri 2002] N. N. Khuri, A. Martin and T.-T. Wu. *Bound States in  $n$  Dimensions (Especially  $n=1$  and  $n=2$ )*. Few-Body Systems, vol. 31, pages 83–89, 2002.
- [Knoop 2012] S. Knoop, J. S. Borbely, W. Vassen and S. J. J. M. F. Kokkelmans. *Universal three-body parameter in ultracold  $^4\text{He}^*$* . Physical Review A, vol. 86, no. 6, page 062705, December 2012.
- [Kraemer 2006] T. Kraemer, M. Mark, P. Waldburger, J. G. Danzl, C. Chin, B. Engeser, A. D. Lange, K. Pilch, A. Jaakkola, H.-C. Nägerl and R. Grimm. *Evidence for Efimov quantum states in an ultracold gas of caesium atoms*. Nature Physics, vol. 440, pages 315–318, March 2006.
- [Kuhnle 2010] E. D. Kuhnle, H. Hu, X.-J. Liu, P. Dyke, M. Mark, P. D. Drummond, P. Hannaford and C. J. Vale. *Universal Behavior of Pair Correlations in a Strongly Interacting Fermi Gas*. Physical Review Letters, vol. 105, no. 7, page 070402, August 2010.
- [Lamé 1818] G. Lamé. Examen des différentes méthodes employées pour résoudre les problèmes de géométrie. Vve Courcier, 1818.
- [Landau 1977] L. D. Landau and E. M. Lifshitz. Quantum Mechanics. Oxford, 1977.
- [Levinsen 2014] J. Levinsen, P. Massignan and M. M. Parish. *Efimov trimers under strong confinement*. ArXiv e-prints, February 2014.
- [Lim 1980] T. K. Lim and B. Shimer. *The Fonseca-Redish-Shanley solvable model for a molecular three-body system and the efimov effect in two dimensions*. Zeitschrift für Physik A Hadrons and Nuclei, vol. 297, pages 185–188, September 1980.

- [Lompe 2010] T. Lompe, T. B. Ottenstein, F. Serwane, A. N. Wenz, G. Zürn and S. Jochim. *Radio-Frequency Association of Efimov Trimers*. Science, vol. 330, pages 940–, November 2010.
- [Martinyanov 2010] K. Martinyanov, V. Makhalov and A. Turlapov. *Observation of a Two-Dimensional Fermi Gas of Atoms*. Physical Review Letters, vol. 105, no. 3, page 030404, July 2010.
- [Meera 2011] M. P. Meera. *Polaron-molecule transitions in a two-Dimensional Fermi gas*. Physical Review A, vol. 83, page 051603, 2011.
- [Mitra 1969] A. N. Mitra. *The Nuclear Three-Body Problem*. Advances in Nuclear Physics, vol. 3, pages 1–69, 1969.
- [Modugno 2003] G. Modugno, F. Ferlaino, R. Heidemann, G. Roati and M. Inguscio. *Production of a Fermi gas of atoms in an optical lattice*. Physical Review A, vol. 68, no. 1, page 011601, July 2003.
- [Morinaga 1999] M. Morinaga, I. Bouchoule, J.-C. Karam and C. Salomon. *Manipulation of Motional Quantum States of Neutral Atoms*. Physical Review Letters, vol. 83, pages 4037–4040, November 1999.
- [Nielsen 1997] E. Nielsen, D. V. Fedorov and A. S. Jensen. *Three-body halos in two dimensions*. Physical Review A, vol. 56, pages 3287–3290, October 1997.
- [Nielsen 1999] E. Nielsen, D. V. Fedorov and A. S. Jensen. *Structure and Occurrence of Three-Body Halos in Two Dimensions*. Few-Body Systems, vol. 27, pages 15–55, 1999.
- [Nielsen 2001] E. Nielsen, D. V. Fedorov, A. S. Jensen and E. Garrido. *The three-body problem with short-range interactions*. Physics Reports, vol. 347, pages 373–459, June 2001.
- [Novoselov 2004] K. S. Novoselov, A. K. Geim, S. V. Morozov, D. Jiang, Y. Zhang, S. V. Dubonos, I. V. Grigorieva and A. A. Firsov. *Electric Field Effect in Atomically Thin Carbon Films*. Science, vol. 306, no. 5696, pages 666–669, 2004.
- [Petrov 2001] D. S. Petrov and G. V. Shlyapnikov. *Interatomic collisions in a tightly confined Bose gas*. Physical Review A, vol. 64, no. 1, page 012706, July 2001.

- [Platter 2009] L. Platter, C. Ji and D. R. Phillips. *Range corrections to three-body observables near a Feshbach resonance*. Physical Review A, vol. 79, no. 2, page 022702, February 2009.
- [Press 2007] William H. Press, Saul A. Teukolsky, William T. Vetterling and Brian P. Flannery. Numerical recipes 3rd edition: The art of scientific computing. Cambridge University Press, New York, NY, USA, 3 édition, 2007.
- [Pricoupenko 2010] L. Pricoupenko. *Crossover in the Efimov spectrum*. Physical Review A, vol. 82, no. 4, page 043633, October 2010.
- [Pricoupenko 2011] L. Pricoupenko. *Isotropic contact forces in arbitrary representation: Heterogeneous few-body problems and low dimensions*. Physical Review A, vol. 83, no. 6, page 062711, June 2011.
- [Ramos 2011] J. G. G. S. Ramos, D. Bazeia, M. S. Hussein and C. H. Lewenkopf. *Conductance Peaks in Open Quantum Dots*. Phys. Rev. Lett., vol. 107, page 176807, Oct 2011.
- [Repp 2013] M. Repp, R. Pires, J. Ulmanis, R. Heck, E. D. Kuhnle, M. Weidemüller and E. Tiemann. *Observation of interspecies  ${}^6\text{Li}$ - ${}^{133}\text{Cs}$  Feshbach resonances*. Physical Review A, vol. 87, no. 1, page 010701, January 2013.
- [Sascha 2011] Z. Sascha, G. M. Bruun and C. J. Pethick. *Polarons and molecules in a two-Dimensional Fermi gas*. Physical Review A, vol. 83, pages 021603–1, 2011.
- [Schmid 1974] Erich W. Schmid and Horst Ziegelmann. The Quantum Mechanical Three-Body Problem. Pergamon Press, 1974.
- [Schmidt 2012a] R. Schmidt, T. Enss, V. Pietila and E. Demler. *Fermi ppolaron in two dimensions*. Physical Review A, vol. 85, page 021602, 2012.
- [Schmidt 2012b] R. Schmidt, S. P. Rath and W. Zwerger. *Efimov physics beyond universality*. European Physical Journal B, vol. 85, page 386, November 2012.
- [Schmidutz 2014] T. F. Schmidutz, I. Gotlibovych, A. L. Gaunt, R. P. Smith, N. Navon and Z. Hadzibabic. *Quantum Joule-Thomson Effect in a Saturated Homogeneous Bose Gas*. Physical Review Letters, vol. 112, no. 4, page 040403, January 2014.

- [Serwane 2011] F. Serwane, G. Zürn, T. Lompe, T. B. Ottenstein, A. N. Wenz and S. Jochim. *Deterministic Preparation of a Tunable Few-Fermion System*. *Science*, vol. 332, pages 336–, April 2011.
- [Simon 1976] B. Simon. *The bound state of weakly coupled Schrödinger operators in one and two dimensions*. *Annals of Physics*, vol. 97, pages 279–288, April 1976.
- [Skornyakov 1956] G. Skornyakov and K. Ter-Martirosian. *Three-body problem with short-range forces. Neutron scattering of deuterons at small energy*. *Zh. Eksp. Teor. Fiz*, vol. 31, page 775, 1956.
- [Sommer 2012] A. T. Sommer, L. W. Cheuk, M. J. H. Ku, W. S. Bakr and M. W. Zwierlein. *Evolution of Fermion Pairing from Three to Two Dimensions*. *Physical Review Letters*, vol. 108, no. 4, page 045302, January 2012.
- [Sørensen 2013] P. K. Sørensen, D. V. Fedorov, A. S. Jensen and N. T. Zinner. *Finite-range effects in energies and recombination rates of three identical bosons*. *Journal of Physics B Atomic Molecular Physics*, vol. 46, no. 7, page 075301, April 2013.
- [Stewart 2010] J. T. Stewart, J. P. Gaebler, T. E. Drake and D. S. Jin. *Verification of Universal Relations in a Strongly Interacting Fermi Gas*. *Physical Review Letters*, vol. 104, no. 23, page 235301, June 2010.
- [Tan 2008] Shina Tan. *Energetics of a strongly correlated Fermi gas*. *Annals of Physics*, vol. 323, no. 12, pages 2952 – 2970, 2008.
- [Thøgersen 2008] M. Thøgersen, D. V. Fedorov and A. S. Jensen. *N-body Efimov states of trapped bosons*. *EPL (Europhysics Letters)*, vol. 83, page 30012, August 2008.
- [Thomas 1935] L. H. Thomas. *The Interaction Between a Neutron and a Proton and the Structure of  $H^3$* . *Phys. Rev.*, vol. 47, pages 903–909, June 1935.
- [Tung 2013] S.-K. Tung, C. Parker, J. Johansen, C. Chin, Y. Wang and P. S. Julienne. *Ultracold mixtures of atomic  $^6Li$  and  $^{133}Cs$  with tunable interactions*. *Physical Review A*, vol. 87, no. 1, page 010702, January 2013.

- [Valiente 2012] M. Valiente, N. T. Zinner and K. Mølmer. *Universal properties of Fermi gases in arbitrary dimensions*. Physical Review A, vol. 86, no. 4, page 043616, October 2012.
- [Volosniev 2011] A. G. Volosniev, D. V. Fedorov, A. S. Jensen and N. T. Zinner. *Model Independence in Two Dimensions and Polarized Cold Dipolar Molecules*. Physical Review Letters, vol. 106, no. 25, page 250401, June 2011.
- [Volosniev 2012] A. G. Volosniev, D. V. Fedorov, A. S. Jensen and N. T. Zinner. *Few-body bound-state stability of dipolar molecules in two dimensions*. Physical Review A, vol. 85, no. 2, page 023609, February 2012.
- [von Stecher 2009] J. von Stecher, J. P. D’Incao and C. H. Greene. *Signatures of universal four-body phenomena and their relation to the Efimov effect*. Nature Physics, vol. 5, pages 417–421, June 2009.
- [Vuletić 1998] V. Vuletić, C. Chin, A. J. Kerman and S. Chu. *Degenerate Raman Sideband Cooling of Trapped Cesium Atoms at Very High Atomic Densities*. Physical Review Letters, vol. 81, pages 5768–5771, December 1998.
- [Werner 2012] F. Werner and Y. Castin. *General relations for quantum gases in two and three dimensions. II. Bosons and mixtures*. Physical Review A, vol. 86, no. 5, page 053633, November 2012.
- [Wild 2012] R. J. Wild, P. Makotyn, J. M. Pino, E. A. Cornell and D. S. Jin. *Measurements of Tan’s Contact in an Atomic Bose-Einstein Condensate*. Physical Review Letters, vol. 108, no. 14, page 145305, April 2012.
- [Yamashita 2002] M. T. Yamashita, T. Frederico, A. Delfino and L. Tomio. *Scaling limit of virtual states of triatomic systems*. Physical Review A, vol. 66, no. 5, page 052702, November 2002.
- [Yamashita 2004a] M. T. Yamashita, L. Tomio and T. Frederico. *Radii in weakly-bound light halo nuclei*. Nuclear Physics A, vol. 735, pages 40–54, April 2004.
- [Yamashita 2004b] Marcelo Takeshi Yamashita. *Sistemas Fracamente Ligados de Trs Corpos: Molculas e Ncleos Exticos Leves*. PhD thesis, Universidade de So Paulo, 2004.



- [Yamashita 2008] M. T. Yamashita, T. Frederico and L. Tomio. *Trajectory of virtual, bound and resonant Efimov states*. Few-Body Systems, vol. 44, pages 191–193, December 2008.
- [Yamashita 2013] M. T. Yamashita, F. F. Bellotti, T. Frederico, D. V. Fedorov, A. S. Jensen and N. T. Zinner. *Single-particle momentum distributions of Efimov states in mixed-species systems*. Phys. Rev. A, vol. 87, page 062702, Jun 2013.
- [Yamashita 2014] M. T. Yamashita, F. F. Bellotti, T. Frederico, D. V. Fedorov, A. S. Jensen and N. T. Zinner. *Dimensional crossover transitions of strongly interacting two- and three-boson systems*. ArXiv e-prints, April 2014.
- [Yefsah 2011] T. Yefsah, R. Desbuquois, L. Chomaz, K. J. Günter and J. Dalibard. *Exploring the Thermodynamics of a Two-Dimensional Bose Gas*. Physical Review Letters, vol. 107, no. 13, page 130401, September 2011.
- [Zürn 2012] G. Zürn, F. Serwane, T. Lompe, A. N. Wenz, M. G. Ries, J. E. Bohn and S. Jochim. *Fermionization of Two Distinguishable Fermions*. Physical Review Letters, vol. 108, no. 7, page 075303, February 2012.